

**ROLE OF SUPER PARAMAGNETIC IRON OXIDE NANOPARTICLES AS A
RADIOTHERAPY SENSITIZER IN COLORECTAL CANCER**

A THESIS SUBMITTED TO



**D.Y. PATIL EDUCATION SOCIETY (DEEMED TO BE UNIVERSITY),
KOLHAPUR**

(Declared u/s 3 of the UGC Act. 1956)

**FOR THE DEGREE OF
DOCTOR OF PHILOSOPHY
IN MEDICAL PHYSICS
UNDER THE FACULTY OF
INTERDISCIPLINARY STUDIES**

BY

Ms. Madhuri Anuje

(M. Sc.)

UNDER THE GUIDANCE OF

ASST. PROF. (DR.) P.N.Pawaskar

M.Sc. Ph.D.

**CENTRE FOR INTERDISCIPLINARY RESEARCH,
D. Y. PATIL EDUCATION SOCIETY (DEEMED TO BE UNIVERSITY), KOLHAPUR,
KOLHAPUR – 416 006 (M.S.) INDIA**

November 2021

CERTIFICATE

This is to certify that the thesis entitled “**Role of superparamagnetic iron oxide nanoparticles as a radiotherapy sensitizer in colorectal cancer**” which is being submitted herewith for the Degree of Doctor of Philosophy in Medical Physics of D. Y. Patil Education Society (Deemed To Be University) Kolhapur is the result of original work completed by **Ms. Madhuri Anuje** under my supervision and guidance and to the best of my knowledge and belief the work embodied in this thesis has not formed earlier the basis for the award of any Degree or similar title of this or any University or examining body.

Place: Kolhapur

Date:

Research Guide

Asst.Prof.(Dr). P.N.Pawaskar

M.Sc. Ph.D

Department of Medical Physics,

D.Y.Patil Education Society

(Deemed to be university

Kolhapur) - 416006

Prof and Head

D.Y.Patil Education Society

(Deemed to be university

Kolhapur)- 416006

DECLARATION

I hereby declare that the thesis entitled, “**Role of superparamagnetic iron oxide nanoparticles as a radiotherapy sensitizer in colorectal cancer**” completed and written by me has not previously formed the basis for the Degree or Diploma or other similar title of this or any other University or examining body.

Place: Kolhapur

Date:

Research Student

Madhuri Anuje

**D. Y. Patil Education Society (Deemed
to be university Kolhapur) -416006**

ACKNOWLEDGEMENT

First and foremost, I have to thank my research supervisor, Dr. P. N. Pawaskar for her inspired guidance, valuable suggestions, insightful criticism, great patience and constant encouragement and support throughout the entire period of my research. Without her assistance and dedicated involvement in every step throughout the process, this dissertation would have never been accomplished. I would like to thank you very much for your support and understanding over these past six years.

I would like to express my deep and sincere gratitude to Dr. V. V. Bhosale, Registrar, D. Y. Patil Education Society (Deemed to Be University) Kolhapur to encourage me in my hard times. He always supported and inspired me to follow my dreams throughout my struggles.

I would like to heartily acknowledge Dr. C. D. Lokhande, Research Director & professor and other staff members. I would like to say thanks Dr. V. M. Khot, Dr. N. D. Thorat, Dr Aravind Gulbake and Dr. Jagruti Meshram, for their valuable discussion regarding the manuscripts of related research articles. I am also thankful to Namrata shinde, Pooja nimbalkar, Puja patil, Ramdas and the entire faculty members of Centre for Interdisciplinary Research for their unwavering support during the time I spent at the University.

I would also like to show gratitude to Dr. S. P. Sardeshmukh, Director, Dr. Aravind Kulkarni and Dr. Jagdish Shinde, Radiation Oncologists, Dr. Vineeta Deshmukh, Deputy Director, Dr. Shweta Gujar, Assistant Director and Dr. Sandeep Chavan, Integrated cancer treatment and research centre, wagholi, pune, for their continuous support and encouragement throughout my research time.

I convey special thanks to my team mate and my friend, Rita Mendonca, Mahavir Thakur, Papiya Debnath and Khushnuma Kainat who has always been there to help me and to support morally, and special thanks to Ajay Sivan to give scientific suggestions about the task.

Most importantly, none of this could have happened without my husband Mr. Pavan Kawade for providing me with unfailing support and continuous assistance throughout my years of study and through the process of researching and writing this thesis. Additionally I owe a tremendous thanks to my uncle Mr. Raghunath Pawar for standing behind me to start my career in my struggling time. I express my deep sense of love to my daughter Niharika and my niece Moksha, whose smile always freshened my mind. I must express my very profound gratitude to my parents, my mother 'Surekha' and father 'Pratap', my sisters, Pratiksha, Pratibha and my aunt Trishala. I would also like to say thanks to my in laws family, Raovso Kawade, Appaso Kawade, Subhash Kawade, Sujata kawade, Asmita Kawade, Bhushan kawade and Priyanka kawade for their understanding nature towards my study. This dissertation stands as a testament to your unconditional love and encouragement.



Madhuri Anuje Kawade

TABLE OF CONTENTS

1	INTRODUCTION TO RADIOTHERAPY	1-39
1.1	Introduction- History of Radiotherapy	1
1.2	Principle of Radiotherapy	5
1.2.1	Direct action	5
1.2.2	Indirect action	7
1.3	Classification of Radiotherapy	9
1.3.1	Photon based radiotherapy	9
1.3.1.1	Radiotherapy types according to aim	10
1.3.1.2	Radiotherapy types according to timing	11
1.3.1.3	Radiotherapy types according to mode	11
1.3.2	Particulate radiotherapy	12
1.4	Radiotherapy Procedure	13
1.4.1	Immobilization	16
1.4.2	Patient positioning	17
1.4.3	Tumour localization	17
1.4.4	CT based treatment planning	21
1.4.4.1	Image manipulation and image fusion	22
1.4.4.2	Defining the volume, growing tools	22
1.4.4.3	Beam's eye view	22
1.4.4.4	Margins	23
1.4.4.5	Plan verification and evaluation	24
1.4.5	Setup and treatment	27
1.4.6	Quality assurance	27
1.5	Technological Advances in Treatment Delivery	30
1.5.1	Conformal three-dimensional radiation therapy (3DCRT)	31

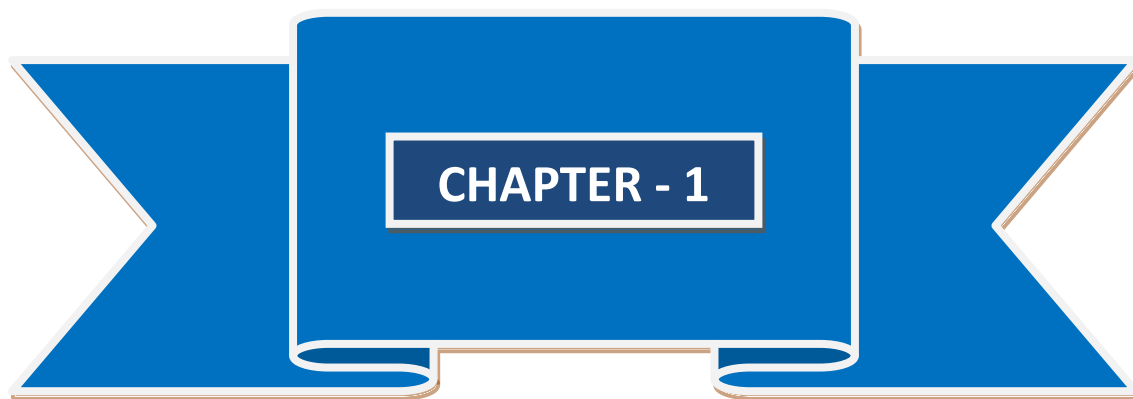
1.5.2	<i>Intensity-modulated radiation therapy (IMRT)</i>	32
1.5.3	<i>Image-guided radiotherapy (IGRT)</i>	33
1.5.4	<i>Stereotactic radiation therapy (SRT)</i>	34
1.5.5	<i>Tomotherapy</i>	34
1.6	<i>Nanoparticles in Radiation Therapy</i>	35
	<i>References</i>	37
2	MAGNETIC NANOPARTICLES	40-68
2.1	<i>Nanotechnology</i>	40
2.2	<i>Physicochemical Properties of Magnetic Nanoparticles</i>	45
2.2.1	<i>Size</i>	45
2.2.2	<i>Shape</i>	46
2.2.3	<i>Nanoparticle charge</i>	48
2.2.4	<i>Solution stability and zeta potential</i>	49
2.2.5	<i>Coating</i>	49
2.3	<i>Magnetic Properties of Nanoparticles</i>	50
2.3.1	<i>Diamagnetic</i>	50
2.3.2	<i>Paramagnetic</i>	51
2.3.3	<i>Ferromagnetic</i>	51
2.4	<i>Therapeutic Uses of Magnetic Nanoparticles</i>	54
2.4.1	<i>Magnetic resonance imaging</i>	54
2.4.2	<i>Magnetic hyperthermia</i>	57
2.4.3	<i>MNPs and targeted drug delivery</i>	59
2.5	<i>Magnetic Nanoparticles as a Radiosensitizer</i>	62
	<i>References</i>	63
3	NANOPARTICLE BASED RADIOSENSITIZERS	69-122
3.1	<i>Introduction to Radiosensitizer</i>	69
3.1.1	<i>Classification of radiosensitizers</i>	70

3.2	<i>Introduction to Nano-radiosensitizer</i>	77
3.3	<i>Classification of Nanoparticle Mediated Radiosensitizers</i>	90
3.3.1	<i>Metal based radiosensitizers</i>	90
3.3.2	<i>Quantum dots in radiosensitization</i>	93
3.3.3	<i>Nonmetal based radiosensitizers</i>	93
3.3.4	<i>Superparamagnetic iron oxide nanoparticles (SPION) as a radiosensitizer</i>	94
3.4	<i>Different Methods for Assessment of Radiosensitization</i>	97
3.4.1	<i>Different approaches for assessment of nano-radiosensitization from cell survival data</i>	97
3.4.1.1	<i>Quantification of radiosensitization by mean inactivation dose (MID)</i>	100
3.4.1.2	<i>Quantification of radiosensitization in terms of alpha and beta parameters</i>	100
3.4.1.3	<i>Quantification of radiosensitization in terms of dose modifying ratio (DMRx%)</i>	101
3.4.1.4	<i>Radiation enhancement factor (REF) using the multi- target model</i>	102
3.4.1.5	<i>Radiation enhancement ratio (RER/SER)</i>	103
3.4.2	<i>Monte Carlo in radiosensitization studies</i>	104
	<i>References</i>	106
4	<i>CHARACTERIZATION AND CYTOTOXICITY STUDY</i>	123 -162
4.1	<i>Introduction</i>	123
4.2	<i>Synthesis of Magnetic Nanoparticles (MNPs) by Chemical Co-Precipitation</i>	126
4.2.1	<i>Steps involved during precipitation</i>	129
4.2.1.1	<i>Liquid mixing/supersaturation</i>	130

4.2.1.2	<i>Nucleation and growth</i>	131
4.2.1.3	<i>Aggregation of the primary particles</i>	132
4.2.2	<i>Factors influencing co-precipitation process</i>	133
4.2.2.1	<i>Effect of raw materials</i>	133
4.2.2.2	<i>Effect of pH</i>	134
4.2.2.3	<i>Effect of temperature</i>	135
4.2.2.4	<i>Effect of concentration</i>	135
4.2.2.5	<i>Effect of solvent</i>	135
4.2.2.6	<i>Effect of additives</i>	136
4.2.2.7	<i>Stirring velocity</i>	136
4.3	<i>Surface Functionalization</i>	136
4.4	<i>Characterization of Magnetic Nanoparticles</i>	138
4.4.1	<i>Structural and phase analysis</i>	139
4.4.1.1	<i>XRD</i>	139
4.4.1.2	<i>FTIR</i>	142
4.4.1.3	<i>TGA</i>	144
4.4.2	<i>Morphological study</i>	146
4.4.2.1	<i>TEM</i>	146
4.4.3	<i>Colloidal stability study</i>	148
4.4.3.1	<i>Zeta potential</i>	148
4.4.3.2	<i>DLS</i>	150
4.4.4	<i>Magnetic characterizations</i>	152
4.4.4.1	<i>VSM</i>	152
4.5	<i>Biocompatibility Study: Cytotoxicity Assays</i>	153
	<i>References</i>	158


5	PEG COATED SPION'S RADIOSENSITIZER EVALUATION	163-185
5.1	Introduction	163
5.2	Experimental	164
5.2.1	Synthesis and characterization of PEG coated and uncoated Fe_3O_4 nanoparticles	164
5.2.2	In Vitro cytotoxicity study of PEG coated and uncoated Fe_3O_4 nanoparticles	167
5.3	Results and Discussion	168
5.3.1	Structural analysis	168
5.3.1.1	X-ray diffraction (X-RD)	168
5.3.1.2	Fourier transform infrared spectrometry (FTIR)	171
5.3.1.3	Thermal gravimetric analysis (TGA)	173
5.3.2	Colloidal stability study	174
5.3.2.1	Zeta potential measurements	174
5.3.2.2	Dynamic light scattering (DLS)	174
5.3.3	Morphological study	175
5.3.3.1	High resolution- transmission electron microscopy (HR- TEM)	175
5.3.4	Magnetization study (VSM)	177
5.4	Cytotoxicity Study (MTT assay)	178
5.5	Conclusion	183
	References	184
6	PEG COATED SPION AS A RADIOSENSITIZER	186-210
6.1	Introduction	186
6.2	Methods and Materials	188
6.2.1	Preparation of bolus phantom	190
6.2.2	CT simulation	191

6.2.3	<i>Irradiation planning</i>	191
6.2.4	<i>Cell culture well plates for radiation exposure</i>	193
6.2.5	<i>Irradiation setup</i>	194
6.2.6	<i>Analysis of cell survival using MTT assay</i>	196
6.2.7	<i>Sensitization enhancement ratio (SER)</i>	196
6.3	<i>Results</i>	197
6.3.1	<i>Cytotoxicity evaluation of PEG coated SPIONs</i>	197
6.3.2	<i>Radiosensitization enhancement by PEG coated SPIONs</i>	198
6.4	<i>Discussion</i>	201
6.5	<i>Conclusion</i>	206
	<i>References</i>	208
7	<i>SUMMARY AND CONCLUSION</i>	211-214
7.1	<i>Introduction</i>	211
7.2	<i>Major Conclusions</i>	213
7.3	<i>Future Scopes</i>	214



INTRODUCTION TO RADIOTHERAPY

The part of this chapter has published in an IOP book



External Field and Radiation Stimulated Breast Cancer Nanotheranostics


CHAPTER 7

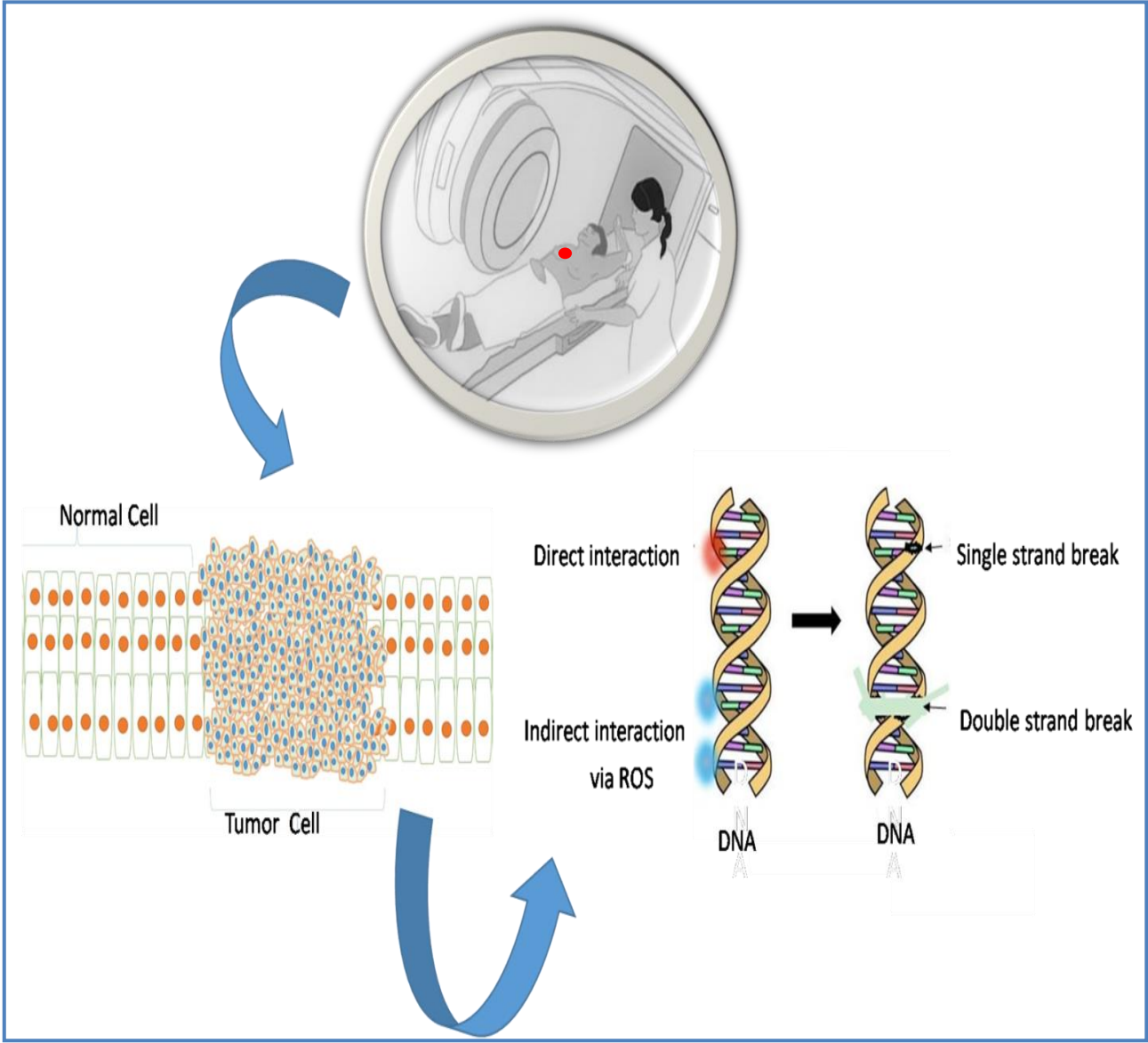
Radiotherapy and breast cancer nanomedicine

Madhuri Anuje, Joanna Bauer and Nanasaheb D Thorat

Published September 2019 • Copyright © IOP Publishing Ltd 2019

Pages 7-1 to 7-78







1.1 Introduction- History of Radiotherapy

Cancer is a major public health problem worldwide; it accounts for a quarter of all deaths and surpasses heart disease as the leading cause of death for people under the age of 85 [1]. Increasing morbidity and fatality due to cancer negatively affects the financial and overall growth of the nation [2]. Cancer can start almost anywhere in the human body, which is made up of trillions of cells. Normally, when the body needs it, human cells grow and divide to form new cells. When cells grow old or become damaged, they die, and new cells take their place. However old or damaged cells which should die, survive. These extra cells can divide and grow without stopping which is called tumors. Management of cancer is a rising concern in an ageing population and is increasingly important in developing countries [3]. Cancer can be treated with various treatment methods including chemotherapy, radiation therapy, immunotherapy, surgery etc. Out of which the most effective one is radiotherapy for the treatment of primary and metastatic tumors, microscopic tumor spread as well as regional lymph nodes [2].

On November 8, 1895, while studying cathode rays, William C. Roentgen discovered x-rays. Roentgen noticed that when he shielded the tube with heavy black cardboard, the green fluorescent light caused a platino-barium screen nine feet away to glow - too far away to be reacting to the cathode rays. He noticed that another type of radiation could produce fluorescence, blacken a photographic plate, ionize a gas and penetrate opaque substances. This unknown radiation he named as X-rays. Further experiments revealed that this new type of ray was capable of passing through most substances, including the soft tissues of the body, but left bones and metals visible. In actuality, his wife Bertha's left hand was one of the first x-ray photographs ever created [4]. In 1896, after learning about Roentgen's finding, Becquerel began looking for a connection between the



phosphorescence he had already been investigating and the newly discovered x-rays. Becquerel thought that the phosphorescent uranium salts he had been studying might absorb sunlight and reemit it as x-ray. Using a method similar to that of Roentgen, Becquerel surrounded several photographic plates with black paper and fluorescent salts like uranium. Becquerel intended to place the concealed photographic paper in the sunlight believing that the uranium absorbed the Sun's energy and then emitted it. Unfortunately, he had to delay his experiment because the skies over Paris were overcast. He placed the wrapped plates into a dark desk drawer. After a few days Becquerel returned to his experiment unwrapping the photographic paper and developing it, expecting only a light imprint from the salts. Instead, the salts left very distinct outlines in the photographic paper suggesting that the salts, regardless of lacking an energy source, continually fluoresced. What Becquerel had discovered was radioactivity [5].

Becquerel's doctoral student Marie Curie In 1898, began her doctoral study of Becquerel's rays. She and her spouse, Pierre, showed that intensity of radiation increases with increase in the amount of uranium in a substance (i.e., directly proportional) and Becquerel rays could be measured using ionizing techniques. Soon she discovered two new radioactive elements, which were named polonium, after her native land of Poland, and radium, because it radiates. These two new elements filled holes in the periodic table and displayed much higher levels of radioactivity than uranium. Over four years, working under poor conditions and spending their own funds, the Curies processed more than a ton of uranium ore to isolate a mere gram of radium salt [5].



After the discovery of x-rays Emil Grubbe observed peeling of his hands on exposure to x-rays. In 1896, He assembled his x-ray machine in Chicago and treated a woman named Rose Lee for breast cancer recurrence. Grubbe has taught approximately 7000 doctors how to use x-rays for medicinal purposes (radiotherapy) [6].

Scientists studied details about the action of radiation on cell survival, its nature and the relationship between time and dose of radiation. By the 1920s, those physicians understood that a fractionated dose is better than a singular large dose in order to reduce normal tissue toxicity. This is one of the most important underlying principles in radiation therapy, known as fractionation. Thereafter, in radiation oncology fractionation lies at the heart of many treatment programs [7]. In 1928, to address the question of radioprotection, the International Commission on Radiological Protection (ICRP) was created [8]. Introduction of an ionizing chamber in 1932, allowed physicians to measure the radiation dose in Rontgen unit [9].

From 1930 to 1950, there was continual scientific advancement in treating patients with deep tumours. The use of radium-based interstitial irradiation (brachytherapy) and the invention of super voltage X-ray tubes capable of delivering energy from 50 kV to 200 kV marked this era (also known as orthovoltage era). The early X-ray devices' inability to create high-energy, deeply penetrating beams was a significant drawback. Deep-seated cancers were so difficult to cure without causing severe skin reactions. Many early proponents of radiation therapy depended on the near proximity or even insertion of radioactive sources within the tumour, a procedure known as brachytherapy. When Pierre Curie suggested to Danlos that a radioactive source may be put into a tumour, this



technique was born. The tumour shrank as a result of the radiation treatment. Ralston Patterson, a radiologist with a deep interest in newer discoveries in the profession, was named Director of the Holt Radium Institute in 1931 and went on to establish a world-renowned center for the treatment of cancer using radiation. Following initial interest in brachytherapy in Europe and the United States, its use dropped in the mid-twentieth century due to concerns about operator radiation exposure from the manual administration of radioactive sources. The introduction of remote after loading systems in the 1950s and 1960s, which allowed radiation to be supplied from a shielded safe, lowered the risk of unnecessary radiation exposure to the operator and patients. Secondly, electron beam treatment is introduced as a potential therapeutic option for treating superficial cancers since it can deliver higher and variable energy [10].

Dr Harold E Johns, a Canadian medical physicist, requested the National Research Council (NRC) to develop Cobalt-60 isotopes for use in a prototype cobalt therapy unit in 1949. On October 27, 1951, a 43-year-old cervical cancer patient received the world's first Cobalt-60 radiation treatment at Victoria Hospital. This was a significant step forward in the fight against cancer. Despite advancements in radiation therapy technology, the Cobalt-60 remains the primary radiotherapy machine in use around the world. It is widely used in developing countries due to its low cost, reliability, and convenience of use. The emergence of novel proton beam delivery devices marked the 1970s and 1980s. Even though computer-assisted proton accelerators were initially used in 1954, it wasn't until the late 1970s that they were successfully used to treat a distinct type of tumour. The main benefit of using ion beams is their controllability, which makes them a better tool for cancer treatment and difficult-to-treat benign conditions [11].



The emergence of high-energy (megavoltage) therapy machines known as Linear Accelerators or LINACS has been an exciting breakthrough. These machines were capable of generating high-energy, deeply penetrating beams, allowing for the first time the treatment of malignancies deep within the body without causing major damage to the skin and other normal tissues. Several technological advances occurred in the field of radiation oncology in the following years. The radiation planning systems underwent a significant transformation with the introduction of computers and newer technological breakthroughs. 3D conformal radiotherapy, a type of radiation therapy in which the fields are tailored so that the radiation dose is largely delivered to the tumour while the surrounding tissues receive little to no radiation dose, was first introduced in the 1990s. Intensity-modulated radiation therapy (IMRT) is an advanced form of three-dimensional conformal radiation therapy (3D CRT). It varies the shape and intensity of radiation given to different sections of the treatment area using sophisticated software and hardware. Radiation therapy is currently undergoing yet another significant technological revolution, this time in the form of Image-Guided Radiation Therapy (IGRT) [12].

1.2 Principle of Radiotherapy

Radiotherapy mostly works by killing or stopping the division of malignant cells. This can be the result of direct interaction or indirect interaction as shown in Figure 1.1.

1.2.1 Direct action

Direct interaction of atoms involves breaking of single strand or double strand (Fig. 1.1) as a result of energy absorption by photoelectric or Compton interaction. DNA strand breaks due to removal of electrons from molecules by sufficient

energy absorption which is called ionization. The cell can usually repair a single broken strand, but two damaged strands nearly always result in cell death [12, 13].

When normal cell DNA is damaged by radiation at doses frequently used in radiotherapy, the protein p53 stops the cell cycle. After the DNA is repaired, the cell re-enters the cell cycle and continues to reproduce. Apoptosis, or programmed cell death, occurs when a cell's DNA cannot be repaired. When the materials used by DNA repair mechanisms are destroyed by high radiation dosages, repair is impossible, the cell loses its ability to proliferate and it dies [14].

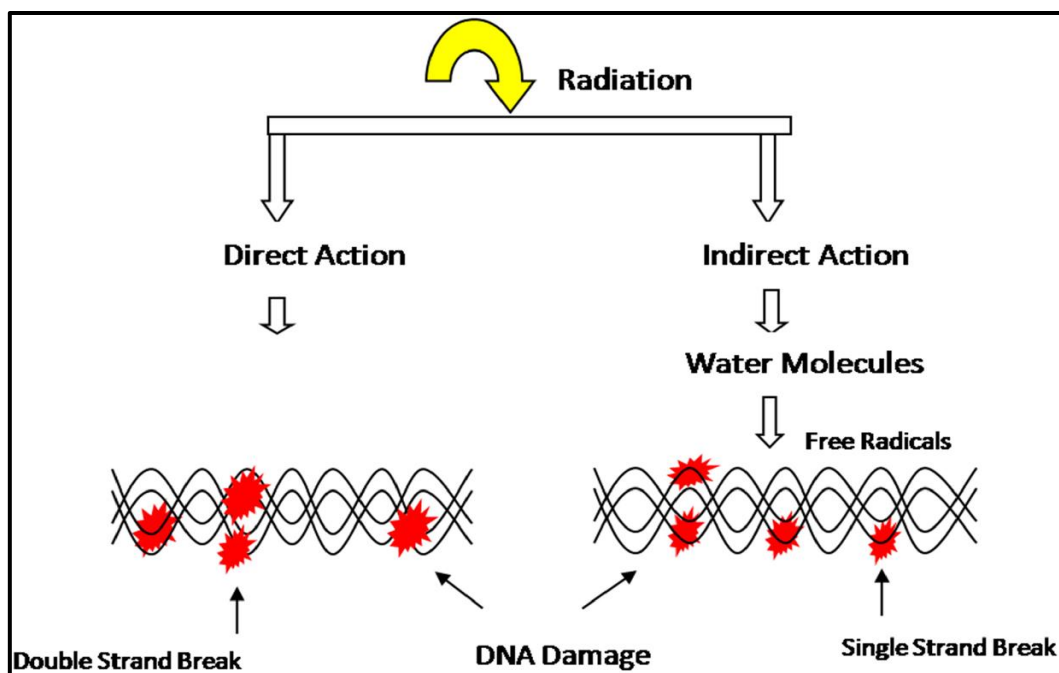


Figure 1.1 Interaction mechanism of radiation with matter

1.2.2 Indirect action

As illustrated in figure 1.2, the indirect effect of radiation on molecules includes the generation of free radicals as a result of radiation energy transfer as well as the resulting molecular damage caused by free radical interactions with DNA. Several studies have shown that the main pathway of DNA damage from both x-rays and gamma rays is through the production of water radicals, with free radicals and other reactive oxygen species (ROS) (e.g., OH^\bullet , NO^\bullet , H^\bullet , and H_2O_2) causing 70% of the damage and secondary electrons and direct fragmentation of the DNA causing 30% of the damage [13,14].

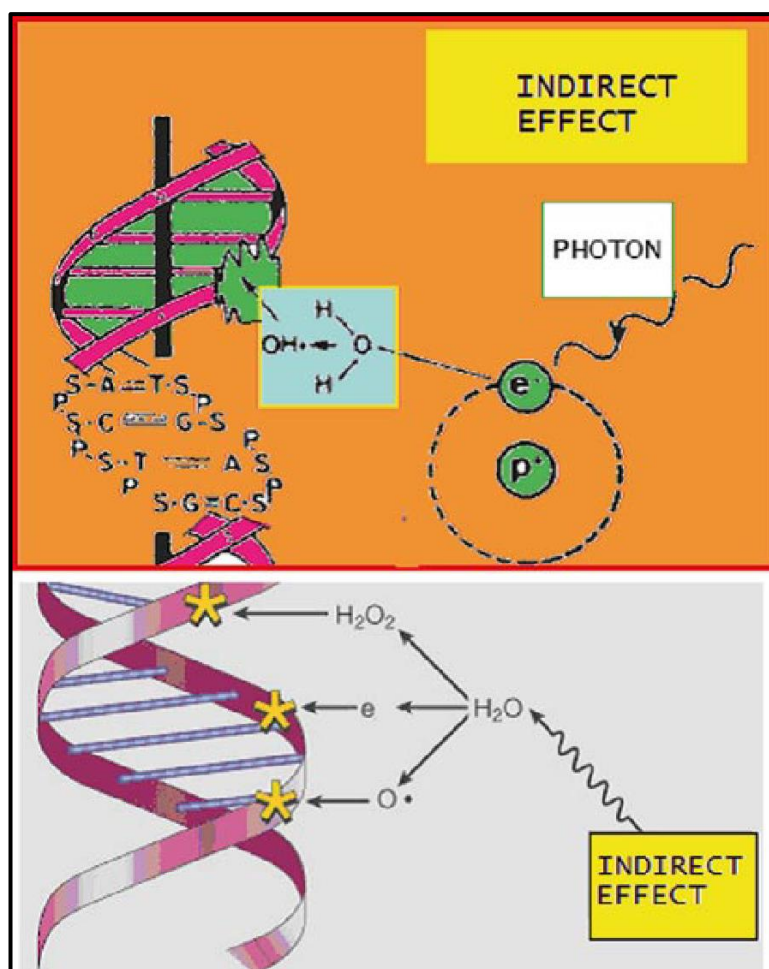


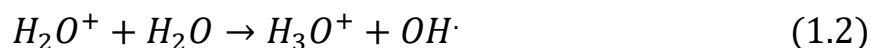
Figure 1.2 Indirect effect of radiation [14]



An atom or molecule with an unpaired orbital electron in the outer shell is known as a free radical. An orbital electron not only spins around its own axis but also rotates around the nucleus of an atom. The spin can be done in either a clockwise or counterclockwise direction. Spins are paired in an atom or molecule with an even number of electrons; that is, for every clockwise spinning electron, there is a counterclockwise spinning electron. This condition is linked to a high level of chemical stability. There is one electron in the outer orbit of an atom or molecule with an odd number of electrons for which there is no other electron with an opposing spin; this is an unpaired electron [13]. This condition is related to the high degree of chemical reactivity. Water makes up 80% of a cell's volume. Ionization happens when radiation interacts with water, as illustrated in equation 1.1.



H_2O^+ is an ion radical. An ion is an electrically charged atom or molecule that has lost one of its electrons. H_2O^+ is both an ion and a free radical since it is charged and has an unpaired electron. Because the main ion radicals have a very short lifetime, on the order of 10^{-10} s, they cannot travel from the cytoplasm to the nucleus, where the DNA is found. As indicated in equation 1.2, the ion radical interacts with another water molecule to generate the extremely reactive hydroxyl radical.





Because the hydroxyl radical has nine electrons, one of them is unpaired. It's a highly reactive free radical that can travel a short distance to reach a cell's most important target. Free radicals, for example, are expected to diffuse to DNA from within a cylinder with a diameter roughly twice that of the DNA double helix (4 nm). The hydroxyl radical is thought to be responsible for around two-thirds of the x-ray damage to DNA in mammalian cells. The damage caused to DNA by radiation can result in a range of various lesions, including base damage, single strand breaks (SSBs) or, less frequently, double strand breaks (DSBs) (Fig. 1.1). In most cases base damage and SSBs can be effectively repaired by cell repair mechanism whereas DSBs, especially when induced at high levels, are difficult to get successfully repaired and therefore more damaging to cells [13, 14].

1.3 Classification of Radiotherapy

On the basis of penetration power and ionization they are classified as photon and particulate based radiotherapy. Photon based radiotherapy is usually classified according to aim, timing and mode of delivery. Classification of radiotherapy depicted in figure 1.3.

1.3.1 Photon based radiotherapy

Photons carry less mass and no charge, so its penetration power is high. X-rays and gamma rays are used to treat various cancers. They are sparsely ionizing radiation and considered as low LET (linear energy transfer) electromagnetic radiation. They have exponential dose deposition with tissue depth, therefore fraction of total dose delivered to healthy tissue lying front of and behind the target. Amount of radiation dose received is being limited by sparing normal tissue in different angles. X-rays are produced by a device that excites electrons (e.g., cathode ray tubes and linear accelerators). In the x-ray therapy, modern

high-energy linear accelerators used to produce photon beams in the range of 4 – 25 MV, while gamma rays originate from the disintegration of radioactive materials (e.g., cobalt-60, radium and cesium) [12].

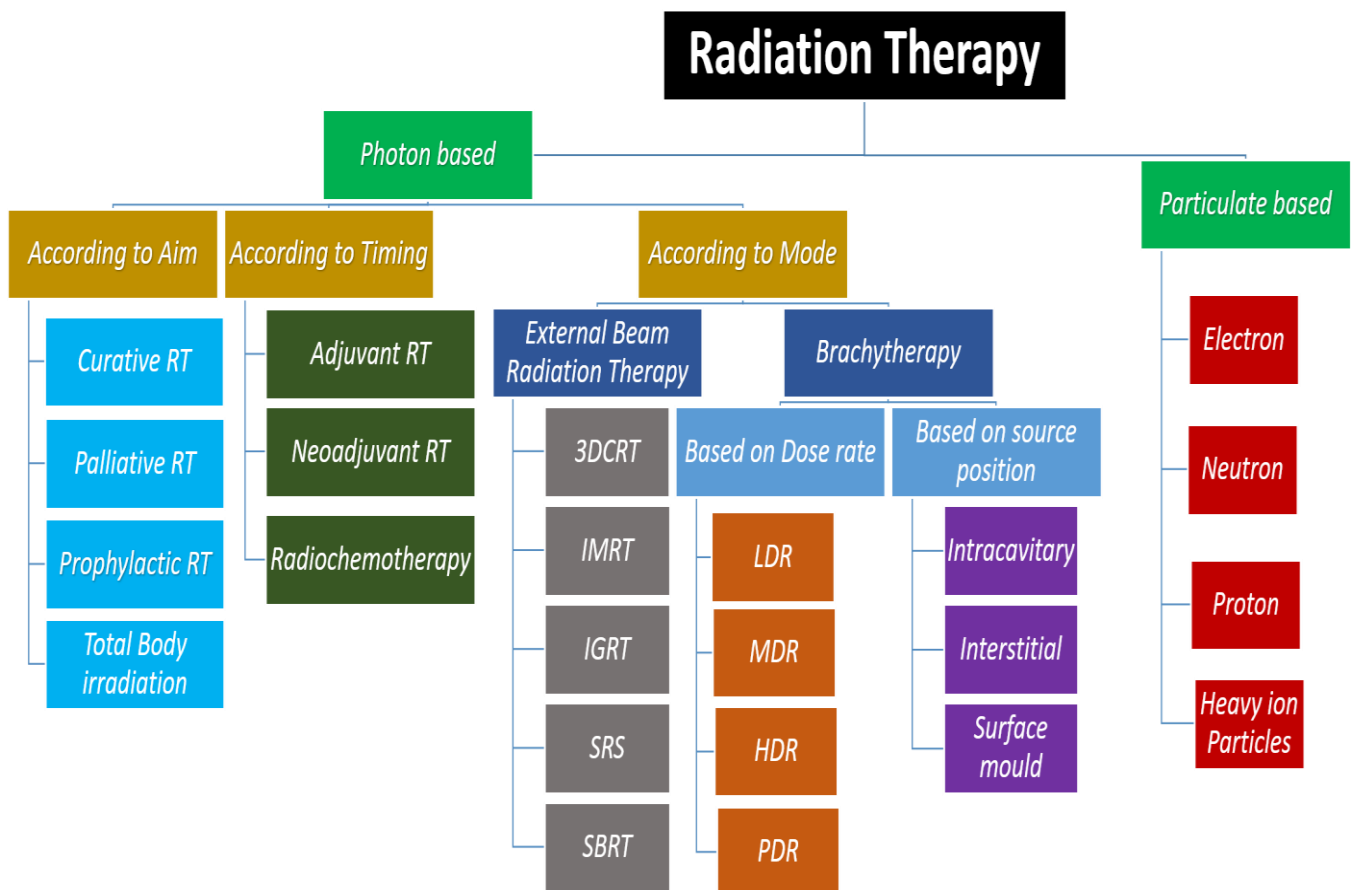


Figure 1.3 Classification of Radiotherapy

1.3.1.1 Radiotherapy types according to aim

- Curative radiotherapy - Here radiation therapy is only intended to cure. For example, it's been applicable in cases of nasopharyngeal cancer, early-stage Hodgkin's lymphoma, early glottic tumors and certain skin malignancies [14].



- Palliative radiotherapy - This is the treatment of cancer symptoms with palliative radiation doses. Applicable in cases of bone metastases, brain metastases, superior vena cava syndrome etc. [14].
- Prophylactic (preventive) radiotherapy - Such kind of application of radiotherapy to prevent possible metastases as well as recurrences. Whole-brain irradiation, for example, is used to treat small cell lung cancer and acute lymphoblastic leukemia [14].
- Total body irradiation (TBI) - In this case, radiation is used to ablate bone marrow in order to inhibit the immune system, destroy leukemic cells and clear space for transplant cells during transplantation of bone marrow [14].

1.3.1.2 Radiotherapy types according to timing

- Adjuvant radiotherapy - It is a kind of treatment in which radiotherapy administered post treatment like surgery, chemotherapy etc. e.g. If radiation delivered post-surgery it is called as postoperative radiotherapy [12,14].
- Neoadjuvant radiotherapy - Radiotherapy administered prior to any other type of treatment modality. e.g., If given before surgery, it is referred to as preoperative radiotherapy [12, 14].
- Radio-chemotherapy - Radiotherapy given concurrently with chemotherapy [12,14].

1.3.1.3 Radiotherapy types according to mode

- External radiotherapy (teletherapy) - External radiotherapy is the use of radiation from outside the body to destroy cancer cells. Teletherapy involves directing high energy radiations from distance usually source to surface distance (SSD) 80 cm for Telecobalt and 100 cm for LINAC.



External-beam therapy is usually delivered by different techniques such as IMRT, IGRT, SBRT, EBRT etc. [12].

- **Brachytherapy (sealed-source radiotherapy)** – Brachytherapy is administered by inserting either permanent or temporary radiation sources into body cavities [12]. In case of internal beam therapy (brachytherapy) radiation is usually given within or near the tumor inside the body by using a brachytherapy machine. It involves radioactive material placed directly into the body. The tumor receives a relatively high dose of radiation, while healthy surrounding tissue receives very little radiation. In some types of cancer these implants may be left in the body permanently. Based on dose rate it is classified as LDR, MDR, HDR and PDR. Two main forms of brachytherapy are intracavitary treatment and interstitial treatment. With intracavitary treatment, the radioactive sources are put into a space near where the tumor is located, such as the cervix and vagina. With interstitial treatment, the radioactive sources are put directly into the tissues, such as the prostate and breast. Another type of brachytherapy is surface mold brachytherapy, which can be used externally to treat some skin cancers [12].

1.3.2 Particulate radiotherapy

Electrons having less penetration power have been widely used for superficial treatments since the early 1950's. In radiotherapy, 6-20 MeV energy range is commonly used for treatment. Electron beams have a characteristically sharp dose drop off beyond the tumor; this characteristic is exploited to treat superficial tumors (up to 5 cm deep). The key applications are (a) administering boost dose to nodes, (b) head and neck cancer treatment, (c) skin and lip cancer treatment, and (d) irradiation of chest wall in case of breast cancer treatment [15].



External-beam radiotherapy carried out using heavier particles such as neutrons, protons and heavy ions (helium carbon). The proton is a newly introduced particle for the treatment of cancer. Its dose distribution with depth is unique. A proton beam deposits a dose with depth gradually in increasing order, at the end of the range of the particle there is a sharp increase in dose which is called Bragg peak [15]. Due to this property of protons or heavy ions there is maximum destructive dose deposition at the tumor site with less radiation to healthy tissue underlying. These are especially useful in pediatric cancers and adult tumors that are situated near critical structures like the spinal cord or the skull base, where the preservation of normal tissue as much possible is critical [16]. Protons can be generated using cyclotrons and synchrotrons while heavy ions are produced using synchro cyclotrons and synchrotrons. Inside a neutron generator, once proton beams are deviated to a target, neutron beams are formed. They have a higher LET than photons and can cause greater DNA damage. The difficulties in producing neutron particles, as well as the building of such treatment facilities, have been the key constraints [16].

1.4 Radiotherapy Procedure

Radiotherapy is performed by a group comprising radiation oncologist, radiation physicist, radiotherapist, social workers etc. [14]. The success of radiation therapy depends heavily on appropriate technological equipment. After a multidisciplinary meeting has taken the decision to use radiotherapy, the radiation oncologist must evaluate reports relating to patient history, physical examinations and especially pathological reports, nuclear imaging reports as well as x-ray reports and add details of these to a patient's chart. After registration, including a brief summary at the bottom of the chart can be beneficial. If there are obvious physical indications, they should be imaged and put to the chart because they

might be useful for assessing therapy success or failure. Such images may also be used for academic studies with the patient's consent.

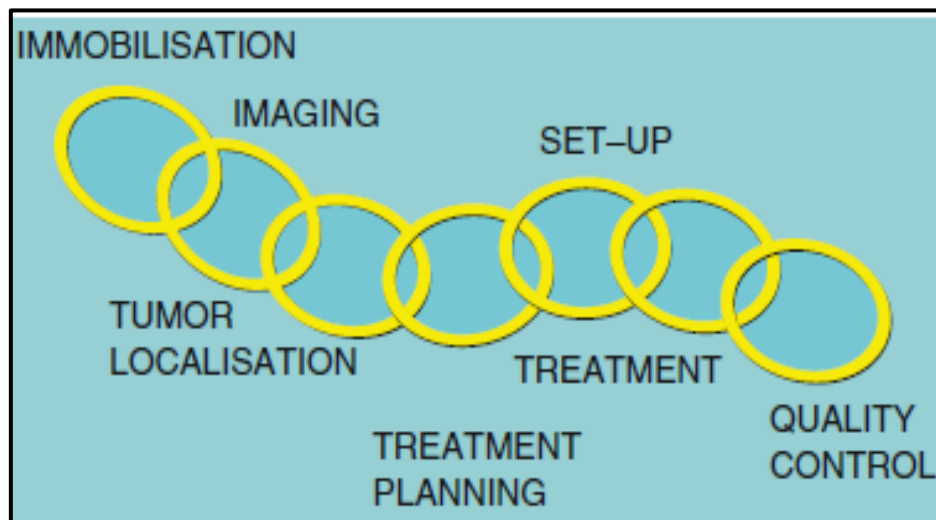


Figure 1.4 Steps involved in radiotherapy [14]

Just after clinical exams, the patient should be notified about his/her illness and therapy according to his/her education. The patient should also be told about the processes and the duration of the procedure for radiotherapy, as well as acute and late effects, start times and preventive measures. The patient and physician should then sign the consent form and provide the patient with one copy and the other with the patient chart. The first phase is then scheduled in radiation therapy – simulation (immobilization, imaging, and tumor localization) [14]. Schematic 1.4 represents steps involved in radiotherapy.

Simulation

Simulation is actually a field determination for radiotherapy by utilizing an x-ray diagnostic machine which is identical to the real teletherapy machine. The patient

is immobilized prior to simulation, and the tumour is located using a direct X-ray scopy machine or serial CT slices.

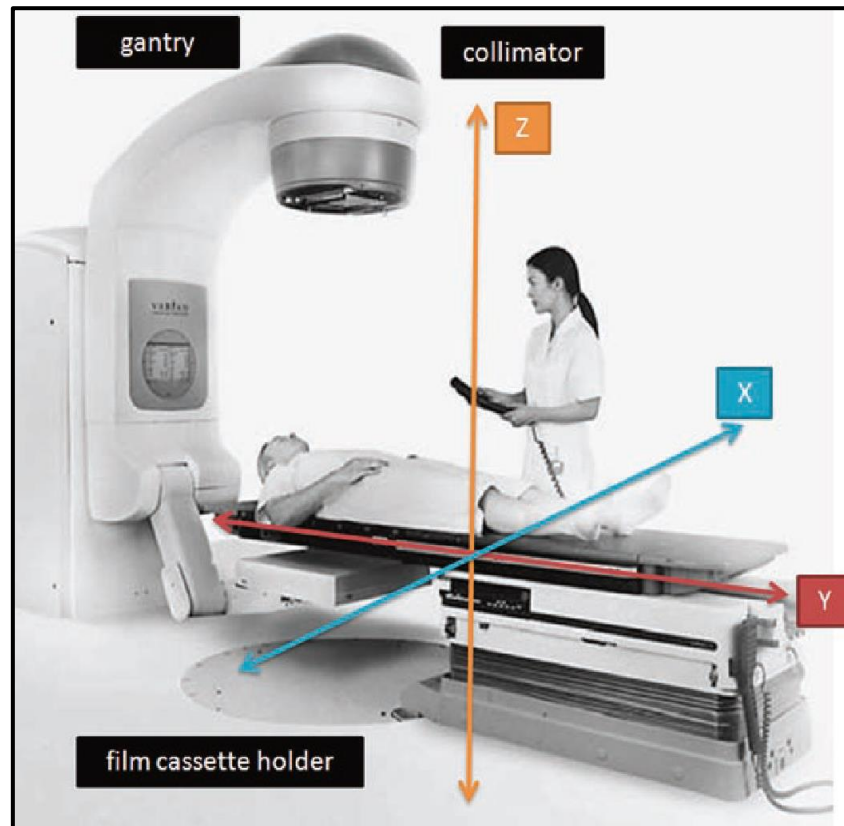


Figure 1.5 A conventional simulator [19]

CT, SPECT, PET, PET-CT or MRI can be used for the simulation. Because it is done directly with the patient, the simulation performed by a traditional simulator is a real-time simulation procedure (Fig.1.5). However, CT, SPECT, PET, PET-CT or MRI simulation is a virtual simulation as the tumour is digitally located [14, 18].

1.4.1 Immobilization

During treatment therapy, the patient should be immobilized. Body movement causes changes in the region of therapy and increases adverse effects, decreasing the success of treatment. The patient should always be positioned in an easily reproducible and convenient manner which will not hinder the radiation irradiation process [14]. Patient immobilization in the treatment position significantly reduces setup errors and will result in a successful treatment delivery. Overdose to nearby critical structure or Under dose to the target can happen due to setup errors. Depending on the treatment site, several immobilization devices are employed. The thermoplastic mask is the most commonly used device for example face masks as shown in figure 1.6.

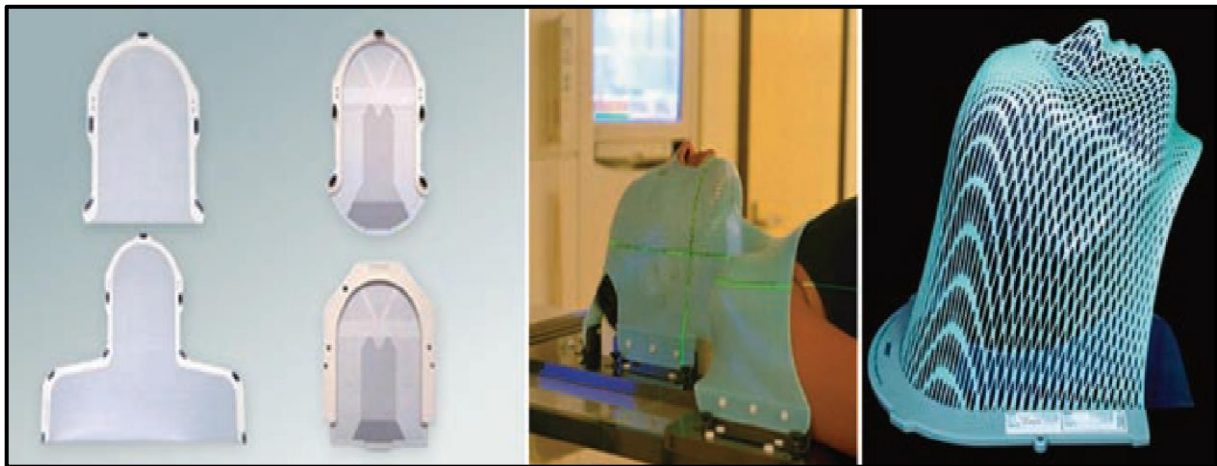


Figure 1.6 Thermoplastic masks [14]

Such mask should be rigid and there will be minimal space between the mask and the patient's body surface. Every day the mask should be examined if it is tight or loose then it will be reworked if necessary. Effective systems must be tolerated and practiced by patients with minimum set up times [14, 18].



1.4.2 Patient positioning

The position of the patient should be carefully chosen and should not vary from planning to treatment. The patient should be stable, relaxed and pleasant throughout treatment as required for ideal for dosimetry. The opening size of the scanners or position of the therapeutic unit head during treatment can put a further limit on the posture of the patient [18]. Both the simulation film and the patient's chart should contain records of the treatment position, like hands on side/hands up or prone/ supine etc. The gantry is then adjusted at distance of source to axis (SAD) of the treatment machine prior to simulation. The required SSD value (typically 80–100 cm) is attained when the patient is positioned on the couch by altering the height of the couch. Last but not least, the field of irradiation is calculated by using the method chosen (Fixed SSD or SAD) [14].

1.4.3 Tumor localization

The patient is in the required position on the simulator couch. The mask, T-arms, knee support, breast board or any similar immobilizing device are accurately placed. The likely fields of radiotherapy are assessed and SSDs calculation carried out based on the thickness of the patient. The simulator software is arranged with intermittent X-ray scopy for field size, gantry angles and collimator angles. Every drain site, palpable mass and scars were marked by pliable wires; in lateral areas of epicanthus, lead markers should be placed for irradiation of the head and neck. During the simulation procedure, these markings are easily seen. Where necessary, IV or oral contrast can be used. Consequently, contrast materials and drugs (e.g., atropine, adrenaline) must be prescribed before simulation; in the simulators' room, they are required for use.

- In gastrointestinal irradiation, an oral solution with barium is commonly used.



- In the imaging of kidneys and bladders the nonionic radiopaque materials are used
- In the pelvic region it is feasible to use radio-opaque rectal and vaginal application or contrast material tamponades.

Treatment and block areas are marked on the patient's skin or mask after the radiation fields have been determined. After that, radiographs are taken in simulations, and protected areas on the film are marked. Focalized blocks will then be made in the block-cutting room for the protected area. The patient is sent home because the manufacturing of blocks is a long procedure. In case of no block preparation or use of standard blocks, the patient can be treated on the same day by sending his/her chart to the physics room to calculate dose. If no blocking unit exists, protected areas are measured by cables and checked in the simulation film. The use of standard blocks saves these areas. The treatment chart should record patient data, other disease-related data and all simulation related parameters. Graphical presentation of the treatment field and date should be mentioned on the treatment chart which will be beneficial for irradiation in future [14,15].

CT Simulation

The mould will be produced for patients who are receiving conformal radiation therapy on the simulation day with a CT, in presence of the medical physicist and radiation oncologist (Fig.1.7a). The patient is forwarded to the nurse for an IV route, if an intravenous contrast material is necessary before CT simulation. The patient is then positioned on the couch of the CT machine with a mask and if necessary, on the CT-couch, the support for the knee, the alpha cradle or any similar device included. Lasers are placed in the midline by region of interest



(ROI). Radio-opaque markers located across laser sections are used to identify reference points (Fig 1.7 b). For every region of the body, reference points are predetermined. There are three points for reference, one craniocaudal and the others on the left and right side. The nurse provides contrast material intravenously if necessary. For any possible anaphylactic reactions, adequate measures should be taken. The CT technician shall make adjustments, if necessary, in the CT room.

Radiation oncologist determines the ROI (which includes serial CT slices) and the thickness of the slices. Following the verification of the area of interest, serial slices are taken. Online networks like a Picture Archive and Communication System (PACS) or Digital Imaging and Medicine Communications (DICOM) are used to send these sections to the treatment planning room. After the completion of CT, the patient should rest at least twenty minutes for any possible adverse reactions [14,15].

All reference points should be tattooed permanently on the body in case of without mask treatment. After transferring the CT slices to a network, a virtual digital simulation is carried out. The CT sections transferred to the Treatment planning software using the above-mentioned network. The radiation oncologist then contours the acquired CT slices using dedicated software which automatically delineates contours of the external body. Then contouring of Gross Tumor Volume (GTV), Clinical Target Volume (CTV), Planning Target Volume (PTV) and organs at-risk (OAR) performed by radiation oncologist [14].

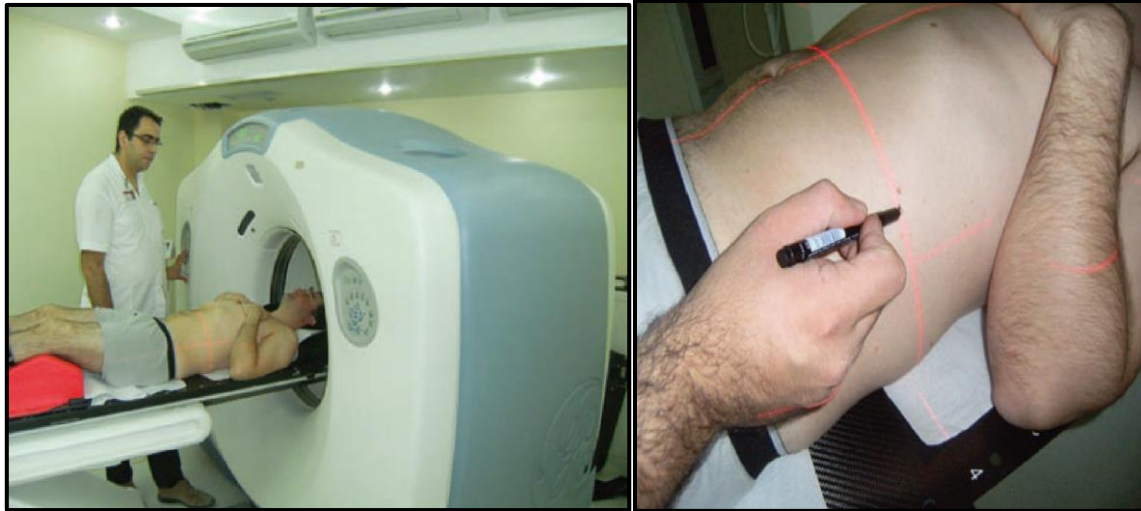


Figure 1.7 a) Patient on a CT couch for simulation b) Determination of reference points [14]

Volume definitions

Precise treatment depends on the definition of volumes. Two documents of the International Commission on Radiation Units and Measurement (ICRU) in detail define the parameters for treatment volume definition. These reports are 50 and 62 "Specifications of Photon Beam Therapy, Recording and Reporting" [20]. A transcript of the definitions is provided below:

Gross tumor volume (GTV) - GTV is the extent and location of the malignant growth which is palpable, visible or demonstrable.

Clinical target volume (CTV) - CTV is the volume of tissue containing GTV and/or microscopic subclinical malignancy that must be removed. This volume has thus been appropriately treated to achieve the aim of therapy, i.e. cure or palliation.

Planning target volume (PTV) - This is a geometric concept and is used to choose the appropriate beam size and beam arrangement, in order to make sure



that the prescribed dose actually is absorbed in the CTV, taking into account the net effect of any potential geometric variations and errors in this way.

Treatment volume (TV) - TV is the volume contained by an isodose surface (line travelling through the same doses) that the radiation oncologist selects and specifies as appropriate for achieving the treatment goal. Normal tissues whose radiation sensitivity may have a substantial impact on treatment planning or prescribed dose are known as organs at risk (OAR).

The supplementary report to ICRU 50, which is ICRU 62, delves deeper into the numerous issues that influence the contours of the PTV. The Internal Margin (IM) is utilized to account for changes in the size, shape, and position of the CTV as a result of anatomical changes caused by organ movement. An additional set-up Margin (SM) must be introduced to account for the uncertainty of patient–beam location. Unlike the IM, which must account for a physiological process, the SM must account for technical issues that produce uncertainty. Improved patient immobilization and set-up accuracy may help to lower the SM. Only procedures like "respiratory gating" or "image guided radiotherapy" can help to minimize IM. The same uncertainties in position will be reflected in the organs at risk (OAR) volumes, necessitating the addition of a margin. The Planning Organs at Risk Volume (PRV) is a concept similar to the PTV.

1.4.4 CT based treatment planning

For many years, imaging using CT scanner has been the primary method for the planning of treatment, and for good cause. It provides us with precise spatial and electron density data. As a result, we know depth and penetration of the radiation when simulating the patient's therapy [18].



1.4.4.1 Image manipulation and image fusion

Nowadays most of the patients were imaged using multiple modalities, such as CT, MRI, or PET, depending on the situation and minimizing drawbacks of each modality. Treatment planning systems (TPSs) allow these data sets to be merged and layered on top of each other. Fusion or registration is the name given to this process. For example, MRI brainstem volume can be outlined in an MRI and translated to CT [18].

1.4.4.2 Defining the volume, growing tools

A precise 3D image of the patient with sufficient tissue contrast allows the GTV and CTV to be identified. TPSs have a number of sketching tools that they can use to shape the required treatment volumes on the virtual patient anatomy. To generate PTV, one must be able to increase CTV. On most TPSs, this can be done automatically, with the CTV increasing uniformly in all directions or more in one direction than others depending on the illness. At this stage, any mistakes can have a negative impact on the clinical outcome, such as missing the tumor or over-irradiating normal tissue. The OAR, which is grown to generate PRVs, goes through a similar volume-growing process [18].

1.4.4.3 Beam's eye view

Beam's eye view (BEV) is a feature which is available across several planning programs. This lets you see the patient as if you were looking through the head of the treatment machine. We can turn patient structures on and off as needed (for example, body contour, PTV, and OAR). This is highly important for structuring the multi leaf collimator (MLC) and jaws so that the PTV is covered and the PRV is avoided.

1.4.4.4 Margins

A big enough treatment field is required for adequate dosage coverage of the PTV. Inexperienced planners frequently make the error of fitting the jaws or MLC up to the edge of the PTV in the BEV. However, because the 50% isodose defines the beam edge, coverage at the PTV's edge will be too cold. We achieve 95% of the maximal dose approximately 0.6 cm inside a 6 MV field, according to a dose profile. As a result, it's preferable to leave a 0.6 to 0.7cm gap between your PTV and the field edge (see Fig. 1.8).

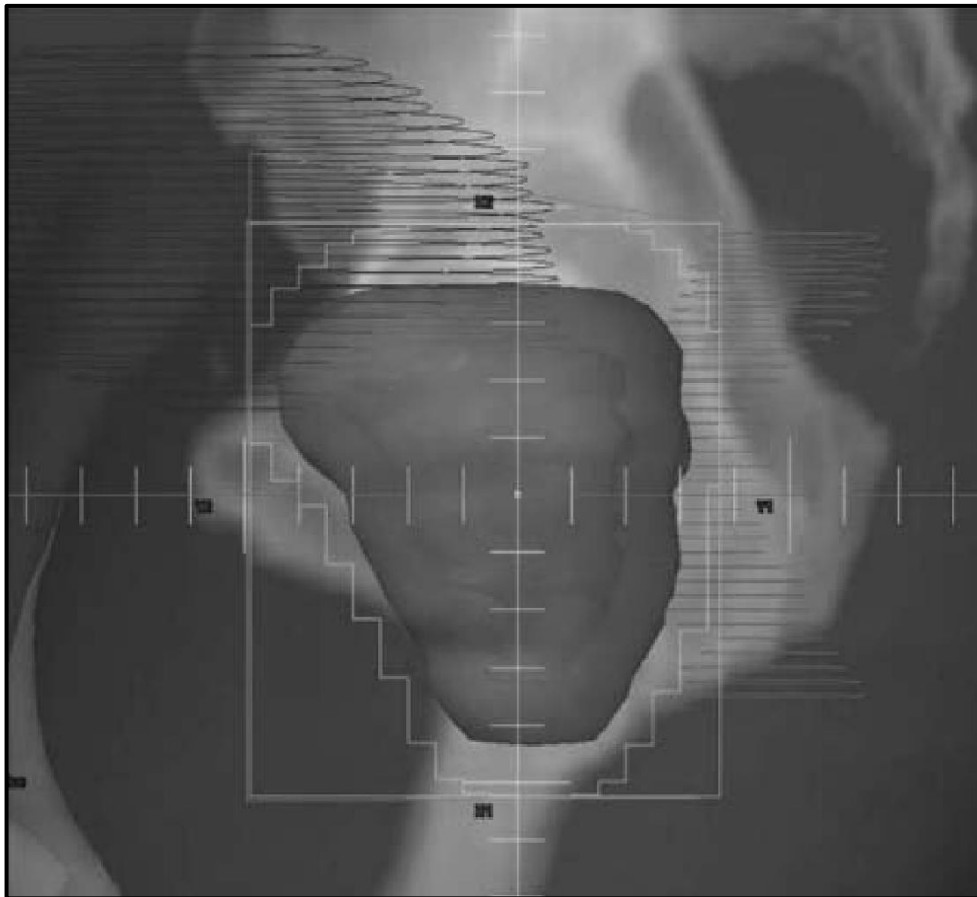


Figure 1.8 BEV showing PTV, bladder and MLC field edges [18].



1.4.4.5 Plan verification and evaluation

Isodose display

After completing the calculation process, the TPS will create isodoses, which are regions of equal dose. Contour lines on a map are equivalent to this. When a TPS calculates a dose, it is actually calculating the dose to a 3D grid of points that encompasses the patient anatomy to be treated. Isodoses are calculated by interpolating dose grid points, however Dosage Volume Histograms (DVH) can be created by calculating doses to individual grid points. DVH is a useful tool for evaluating and comparing plans.

Dose volume histograms

A DVH is a two-dimensional diagrammatic display of the three-dimensional dose distribution for specific organs. It can be used to evaluate and compare different treatment options. DVHs, on the other hand, do not substitute complete isodose distribution. They can't tell you where the dose is in the organ since they lack geometric knowledge.

In radiotherapy, there are two types of DVH.

➤ Differential (frequency) DVH

Within each dosage bin, such as 0-1Gy, the differential DVH shows the volume of the organ that receives the dose. The display of dose to target volumes is useful since the minimum and maximum doses may be easily seen. The Differential DVH depicts the uniformity of a structure's dose (Fig. 1.9). This DVH, on the other hand, isn't very useful for OAR.

➤ Integral (cumulative) DVH

The cumulative DVH for each volume receiving at least a certain dose value is plotted. Because it incorporates the straight histogram, it always

starts at 100%. (100 percent of organ that receives at least 0 percent of dose). The Integral DVH is the most frequent model to evaluate PTV and OAR data (Fig. 1.10). The two most common uses of this DVH are to see the:

1. Global maximum received by an organ (serial organs), such as spinal cord maximum.
2. Dose received by a certain volume of an organ (parallel organs), such as V_{20} of lung.

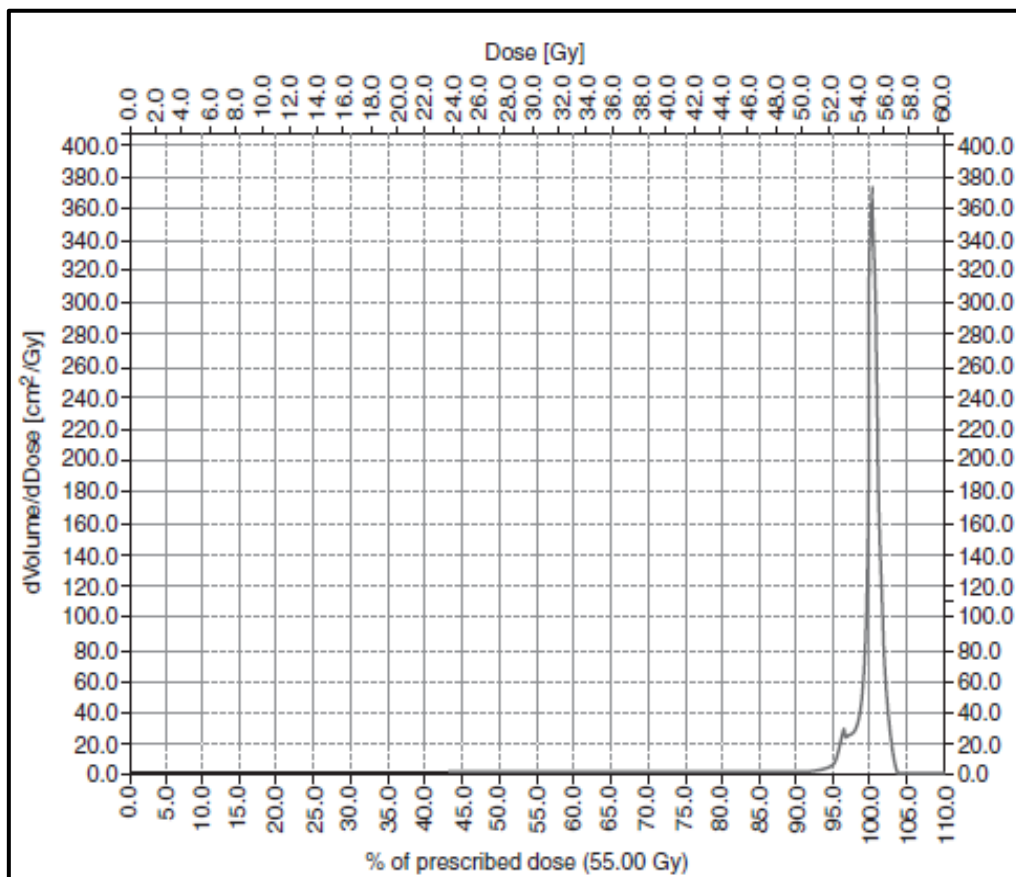


Figure 1.9 Differential DVH showing PTV coverage [18]

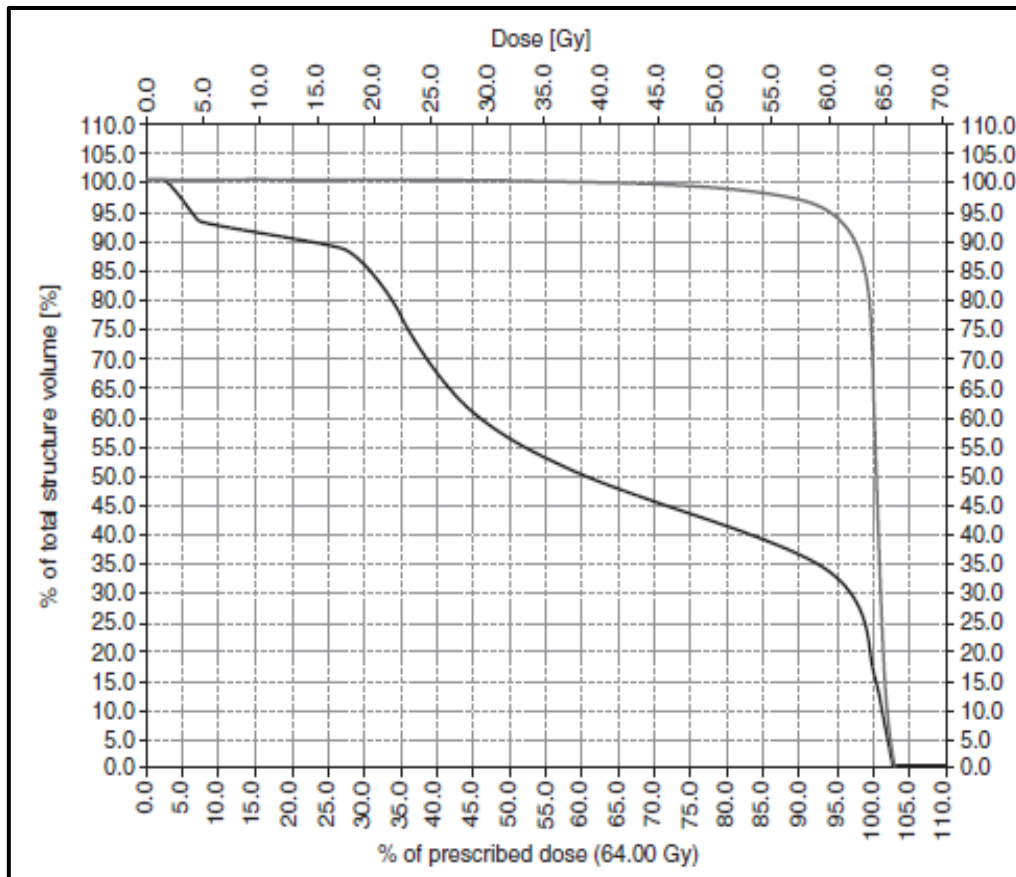


Figure 1.10 Integral DVH showing PTV and OAR data [18]

Digitally reconstructed radiographs (DRR)

The CT image sets which are used to create the treatment plan can also be used to create DRRs, which are simply the images that look like standard X-ray radiographs. For each treatment field in the plan we can generate separate DRRs. The TPS does this by drawing rays across the CT set along the beam path using the treatment field geometry. The CT electron density information allows the TPS to create low and high contrast areas on a film/detector, similar to what a planar X-ray beam would do. This DRR can then be compared to x-ray pictures taken on the treatment unit to ensure that the patient setup is accurate. In virtual simulation, DRRs are utilized to substitute simulator visuals. PTV, OAR, and field shape are superimposed on a DRR in Figure 1.8.

1.4.5 Setup and treatment

The radiation oncologist and medical physicist should be present for the first patient treatment (i.e., during setup) and should follow up with the patient on a regular basis throughout radiotherapy. Both traditional and sophisticated radiotherapies fall within this category. An ergonomic therapy plan must be carefully evaluated by the physician. After carefully completing patient setup on the couch, port films are obtained on a regular basis and compared to simulation films (Fig. 1.11). After that, the patient's position is modified properly. In more advanced procedures, TPS-created digitally reconstructed radiographs are compared to portal pictures captured by an electronic portal imaging device (EPID) (e.g., conformal RT, IMRT).

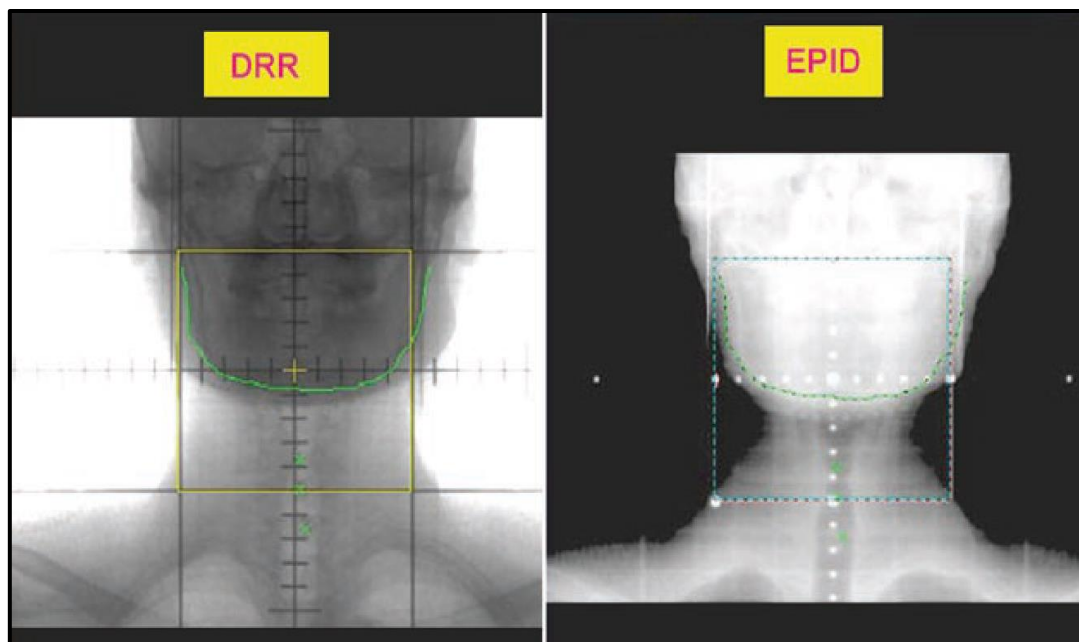


Figure 1.11 Imaging of DRR and EPID

1.4.6 Quality assurance

A complete quality assurance procedure is required to ensure that the finest possible care is provided to the patient. A radiotherapy manager with overall



responsibility for implementation must develop a quality assurance strategy while major portions of this job may be assigned to other adequately trained and certified members of the radiotherapy team. External accreditation visits supplement internal quality assurance methods. Before the trials begin, individual treatment strategies can be tested. Phantom measurements are frequently employed to ensure that all parameters, such as dose uniformity, output measurement and beam matching, are in good working order. Any internal or external system must be examined on a regular basis, with all activity documented according to a set process. Tolerances and actions to be done if the reference values are exceeded must be defined. Every portion of the system must have a departmental mechanism for investigating deviations [21].

Practical considerations

The following routine checks must be included in the quality assurance protocol:

- Machine checks
- Dosimetry protocols
- Planning checks
- Patient documentation.

Machine checks

Calibration data is gathered during the installation and acceptance of a new machine to serve as a reference point for further checks. For finding systemic deviations, inter-comparisons between different institutions or with national or international norms are useful. After that, quality control should guarantee that a machine meets its specifications and is safe for both employees and patients. It should ensure dose accuracy, prevent severe errors, reduce machine downtime and stimulate preventative equipment maintenance. Each machine should have



its own quality control procedure that specifies the tests to be carried out. Parameters to be tested, such as staff responsibilities, frequency of measurement, tolerances, reference values, action to be taken in the event of deviation and rules for documentation are among the ways to be utilised to maintain consistency in the operation of each machine. Dosimetry, beam alignment and safety checks must be tested on a daily, weekly, and monthly basis. Mechanical, optical and computer hardware and software systems are all tested on a regular basis. Where correction is required, action should be taken before treatment may begin. All imaging equipment and treatment planning systems should be subjected to the same scrutiny. The results of daily checks must be recorded in the treatment units control rooms and radiotherapists must also document any machine malfunctions. A separate log book is kept for any other checks, actions and maintenance tasks. All members of the team must work well. A physicist who oversees all quality control activities ensures that tests are up to par and notifies the oncologist if there are any significant variations [21].

Dosimetry protocols

Checks for dose monitor calibration, beam flatness and symmetry, beam quality evaluation and beam output measurement are included here. TLDs and silicon diodes used for in vivo dosimetry must also be examined and calibrated on a regular basis [21].

Planning checks

Nowadays most of the treatment prescriptions are in electronic format and computer systems coupled to therapy units automatically record treatment delivery parameters. These systems' activity reports can be utilised for auditing and a central collection of these output data could provide highly helpful



information about radiotherapy delivery design. Individual weekly reviews of patients' treatment data are recommended to ensure that treatment is being given as intended [21].

Patient documentation

Electronic technologies are becoming more widely used. To enable dependable rapid access, radiation therapy data are normally maintained separate from other medical documentation. The patient should be identified in the records as well as the clinical history and examination findings, histological diagnosis, tumour staging and planned treatment strategy should be obtained from records. Written treatment policies for specific tumour sites should be in place, and data should be kept so that treatment outcomes may be evaluated afterwards. It is necessary to obtain written consent for therapy. At the conclusion of treatment, a summary documenting the actual treatment parameters must be provided and the patient's continued care must be ensured. Maintaining a high-quality programme, as indicated above, is critical for safe treatment delivery. It can only be accomplished if each team member understands their responsibilities and if all quality control activities are well coordinated by a highly qualified physicist working with the person in charge of the radiotherapy department's overall administration. Any efficient quality assurance system must consequently include thorough training for all employees [21].

1.5 Technological Advances in Treatment Delivery

Novel imaging methods, more powerful computers and software and new delivery systems such as improved linear accelerators, have all aided in achieving the goal of radiotherapy, which is to give a high dose to the tumor while preserving normal tissue.



1.5.1 Conformal three-dimensional radiation therapy (3DCRT)

3DCRT is a radiation technology in which three-dimensional anatomical data obtained from CT, MRI or PET imaging modalities are used to make the dose volume fit closely to the target. With the help of modern computer software and technology, the goal is to administer the maximal dose to the target area while sparing as many surrounding structures as feasible [14]. 3D conformal radiation (3DCRT) combines 3D CT tumor visualization with the linear accelerators capacity to modify the beam both geometrically and by changing the photon fluence. The final PTV, which was developed using 3D growth algorithm software and departmental protocols while taking OAR into account, was agreed upon by the radiation oncologist and medical physicist. Understanding the requirements for homogeneity of dose distribution, tumor cell density pattern within the PTV, avoidance of maximum or minimum dose spots in 3D, dose constraints to adjacent OAR and review of a preliminary plan of likely beam arrangements are all discussed between oncologist and medical physicist. Static and coplanar beams with MLC or conventional blocks shaping the volume make up a basic 3DCRT. DVHs may aid in the selection of the best plan for coplanar non-standard beam configurations but they do not show which region of the organ is receiving a high or low dosage; DVHs of the PTV, CTV and all PRVs are required for later clinical result correlation. The final dose plan is chosen by analyzing 3D physical dose distributions and DVHs at the end of treatment planning. To reduce transfer mistakes between CT, treatment planning and the treatment unit, good communication between the radiotherapist, medical physicist and clinician is critical. Part of conformal therapy may entail the use of mixed beams that combine photons and electrons. Bolus, wedges, compensators, MLCs and shielding blocks can all be used to modify beams. Skin dose optimization is performed by employing greater megavoltage energies to create



a skin sparing effect or by maximizing skin dosage using tissue equivalent bolus. For pelvic treatments, higher beam energies in the range of 10–18 MV are preferred to enhance dosage to the center while reducing damage to the skin and subcutaneous tissues. For breast and head & neck cancers, lower energies (6-8 MV) are used. Lower energies help us to avoid excessive skin sparing. To deliver therapy, MLCs with many leaves or shields that can block part of the radiation beam to preserve critical structures are utilised. Modern MLCs typically contain 20–80 leaves stacked in opposing pairs that may be positioned using a computer to create an uneven beam that conforms to the intended shape. This approach not only eliminates the risk of alloy block fabrication and use, but it also enables for quick shaping adjustments to fit the PTV's beam's eye view [15, 21].

1.5.2 Intensity-modulated radiation therapy (IMRT)

Intensity-modulated radiation therapy (IMRT) is a radiation therapy technique in which non-uniform fluence is given to the patient from any given gantry angles to optimize the complex dose distribution [15]. Radiation oncologists may now design irregularly-shaped radiation beams that precisely adapt to the tumor and are dynamic enough to avoid important structures because of the development of computer-controlled modulation of photon intensity and the creation of inverse planning software. Little leaflets known as multi-leaf collimators (MLC) are employed in IMRT to adjust the beam pattern during delivery, ensuring that the shape of the beam is more closely wrapped around the tumor. Radiation oncologists can use IMRT to enhance the amount of radiation delivered to specific tumor sites, deal more effectively with tumor cells that are resistant to treatment and extend the area covered by high-dose radiation to lymph nodes. Unlike traditional planning procedures, where dose distribution can only be



changed through trial and error (by adjusting the field weight, angle and shape, for example), with IMRT, the radiation oncologist designs the doses and dose/volume limits for the tumor and surrounding normal organs. The Treatment Planning System (TPS) determines the ideal fluence of each field, resulting in a dose distribution that is personalized to the patient (inverse planning). Traditionally, IMRT was delivered with a traditional LINAC with static field geometry. Multiple static fields IMRT has been converted into constantly rotating gantry intensity modulation in IMRT approaches to reduce treatment times employing arc therapy [23]. IMRT is now available in many clinical departments and can be given with linear accelerators, tomotherapy devices or static or dynamic multi-leaf collimators. This has resulted in therapeutic index improvements for a variety of tumor types, including head and neck cancers, prostate cancers and gynecological malignancies [24].

1.5.3 Image-guided radiotherapy (IGRT)

Image-guided radiation therapy (IGRT) is a type of radiation therapy that uses image guidance at various phases of the treatment, such as patient data collection, patient setup, treatment simulation, treatment planning and target localization [15]. These methods employ imaging technology to detect concerns resulting from inter- and intra-fractional changes in patient setup and anatomy, such as the shapes and volumes of treatment targets, organs at risk and normal tissues in the surrounding area [15]. For image guiding, imaging devices that are accessible in the treatment room or mounted directly on the accelerator have been developed. On-board imagers are imaging systems placed on accelerators (OBIs). One example is the use of daily cone-beam CT scans before each treatment. Because of the enhanced precision, dose escalation is now possible, which has improved



the therapeutic index for various tumor sites, including head and neck cancers and prostate cancers [24].

1.5.4 Stereotactic radiation therapy (SRT)

This method is only available in a few hospitals but it has been used for a long time, primarily to treat tiny brain tumors and arteriovenous malformations. A stereotactic frame that is affixed to the patient's skull and allows for patient placement accuracy of 1mm. The dose of radiation can be provided in a single fraction or numerous fractions and it can be used instead of surgery. Multiple cobalt (Co-60) sources placed in a half circle, irradiate a very conformal volume by blocking chosen collimator apertures with different collimation helmets for varied time intervals in the gamma knife device.

Multiple arc therapy can also be delivered using a linear accelerator with specific collimators. Because of the severe dose gradients and challenges with electron equilibration with extremely small photon beams, this technology needs meticulous quality control. It will also require close collaboration among a group of experts in imaging, neuro anatomy, tumor care and physics. Some small-volume lung and liver cancers may benefit from this treatment [21].

1.5.5 Tomotherapy

Serial and helical tomotherapy are the two kinds of tomotherapy. Serial tomotherapy is performed with a MiMIC collimator system installed on a traditional linac gantry. The table is also equipped with a crane, which allows it to be moved with extreme precision. After that, IMRT is administered in a series of arcs. In contrast, helical tomotherapy makes use of a specialized tomotherapy unit. It comprises a 6 MV linac put on top of a CT that performs IMRT using



spiral movements similar to CT. IMRT and simulations are carried out on the same equipment [14].

1.6 Nanoparticles in Radiation Therapy

Radiation therapy includes drawbacks, including the risk of harm to normal tissue in the surrounding area. Another downside is that some tumour cells are further away from the radiation source, receiving a reduced photon beam intensity as a result. Furthermore, cancer cells can develop radiation resistance. Normally, the mitotically active tumor cells' sensitivity is only slightly higher than that of the surrounding normal tissue. As a result, the lower amount of radiation required to destroy tumor tissue may only damage rather than kill normal tissue. However, tumor cells' resistance to dosed radiation necessitates higher doses, which finally results in the death of healthy tissue [25].

Even while great advances in the field of radiation oncology have resulted in better concentrating and more controlled doses of ionizing radiation, there are still some serious concerns with the therapy. Radiation resistances as well as the therapeutic system's fundamental weaknesses make it a balancing act between therapeutic benefits and physiological drawbacks. Many methods have been tried to improve its efficacy while lowering its toxicity. The three major approaches to improve therapeutic index are (I) increasing radiosensitization of tumour tissue; (II) reversing radiation resistance in tumour tissue; and (III) boosting radioresistance of healthy tissue [25].

Radiation sensitization is the process of making tumor tissues more vulnerable to radiation-induced damage. As a result, radiosensitizers are medicinal or otherwise inert substances that improve radiation therapy outcomes [25]. The use of



nanoparticles in radiation therapy has a lot of potential. It may be able to eliminate cancer tumors with nanoparticles while causing minimal damage to healthy tissue and avoiding the major side effects those radiation therapy treatments routinely induce. Nanomaterials with well-developed synthetic techniques, minimal cytotoxicity, high biocompatibility and simplicity of functionalization show promise as radiosensitizers [2].



References

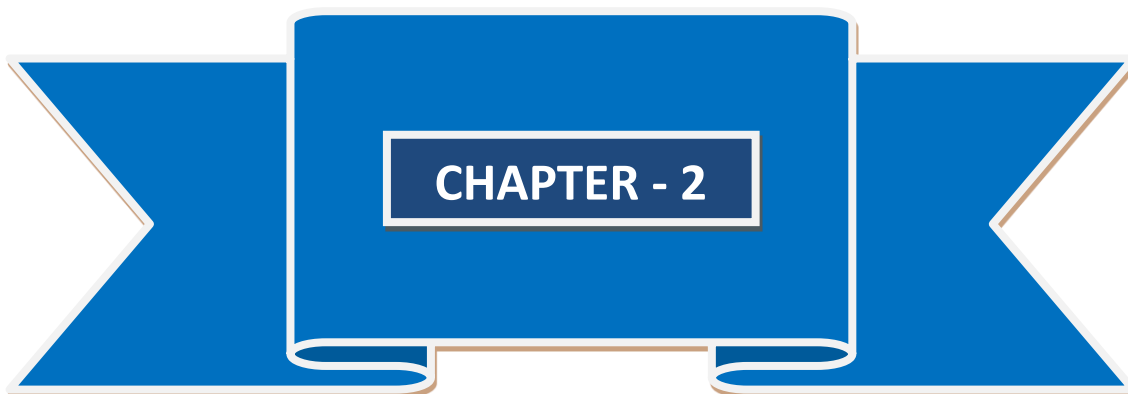
1. Siegel R, Naishadham D, Jemal A. Cancer statistics. CA: A Cancer Journal for Clinicians, 2012, 62, 10-29.
2. Anuje M, Pawaskar P N et al; Synthesis and cytotoxicity evaluation of poly (ethylene) glycol coated iron oxide nanoparticles for radiotherapy application, J Med Phy, 2021, 46(3), 154-161.
3. Thariat J, Hannoun Levi J M, Sun Myint A, Vuong T, Gérard J P; Past, present, and future of radiotherapy for the benefit of patients. Nat. Rev. Clin. Oncol. 2013, 10, 52–60.
4. Röntgen W C. Ueber eine neue Art von Strahlen. Vorläufige Mitteilung. Sitzung; Sitzungsberichte der physikalisch-medizinischen Gesellschaft zu Würzburg; 1895, 30, 132–141.
5. Becquerel A H, Curie P. Action physiologique des rayons de radium. Compt. Rend. Acad. Sci. 1901, 132, 1289–1291.
6. Grubbe E H. Priority in the therapeutic use of X-rays. Radiology; 1933, 21, 156–162.
7. Coutard H. Principles of X-ray therapy of malignant disease. Lancet. 1934, 2, 1–12.
8. Taylor L S. History of the International Commission on Radiological Protection (ICRP), Health Phys. 1958 Sep, 1(2), 97-104.
9. Theraeus R A. A study of ionization method for measuring the intensity and absorption of roentgen rays and of the efficiency of different filters used in therapy. Acta Radiol. 1932, 15, 1–86.
10. Courant E D. Early Milestones in the Evolution of Accelerators. In Chao AW, editor. Reviews of Accelerator Science and Technology. Singapore: World Scientific; 2008, 1, 1–5.



11. Gianfaldoni S, Gianfaldoni R, Wollina U, Lotti J, Tchernev G and Lotti T. An overview on radiotherapy: from its history to its current applications in dermatology, J. Med. Sci. 2017, 5,521–5.
12. Anuje M, Bauer J and Thorat N. Chapter 7 Radiotherapy and breast cancer nanomedicine. In Thorat N, Bauer J (eds). External Field and Radiation Stimulated Breast Cancer Nanotheranostics. 2019,7-9. ISBN: 978-0-7503-2416-8.
13. Hall E J. Radiobiology for the radiologist. Lippincott Williams & Wilkins, Philadelphia,2000,7, 558.
14. Murat B, Gokhan O, Cuneyt E. Basic Radiation Oncology, Springer Heidelberg Dordrecht London New York, 2010,4, 86.
15. Khan F M. The Physics of Radiation Therapy. Philadelphia, PA: Lippincott Williams & Wilkins, 2010, 4.
16. Baskar R, Lee K A, Yeo R, Yeoh K W. Cancer and radiation therapy: current advances and future directions. Int J Med Sci. 2012, 9(3), 193-9.
17. Symonds P, Deehan C, Meredith C, and Mills J; Walter and Miller's Textbook of Radiotherapy: Radiation Physics, Therapy and Oncology, Churchill Livingstone, New York.2012, 7.
18. Sibtain A, Morgan A, and MacDougall N. Radiotherapy in practice: Physics for clinical oncology. Oxford: Oxford University Press.2012.
19. ICRU Report 50. Prescribing, recording and reporting photon beam therapy. International Commission on Radiation Units and Measurements. 1993.
20. ICRU Report 62. Prescribing, recording and reporting photon beam therapy (supplement to ICRU Report 50). International Commission on Radiation;1999.




21. Dobbs J, Barrett A, Morris S, Roques T. Practical radiotherapy planning. London: Arnold. 2009.
22. Lee T F, Yang J, Huang E Y, et al. Technical advancement of radiation therapy. Biomed Res Int 2013; 2014:549–56.
23. Garibaldi C, Jereczek-Fossa B A, Marvaso G, Dicuonzo S, Rojas D P, Cattani F, et al. Recent advances in radiation oncology. Cancer medical science 2017, 11, 785.
24. Baskar R, Lee K A, Yeo R and Yeoh K W. Cancer and radiation therapy: current advances and future directions. Int. J. Med. Sci, 2012, 9, 193–199. doi:10.7150/ijms.3635
25. Kwatra D, Venugopal A, Anant S. Nanoparticles in radiation therapy: a summary of various approaches to enhance radiosensitization in cancer. Transl Cancer Res. 2013, 2(4), 330–42.





MAGNETIC NANOPARTICLES

The part of this chapter has published in an Elsevier book

 Access through your institution

Purchase PDF

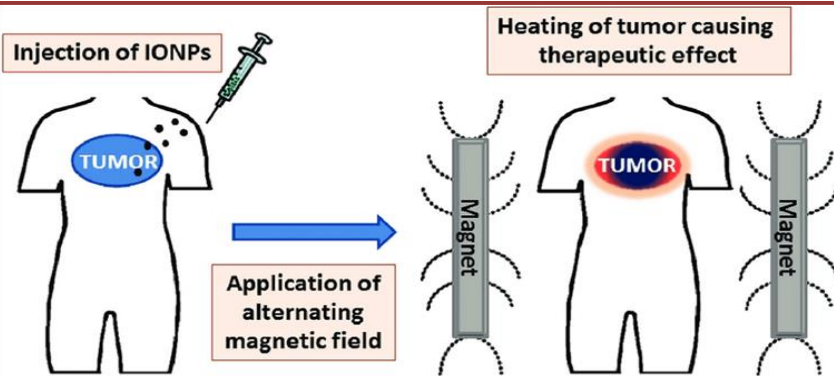
 **Nanomedicines for Breast Cancer Theranostics**
Micro and Nano Technologies
2020, Pages 193-243



10 - Cellular interaction and toxicity of nanostructures

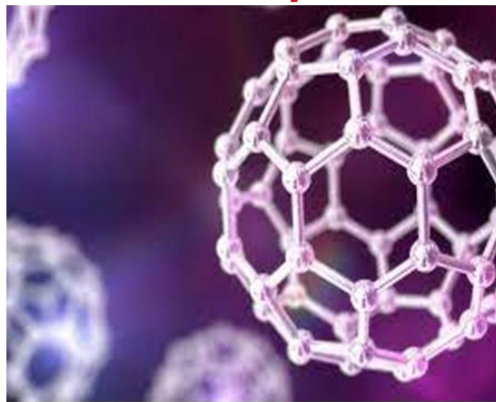
Madhuri Anuje ^{1, 2}, Ajay Sivan ², Vishwajeet M. Khot ¹, P.N. Pawaskar ¹

Show more ▼



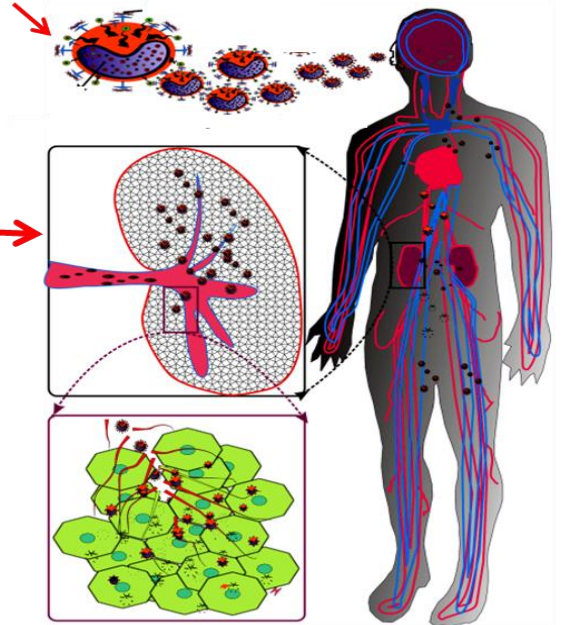
Hyperthermia

Application of Nanoparticle

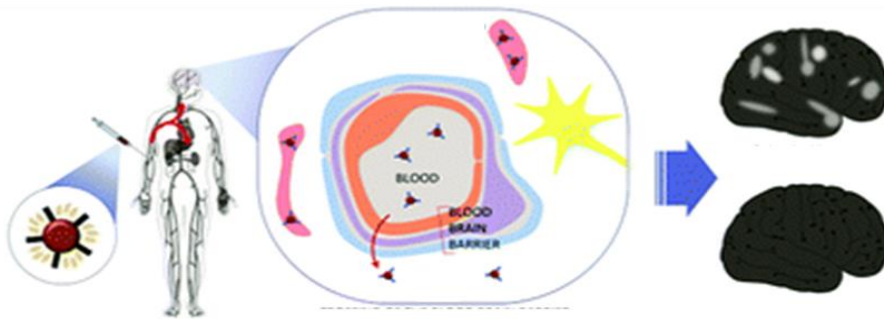


MRI Imaging

Drug functionalize with nanoparticle



Drug delivery



Intravenous injection of nanoparticles



2.1 Nanotechnology

On December 29, 1959, the idea of Nanotechnology was triggered by Famous physicist Richard Feynman at an American Physical Society meeting held at California Institute of Technology. In his talk entitled “*There’s plenty of room at the bottom*” he described a process in which scientists would be able to manipulate and control individual atoms and molecules. Nanotechnology is the branch of technology that deals with dimensions and tolerances of less than 100 nanometers. The term Nanotechnology was coined by Norio Taniguchi in 1974. The pioneering of the scanning tunnelling microscope in 1981 and the finding of fullerene in 1985 were two key innovations in Nanotechnology. The field earned scientific, political and commercial attention in the early 2000’s and a different kind of “Nanotech” products are available in the market today. It should be appreciated that nanotechnology is not in itself a single emerging scientific discipline, but rather, a meeting of different traditional sciences, such as, chemistry, physics, materials science, engineering, electronics, biology and to bring together the required collective expertise needed to develop these novel technologies.

Nanotechnology can be defined as the design and manufacturing of structures, gadgets and systems at the nanometer scale by regulating shape and size. At nanometer range, consideration of individual molecules and interacting groups of molecules in relation to the bulk macroscopic properties of the material or device becomes important, as it has a control over the fundamental molecular structure, which allows control over the macroscopic chemical and physical properties [1]. The properties of materials can be different at the nanoscale for two main reasons: First, nanomaterials have a relatively larger surface area when compared to the same mass of material produced in a larger form. This can make materials more



chemically reactive (in some cases materials that are inert in their larger form are reactive when produced in their nanoscale form) and affect their strength or electrical properties. Second, quantum effects can begin to dominate the behavior of matter at the nanoscale – particularly at the lower end – affecting the optical, electrical and magnetic behavior of materials. A nanostructured material is defined by the International Organization for Standardization (ISO) as a “material with any external nanoscale dimension or having internal nanoscale surface structure.”

One of the most high-impact areas where nanotechnology offers remarkable potential and promise is disease detection and therapy [2-3]. Nanomedicine is defined by the National Institutes of Health (NIH) as the use of nanotechnology for disease treatment, diagnosis, monitoring and control of biological systems. Nanomedicine takes advantage of materials improved and unique physical, chemical and biological properties at the nanoscale scale.

Research into the rational delivery and targeting of therapeutic, pharmacological and diagnostic substances is currently at the forefront of Nanomedicine projects. These therapeutic and diagnostic therapies entail the identification of specific targets, such as cells and receptors, associated with certain clinical problems, as well as the selection of appropriate nanocarriers to elicit the desired responses with the least amount of side effects. Both theoretically and practically, a survey of fundamental difficulties related to nanomaterial biocompatibility has begun. The US Food and Drug Administration has considered the challenging problems regarding the future approval of nanomedical products. It is clear that plans are being made for our society to develop nanomedicine in order to improve human health. Before nanomedicine may be employed in clinics, the fundamental mechanisms of nanomedicine must be completely investigated, as well as clinical



trials and validation methods. For example, while it is hoped that biological entities such as proteins, DNA and other biopolymers will be directly employed for biosensor applications, severe challenges such as biocompatibility and robustness may obstruct these efforts [4].

Nanomaterials (NMs) are classified on the basis of material, dimension and origin as shown in figure 2.1. Most NMs can be generally classified into four material-based categories viz. organic, inorganic, composite and carbon-based [5]. Dendrimers, liposomes, micelles, polymer NPs etc. are usually known as organic nanostructures. These nanostructures are nontoxic, biodegradable and some of their structures, e.g., liposomes and micelles, have hollow cores (also known as nanocapsules). They are sensitive to electromagnetic and thermal radiation, i.e., light and heat. Inorganic nanostructures include metal and metal oxide NPs. The commonly used metals for nanoparticle synthesis are aluminium (Al), cadmium (Cd), cobalt (Co), copper (Cu), gold (Au), iron (Fe), lead (Pb), silver (Ag) and zinc (Zn). The metal oxide-based nanoparticles are synthesized to alter the properties of their respective metal-based nanoparticles, for example nanoparticles of iron (Fe) instantly oxidizes to iron oxide (Fe_2O_3) in the presence of oxygen at room temperature that increases its reactivity compared to iron nanoparticles. Metal oxide nanoparticles are synthesized mainly due to their increased reactivity and efficiency [5]. The commonly synthesized are Aluminium oxide (Al_2O_3), Cerium oxide (CeO_2), Iron oxide (Fe_2O_3), Magnetite (Fe_3O_4), Silicon dioxide (SiO_2), Titanium oxide (TiO_2) and Zinc oxide (ZnO). These nanoparticles have exceptional properties when compared to their metal counterparts. Nanocomposites can be described as multiphase nanostructures with one phase being at the nanoscale dimension. They can either combine nanostructures with other NPs or NPs with bulk-type or larger materials (e.g., hybrid nonporous materials) or more complicated structures. Nanocomposites



can be any combination of metal-based, carbon-based, or organic-based nanostructures with any form of ceramic, metal, or polymer bulk materials [5]. Nanostructures made of carbon are known as carbon-based nanostructures. They can have different morphologies, such as ellipsoid, hollow tube or sphere. Generally, these nanostructures can be classified into diamonds, fullerenes (C_{60} , C_{80} , and C_{240}), carbon nanotubes (CNTs), graphene and carbon nanofibers [5].

Based on dimension NM classified as 0D, 1D, 2D and 3D NMs (Fig. 2.1). In zero dimensional structures (0D) all three dimensions are in the range of 1 to 100 nm. Example - quantum dots. In one dimensional nanostructure (1D) two dimensions fall anywhere in the range of 1 to 100 nm and one dimension larger than 100 nm. Examples include nanofibers, nanowires, nanorods, nanobelts, nanoribbons. Two-dimensional structures (2D) benefit from two dimensions larger than 100 nm, e.g., Nano-coatings, nanofilm, nanodisc, nanoplate, nanosheet. Three dimensional nanostructures (3D) materials have three dimensions larger than 100 nm, but components of their microstructures are at nanoscale, e.g. Nanocrystalline or nanoporous materials such as Nanoballs (dendritic structures), nanocoil, nanocones, nanopillars, nanoflowers.

Based on origin NM classified as natural and synthetic (engineered) nanomaterials (Fig. 2.1). Natural nanomaterials are produced in nature either by biological species or through anthropogenic activities. Synthetic (engineered) nanomaterials have been manufactured by humans to have certain required properties for desired applications and are produced by mechanical grinding, engine exhaust and smoke or are synthesized by physical, chemical, biological or hybrid methods.

Nanotechnology emerged as a promising field of science with a variety of applications in energy storage, biotechnology, medicine, sensing and healthcare

monitoring and in each aspect of nature. Owing to the significant characteristics of the smaller size, easy modification and tunable physical and chemical properties, magnetic nanomaterials have gained potential fame in the nanomedicine area. In terms of therapeutic and diagnosis, magnetic nanoparticles (MNP) cannot be replaced with any other material [6].

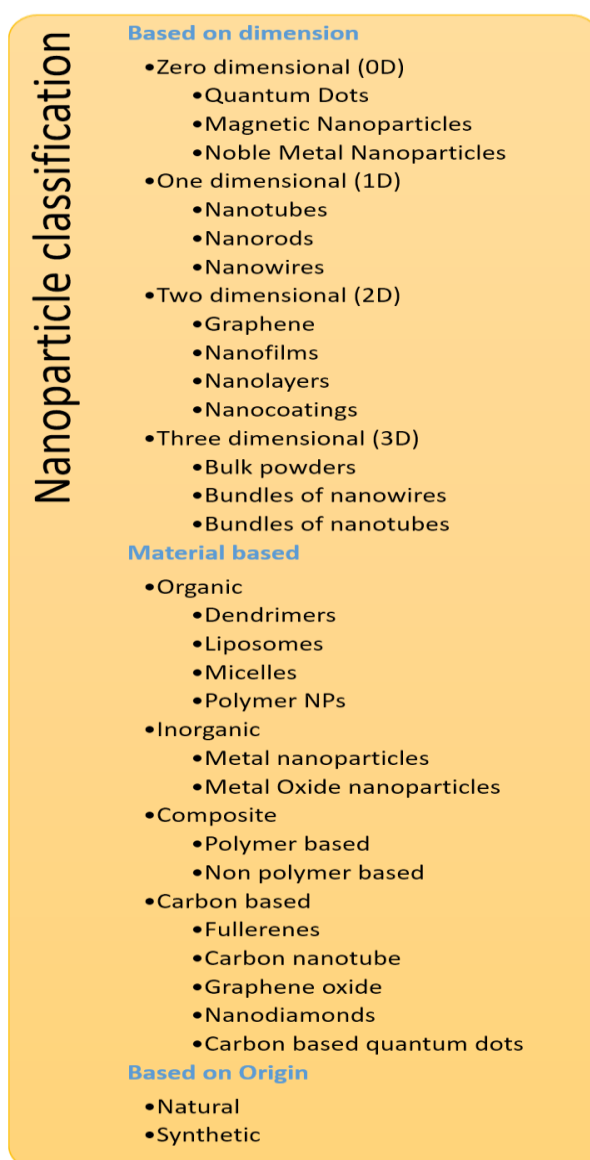


Figure 2.1 Classification of nanoparticles

Nowadays, MNPs have been used for different applications including magnetic biosensing (diagnostics), magnetic imaging, magnetic separation, drug delivery



and hyperthermia therapy etc [7]. Surface functionalization and coating of ferromagnetic and superparamagnetic nanoparticles not only make them biocompatible but also effective for drug delivery and killing cancer cells [6]. The Properties and applications of MNPs are discussed below.

2.2 Physicochemical Properties of Magnetic Nanoparticles

Superparamagnetic nanoparticles are getting popular as prospective agents for a wide range of applications in oncology. However, for these applications to work, a precise set of biological and physicochemical qualities must be united in nanoparticles [8]. Different physical features of NPs, such as size, shape, surface charge, solution stability and coating, must be investigated in order to assess their suitability for biological and biomedical applications and to assist those involved in developing and manufacturing nanoparticles.

2.2.1 Size

Oral SPIONs with a hydrodynamic diameter of 300 nm–3.5 mm, standard SPIONs (SSPIO) with a hydrodynamic diameter of 50–150 nm, and ultra-small SPIONs (USPIO) with a hydrodynamic diameter of less than 50 nm are the three primary categories of SPIONs. SPIONs with a size of 10–100 nm is ideal for intravenous delivery. [9, 10, 11, and 12].

A variety of biological parameters influence the size of nanoparticles that should be used for a specific purpose. At first, nanoparticles aggregate in locations with enhanced vascular permeability, such as tumours and inflammatory tissues, in a nonspecific manner [9]. Second, various aspects of the target tissue's vasculature should be evaluated, with the diameter of fenestrae being the most important. Non-fenestrated, fenestrated and sinusoidal capillaries are the three types of normal capillaries. The fenestrae of fenestrated capillaries are 80 nm in diameter,



but the openings between the cells of sinusoidal capillaries are larger [13]. The typical pore size of tumour vasculature ranges from 380 to 780 nanometers [9]. Third, tumours have wider vascular fenestrae; nevertheless, the larger the size of nanoparticles, the more difficult it is for them to traverse through the extracellular space [9] and the more reliant on transcytosis for their effects [14].

For in vivo research, tiny nanoparticles with a size of 10 to 50 nm are the optimum choice; these nanoparticles provide several advantages [15]:

- For smaller size nanoparticles with superparamagnetic features, it is feasible to improve colloidal stability and avoid aggregation. The dipole-dipole interaction is proportional to the sixth power of the particle radius (r^6). Therefore, by reducing size, the dipolar interactions become small and the particle agglomeration is decreased.
- For a given volume, surface area of small nanoparticle's is high. It has the potential to increase the efficiency of the coating and targeting processes.
- At pH = 7, small NPs can be stable in water.

2.2.2 Shape

NPs shape (Fig. 2.2) has a great impact on cellular intake. The biodistribution, circulation duration and residency time of NPs inside cells are all influenced by the shape of the NPs chosen. Furthermore, specific cells can be targeted by regulating the shape [16]. The shape of nanoparticles affects cellular uptake, extravasation and tumour accumulation. To begin with, nanoparticle shape affects macrophage phagocytosis. When compared to spherical nanoparticles, elongated nanoparticles have a lower likelihood of being absorbed by phagocytic cells [16]. In addition to prolonged circulation, the elongated nanoparticles with high length-to-diameter ratios and greater surface area contribute to their superior tumour deposition, which could be due to changes in direction of blood flow in mazy

tumour vessels, causing the elongated nanoparticles to tumble and collide with the vessel walls [8].

Compared to spherical NPs, elongated NPs have a better capability for attaching to cells. Because of the spherical particles' round shape, binding sites which may engage with receptors on target cells are less. While elongated NPs have a larger surface area than spherical NPs, this allows for multivalent interactions between these particles and the cell surface [16]. Particularly after modifying the surface, elongated NPs have a larger surface area and are better able to interact with surface membranes of the cell due to their shape [16].

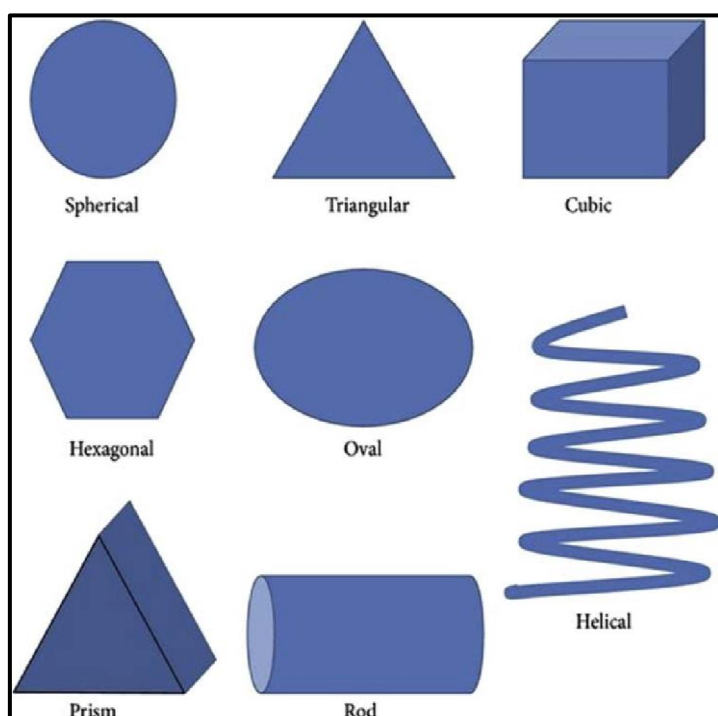


Figure 2.2 Different shapes of nanoparticles [16].

Furthermore, in vitro and in vivo tests have revealed that NPs with rod shape have a higher proclivity and efficacy for endothelial cells. Endosome membranes can be penetrated by NPs with a sharpened shape, which then localise to the



cytoplasm. As a result, their exocytosis was lower than that of spherical particles [16].

2.2.3 Nanoparticle charge

Cell membrane made up of lipid bilayer has a negatively charged outer surface, and endocytosis (membrane internalisation) is charge dependent [17]. The charge of the particles being opsonized determines whether proteins opsonize them and hence facilitate phagocytosis [18]. The charge of extracellular matrix components varies and as a result, their attraction for external substances varies as well [18]. The zeta potential should not be confused with nanoparticles' surface charge. Iron oxide nanoparticles can be or positively charged, negatively charged or neutral, depending on the synthesis components [19]. Neutral nanoparticles have a slower absorption rate than charged nanoparticles due to the aforementioned biological variables but negative and positive nanoparticles have different clearance speeds and biodistribution [18, 19]. Finally, nanoparticles that are neutral or slightly negatively charged have a longer circulation duration [18].

The steric stabilisation of NPs by nonionic polymers aids particle stability by limiting the direct interaction within the phagocytic system and cell. By creating barrier layers on particle surfaces using polyethylene glycol (PEG), a neutral and hydrophilic polymer, low opsonization, increased blood circulation time and escape from opsonization by the protein system can be achieved [16]. The uptake of PLGA NPs coated with PEG was 5 times higher than the unmodified form [16]. The addition of folic acid and PEG to the surface of NPs prevents protein adsorption and identification by macrophages. As a result, these NPs with surface functionalization are easily absorbed by tumours, resulting in effective and targeted cancer treatment [16].



2.2.4 Solution stability and zeta potential

Because of the greater magnetic attraction within the particles, SPIONs with bare surfaces tend to aggregate; thus, stabilisers such as inorganic compounds, carboxylates and polymeric compounds are commonly used to improve nanoparticles stability in suspension [20]. Different factors such as charge of the nanoparticles, the ionic concentration and strength of the solution affects the zeta potential (ζ) of the particle [21]. Suspensions of slightly charged nanoparticles or neutral (with a zeta potential between -25 and $+25$ mV) are susceptible to coagulation [18]. For nanoparticles to be useful, the zeta potential must be less than -25 mV or greater than $+25$ mV. In order to modify the zeta potential of nanoparticle formulation, one can use numerous coatings.

2.2.5 Coating

For targeted drug delivery, NPs must have a long blood circulation period in the body in order to recognise their specific region of interest. Opsonins, a blood serum protein that binds to the hydrophobic surface of NPs and reduces circulation time by triggering an immune response that permits phagocytosis of the NPs after they are recognised as foreign particles. As a result, current research has focused on applying a hydrophilic protective layer to normal hydrophobic NP surfaces. This hydrophilic coating prevents targeted nanocarriers from opsonization and extends their blood circulation half-life. Polymer types like polyvinyl pyrrolidone and PEG can be used to make hydrophilic-coated NPs [16]. Surface coating can be provided by PEG and PEG-based copolymers. In the presence of PEG, nanoparticles have a half-life of almost 7 hours, whereas in the absence of PEG, it is less than a minute [22].



2.3 Magnetic Properties of Nanoparticles

Movements of particles such as electrons, holes, protons, positive and negative ions that have both mass and electric charges produce magnetic effects. A spinning electric-charged particle creates a magnetic dipole, so called magneton. A magnetic moment is a quantity that represents the magnetic strength and orientation of a magnet or any other object that creates a magnetic field. In other words, a magnetic moment refers to a magnetic dipole moment, the component of the magnetic moment that can be represented by a magnetic dipole. A magnetic dipole is a magnetic north pole and a magnetic south pole separated by a small distance. Susceptibility and permeability are two characteristics that affect how substances behave when exposed to an external magnetic field. As illustrated in equation 2.1.

$$M = \chi H \quad (2.1)$$

Susceptibility (χ) is defined as a measure of a material's magnetization level (M) under an external magnetic field (H). It's a proportionality factor with no dimensions. The permeability of a substance is defined as its resistance to the formation of a magnetic field. All materials are categorized into many classes based on their susceptibility to magnetic fields [15]. MNPs are classed as diamagnetic, paramagnetic, ferromagnetic, ferrimagnetic or antiferromagnetic based on their net magnetization with and without application of magnetic field.

2.3.1 Diamagnetic

Magnetic dipoles do not exist in diamagnetic materials when there is no magnetic field (Fig. 2.3 (a)). In case of diamagnetic materials, a magnetic dipole is formed and is orientated in the opposite direction to the applied field [23]. As a result,

their susceptibility is low and negative (-10^{-6} to 10^{-3}). When the external field is removed, the spins return to their original position and lose their magnetic properties. Diamagnetic materials include water, wood, quartz (SiO_2), copper, silver and the majority of organic molecules. The fact that all of these materials contain filled electronic subshells is a common feature [15].

2.3.2 Paramagnetic

After a magnetic field is applied, paramagnetic substances exhibit a weak magnetic field that lies parallel to the applied external field. Magnetic dipoles present in paramagnetic materials, as shown in figure 2.3 (b), but only after applying an external magnetic field these dipoles are aligned [23]. These have a positive susceptibility and are in the range of (10^{-5} to 10^{-3}). Their magnetic moment disappears when the external field is removed. Paramagnetic characteristics are seen in aluminium, oxygen, magnesium, and lithium [15].

2.3.3 Ferromagnetic

Magnets with a large and positive susceptibility are referred to as ferromagnetic materials. External fields, temperature and atomic structures all influence the susceptibilities of ferromagnetic materials. Even after the magnetic field has been removed, their magnetic properties persist.

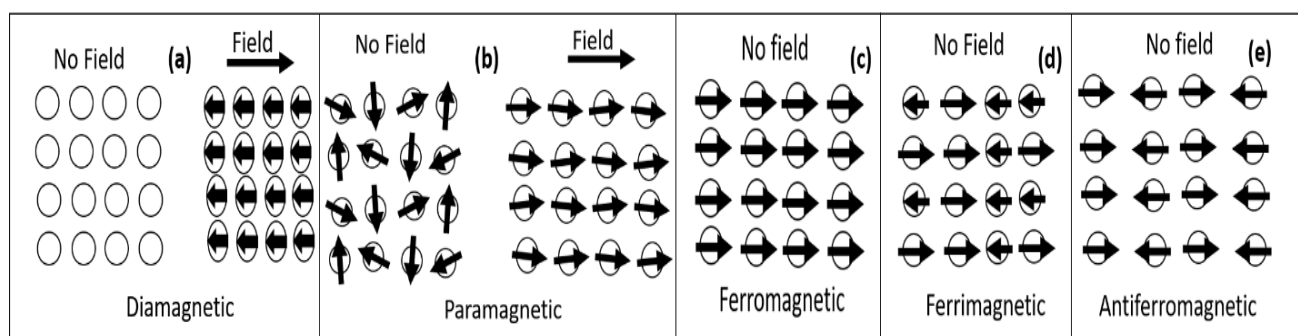


Figure 2.3 Magnetic dipoles and their behavior with and without magnetic field. Materials classification based on the alignment and response of magnetic dipoles.



The spins of the substance are aligned with the field after a strong magnetic field is applied. The maximum magnetization, also known as saturation magnetization, is achieved at this time. The return of spins to their original directions occurs when the magnitude of the applied field is lessened, resulting in a drop in total magnetization. The magnetic moment of these materials, on the other hand, is stable even in zero field, which means that without applied magnetic field magnetization shows their fundamental character. With no magnetic field ferromagnetic materials have net magnetic dipole moments (Fig. 2.3 (c)).

The atomic level magnetic dipole moments in antiferromagnetic and ferrimagnetic materials (Fig. 2.3 (d) and (e)) are identical to those in ferromagnetic materials but neighboring dipole moments that are not parallelly aligned cancel effectively [23]. Furthermore, tiny ferromagnetic substances with sizes in the tens of nanometers exhibit a single high magnetic moment. Magnetic nanoparticles have magnetic responses similar to paramagnetic materials, with a zero average magnetic moment, with no external field and a rapidly increasing magnetic moment when an external field is applied in the field's direction. At temperatures beyond the so-called blocking temperature, this phenomenon occurs. In fact, they exhibit superparamagnetic characteristics in this state [23]. In comparison to paramagnetic materials, they have higher magnetic susceptibilities. They can sustain colloidal stability and be helpful for biomedical applications because of this feature [15]. Superparamagnetic nanoparticles (SPNs) lose their magnetic properties after the external field is removed and thus have no attraction for one another, reducing aggregation of nanoparticles. This property makes them applicable in drug delivery and MRI. More significantly, because SPNs have a strong sensitivity to applied magnetic fields, they allow for improved control over the application of their magnetic properties [23].

The saturation magnetization occurs when all of the magnetic dipoles align in an applied magnetic field and it is the greatest magnetization attainable for MNPs. A typical magnetization curve is as shown in figure 2.4. Figure highlights the positions on the curve associated with saturation magnetization (M_s), remanent magnetization (M_r) and coercivity (H_c).

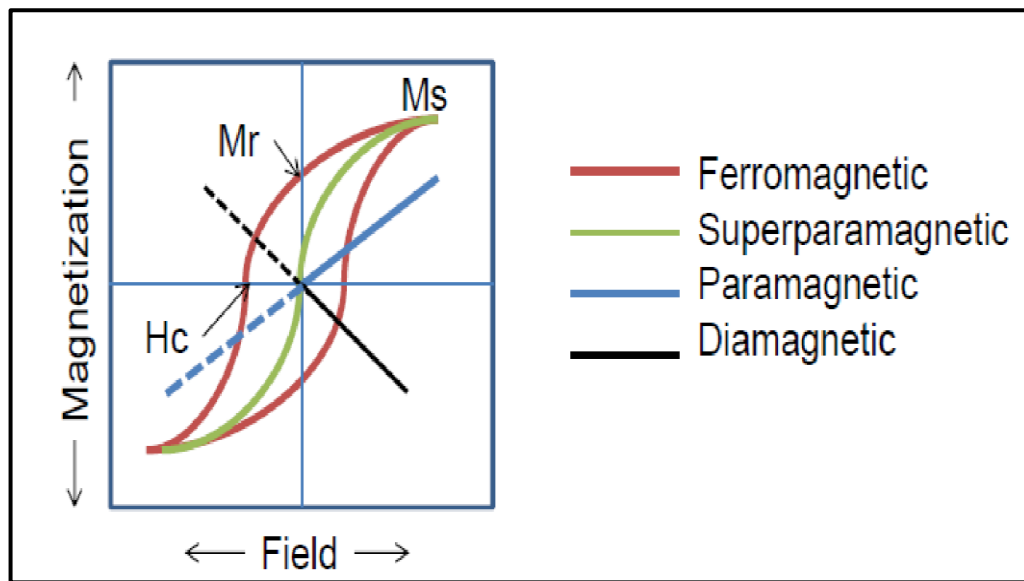


Figure 2.4 Magnetic behaviours influenced by an applied field. The X-axis represents the applied field (Oe), and the Y-axis represents sample magnetization as a function of field exposure (emu/g) [23].

Where M_s is maximum induced magnetization, M_r refers to remaining induced magnetization after removal of an applied field and H_c is the intensity of an external coercive field required to bring the magnetization to zero. In same figure, ferromagnetic nanoparticles (red loop), superparamagnetic nanoparticles (green line (sigmoid curve)), paramagnetic nanoparticles (blue line) and diamagnetic nanoparticles (black line) responses is also depicted [23].

2.4 Therapeutic Uses of Magnetic Nanoparticles

Magnetic nanoparticles (MNPs) have a variety of applications, including magnetic resonance imaging (MRI) techniques, drug delivery systems and magnetic hyperthermia. MNPs are used in a variety of ways, as shown in figure 2.5.

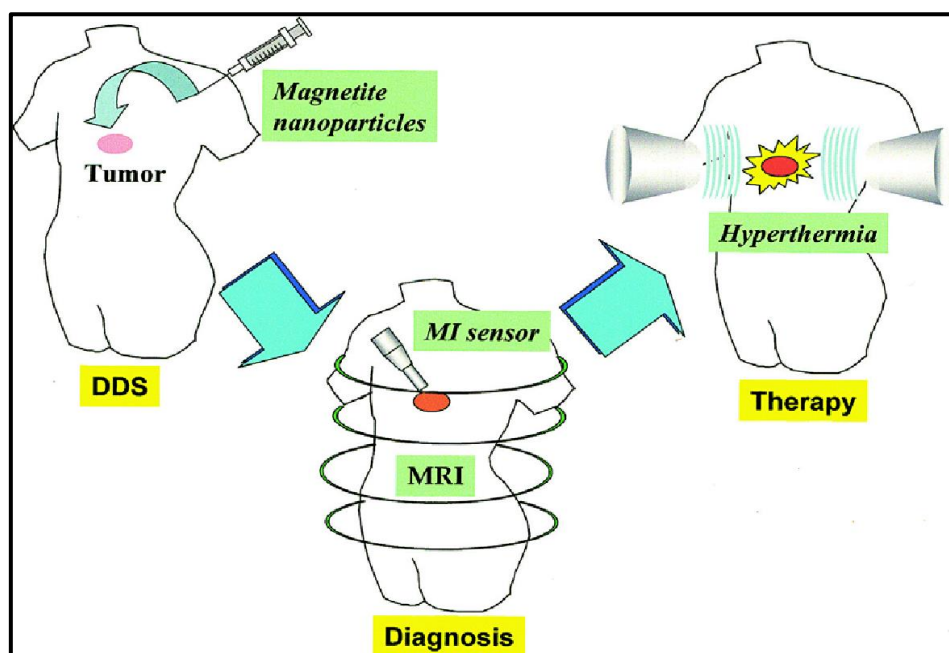


Figure 2.5 Schematic illustration of the therapeutic strategy using magnetic particles.

2.4.1 Magnetic resonance imaging

MRI is a noninvasive imaging technique that can generate high-resolution anatomical images. MRI, unlike other imaging techniques, does not employ ionising radiation for imaging, instead relying on protons magnetic properties to create images. It is a widely used approach for diagnosing soft tissue or cartilage diseases, allowing malignant and normal tissues to be distinguished [25]. In comparison to other MRI contrast agents such as chelates of paramagnetic ions like Gd^{3+} diethyle-netriamine-penta-acetic acid (Gd^{3+} DTPA), iron oxide NPs are



remarkable MRI contrast agents [26-28] because of their transverse relaxation feature with great sensitivity. The goal of this modality is to visualise molecular aspects of physiological or pathological processes in living organisms before they emerge as anatomic alterations.

Water molecules make up the majority of the human body. Each water molecule has two protons or hydrogen nuclei. The great prevalence of hydrogen in the body as well as the magnetic properties of the proton in a hydrogen atom are used in MRI. Because protons spin, hydrogen atoms produce a modest magnetic field. When a human enters the scanner's strong magnetic field, the magnetic moments (a measure of a particle's ability to align with a magnetic field (B_0)) of some of these protons shift and align with the applied field's direction which is known as longitudinal magnetization (M). The net magnetization vector moves 90 degrees towards the transverse plane after technicians employ radio frequency pulses to drive protons into a high-energy, in-phase condition.

The excited condition of nuclei that have absorbed radio frequency energy will not last very long. They revert to their former state and emit a radio frequency signal into the environment. These signals are detected by MRI detectors positioned all across the body. In MRI, the following two nuclear processes are used.

Spin-lattice relaxation (T_1 relaxation)

The spin state of a nucleus changes as it absorbs a photon at its Larmor frequency. The nucleus, on the other hand, will not remain in this excited condition. After emitting a photon, it will revert to its original state. The spin-lattice relaxation time, which is determined by the constant T_1 , is the amount of time it takes to perform this. The energy exchange between the spins and the surrounding lattice causes longitudinal relaxation (T_1) (spin-lattice relaxation). RF energy is released



back into the surrounding lattice as spins transition from a high to a low energy state.

Spin-spin relaxation (T_2 relaxation)

Spin-spin relaxation is another form of relaxation employed in MRI. Gradient coils change the principal magnetic field, allowing MRI to image in the x, y, or z axes. Change in the magnetic field affects the nuclei's Larmor frequency. Protons precess in-phase and out-of-phase in the direction of the primary magnetic field is directly proportional to the magnetic field's strength. Since they spin at different frequencies, the nucleus will gradually end up out of phase or spin at different times. Transverse relaxation (T_2) results from spins getting out of phase. As spins move together, their magnetic fields interact (spin-spin interaction), slightly modifying their precession rate. These interactions are temporary and random. Thus, spin-spin relaxation causes a cumulative loss in phase resulting in transverse magnetization decay. The loss of signal caused by the phase difference between these nuclei is used in MRIs to create the image. Magnetic field inhomogeneities causes protons to de-phase significantly quicker than T_2 ; T_2^* is the sum of T_2 relaxation and these inhomogeneities [29]. The change in net magnetic vector, which is subsequently produced from relaxation of protons from the transverse to the longitudinal plane, utilised to scan tissues.

Quality of MRI images can be improved by using contrast agents which can be categorised according to their capacity to affect T_1 , T_2 or T_2^* relaxation times [30]. Longitudinal (T_1) relaxation times of water protons in images get affected by T_1 contrast agents, resulting in bright positive signal intensity and increased cell visibility. T_2/T_2^* agents provide intensities of dark negative signal in images by varying the water proton's transverse (T_2/T_2^*) relaxation times. Magnetic nanoparticle (MN) based contrast agents mostly affect T_2^* relaxation [31]. When



exposed to and separated from an external magnetic field, magnetic nanoparticles with superparamagnetic properties can rapidly flip the orientation of the protons within their core, providing SPIONs exceedingly high relaxivity values [32].

MNs have also been used to monitor specific cells in addition to imaging [33]. For general imaging applications, a range of non-specific iron oxide-based contrast agents are available [34]. MRI resolution can be improved by simplifying accumulation of tumor-specific targeting moieties with attached MNs in cancer sites. For example, conjugation of anti-glypican antibodies and anti-fetoprotein to the MN shell can be used to target tumour in hepatocellular carcinoma [35].

2.4.2 Magnetic hyperthermia

Hyperthermia and photothermal therapy are known oldest therapies currently used as an anti-cancer therapy where the tumor temperature is increased to kill cancer cells and improve the effectiveness of other therapies such as radiation or chemotherapy. Heating was indicated as a potential cure for some ailments more than 4000 years ago, when the concept of hyperthermia was first proposed. Hyperthermia has recently gained a lot of attention, indicating that it could be used in cancer treatment. The utilisation of MNPs as heat mediators, in particular, is promising for the development of novel thermotherapy treatments, especially in combination with traditional cancer treatments such as surgery, radiotherapy and chemotherapy. Hyperthermia is characterized as an excessively high body temperature [36]. The malignant cell killing pathway in local magnetic hyperthermia therapy is depicted in figure 2.6. The mechanisms of heat generation by magnetic nanoparticles (MNP) depend on the magnetic action of the nanoparticles used in hyperthermia.

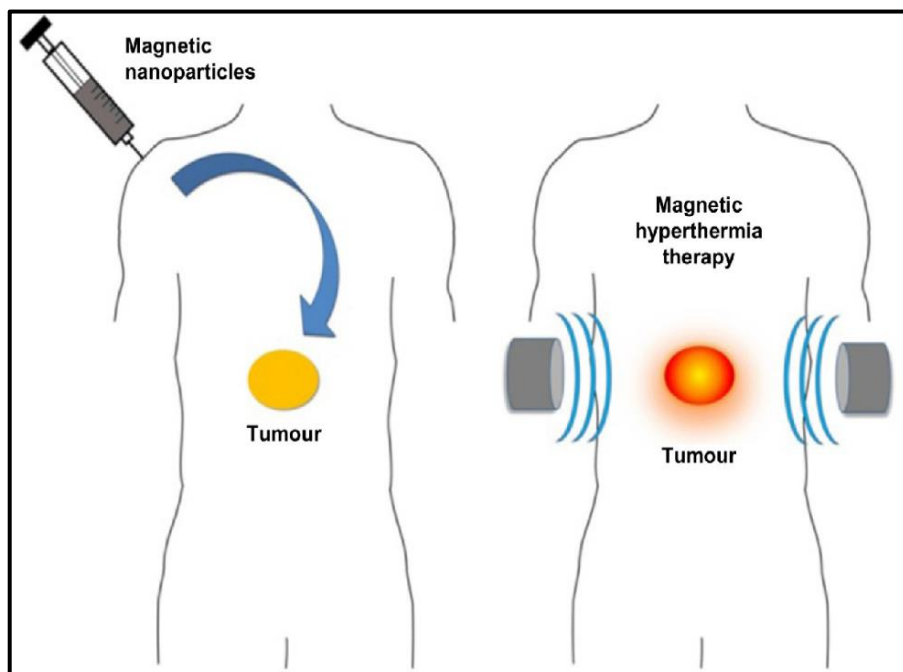


Figure 2.6 General procedure for local magnetic hyperthermia [37]

For paramagnetic materials, heat generation caused by two different types of magnetic relaxation mechanisms i.e., the relaxation of magnetic moments inside the particle volume (Neel relaxation) or the relaxation of magnetic moments fixed to the particles (Brownian relaxations) [37] (Fig. 2.7). In the case of ferromagnetic materials, thermal dissipation is due to hysteresis losses. The contribution of each process depends strongly on the nanoparticle size. For example, in small nanoparticles (size, 20 nm), heat dissipation is due to the Neel and Brownian relaxations with negligible contribution of hysteresis loss [38]. For larger single-domain (Size of NPs 100 nm and above) particles, hysteresis losses are significant [39].

Due to Neel and Brownian relaxation, superparamagnetic materials are applicable in magnetic hyperthermia while not exhibiting hysteresis (under normal conditions). Nanoparticles, in presence of magnetic field, first align parallel or antiparallel to applied magnetic field. Brownian relaxation is the time delay

between the reversal of the magnetic field and the reversal of magnetization. Brownian relaxation generates heat in this environment by causing agitation between MNPs with their surrounding media, such as blood [25]. Brownian

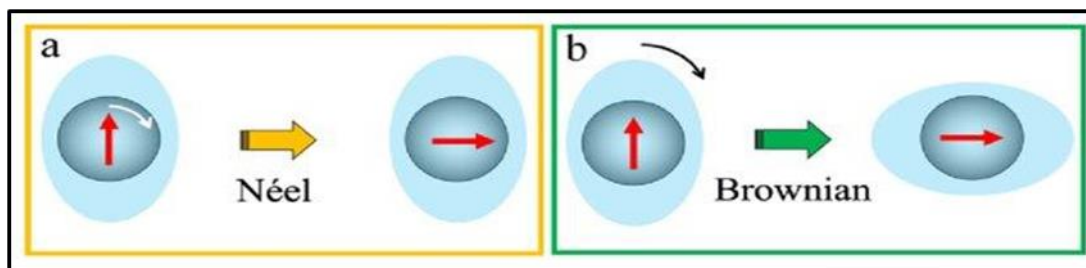


Figure 2.7 (a) Néel relaxation is the rotation of magnetic moment inside a stationary MNP. (b) Brownian relaxation is the rotation of entire MNP along with the magnetic moment.

relaxation is assumed to be size and viscosity dependent because when MNP size and carrier fluid viscosity increase, Brownian relaxation duration increases as well [40]. Only after relaxation of MNPs clinicians can re-magnetize them and are thus magnetizable again.

The specific absorption rate (SAR), which is the measure of heat generated per unit gram of magnetic material and per unit time, is used to determine the heating efficiency of magnetic nanoparticles using an alternating (AC) magnetic field. It's also known as a rate of energy absorption by the body when it's exposed to a radio frequency (RF) electromagnetic field.

2.4.3 MNPs and targeted drug delivery

Magnetic nanoparticles (MNP) have been developed for localized drug delivery for cancer patients. These are directed to the tumor, by acting as a drug carrier. Once the drug has reached the patient's bloodstream, a magnetic field is applied to retain the particles in the targeted site of the tumor. This has become one of the most promising treatment options for cancer patients today.



Superparamagnetic Nanoparticles (SPNs) within the size range of less than 10 nm, due to the presence of a single domain state, behave magnetic only under the influence of external magnetic field and become inactive once removed [41]. This property of superparamagnetic materials results in potential advantages to deliver therapeutics onto specific sites under the influence of external magnetic fields and can be returned to their nonmagnetic states by removing external magnetic fields to allow them to be excreted (Fig. 2.8) [41]. A variety of MNPs and microparticle carriers have been evolved to deliver drugs to specific target sites in vivo for more than 30 years [41]. Various kinds of MNPs have been used, including iron oxide (e.g., Fe_3O_4 and MFe_2O_4 ($\text{M} = \text{Mn}$, Co and Zn)), alloys (e.g. Iron–platinum (FePt), Platinum-cobalt (PtCo) and Iron-cobalt (FeCo)), and multifunctional MNPs with core/shell, dumbbell or multicomponent hybrid structures [41]. Micelles, [42-44], liposomes NPs [44-46], dendrimers [47], and polymers [48] are examples of macromolecular structures intended for drug delivery systems. The drug is entrapped, attached, adsorbed or encapsulated into or onto nano-matrices in various ways [49]. In an ideal scenario, they would attach a pharmaceutical drug to their surface or bulk and deliver it to the target organ. Micelles, [42-44], liposomes NPs [44-46], dendrimers [47] and polymers [48] are examples of macromolecular structures intended for drug delivery systems. The drug is entrapped, attached, adsorbed or encapsulated into or onto nano-matrices in various ways [49]. In an ideal scenario, they would attach a pharmaceutical drug to their surface or bulk and deliver it to the target organ. The surface chemistry, charge and size of the magnetic particles are very crucial in these applications, and they have a significant impact on both the blood circulation time and the biodistribution of the particles throughout the body [50]. Furthermore, the size of magnetic particles has a significant impact on their magnetic properties and internalisation [51]. Larger NPs with a diameter higher

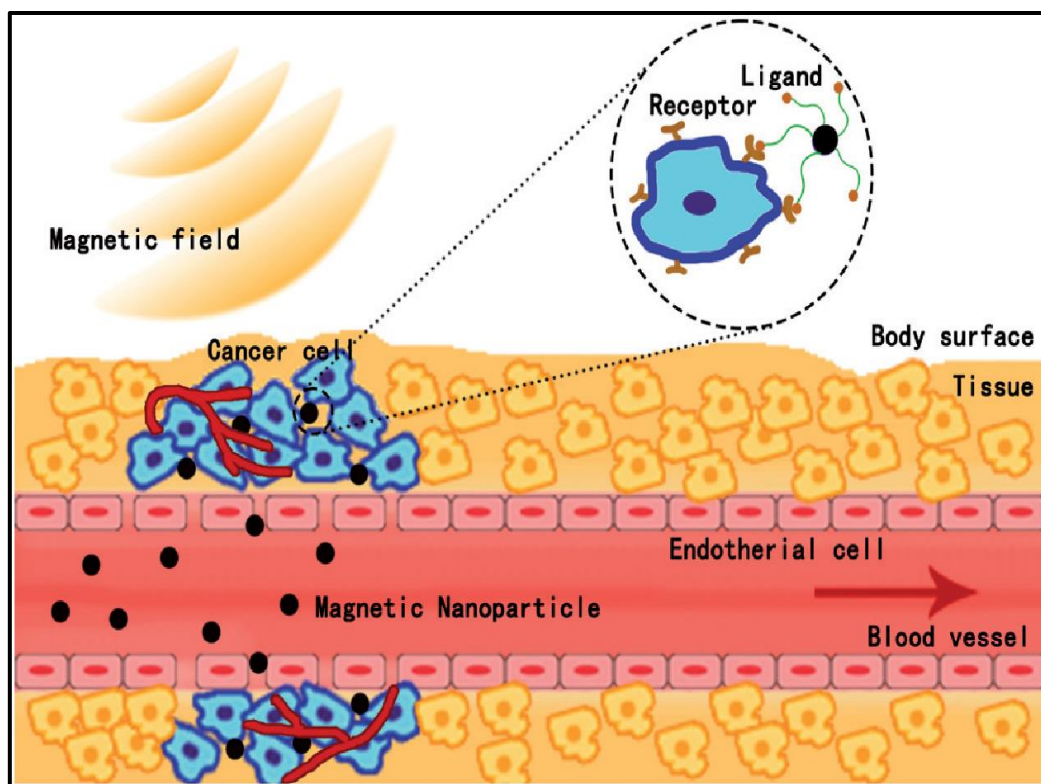


Figure 2.8. Schematic representation of a magnetic drug delivery system using an external magnetic field [41].

than 200 nm, for example, are often sequestered by the spleen as a result of mechanical filtration and eventually removed by the cells of the phagocyte system, resulting in reduced blood circulation times. Superparamagnetic NPs with a narrow size range are simple to synthesize and can be functionalized with a variety of polymers, making them useful and targetable agents. Because of their high surface area to volume ratio, MNPs agglomerate and adsorb plasma proteins. Due to their hydrophobic surface, the body's reticuloendothelial system (RES), primarily the kupffer cells in the liver, ingest these NPs. By limiting or eliminating protein adsorption to the NPs, surface coverage by polymeric surfactants over the NPs significantly enhances blood circulation time [52].



2.5 Magnetic Nanoparticle as a Radiosensitizer

Radiation therapy is one of the most crucial therapeutic techniques for cancer treatment alongside surgery and chemotherapy. It entails the precise delivery of ionising radiation to tumour tissue, resulting in the destruction of tumour cells. The process of increasing the sensitivity of tumour tissues to radiation damage is known as radiation sensitization. Efficacy of radiation treatment can be increased using therapeutic or otherwise inert substances known as radiation sensitizers. Iron oxide nanoparticles, a type of magnetic nanoparticle (MNP), are amongst the nanomaterials which have been suggested as effective radiation sensitizers [53]. Magnetite (Fe_3O_4) or maghemite ($\gamma\text{Fe}_2\text{O}_3$) are the main components of superparamagnetic iron oxide nanoparticles (SPIONs). Superparamagnetic characteristics of these nanoparticles allow them to be aimed and localised to a specific organ using an applied magnetic field [54]. SPIONs are highly biocompatible with minimal toxicity to normal tissues and making them suitable for use in therapy [54]. These nanoparticles can cause cytotoxicity by producing reactive oxygen species (ROS) such as superoxide anion, hydroxyl radical, hydrogen peroxide, and hydroperoxyl radical which can damage DNA and other cell organelles [54, 55].

SPIONs attracted great attention as potential radiosensitizers in radiotherapy [56]. SPIONs shared similar intriguing properties with gold nanoparticles such as non-toxic, easy to synthesis, size variation and targeting structural modification [56]. In contrast to gold nanoparticles, SPIONs are relatively more cost effective and employ the unique superparamagnetic properties. SPIONs as an effective candidate were investigated pre-clinically in radiotherapy and results indicated the potential of SPIONs as multifunctional agents for cancer diagnostic and therapy [56].



References

1. Silva G A. Introduction to nanotechnology and its applications to medicine. *Surg Neurol*, 2004, 61, 216-20.
2. Nouailhat A. An Introduction to Nanoscience and Nanotechnology. 1st edition, John Wiley, New York, NY, USA, 2008.
3. Varadan V K, Chen L, Xie J. Nanomedicine: Design and Applications of Magnetic Nanomaterials, Nanosensors and Nanosystems. Wiley, London, UK, 2008.
4. Roco M C. Nanotechnology: convergence with modern biology and medicine. *Curr. Opin. Biotechnol*, 2003, 14, 337.
5. Jeevanandam J, Barhoum A, Chan Y S, Dufresne A, Danquah M K. Review on nanoparticles and nanostructured materials: history, sources, toxicity and regulations, *Beilstein J Nanotechnol*, 2018, 9, 1050-1074.
6. Iqbal M Z, Dar G I, Ali I, Wu A. Magnetic Nanomedicine. In: Xue X. (eds) *Nanomedicine in Brain Diseases*, Springer, Singapore, 2019.
7. K. Wu, et al. Magnetic nanoparticles in nanomedicine: a review of recent advances *Nanotechnology*. 2019, 30, 502003.
8. Chmykhalo V, Belanova A, Belousova M, Butova V, Makarenko Y, Khrenkova V, Soldatov A, Zolotukhin P. Microbial-based magnetic nanoparticles production: a mini-review. *Integrative Biology*, 2021, 13 (4), 98–107.
9. Heneweer C, Gendy S E, Penate-Medina O. Liposomes and inorganic nanoparticles for drug delivery and cancer maging. *TherDeliv*, 2012, 3, 645–656.
10. Durymanov M O, Rosenkranz A A, Sobolev A S. Current approaches for improving intratumoral accumulation and distribution of nanomedicines. *Theranostics*



- 2015, 5, 1007–1020.
11. Devarajan P V, Jindal A B, Patil R R, Mulla F, Gaikwad R V, Samad A. Particle shape: a new design parameter for passive targeting in splenotropic drug delivery. *J Pharm Sci*, 2010, 99, 2576–2581.
 12. Yu F, Yang V C. Size-tunable synthesis of stable superparamagnetic iron oxide nanoparticles for potential biomedical applications. *J Biomed Mater Res A*, 2010, 92, 1468–1475.
 13. Webster D M, Sundaram P, Byrne M E. Injectable nanomaterials for drug delivery: carriers, targeting moieties, and therapeutics. *Eur J Pharm Biopharm*, 2013, 84, 1–20.
 14. Akita H, Fujiwara T, Santiwarangkool S, Hossen N, Kajimoto K, El-Sayed A, Tabata Y, Harashima H. Transcytosis-targeting peptide: a conductor of liposomal nanoparticles through the endothelial cell barrier. *Small*, 2016, 12, 1212–1221.
 15. Yadollahpour A, Rashidi S. Magnetic nanoparticles: a review of chemical and physical characteristics important in medical applications. *Orient J Chem*, 2015;31(1), 25–30.
 16. Anuje M, Sivan A, Khot V M, Pawaskar P N. Cellular interaction and toxicity of nanostructures In: *Nanomedicines for Breast Cancer Theranostics*. Elsevier, 2020, 193–243.
 17. Murayama S, Nishiyama T, Takagi K, Ishizuka F, Santa T, Kato M. Delivery, stabilization, and spatiotemporal activation of cargo molecules in cells with positively charged nanoparticles. *Chem Commun (Camb)* 2012, 48, 11461–11463.
 18. Durymanov M O, Rosenkranz A A, Sobolev A S. Current approaches for improving intratumoral accumulation and distribution of nanomedicines. *Theranostics*, 2015, 5, 1007–1020.



19. Chouly C, Pouliquen D, Lucet I, Jeune JJ, Jallet P. Development of superparamagnetic nanoparticles for MRI: effect of particle size, charge and surface nature on biodistribution. *J Microencapsul*, 1996, 13, 245–255.
20. Shukla S, Jadaun A, Arora V, Sinha RK, Biyani N, Jain VK. In vitro toxicity assessment of chitosan oligosaccharide coated iron oxide nanoparticles. *Toxicol Rep*. 2015, 2, 27–39.
21. Dilnawaz F, Singh A, Mohanty C, Sahoo SK: Dual drug loaded superparamagnetic iron oxide nanoparticles for targeted cancer therapy. *Biomaterials*, 2010, 31, 3694– 3706.
22. Yoo J W, Chambers E, Mitragotri S. Factors that control the circulation time of nanoparticles in blood: challenges, solutions and future prospects. *Current pharmaceutical design*. 2010, 16, 2298–2307.
23. Kolhatkar A G, Jamison A C, Litvinov D, Willson R C, Lee T R. Tuning the magnetic properties of nanoparticles. *Int. J. Mol. Sci*. 2013, 14, 15977–16009.
24. Ito A, Shinkai M, Honda H, Kobayashi T. Medical application of functionalized magnetic nanoparticles. *J. Biosci. Bioeng*. 2005, 100, 1–11.
25. Williams HM. The application of magnetic nanoparticles in the treatment and monitoring of cancer and infectious diseases. *Biosci. Horiz. Int. J. Stud. Res*. 2017, 10.
26. Laurent S, Forge D, Port M, Roch A, Robic C, Elst L V and Muller R N. *Chem. Rev*. 2008, 108, 2064.
27. Gupta A K, Gupta M. Synthesis and surface engineering of iron oxide nanoparticles for biomedical applications, *Biomaterials*. 2005, 26(18), 3995-4021.
28. Kroft L J, Doornbos J, van der Geest R J, van der Laarse A, van der Meulen H, de Roos A. Ultra-small superparamagnetic particles of iron oxide (USPIO)



- MR imaging of infarcted myocardium in pigs. *Magn Reson Imaging*. 1998, 16(7), 755–63.
29. Kamada K, Houkin K, Hida K. et al. Localized proton spectroscopy of focal brain pathology in humans: Significant effects of edema on spin-spin relaxation time, *Magnetic Resonance in Medicine*. 1994, 31 (5), 537–540.
30. Kato H, Kanazawa Y, Okumura M. et al. Lanthanoid endohedral metallofullerenols for MRI contrast agents, *Journal of the American Chemical Society*. 2003, 125 (14), 4391–4397.
31. Qin J, Laurent S, Jo Y S. et al. A high-performance magnetic resonance imaging T2 contrast agent. *Advanced Materials*. 2007, 19 (14), 1874–1878.
32. Nelson N R, Port J D, Pandey M K. Use of Superparamagnetic Iron Oxide Nanoparticles (SPIONs) via Multiple Imaging Modalities and Modifications to Reduce Cytotoxicity: An Educational Review. *J. Nanotheranostics*. 2020, 1, 105-135.
33. Nitin N, LaConte L E W, Zurkiya O. et al. Functionalization and peptide-based delivery of magnetic nanoparticles as an intracellular MRI contrast agent, *Journal of Biological Inorganic Chemistry*. 2004, 9 (6), 706–712.
34. Tan H, Xue J M, Shuter B. et al. Synthesis of PEOlated $\text{Fe}_3\text{O}_4@ \text{SiO}_2$ nanoparticles via bioinspired silification for magnetic resonance imaging, *Advanced Functional Materials*. 2010, 20 (5), 722–731.
35. Li Y W. Preparation of magnetic resonance probes using one pot method for detection of hepatocellular carcinoma, *World Journal of Gastroenterology*. 2015, 21 (14), 4275–4283.
36. Gilchrist R K, Medal R, Shorey W D, Hanselman R C, Parrott J C, Taylor C B. Selective inductive heating of lymph nodes. *Ann. Surg*. 1957, 146, 596–606.



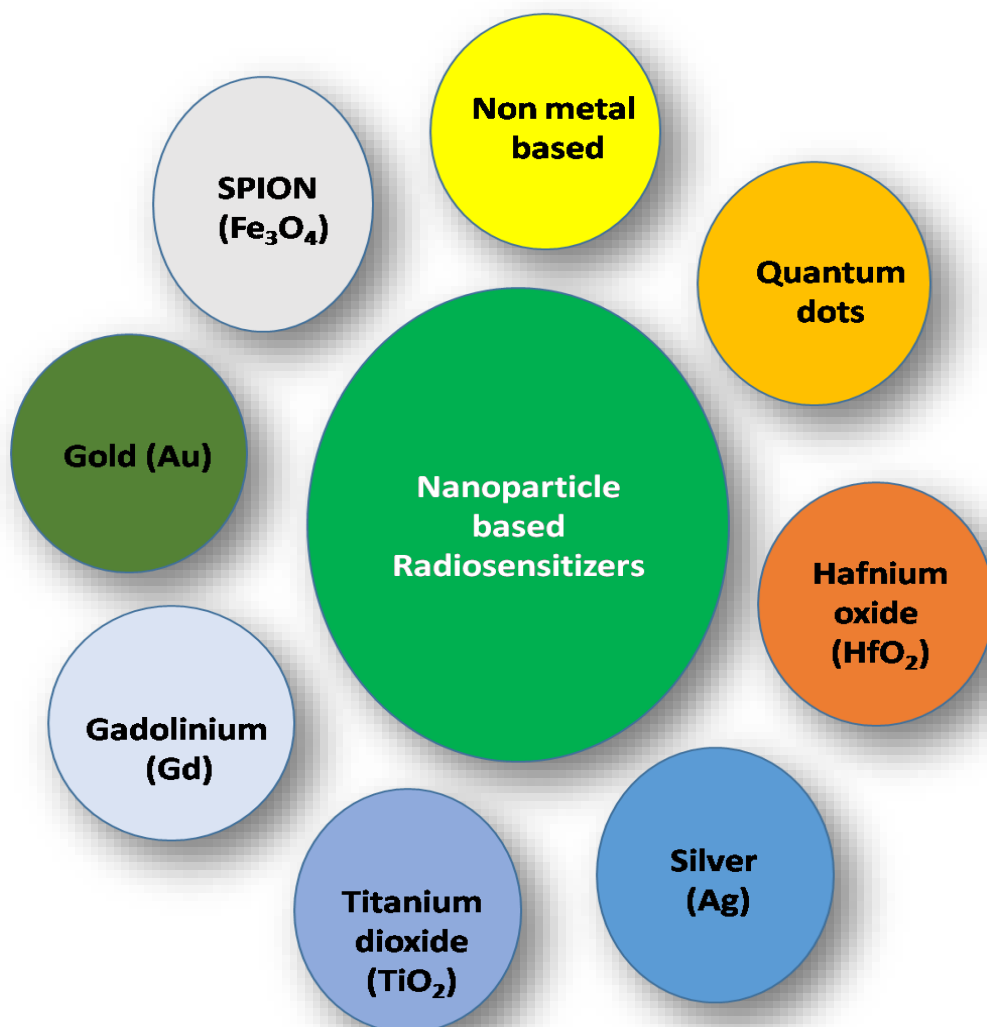
37. Lemine OM. Chapter 7 - Magnetic Hyperthermia Therapy Using Hybrid Magnetic Nanostructures, Editor(s): Raghvendra Ashok Bohara, Nanasaheb Thorat, In Micro and Nano Technologies, Hybrid Nanostructures for Cancer Theranostics. Elsevier, 2019, 125-138.
38. Brazel CS. Magneto Thermally-responsive nanomaterials: combining magnetic nanostructures and thermally-sensitive polymers for triggered drug release. *Pharmaceutical Res.* 2009, 26, 644–56.
39. Alison E D, Benjamin A E. Heating efficiency in magnetic nanoparticle hyperthermia *Journal of Magnetism and Magnetic Materials.* 2014, 354, 163-172.
40. Kötitz R, Fannin P C, Trahms L. Time-domain study of Brownian and Neel relaxation in ferrofluids, *Journal of Magnetism and Magnetic Materials.* 1995, 149 (1–2), 42–46.
41. Xiong F, Huang S, Gu N. Magnetic nanoparticles: Recent developments in drug delivery systems. *Drug Dev. Ind. Pharmacy.* 2018, 44 (5), 697–706.
42. <http://www4.ncsu.edu/~hubbe/Defnitns/DefnitnGIFs/Slide41.GIF>
43. Surface functionalizing SPM iron oxide NPs using nitrocatechol anchors. Ph.D. thesis submitted to Eth Zurich by E. Amstad, 2010, 27
44. http://www.woparticles.malvern.com/LabEng/industry/colloids/dlvo_theory.html
45. Sun C, Lee Jerry S H, Zhang M. Magnetic nanin MR imaging and drug delivery. *Adv Drug Deliv Rev.* 2008, 60, 1252 – 1265.
46. Jun Y W, Lee J H, Cheon J. Chemical Design of Nanoparticle Probes for High-Performance Magnetic Resonance Imaging. *Angewandte Chemie International Edition.* 2008, 47: 5122-5135.
47. Na H B, Song I C and Hyeon T. Inorganic Nanoparticles for MRI Contrast Agents. *Adv. Mater.* 2009, 21, 2133-2148.



48. Liese A, Hilterhouse L. Evaluation of immobilized enzymes for industrial applications. *ChemSoc Rev.* 2013, 42, 6236–6249.
49. Salunkhe A B, Khot V M, Pawar S H. Magnetic Hyperthermia with Magnetic Nanoparticles: A Status Review. *Curr. Top. Med. Chem.* 2014, 14, 572–594.
50. Kenneth J W, Andrew E S, David F R. Magnetically Responsive Microspheres and Other Carriers for the Biophysical Targeting of Antitumor Agents, Editor(s): Silvio GA. Goldin, FH, Kopin IJ, Schnitzer RJ. In *Advances in Pharmacology*, Academic Press. 1979, 16, 213–271.
51. Hao R, Xing R, Xu Z, Hou Y, Gao S, Sun S. Synthesis, Functionalization, and Biomedical Applications of Multifunctional Magnetic Nanoparticles. *Adv. Mater.* 2010, 22, 2729–2742.
52. Surface Functionalized Water-Dispersible Magnetite NPs: Preparation, Characterization and the Studies of Their Bioapplications. Ph. D. Thesis submitted to University of New Orleans by H. Qu, 2012, 15.
53. Kolhatkar K, Petryk A. Radiosensitization with Magnetic Nanoparticles, Department of Biomedical Engineering, University of Bridgeport, Bridgeport, CT.
54. Kwatra D, Venugopal A, Anant S. Nanoparticles in radiation therapy: a summary of various approaches to enhance radiosensitization in cancer. *Transl Cancer Res.* 2013, 2(4), 330–342.
55. Anuje M, Pawaskar P N, Khot V M et al. Synthesis and cytotoxicity evaluation of poly (ethylene) glycol coated iron oxide nanoparticles for radiotherapy application. *Journal of Medical Physics*, 2021, 46(3), 154–161.
56. Rahman W N, Kadian S N M, Ab Rashid R, Abdullah R et al. characteristic of superparamagnetic iron oxide nanoparticles in electron beam radiotherapy and brachytherapy, *IOP Conf. Series: J. Phys. Conf.* 2019, 1248, 012068

CHAPTER - 3

NANOPARTICLE BASED RADIOSENSITIZERS



3.1 Introduction to Radiosensitizer

Cancer is still one of the most serious threats to human health. According to the World Health Organization (WHO), cancer claimed the lives of 8.8 million people globally in 2015 and the International Agency for Research on Cancer (IARC) predicts that number would rise to 13 million by 2030 [1]. Radiotherapy, surgery, chemotherapy, targeted therapy, immunotherapy, hormone therapy, precision medicine and stem cell transplantation have all been developed in recent years to improve cancer therapy. Radiotherapy (RT) is one of the most significant and successful methods for killing or controlling malignancies [2, 3]. Marie Curie, a Nobel Laureate, was one of the first to deeply study radioactivity and its effects on human cells. Because it can cause varied DNA damage and cellular death in target regions (clinical and/or subclinical lesions), ionizing radiation is used as a therapeutic approach [4]. Cancer cells reproduce uncontrollably, they are more vulnerable to radiation-induced DNA damage [5]. More than 60% of cancer patients now receive radiotherapy as part of their anti-cancer treatment [6], which is delivered via a variety of modalities including as external beam (electrons, protons, photons) and brachytherapy (internal radioactive source). The manner in which it is used is determined by the clinical indications.

Cancer cells are exposed to high-energy photon radiation in radiotherapy (RT), such as gamma rays, X-rays and other radiations. Tumor cells and tissues were killed by either direct interaction or indirect interaction. Double strand breaks and single strand breaks occur in DNA as a result of direct radiation interaction, resulting in necrosis, apoptosis or even the termination of cell division and proliferation (As discussed in chapter 1 section 1.2). In the case of indirect action, radiation generates reactive oxygen species (ROS), which causes cellular stress, damage to

biomolecules and changes cellular signalling pathways. According to clinical studies, more than half of patients (roughly 70%) require RT, where specific radiation doses are delivered using controlled linear accelerators to a metastatic tumour or exact regions within the tumour [7]. Despite the fact that the above-mentioned novel technologies have substantially improved the therapeutic effect, hurdles such as tumor heterogeneity, cancer stem cells and damage to normal tissue make it difficult to cure tumors with RT alone. Radiosensitizers that can boost tumor tissue's radiosensitivity while reducing toxicity to normal tissue pharmacologically are expected to be an effective technique to improve RT.

Because of insufficient vascularization, many types of solid tumors have hypoxic cells. These cells are X-ray resistant. It's hypothesized that their high radio-resistance is to blame for certain radiation failures. One of the newest and most promising approaches to dealing with hypoxic cells is the use of oxygen-mimetic medicines. Because they are not used by the respiratory metabolism, these medicines will diffuse more rapidly from capillaries to hypoxic cells than oxygen. They then expose the hypoxic cells to X-rays while leaving the well-oxygenated normal tissues unaffected [8].

3.1.1 Classification of radiosensitizers

Radiosensitizers are chemicals that achieve greater tumour inactivation along with radiation than the additive effect of each modality would imply. Radiosensitizers were divided into five groups by G E Adams, a pioneer in the field of RT [8, 9]:

(1) Intracellular thiols (-SH) suppression

Bridges discovered that the chemical compound N-ethylmaleimide (NEM) sensitized irradiated bacterium cultures in 1960. While in some situations, less sensitization is observed for well-oxygenated bacteria, hypoxic cells are usually much more sensitive. NEM is used as an antioxidant in the rubber industry. SH compounds are naturally found in cells and act as radiation shields; however, removing these thiols through a chemical reaction with NEM may enhance sensitivity of radiation. It is undeniable that rapid reaction of NEM with SH compounds may contribute to the compounds sensitising effect [10]. However, investigations using a rapid mixing apparatus [11] have shown that sensitization of anoxic bacteria by NEM occurs when radiation exposure is carried out as soon as the sensitizer comes into contact with the cells. Because the short contact period is thought to be far too little for any chemical interaction within the SH groups and NEM, it was determined that quick radiation-chemical free-radical reactions are the major mechanism of NEM sensitization. Other SH compounds, such as neoarsphenamine [12], p-chloromercuribenzoate and iodoacetamide have shown to be effective sensitizers in vitro. Rapid mixing investigations [13] suggest that iodoacetamide's sensitizing effect is attributable to a cytotoxic material generated by radiation action on the sensitizer.

(2) Formation of cytotoxic substances by radiolysis of the radiosensitizer

In addition to iodoacetamide, a few additional chemicals have an apparent sensitising effect as a result of the production of cytotoxic products of radiation action on the sensitizer. The action of cupric ion (Cu^{2+}), which has been

demonstrated to be a very powerful hypoxic bacteria sensitizer [14] is of special interest here.

(3) Inhibitors of repair of biomolecules

It is now well documented that enzymatic mechanisms can naturally heal some of the damage caused by irradiation mammalian cells. Chemical substances that either inactivate enzyme systems that are responsible for repair function or modify lesions caused by the initial radiation in such a way that it cannot be repaired. This process is thought to be responsible for impact of drug like actinomycin D [15] and a recent study reveals that due to inhibition of repair mechanism, the sensitizing effect observed for 2, 4-dinitrophenol when irradiated on *Escherichia coli* mutant [16].

(4) Incorporation of thymidine analogs into DNA

The bromo derivative 5-BUdRs (Bromodeoxyuridine Sensitizing) activity necessitates its integration into the cell's DNA structure. It only works on dividing cell populations [9]. 5-BUdR is a synthetic nucleoside analogue having a thymidine-like molecular structure. BUdR can be integrated in place of thymidine in freshly generated DNA molecules of dividing cells during the S phase of the cell cycle (when DNA replication occurs) [17]. Unfortunately, when 5-BUdR is introduced, both well-oxygenated and hypoxic cells become sensitive. When 5-BUdR is included, the output of discrete radiation-chemical lesions increases, which might cause irreversible biological damage [18]. A mechanism of transport of electrons by long-range intramolecular distance has been suggested [19] and studies with 5-BUdR based on fast luminescence have shown that energy in some form can emigrate substantial lengths along the DNA chain [20].

(5) Oxygen mimics that have electrophilic activity

Oxygen mimetics have a stronger electron affinity and better diffusion qualities to anoxic tissue than oxygen because they use the chemical features of molecular oxygen as a template. Because oxygen mimetics can hypothetically substitute oxygen in “fixing” radiation-induced DNA damage, the damage becomes irreversible and thus fatal. As a result, oxygen mimetics are referred to as “true radiosensitizers.” Nitro-containing chemicals and nitric oxide (NO) are the most common oxygen mimics [21].

Radiosensitizers can be categorised into three categories depending on their architectures, according to current research: small molecules, macromolecules and nanomaterials [22]. Small molecules have dominated biomedical research until recently but the usage of bigger chemical structures, such as proteins or nanoparticles, has increased in recent decades, leading to spectacular and often unexpectedly innovative research [23]. Great strides have been made in understanding the laws that regulate cellular absorption, which reveal that the size of molecules has the greatest impact on cell internalization. Macromolecules like proteins and nucleic acids, for example, are rarely able to enter cells. Larger sizes of nanoparticles appear to enhance ingestion via endocytic pathways, allowing the particles to remain trapped in lysosomes and endosomes [23].

I) Small molecules (0.1-1nm)

Oxygen

One of the most problematic aspects of radiation therapy is hypoxia in the tumour microenvironment. In a hypoxic microenvironment, cancer cells are considerably

more radiation resistant than cancer cells in a normal oxygen microenvironment [1]. Through its particular electrical arrangement, oxygen, a potent radiosensitizer, aids in the creation of free radicals. Because oxygen is the most electrophilic biological molecule, the incident radiation's electrons can rapidly decrease it. After an oxygenated tumor is irradiated, energy transfer causes water to be radiolyzed, resulting in the creation of an ion radical, which subsequently interacts with another water molecule to generate the extremely reactive hydroxyl radical ($\text{OH}\cdot$). Following an interaction with the hydroxyl radical, oxygen produces peroxide. The peroxide then causes permanent DNA damage and cell death [1, 21].

More research is being done to tackle hypoxia problems, such as oxygen-carrying substitutes in blood and oxygen tanks to precise processes that proportionate variations in partial pressure of oxygen (PO_2) between malignancies and healthy tissue [24,25]. Kochi oxydol radiation therapy for unresectable carcinomas (KORTUC), a novel radiosensitizer, is being tested in a Phase I/II clinical trial (NCT02757651) for the treatment of malignant tumours [26].

Oxygen mimics

The oxygen effect's broad application led researchers to hunt for additional elements that might have a similar impact. Because oxygen is paramagnetic, nitric oxide (NO), an isoelectronic paramagnetic gas was examined and shown to be an effective sensitizer. Nitroxyl based, firstly introduced radiosensitizer, triacetoneamine-N-oxyl (TAN), proved to be successful [27]. More effective nitroxyl sensitizers have since been discovered, including 2, 2, 6, 6-tetramethyl-4-piperidinol-N-oxyl and norpseudopelletierine-N-oxyl [28].

Nitrobenzene is the prototypical electron-affinity radiosensitizer, followed by nitroimidazole and its derivatives [1]. Enzymatic and radiation-induced redox reactions occur in nitroimidazoles. These agents are inert by nature and their action is triggered only when ionizing radiation is used to "fix" or stabilize DNA radical lesions in oxygen-deficient cells [28]. Misonidazole, a 2-nitroimidazole, is one of the first nitroimidazoles to be produced.

Active compounds from chinese herbs

Curcumin, resveratrol, dihydroartemisinin, and paclitaxel are potent chemicals found in Chinese herbs that have recently been discovered to improve tumor sensitivity in radiation [1].

Small molecules range in size from 0.1 to 1 nanometer. This description encompasses a large percentage of currently used medical drugs. Small molecules can be designed to permeate cells through simple diffusion, which requires that they are at least partially soluble in the lipid bilayer. As a result, such tiny molecules are able to pass through biological barriers, penetrate cells and even gain access to cell organelles [23].

II) Macromolecules (10-1000nm)

Proteins and nucleic acids have the potential to be effective therapeutic agents for a variety of ailments. Due to their bulk, macromolecules cannot enter the cell membrane via simple diffusion, as tiny molecules can [23].

For example, short peptides and antibodies have a greater affinity for receptors and antigens, which are highly expressed on tumour surface, making them applicable as radiosensitizers [30]. HER3-ADC is a maytansine-based antibody-drug combination that inhibits DNA damage repair and hence increases radiosensitivity in HER3-positive pancreatic cancer cells [31]. MicroRNAs (miRNAs) are non-coding single-stranded RNA molecules with roughly 22 nucleotides that are encoded by endogenous genes. Some specific miRNAs have been discovered to boost radiation efficacy and can be exploited as radiotherapy sensitization targets, according to study [32, 33, and 34]. MiR-621, which targets SETDB1 in hepato-cellular carcinoma, can be utilized directly as a tumor radiosensitizer [35].

siRNA, also known as silencing RNA or short interfering RNA, is a type of noncoding RNA molecule with a double-stranded RNA molecule with a length of 20–27 base pairs, similar to miRNA, that operates through the RNA interference (RNAi) pathway [36]. HuR is a protein linked to radiation resistance, knockdown by siRNA, leading to DNA damage and increased radiosensitivity [37]. Oligonucleotides, like siRNAs, play an important function in gene expression regulation. Antisense oligonucleotides have a lot of potential as radiosensitizers since they are simple to design and make [38]. Telomerase is expressed in a wide range of cancers (>85%), however it is not found in normal tissues. In telomerase-positive tumour cells, radiolabeled oligonucleotides targeting the RNA subunit of telomerase were discovered to limit telomerase expression, resulting in DNA damage and cell death [39].

III) Nanoparticles (1-100nm)

Radiosensitizers have been identified in a wide range of chemicals and materials. Nanoparticles have made recent advances, allowing them to be proposed as new radiosensitizers. Nanoparticles (NPs) are particles with a diameter of 1 to 100 nanometers [40]. The cellular absorption of NPs must differ from that of molecules due to their relatively large size. NPs, for example, are actively absorbed into the cell via several endocytic pathways, whereas most molecules are unable to internalize cells efficiently on their own (*vide supra*) [23]. Engineered NPs have also been proposed to improve the cellular permeability of small molecules and proteins due to their effective absorption [23]. The rationale for this uptake ability is because NPs have a vast, highly energetic surface that can interact with biomolecules, such as those that make up the cell membrane [23].

Nanoparticles have more cell penetration and fewer side effects than conventional radio sensitizers (mentioned above) as well as a better enhanced permeability and retention (EPR) effect [41]. Multiple techniques have been proposed to increase the radiation dose to the tumor using nanoparticles, including metal-based nanoparticles (NPs), quantum dots, super paramagnetic iron oxides and non-metal-based NPs [42].

3.2 Introduction to Nano-radiosensitizer

Because of their excellent physical and chemical properties, such as the ease of synthesizing NPs with ideal sizes and components, their favorable biocompatibility and biodegradability and their specific targeting ability due to the enhanced permeation and retention effect (EPR) [43], nanoparticles have piqued the interest of researchers. Radiation sensitizers have provided innovative and valuable tools for

cancer imaging, diagnosis and treatment. To date, a wide range of NPs, including gold, iron, bismuth, titanium and carbon, have been used as potential tumor-selective radio-sensitizers. Various approaches used for radiosensitization have been listed in table 3.1 and figure 3.1.

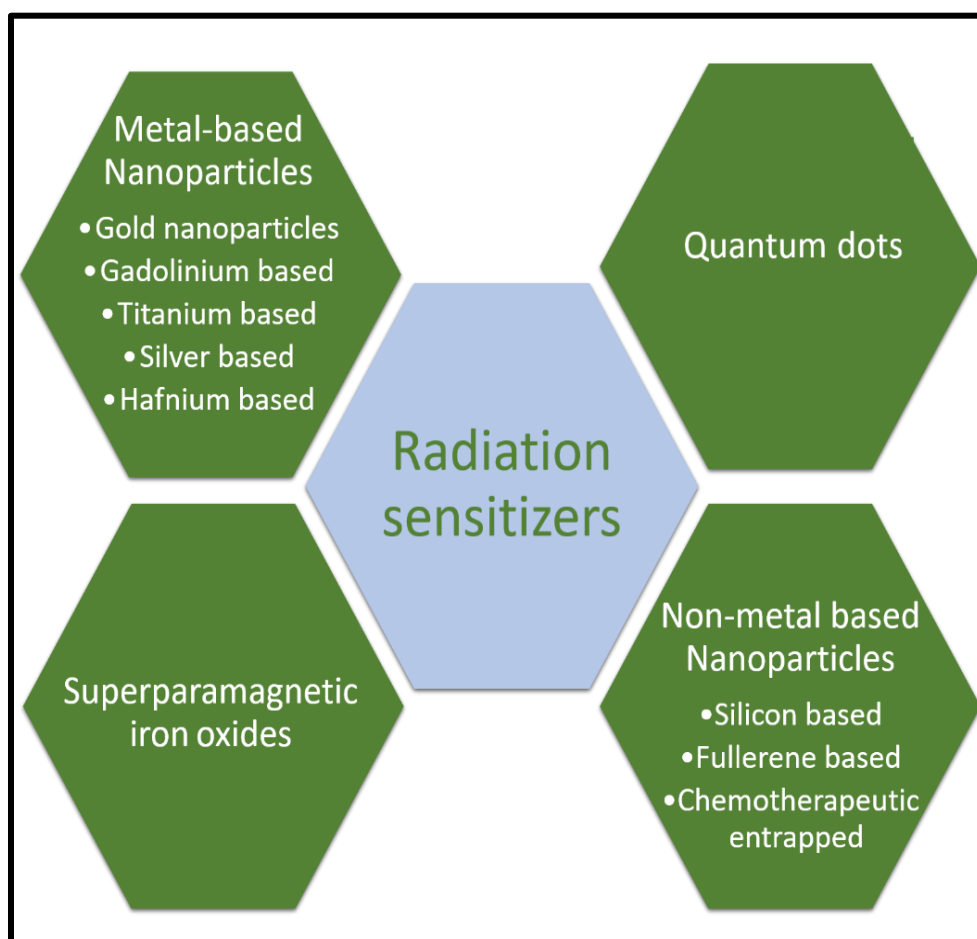


Figure 3.1 Classification of Radiosensitizers

Radiosensitizers are chemical or pharmacologic agents that increase cancer cells sensitivity to radiation. Ideal sensitizers should be able to selectively sensitize, be chemically stable and slowly metabolized, be effective throughout the cell cycle and



be effective at low daily radiation doses. The sensitizer enhancement ratio (SER) or dose enhancement factor (DEF) is most commonly used to describe the relative efficacy of a radiosensitizer to a specific cell. The SER and DEF are the dose ratios of radiation alone versus radiation plus cell sensitizer to produce the same biologic effect. If the SER values were greater than one, the combination of the agents was acting as a radiosensitizer. If they were less than one, the drug was classified as a radioprotector [43].

**Table 3.1** Various approaches of nanoparticle radiosensitizer

Reference	Nanoparticle	Size (nm)	Concentration	Radiation Source/Energy	Dose / Dose rate	Cell line	Outcomes (DMF/DEF/SER)
44	Au	50	0.2 mg/ml	^{125}I (28KeV)	2.1-4.5 cGy/h	HeLa	1.7-2.3
45	Gd	5	0.4-2 mMol	-	2 Gy	SQ20B	-
46	Ti	60	225 nMol	250 kV	0-3 Gy	RD, RH30, MCF7	-
47	Fe, Bi	10 & 30	100 mg/mL	40 kV	-	HeLa, MG-63	-
48	Au	30	0.8 mg	100 kV	11 Gy	MDA-MB-361	0.74
49	Au (PEG)	4.8-46.6	-	^{137}Cs	-	HeLa	-
50	Hf	50	64 g/l.	^{60}Co	4 Gy	HT1080	1.4
51	Au	1.9	10 $\mu\text{g/mL}$ - 2 mg/mL	160KV	3 Gy	DU145, MDA-MB-231, L132	-



52	Au (thio-glucose)	14	1 nM, 5 nM	90 KV, 6 MV	10 Gy	SK-OV-3 (HTB-77)	-
53	Au	5-13	4.2 mg	Electrons, 60 keV	-	DNA strand	-
54	Au	1.9	-	160 KVp, 6 MV, 15 MV, 6 Mev, 16 Mev	0-6 Gy	L132, DU145 MDA-MB-231	0.92- 1.41
55	Au (PEG)	50	1mM	6 MV	5 Gy	LNCaP	-
56	Gd (DTPA)	5	0.5 - 2 mM	6 MeV	2-8 Gy	U87	-
57	Au	-	-	200 KV	1- 10 Gy	NIH 3T3, DU-145, H460	1.65 and 1.23
58	Au (PEG)	6.1	400, 500 uM Or 1000 uM	6.5 keV, 45 kV, 160 kV, 6 MV, 3 MV (proton)	1-10Gy	EMT-6 CT26	-



59	Au	1.9	10 and 100 $\mu\text{g ml}^{-1}$	160 keV	-	DU-145 and PC-3, L-132, MDA-231-B and MCF-7, T98G AGO-1522B	-
60	Pt	3	18 μl	276 MeV/amu	0-260 Gy	DNA strand	1.63, 2.17
61	Au	2	1.0 mM/L	80 kV	10 Gy	BAECs	2
62	Au	37.5	3.3 1010, 1.65 109 mol/L	8, 24.4 and 49 keV	0-150 Gy	Hscen2 protein	-
63	Au	8 to 92	700 μL , 0.05 nM	14.8 to 70 keV	0-5 Gy	DNA solution	-
64	Au	1.9	0.125, 0.25, 0.5, 1.0 mM	80 kV, 150 kV, 6 MeV, 12 MeV	0-5 Gy	BAECs	1.4 to 24.6
65	Au (Glucose)	10.8	15 nM	^{137}Cs	2 Gy	DU-145	-



66	La (Cerium)	10-12	1.2 mg/mL	^{137}Cs	-	-	-
67	Au	13	10.72 nM (180 $\mu\text{g/mL}$)	200 kV	0-10 Gy	B16F10	-
68	Au (PEG)	4.7	500 μM	6 Mv	2 Gy	CT26	-
69	Au (Glucose)	1.9	5.5 $\mu\text{M/mL}$	$^{12}\text{C}^{6+}$ ion	0.9, 1.9, 2.8, 3.7 and 4.6 Gy	HeLa	1.39
				^{60}Co	1.8, 4.6, 7.4, 9.2 and 13.8 Gy.		1.52
70	Au	50	-	105 kVp, 220 kVp, 6 MV	2.3 Gy/min	HeLa	1.43



71	Au (Glucose)	13	5 nM	6 MV	10 Gy	A549	1.49
72	Au	1.9 & 15	10 mg /mL	50 keV	15 Gy	F98	1.92 & 1.40
73	Bi	50	0.5 mM	100 kVp	10 Gy		1.94
74	Au (PEG)	23	1 mM	150 kVp	4 Gy	U251	-
75	Ti	10	1 µg/ml	6 MV	0, 0.5, 1, 2, 5 and 10 Gy	SNB-19, U87MG	-
76	Fe (citrate)	3-20	0.1 mg Fe/mL	120 kVp	3 Gy	MCF-7	-
77	Si	3	6.4 µM	4 MV	1 Gy	C6	-
78	Au	5-250	-	100 kVp	1 -10 Gy	-	1.46, 7.68



79	Nanoparticle Conjugate	48	48 nM	6 MV	6 Gy– 10 Gy – 20 Gy-30 Gy	H460	-
80	Au (PEG)	28.9-47	10 μ M	-	5 Gy	A549, A431, RKO	-
81	CdSe (PEG)	2.1	-	6 MV	2 - 8 Gy	H460	-
82	Ce	6-8	50 μ g/ml	10 MV and 150 kVp	-	9L	-
83	TiO ₂ , ZnS:Ag, CeF ₃ , CdSe, CdTe	100	3.0 mg/ml	20-65, 20-90, 20-170, 20-160	1 - 5 Gy	HeLa	-
84	Au	1.9	1 mmol/L or 0.197 mg/mL	30–100 keV	-	Bovine aortic endothelial cells	1.3 -3.47
85	Si	1	0.1 mg/ml	-	3 Gy	MCF-7, 3T3	-



86	Au	05-10	0–100 µg/mL	⁶⁰ Co	10 Gy	HeLa	5.18
87	Au	2	2 µM	-	0, 2, 4 Gy	EC1	-
88	Ag	15.38	0.1 mM	6 MV	4 Gy	U251	-
89	Gd	2-5	0.5, 5.0, and 10.0 µg/mL	Carbon ion Radiation- 100 MeV/u,	0.5 and 2 Gy	A549, NH1299 and NH1650	1.10 (A549), 1.11 (NH1299) and 1.20 (NH1650)
90	CuO	-	10 µg/mL	6 MV	0, 2, 4, 6, and 8 Gy	MCF-7	-
91	FeO	9–12	100 mg/mL or 500 mg/mL	-	5 Gy	A549	-
92	ZnO	-	0-100 mg/ml	6 MV	3 Gy	SMMC-7721	-



93	PAA-TiO _x	50	-	150 kV	0-30 Gy	MIAPaCa-2 human pancreatic cancer cell line	-
94	Gd-doped ZnO	9	10 & 20 µg/mL	6 MV	2, 4, 6 and 8 Gy	SKLC-6 cells	1.47 & 1.61
95	Au-Bi ₂ S ₃	30-40	50 kV	-	6 Gy	HeLa, 4T1 cells and HUVECs	-
96	GQDs	~18	50, 100 and 200 µg/mL	-	3, 6 Gy	SW620 and HCT116	-
97	Ag	~20	0, 5, 10 and 15 µg/ml	UV-C	1 mW/cm ²	TK6	-
98	Bi ₂ S ₃ -MoS ₂	~50	200 µg mL ⁻¹	160 Kev	0, 2, 4, 6, and 8 Gy	L929	-
99	ZnO (SiO ₂)	80– 100	-	200 kVp	2, 4, 7 or 10 Gy	LNCaP, Du145	-
100	Fe ₃ O ₄ @ZnO	200	-	6 MV	3 Gy	SMMC-7721	-



101	TiO ₂ (PEG / Aminopropyl)	~30	0, 0.5, 1 and 4 mM	80 kV, 6 MV	0-8 Gy, 15/40 Gy	HaCaT, DU145	-
102	BaWO ₄ (PVP)	318 ± 72	3, 6, 12, 24, 48, 96, 192 µM	50 kV	5 Gy	4T1	-
103	TiO ₂ (Gd)	20	0.1 mg/mL	-	4 Gy	MCF-7	-
104	Au	30,50, 100	-	6MV	0, 2, 5, 7, 10 Gy	-	1.1, 1.17 and 1.12
105	Au (PEG-R8)	6.3±1.1	100, 200, 400, 800, 1,600 nM	6 MV	0,2,4,6,8, 10 Gy	LS180	1.13-1.59
106	Pd	~14	60 µg/mL	-	0, 2, 4, 6, and 8 Gy	MCF-7	1.54
107	Fe (Citrate)	6–25	0.1 mg/mL	6 MV	0,2,4,6,8 Gy	MCF-7 and MDAH-2447	1.49 and 1.39



108	Fe (Dextran & cross-linked dextran)	4.04 & 4.18	0-100 $\mu\text{g Fe mL}^{-1}$	73 keV	0.5, 1, 2, 4, 6, 8 and 10 Gy	HeLa	-
109	Fe (Dextran)	-	10, 40, and 80 $\mu\text{g/ml}$	6 and 12 MeV	0, 2, 4, 6, and 8 Gy	HeLa	1.13, 1.19, 1.25
						MCF 7	1.26, 1.28, 1.29
110	Ag (PEG)	18–45	17 $\mu\text{g/mL}$	320 kVp	0, 2, 4, and 6 Gy	HCT116 & HT29	1.18 & 1.125
111	Au	50	10, 20, 50 and 100 μM	9 MV	2, 4, 6 and 8 Gy	HT29	1.4
112	Fe ₃ O ₄ @Ag	10.59 \pm 1.07	Fe/Ag : 0/0, 0.77/0.26, 3.90/1.30, 7.73/2.60 and 70.30/23.60 $\mu\text{g/mL}$	6 MeV	0, 2, 4, 6 and 8 Gy	U251	1.8

3.3 Classification of Nanoparticle Mediated Radiosensitizers

3.3.1 Metal based radiosensitizers

In recent years, there has been a surge in interest in utilising formulations to boost radiotherapeutic effects, notably employing nanoparticles based on metals (such as gold) (41). The Photoelectric and Compton Effects enable metal nanoparticles which are densely packed to selectively absorb and/or scatter high-energy radiation. The photoelectric effect is determined by $(Z/E)^3$, where Z is the atomic number of the targeted molecule and E is the energy of the incoming photon. The emission of scattered photons, photoelectrons, Compton electrons, auger electrons and fluorescence photons target the tumour cells. Photoelectron scattering, which occurs when photons are irradiated on metal surfaces, has also been postulated as a mechanism for enhanced activity. When all of these characteristics are combined, the therapeutic radiation dose is reduced resulting in minimal damage to healthy tissue. Nanoparticle Enhanced X-ray Therapy or NEXT, is a term used to describe the use of nanomaterial radiosensitizers.

Gold is ideal for photosensitization reactions because it has a high atomic number ($Z=79$) and is very inert to interact with tissue. Figure 3.2 summarises the interaction of radiation with high- Z nanoparticles and the outcomes. Gold nanoparticles are highly biocompatible and by attaching targeting moieties such as antibodies, improve the radiation effect over a larger tumor area. Other properties of gold nanoparticles include the ability to deliver a large number of gold atoms to tumor tissue with ease, the ability to vary the size or shape of gold nanoparticles in order to obtain a better therapeutic approach, the ability to be well absorbed into systemic circulations for better permeation into tumor tissue and a lower rate

of clearance [41]. Along with these benefits, there are also downsides to using gold nanoparticles, such as the high cost of material and formulation [41].

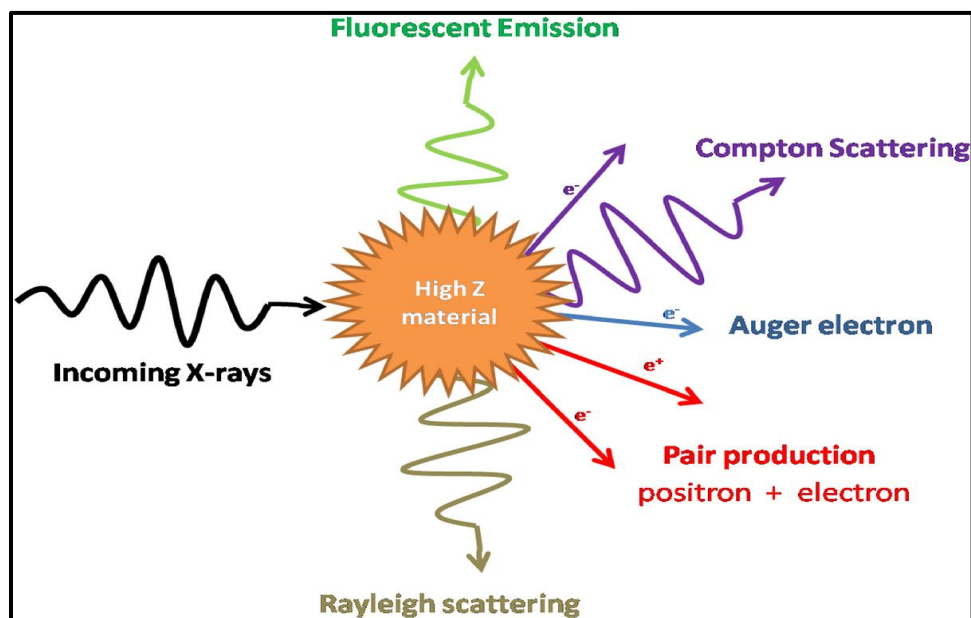


Figure 3.2 Different Interaction of X-rays with high-Z material nanoparticles [41]

Gadolinium (Gd, $Z=64$) was discovered to be a novel type of radiation sensitizer that could also be utilized in magnetic resonance imaging. When exposed to hydrated electrons, it creates pi-radical cations with greater circulation time. It was observed to be a good sensitizer when in vitro study was carried out on HT-29 cells and mouse mammary cancer model [43]. Gadolinium neutron capture treatment (NCT) is a therapeutic approach for cancer therapy that uses the "Gadolinium neutron capture reaction" generated by thermal neutron irradiation. This process produces long-range gamma rays, internal conversion electrons, X-rays and Auger electrons with increased total kinetic energy. The efficacy of this cancer therapy was tested using Chitosan nanoparticles coated with Gadolinium-157. This formulation was

administered intratumorally into mice with subcutaneous melanoma, followed by thermal neutron irradiation. Mice given the Gd nanoparticle exhibited a significantly better therapeutic response than mice given the gadolinium solution alone [113].

Titanium dioxide has also been demonstrated to be useful in photo catalytic chemistry for destroying cancer cells (39). Its mode of action is based on the formation of reactive oxygen species in response to UV radiation photo excitation. The substance is less effective for deep-seated tissues due to the low penetration depth of UV radiation. Titanium nanoparticles containing gadolinium were created and further improved with additional rare earth metals to make them more sensitive to X-ray based stimulation [114].

Radiosensitizing capabilities of silver nanoparticles ($Z=47$) are similar to those of gold nanoparticles. Silver nanoparticles, like other high-atomic-number atoms, use comparable modes of action for radiosensitization effects. They are less biocompatible than gold nanoparticles but they are less expensive. For cancer radiation therapy, silver nanoparticles have been used alone or in conjunction with other metal oxides such as Fe_3O_4 [41].

Other rare earth metals and high- Z elements, such as hafnium oxide (HfO_2), have been used to make nanoparticles. Photo-luminescent characteristics of HfO_2 have been discovered. They cause biological components to be damaged by heat stress [41].

3.3.2 Quantum dots in radiosensitization

In the early 1980s, quantum dots were found. They are nanocrystals constructed of semiconductor materials that, due to their small size, exhibit quantum mechanical features. Their semiconductor properties are inferior to those of bulk semiconductors. As radiosensitizers, quantum dots composed of CaF, LaF, ZnS, or ZnO have been recommended [41]. A prominent issue of discussion has been the development of photosensitizing quantum dots [41]. The quantum dot's mechanism of action is based on the idea that when visible light is absorbed by them, radicals are produced. The therapy's total adverse effects are dramatically reduced because these light waves are significantly less harmful than X-rays. The fundamental drawback of this technology is that visible light waves have a short penetration depth, therefore therapies based on these processes will only be successful for surface cancers [115].

3.3.3 Nonmetal based radiosensitizers

Silica is used as a coating medium for most nanoparticles containing heavy metals for radiosensitization, such as FeO_4 , gold or multicomponent cores [41]. Furthermore, silica-only nanoparticles have been studied for their possible function in radiosensitization.

C60 is a fullerene with a distinctive globular structure made up of 32 separate member rings and 60 carbon atoms that was found in the early 1990s. In cancer cells, fullerene C60 activates particular autophagy markers and possesses potent anti-cancer activities [116]. Because it is exceedingly poisonous to normal tissues, its therapeutic utility is limited [117]. Researchers used quantities that were non-toxic

to healthy cells to investigate the effect of nanocrystals of underivatized fullerene C60 (Nano-C60) on radiosensitization.

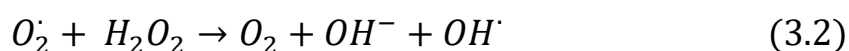
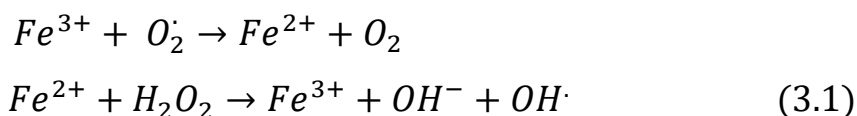
To work as radiosensitizers, polymeric nanoparticles have been made utilizing a variety of chemotherapeutic drugs, either alone or in combination. Paclitaxel is a potent chemotherapeutic drug that is also known to be a radiation sensitizer that is unique to the cell cycle [118]. This is because it halts cell cycle progression at G2/M, the most vulnerable stage of the cell cycle to radiation damage. Etanidazole, on the other hand, is a nitroimidazole hypoxic radiosensitizer. Other chemotherapeutic agents, such as cisplatin, doxorubicin have been employed as radiosensitizers as well [41].

3.3.4 Superparamagnetic iron oxide nanoparticles (SPION) as a radiosensitizers

Typically, iron oxides nanoparticles, one of commonly used compounds for biomedical applications such as contrast agents for magnetic resonance imaging (MRI), Colloidal mediators for cancer magnetic hyperthermia, targeted drug delivery and cell separation techniques [119]. SPIONs have many favorable features due to which their use in diagnosis and therapy arises including; physically and chemically stable, environmentally safe, cheapness, ease of synthesis, biocompatibility, reproducibility in wide range of diameters, applicability to be coated with variety of surface coatings and ability of tumor specific cytotoxic heating when excited by external alternating magnetic field (AMF) [120]. However, when superparamagnetic iron oxide nanoparticles (SPIONs) reach smaller sizes (about 10–20 nm for iron oxide), superparamagnetic properties become evident, so

that the particles achieve a better performance for most of the aforementioned applications [119]. Superparamagnetic enables to guide SPIONs to tumor area by using external inhomogeneous magnetic field while biocompatibility allows for their medical application [120].

Because cancer cells are more susceptible to oxidative insults than normal cells due to their rapid proliferation and metabolic activity, so additional ROS stress induced by external agents can overwhelm the relatively low antioxidant capacity of cancer cells, disrupting redox homeostasis and causing tumour cell toxicity [121]. Hematite (Fe_2O_3), maghemite (Fe_2O_3) and magnetite (Fe_3O_4 ; Iron (II, III) Oxide) are three natural varieties of SPIONs [119]. Based on cytotoxicity evolution and its composition, Fe_3O_4 found to be cytotoxic as it containing Fe^{2+} ions and help in the formation of reactive oxygen species (ROS) such as hydroxyl radical (60% - 90% of all DNA lesions), superoxide anion, hydrogen peroxide, and hydroperoxyl radical (e.g. $\text{OH}\cdot$, O_2^- , H_2O_2 , $\text{HO}_2\cdot$), which provides oxidative stress [119]. From the interaction between superoxide and hydrogen peroxide, the Haber-Weiss process produces the extremely reactive hydroxyl radical. This reaction is thermodynamically unfavorable in biological systems and it was discovered that it requires a catalyst to proceed in aqueous solution with a second order rate constant of zero [121]. The iron-catalyzed Haber-Weiss reaction, which employs Fenton chemistry (Iron catalyzed oxidation process in which highly reactive radicals are formed from hydrogen peroxide) is now widely regarded as the most important mechanism for the generation of highly reactive radicals in biological systems [121]. The Fenton chemistry reaction set is shown as equation 3.1, and the Haber-Weiss reaction (net reaction) is shown as equation 3.2.



Once iron oxide nanoparticles enter the cell, they stimulate the production of ROS via one of two mechanisms: either the release of iron ions into the cytosol, where chelation (type of bonding of ion or molecule to metal) occurs, resulting in the iron ions participating in the Haber-Weiss cycle or the surface of the iron oxide nanoparticle may act as a catalytic site [120,121].

Efficacy of radiation therapy can be increased, with use of SPIONs nanoparticles as a sensitizer. Radiation therapy promotes leakage of electrons from the electron transport chain of the mitochondrial inner surface. This leakage of electrons forms superoxide anion ($O_2 \cdot^-$). Once generated, $O_2 \cdot^-$ is dismutated to hydrogen peroxide (H_2O_2) by superoxide dismutase. Iron oxide nanoparticles can then catalyze the reaction from hydrogen peroxide to the highly reactive hydroxyl radical [119, 91].

Interaction of radiation with nanoparticles involves ejection of electrons and scattered photons via Photoelectric and Compton Effect. Interaction of these electrons may be direct or indirect (as shown in Fig. 3.3). In Indirect action these electrons produce ROS which in turn attack on DNA to kill cancer cells. Indirect action accounts for around two-thirds of the biological damage produced by radiation [119]. The formation of reactive oxygen species (ROS) by SPIONs with radiation improves the therapeutic effectiveness of radiotherapy.

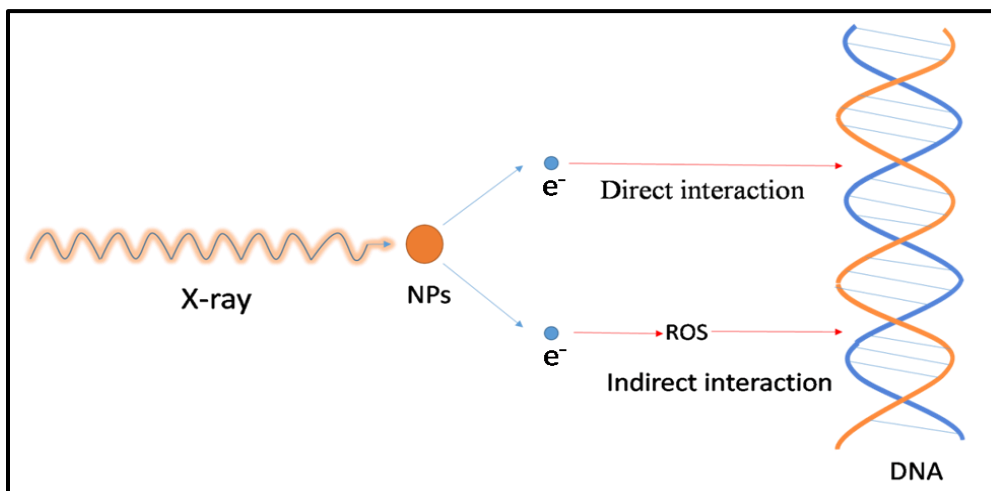


Figure 3.3 Illustration of mechanism of radiation damage (DNA damage) directly or indirectly in presence of nanoparticles

3.4 Different Methods for Assessment of Radiosensitization

Radiosensitization has been assessed using a variety of tests and quantitative approaches. Of which some are discussed below.

3.4.1 Different approaches for assessment of nano-radiosensitization from cell survival data

The clonogenic (or colony formation) assay, developed by Puck and Markus nearly 60 years ago [122], is the most widely used method in radiobiology for determining treatment efficacy. This in vitro approach evaluates the potential of a single cell to expand into a colony, i.e., to multiply indefinitely, in order to measure the cytotoxicity of radiation. A cell is radiobiologically dead if its reproductive viability to produce progeny has been lost [122]. This sort of test has become the most widely used method for assessing the radiosensitivity of various cell lines and it is assumed the "gold standard" in the field. The survival fraction (SF) (colonies generated post

treatment) is plotted as a function of radiation dose (D) in colony formation experiments [122]. The clonogenic assay has long been used to assess cell radiation survival. It is a well-established standard but it is also complicated and time-consuming [123].

Other techniques for determining the survival fraction have been developed, such as the trypan blue exclusion test and methylthiazol-tetrazolium (MTT) assay. MTT assay is superior to other varieties because it is simple to use, safe, reliable and it is extensively used to measure cell viability and cytotoxicity studies [124]. A linear-quadratic (LQ) model is used to fit the survival data experimental curve, which is represented by equation 3.3.

$$SF = e^{(-\alpha D - \beta D^2)} \quad (3.3)$$

Where SF is the fraction of surviving cells, α and β are linear and quadratic parameters of the model respectively and D is the radiation dose delivered [122].

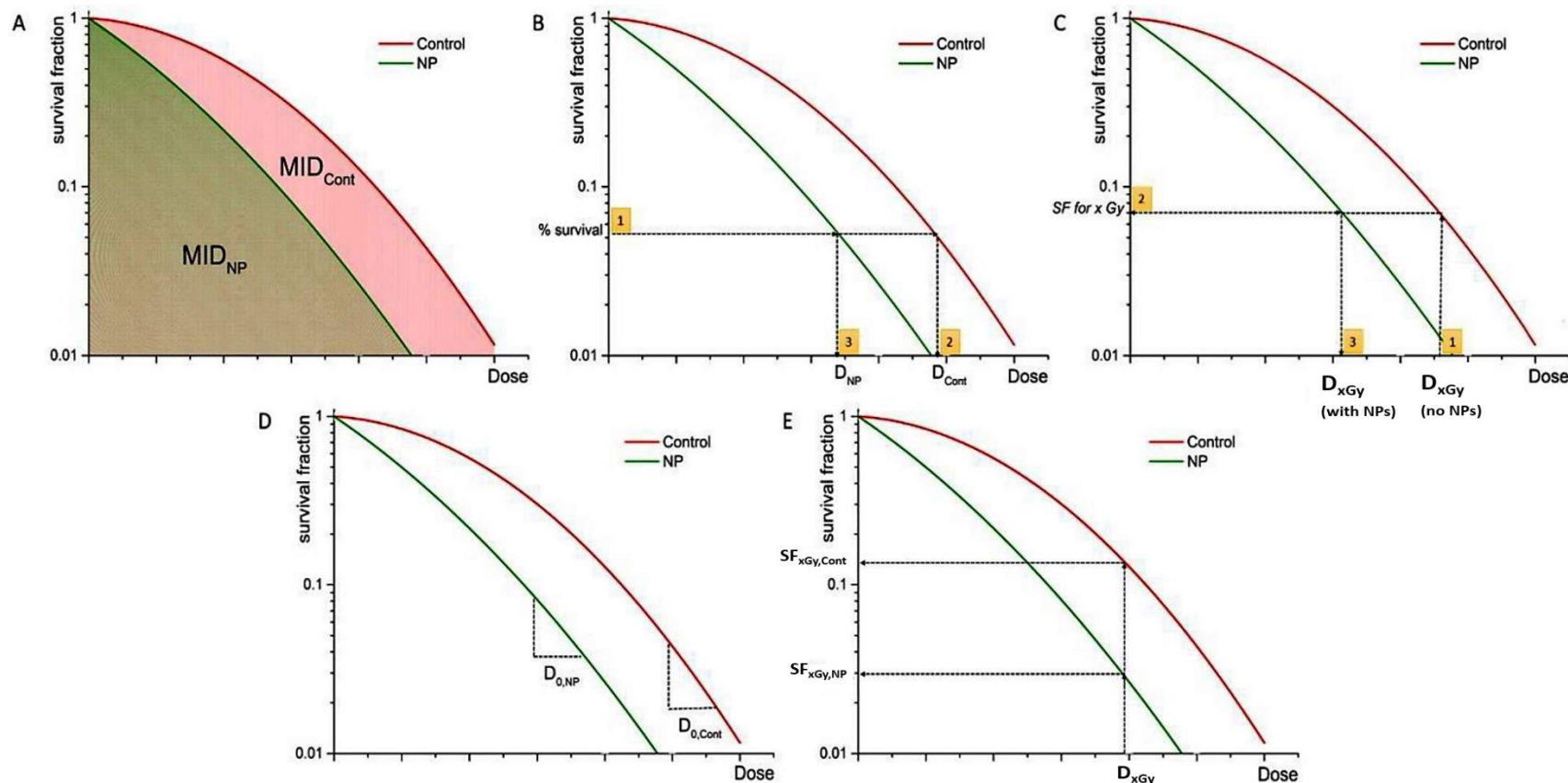


Figure 3.4 The following equations were used to compute the NP-mediated radiation enhancement effect using cell survival data: (A) $SER_{NP} = MID_{Cont} / MID_{NP}$; (B) $DMR_{x\%} = D_{Cont} / D_{NP}$ at $x\%$ effect: (1) percent survival is chosen, (2) dose D_{Cont} is assessed, and (3) dose D_{NP} for the same percent survival is assessed. (C) $DEF_x = D_{x,Gy} \text{ (no NPs)} / D_{x,Gy} \text{ (with NPs)}$ is calculated using the following procedures to estimate the SF level: (1) $D_{x,Gy} \text{ (no NP)}$ is chosen, (2) SF at $D_{x,Gy} \text{ (no NP)}$ is assessed, and (3) $D_{x,Gy} \text{ (with NPs)}$ is calculated; (D) $REF = D_{0,NP} / D_{0,Cont}$; (E) $RER_{xGy} = SF_{xGy,Cont} / SF_{xGy,NP}$ [122].

3.4.1.1 Quantification of radiosensitization by mean inactivation dose (MID)

The Mean Inactivation Dose (MID) is a method for comparing survival curves using a single parameter that takes the entire survival curve into account. Kellerer and Hug [125] were the first to propose the MID theory. For a given nanoparticle concentration, several authors calculated the ratio of MIDs of non-exposed cells to MIDs of nanoparticle exposed cells, which they called the quantity sensitizer enhancement ratio (Fig. 3.4A) (SER_{NP}).

$$SER_{NP} = \frac{MID_{Cont}}{MID_{NP}} \quad (3.4)$$

The subscripts NP and Cont stand for nanoparticle and control (radiation alone) survival curves, respectively. The MID approach has various advantages, including being representative of the entire cell population, minimizing survival curve volatility and taking into consideration the entire survival curve. As a result, MID appears to be a useful measure for determining the intrinsic radio-sensitivity of biological cell systems and it is supported by ICRU Report 30 [126].

3.4.1.2 Quantification of radiosensitization in terms of alpha and beta parameters

The LQ model's linear (α) and quadratic (β) parameters could be utilized to characterize the nanoparticle enhancement effect more broadly. Although these characteristics are frequently stated in the majority of NP radiobiological studies [127], not all of them describe the difference in α and β for irradiations with and without NPs, qualitatively or quantitatively. Despite the fact that the LQ model is

phenomenological, the alpha parameter is commonly connected with the production of complicated deadly DNA damage, whilst the beta parameter is related with the formation of sub-lethal lesions. The α/β ratio is a commonly used measure in radiotherapy to determine a sample's innate radiosensitivity. Assessing the change of the α/β parameter would be beneficial for assessing the radiobiological impact of specific NPs, assuming that NPs interfere with cellular repair mechanisms. Any changes in the system's radio-sensitivity caused by the NPs would be indicated by changes in the α/β ratio. At this time, no investigation or study has used this technique [122].

3.4.1.3 Quantification of radiosensitization in terms of dose modifying ratio ($DMR_{x\%}$)

The Dose Modification Ratio (DMR) is also suggested by the ICRU Report 30 as a metric to evaluate discrepancies between survival curves (Fig. 3.4B). This is defined as the ratio of the dose required to produce the same effect (x %) under reference conditions:

$$DMR_{x\%} = \frac{D_{Cont}}{D_{NP}} \text{ (for } x\% \text{ survival)} \quad (3.5)$$

Although the DMR may be effect-dependent, it still necessitates a complete set of survival data as well as the use of a cell survival model that is tailored to the experimental data. When two dose responses are associated by a constant factor on the dose scale, the dose modification ratio (DMR) is defined as the dose modification factor (DMF) [122].

DMR at the 2 Gy survival level (SF2)

The early slope of the survival curve (rather than the ultimate slope) has been demonstrated to correspond well with clinical outcomes in previous research. The survival level at a dose of 2 Gy, known as SF₂, is thought to best define this initial portion of the survival curve. The typical individual dose of traditional radiotherapy fractionation delivery is also 2 Gy. As a result, several writers [128] examining nanoparticle efficacy in vitro have used this quantity to determine the survival threshold at which the DMR should be calculated. Although less common, using such an approach, a Dose Enhancement Factor (DEF) (Fig. 3.4C) has been defined as the ratio of doses which lead to the same levels of cell survival as a particular dose delivered to the control sample (e.g., 2 Gy).

$$DEF_{xGy} = \frac{\text{Dose of } x \text{ Gy (no NP)}}{\text{The dose required to achieve the same SF in test sample (with NP) as in control samples (with } x \text{ Gy)}} \quad (3.6)$$

3.4.1.4 Radiation enhancement factor (REF) using the multi-target model

The multi-target model, which was created to handle the straight portion of the high dose region of the survival curve and is provided by the following equation, provides an alternative technique for measuring the radiobiological effect of NPs:

$$SF(D) = \left[1 - \left(1 - e^{-\frac{D}{D_0}} \right)^n \right] \quad (3.7)$$

D₀ (the dosage necessary to reduce cell survival to 37 percent of its initial value at any point on the final near exponential portion of the curve) and the extrapolation

number n in this model explain the slope of the survival curve (a measure of the width of the shoulder). Using the multi-target single hit ($n=1$) paradigm, Cui et al. [129] defined the radiosensitivity enhancement factor (REF) (Fig. 3.4D) as the ratio of the D_0 factors for the NP and control exposures:

$$REF = \frac{D_{0,NP}}{D_{0,Cont}} \quad (3.8)$$

In contrast to DMR and the previously described approaches, the parameter associated with the reference radiation appears in the denominator when evaluating such radiosensitization factors. The multi-target model appears to provide a better explanation of experimental data than the linear-quadratic model in assessing the NP effect for high dosage levels. Cui et al. [129] are the only ones who have used this method so far.

3.4.1.5 Radiation enhancement ratio (RER/SER)

Instead of researching and defining radiobiological concepts on an isodose basis, which would require the ratio of effects, all radiobiological concepts have been examined and defined on an iso-effect basis, which requires the ratio of doses (well defined for all radiation types). Many researchers have established that comparing the different degrees of effects following a specific radiation dose for describing the radiobiological effect of NPs. As a result, the Radiation Enhancement Ratio (RER_{xGy}) (Fig. 3.4E) has been defined as the ratio of survival fractions without NPs to those with NPs for a given dose:

$$RER_{xGy} = \frac{SF_{xGy,Cont}}{SF_{xGy,NP}} \quad (3.9)$$

Although confined to cell survival studies, this method of evaluation has the advantage of immediately illustrating the degree of variance in the biological response generated by NPs at a certain dose level. Such a strategy necessitates a precise measurement of the dosage absorbed in the presence of NPs and presupposes that the radiation quality remains unchanged. RER_{xGy} has been referred to as a sensitizer enhancement ratio (SER) or a dose enhancement factor (DEF) in the literature [122].

3.4.2 Monte Carlo in radiosensitization studies

High-Z NPs have a greater photoelectric absorption coefficient than water or soft tissue, making them a possible dosage enhancer. While in vitro experiments show that Au-NPs have radiosensitizing characteristics, the level of radiosensitization predicted from mass-energy absorption and NP concentration [130] appears to differ from the observed experimental findings. According to macroscopic theoretical projections based on the ratio of the mass-energy absorption coefficients of gold and soft tissue, adding 1% of gold by mass to the tumor after exposure to a keV photon source roughly doubles the dosage received [131]. Experimental data, on the other hand, demonstrates that far smaller amounts of gold nanoparticles are required to achieve effects equivalent to twice the absorbed dose, underscoring the limitations of macroscopic theoretical models.



There are numerous methods for determining the dosage distribution as a result of a certain irradiation and NP combination at the micrometer and nanoscale level. The majority of theoretical research exploring radio-sensitizing effects of high-Z nanoparticles uses Monte Carlo methods to analyse dose distributions and predict radiosensitization effects. These methods, which are based on computed cross-sections for a variety of physical interactions, are used to model individual photon and electron interactions with matter in a probabilistic manner. Modeling all of the interactions between the primary and secondary particles allows us to accurately predict dose depositions down to the micrometre and nanometer level. This provides a more accurate image of nanoparticles' impact on dosage absorption, as well as a valuable tool for analysing changes in biological efficiency as a function of the complexity of DNA lesions [122].

Several specific Monte Carlo packages have been used to investigate high-Z nanoparticle radio-enhancement, including EGSnrc [132], Geant4 [133], PENELOPE, MCNP5, MCNPX, and NORTEC. These MC simulations used simplified geometries and produced preliminary data that might be used to support high-Z nanoparticle irradiation. Aside from the mismatch between theoretical and experimental data already discussed, there is significant heterogeneity among Monte Carlo experiments undertaken by different groups. This is due to the high requirement for exact input parameters, which are usually derived from experimental data [122], as well as the complexity of MC simulations.



References

1. Gong L, Zhang Y, Liu C, Zhang M, Han S. Application of Radiosensitizers in Cancer Radiotherapy. *Int J Nanomedicine*. 2021, 16, 1083-1102.
2. Barcellos-Hoff M H, Park C, Wright E G. Radiation and the microenvironment—tumorigenesis and therapy. *Nat Rev Cancer*. 2005, 5(11), 867–75.
3. Bernier J, Hall E J, Giaccia A. Radiation oncology: a century of achievements. *Nat Rev Cancer*. 2004, 4(9), 737–47.
4. Jackson SP, Bartek J. The DNA-damage response in human biology and disease. *Nature*. 2009, 461(7267), 1071–8.
5. Baskar R, Lee K A, Yeo R, Yeoh K W. Cancer and radiation therapy: current advances and future directions. *Int J Med Sci*. 2012, 9(3), 193–9.
6. Schaue D, McBride W H. Opportunities and challenges of radiotherapy for treating cancer. *Nat Rev ClinOncol*. 2015, 12(9), 527–40.
7. Ge Y, Wu Q J. Knowledge-based planning for intensity-modulated radiation therapy: a review of data-driven approaches. *Med Phys*. 2019, 46(6), 2760–2775.
8. Fowler J F, Adams G E, Denekamp J. Radiosensitizers of hypoxic cells in solid tumors. *Cancer Treat Rev*. 1976, 3(4), 227–256.
9. Adams G E. Chemical radiosensitization of hypoxic cells. *Br Med Bull*. 1973, 29(1), 48–53.
10. Tallentire A, Jacobs G P. Radiosensitization of Bacterial Spores by Ketonic Agents of Differing Electron-affinities, *International Journal of Radiation*



- Biology and Related Studies in Physics, Chemistry and Medicine. 1972, 21(3), 205-213.
11. Adams G E, Cooke M S, Michael B D. Rapid-mixing in radiobiology. *Nature*, 1968, 219, 1368-1369.
 12. Kligerman M M, Schulhof L. Sensitization of bacteria to X-ray by Neoarsphenamine. *Radiation Res.* 1969, 39, 571–579.
 13. Dewey D L, Michael B D. The mechanism of radiosensitisation by iodoacetamide, *Biochemical and Biophysical Research Communications*. 1965, 21(4), 392-396.
 14. Cramp WA. The Toxic Action on Bacteria of Irradiated Solutions of Copper Compounds. *Radiat Res.* 1967, 30 (2), 221–236.
 15. Elkind M M. Whitmore G F, Alescio T. Actinomycin D-Suppression of recovery in x-irradiated mammalian cells. *Science*. 1964, 143, 1454-1457.
 16. Van der Schueren E, Smith K C, Kaplan H S. In: Abstr. Ann. Meet. Radiat. Res. Soc., Portland, Oregon, 1972.96-97.
 17. Kee N, Sivalingam S, Boonstra R, Wojtowicz J M. The utility of Ki-67 and BrdU as proliferative markers of adult neurogenesis. *Journal of Neuroscience Methods*. 2002, 115 (1): 97–105.
 18. Kaplan H S (1970) In: Moroson, H, Quint U M. Radiation protection and sensitization, pp. 35-42. (Proceedings of the Second Symposium on Radiosensitizing and Radioprotective Drugs, Rome, 6-8 May 1969) Taylor & Francis, London
 19. Adams G E. The general applications of pulse radiolysis to current problems in radiobiology. *Current Topics Radiat. Res.* 1967, 3, 37–93



20. Fielden E M, Lillicrap S C (1970) In: Moroson, H. & Quintiliani, M., ed. Radiation protection and sensitization, pp. 81-86. (Proceedings of the Second Symposium on Radiosensitizing and Radioprotective Drugs, Rome, 6-8 May 1969) Taylor & Francis, London
21. Oronsky B T, Knox S J, Scicinski J. Six degrees of separation: the oxygen effect in the development of radiosensitizers. *Transl Oncol.* 2011, 4(4), 189–198.
22. Wang H, Mu X, He H, Zhang X D. Cancer radiosensitizers. *Trends Pharmacol Sci.* 2018, 39(1), 24–48.
23. Mosquera J, García I, Liz-Marzán LM. Cellular uptake of nanoparticles versus small molecules: a matter of size. *Acc Chem Res.* 2018, 51, 2305–13.
24. Cabrales P, Intaglietta M. Blood substitutes: evolution from noncarrying to oxygen- and gas-carrying fluids. *ASAIO J.* 2013, 59 (4), 337–354.
25. Hardavella G, Karampinis I, Frille A, Sreter K, Rousalova I. Oxygen devices and delivery systems. *Breathe (Sheffield, England).* 2019, 15 (3), e108–e116.
26. Ogawa Y, Kubota K, Ue H, et al. Phase I study of a new radiosensitizer containing hydrogen peroxide and sodium hyaluronate for topical tumor injection: a new enzyme-targeting radiosensitization treatment, Kochi oxydol-radiation therapy for unresectable carcinomas, type II (KORTUC II). *Int J Oncol.* 2009, 34, 609–618.
27. Peter T E. Enhancement of the Sensitivity of Anoxic *Escherichia coli* B/r to X-Rays by Triacetoneamine-N-Oxyl. *Radiat Res.* 1967, 30 (4), 841–849.
28. Emmerson P T, Fielden E M, Johansen I. A possible steric factor in the sensitization of anoxic bacteria to X-rays by N-oxyl radicals. *Int. J. Radiat. Biol.* 1971, 19, 229-236.



29. Spisz P, Zdrowowicz M, Makurat S, et al. Why does the type of halogen atom matter for the radiosensitizing properties of 5-halogen substituted 4-thio-2'-deoxyuridines? *Molecules*. 2019, 24 (15), 2819.
30. Lhuillier C, Rudqvist N-P, Elemento O, Formenti S C, Demaria S. Radiation therapy and anti-tumor immunity: exposing immunogenic mutations to the immune system. *Genome Med*. 2019, 11 (1), 40.
31. Bourillon L, Bourgier C, Gaborit N, et al. An auristatin-based antibody-drug conjugate targeting HER3 enhances the radiation response in pancreatic cancer. *Int J Cancer*. 2019, 145 (7), 1838–1851.
32. Gandellini P, Rancati T, Valdagni R, Zaffaroni N. miRNAs in tumor radiation response: bystanders or participants?. *Trends Mol Med*. 2014, 20(9), 529–539.
33. de Jong M C, Ten Hoeve J J, Grénman R, et al. Pretreatment micro RNA expression impacting on epithelial-to-mesenchymal transition predicts intrinsic radiosensitivity in head and neck cancer cell lines and patients. *Clin Cancer Res*. 2015, 21, 5630–5638.
34. Huang A, Ono Y. Estimation of wrist flexion angle from muscle thickness changes measured by a flexible ultrasonic sensor. *IEEE*. 2016, 141, 188–191.
35. Shao Y, Song X, Jiang W, et al. MicroRNA-621 acts as a tumor radiosensitizer by directly targeting SETDB1 in hepatocellular carcinoma. *MolTher*. 2019, 27(2), 355–364.
36. Gu J, Li Y, Zeng J, et al. Knockdown of HIF-1 α by siRNA- expressing plasmid delivered by attenuated Salmonella enhances the antitumor effects of cisplatin on prostate cancer. *Sci Rep*. 2017, 7(1), 7546.



37. Mehta M, Basalingappa K, Griffith JN, et al. HuR silencing elicits oxidative stress and DNA damage and sensitizes human triple-negative breast cancer cells to radiotherapy. *Oncotarget*. 2016, 7(40), 64820–64835.
38. Wang H, Mu X, He H, Zhang X D. Cancer radiosensitizers. *Trends Pharmacol Sci*. 2018, 39(1), 24–48.
39. Jackson M R, Bavelaar B M, Waghorn P A, et al. Radiolabeled oligonucleotides targeting the RNA subunit of telomerase inhibit telomerase and induce DNA damage in telomerase-positive cancer cells. *Cancer Res*. 2019, 79(18), 4627–4637.
40. Praetorius N P, Mandal T K. Engineered nanoparticles in cancer therapy. *Recent Pat Drug Deliv Formul*. 2007, 1, 37-51.
41. Kwatra D, Venugopal A, Shrikant A. Nanoparticles in radiation therapy: a summary of various approaches to enhance radiosensitization in cancer. *Translational Cancer Research [Online]*. 2013, 2.4, 330-342.
42. Babaye A B, Malekzadeh R, Pournaghi A F, et al. Main Approaches to Enhance Radiosensitization in Cancer Cells by Nanoparticles: A Systematic Review. *Adv Pharm Bull*. 2021, 11(2), 212-223.
43. Young S W, Qing F, Harriman A, et al. Gadolinium (III) texaphyrin: a tumor selective radiation sensitizer that is detectable by MRI. *Proc Natl Acad Sci U S A* 1996, 93, 6610-6615.
44. Ngwa W, Korideck H, Kassis A I, Kumar R, Sridhar S, Makrigiorgos G M, et al. In vitro radiosensitization by gold nanoparticles during continuous slow-dose-rate gamma irradiation with I-125 brachytherapy seeds. *Nanomedicine*. 2013, 9, 25-27.



45. Rima W, Sancey L, Aloy M T, Armandy E, Alcantara G B, Epicier T, et al. Internalization pathways into cancer cells of gadolinium-based radiosensitizing nanoparticles. *Biomaterials*. 2013, 34, 181-195.
46. Townley H E, Rapa E, Wakefield G, Dobson P J. Nanoparticle augmented radiation treatment decreases cancer cell proliferation. *Nanomedicine*. 2012, 8, 526-536.
47. Hossain M, Luo Y, Sun Z, Wang C, Zhang M, Fu H, et al. X-ray enabled detection and eradication of circulating tumor cells with nanoparticles. *BiosensBioelectron*. 2012, 38, 348-354.
48. Chattopadhyay N, Cai Z, Kwon Y L, Lechtman E, Pignol J P, Reilly R M. Molecularly targeted gold nanoparticles enhance the radiation response of breast cancer cells and tumor xenografts to X-radiation. *Breast Cancer Res Treat*. 2013, 137, 81-91.
49. Zhang X D, Wu D, Shen X, Chen J, Sun Y M, Liu P X, et al. Size-dependent radiosensitization of PEG-coated gold nanoparticles for cancer radiation therapy. *Biomaterials*. 2012, 33, 6408-19.
50. Maggiorella L, Barouch G, Devaux C, Pottier A, Deutsch E, Bourhis J, et al. Nanoscale radiotherapy with hafnium oxide nanoparticles. *Future Oncol*. 2012, 8, 1167-81.
51. Coulter J A, Jain S, Butterworth K T, Taggart L E, Dickson G R, McMahon S J, et al. Cell type-dependent uptake, localization, and cytotoxicity of 1.9 nm gold nanoparticles. *Int J Nanomedicine*. 2012, 7, 2673-85.



52. Geng F, Song K, Xing J Z, Yuan C, Yan S, Yang Q, et al. Thio-glucose bound gold nanoparticles enhance radio-cytotoxic targeting of ovarian cancer. *Nanotechnology*. 2011, 22, 285101.
53. Xiao F, Zheng Y, Cloutier P, He Y, Hunting D, Sanche L. On the role of low-energy electrons in the radiosensitization of DNA by gold nanoparticles. *Nanotechnology*. 2011, 22, 465101.
54. Jain S, Coulter J A, Hounsell A R, Butterworth K T, McMahon S J, Hyland W B, et al. Cell-specific radiosensitization by gold nanoparticles at megavoltage radiation energies. *Int J Radiat Oncol Biol Phys*. 2011, 79, 531-539.
55. Sim L, Fielding A, English M, Waclawik E, Rockstroh A, Soekmadji C, et al. Enhancement of biological effectiveness of radiotherapy treatments of prostate cancer cells in vitro using gold nanoparticles. Coogee Beach, Sydney, NSW: 2011 International Nanomedicine Conference. 2011
56. Mowat P, Mignot A, Rima W, Lux F, Tillement O, Roulin C, et al. In vitro radiosensitizing effects of ultrasmall gadolinium based particles on tumour cells. *J Nanosci Nanotechnol*. 2011, 11, 7833-9.
57. Xing J Z, Xiaoyan Y, Jie C, Biao H, Roa W. Electronic dynamic cellular sensor used to measure gold nanoparticles enhanced radiotherapy. *Life Science Systems and Applications Workshop (LiSSA)*, 2011 IEEE/NIH. 2011, 20-23.
58. Liu C J, Wang C H, Chen S T, Chen H H, Leng W H, Chien C C, et al. Enhancement of cell radiation sensitivity by pegylated gold nanoparticles. *Phys Med Biol*. 2010, 55, 931-945.
59. Butterworth K T, Coulter J A, Jain S, Forker J, McMahon S J, Schettino G, et al. Evaluation of cytotoxicity and radiation enhancement using 1.9 nm gold



- particles: potential application for cancer therapy. *Nanotechnology*. 2010, 21, 295101.
60. Porcel E, Liehn S, Remita H, Usami N, Kobayashi K, Furusawa Y, et al. Platinum nanoparticles: a promising material for future cancer therapy? *Nanotechnology*. 2010, 21, 85103.
61. Rahman W N, Wong C J, Yagi N, Davidson R, Geso M. Dosimetry And Its Enhancement Using Gold Nanoparticles In Synchrotron Based Microbeam And Stereotactic Radiosurgery. *AIP Conference Proceedings*. 2010, 1266, 107-110.
62. Brun E, Duchambon P, Blouquit Y, Keller G, Sanche L, Sicard-Roselli C. Gold nanoparticles enhance the X-ray-induced degradation of human centrin 2 protein. *Rad Phys Chem*. 2009, 78, 177-183.
63. Brun E, Sanche L, Sicard-Roselli C. Parameters governing gold nanoparticle X-ray radiosensitization of DNA in solution. *Colloids and surfaces B, Biointerfaces*. 2009, 72, 128-134.
64. Rahman W N, Bishara N, Ackerly T, He C F, Jackson P, Wong C, et al. Enhancement of radiation effects by gold nanoparticles for superficial radiation therapy. *Nanomedicine*. 2009, 5, 136-142.
65. Roa W, Zhang X, Guo L, Shaw A, Hu X, Xiong Y, et al. Gold nanoparticle sensitize radiotherapy of prostate cancer cells by regulation of the cell cycle *Nanotechnology*. 2009, 20, 375101.
66. Withers N J, Plumley J B, Triño N D, Sankar K, Akins B A, Rivera A C, et al. Scintillating-nanoparticle-induced enhancement of absorbed radiation dose. *SPIE Proceedings*; 2009, 718917-8.



67. Chang M Y, Shiau A L, Chen Y H, Chang C J, Chen HH W, Wu C L. Increased apoptotic potential and dose-enhancing effect of gold nanoparticles in combination with single-dose clinical electron beams on tumor-bearing mice. *Cancer Sci.* 2008. 99. 1479-1484.
68. Liu C J, Wang C H, Chien C C, Yang T Y, Chen S T, Leng W H, et al. Enhanced x-ray irradiation-induced cancer cell damage by gold nanoparticles treated by a new synthesis method of polyethylene glycol modification. *Nanotechnology.* 2008, 19, 295104.
69. Kaur H, Pujari G, Semwal M K, Sarma A, Avasthi D K. In vitro studies on radiosensitization effect of glucose capped gold nanoparticles in photon and ion irradiation of HeLa cells. *NuclInstrum Methods Phys Res, Sect B.* 2013, 301, 7-11.
70. Chithrani D B, Jelveh S, Jalali F, van Prooijen M, Allen C, Bristow R G, et al. Gold nanoparticles as radiation sensitizers in cancer therapy. *Radiat Res.* 2010, 173, 719-728.
71. Wang C, Li X, Wang Y, Liu Z, Fu L, Hu L. Enhancement of radiation effect and increase of apoptosis in lung cancer cells by thio-glucose-bound gold nanoparticles at megavoltage radiation energies. *J Nanopart Res.* 2013, 15, 1-12.
72. Bobyk L, Edouard M, Deman P, Vautrin M, Pernet-Gallay K, Delaroche J, et al. Photoactivation of gold nanoparticles for glioma treatment. *Nanomedicine.* 2013, 9, 1089-97.
73. Alqathami M, Blencowe A, Yeo U J, Franich R, Doran S, Qiao G, et al. Enhancement of radiation effects by bismuth oxide nanoparticles for



- kilovoltage x-ray beams: A dosimetric study using a novel multi-compartment 3D radiochromic dosimeter. *J PhysConf Ser.* 2013, 444, 012025.
74. .
75. Mirjolet C, Papa A L, Crehange G, Raguin O, Seignez C, Paul C, et al. The radiosensitization effect of titanate nanotubes as a new tool in radiation therapy for glioblastoma: a proof-of-concept. *RadiotherOncol.* 2013, 108, 136-142.
76. Klein S, Sommer A, Distel L V, Neuhuber W, Kryschi C. Superparamagnetic iron oxide nanoparticles as radiosensitizer via enhanced reactive oxygen species formation. *BiochemBiophys Res Commun.* 2012, 425, 393-397.
77. David Gara P, Garabano N, LlansolaPortoles M, Moreno M S, Dodat D, Casas O, et al. ROS enhancement by silicon nanoparticles in X-ray irradiated aqueous suspensions and in glioma C6 cells. *J Nanopart Res.* 2012, 14, 1-13.
78. Misawa M, Takahashi J. Generation of reactive oxygen species induced by gold nanoparticles under x-ray and UV Irradiations. *Nanomedicine.* 2011, 7, 604-614.
79. Wang L, Yang W, Read P, Larner J, Sheng K. Tumor cell apoptosis induced by nanoparticle conjugate in combination with radiation therapy. *Nanotechnology.* 2010, 21, 475103.
80. Jeong S Y, Park S J, Yoon S M, Jung J, Woo H N, Yi S L, et al. Systemic delivery and preclinical evaluation of Au nanoparticle containing beta-lapachone for radiosensitization. *J Control Release.* 2009, 139, 239-245.
81. Yang W, Read P W, Mi J, Baisden J M, Reardon K A, Larner J M, et al. Semiconductor nanoparticles as energy mediators for photosensitizer-enhanced radiotherapy. *Int J RadiatOncolBiol Phys.* 2008, 72, 633-635.



82. Briggs A, Corde S, Oktaria S, Brown R, Rosenfeld A, Lerch M, et al. Cerium oxide nanoparticles: influence of the high-Z component revealed on radio resistant 9L cell survival under X-ray irradiation. *Nanomedicine*. 2013, 9, 1098-10105.
83. Takahashi J, Misawa M. Analysis of Potential Radiosensitizing Materials for X-Ray-Induced Photodynamic Therapy. *Nanobiotechnol*. 2007, 3, 116-126.
84. Rahman W N, Corde S, Yagi N, Abdul Aziz S A, Annabell N, Geso M. Optimal energy for cell radiosensitivity enhancement by gold nanoparticles using synchrotron-based monoenergetic photon beams. *Int J Nanomedicine*. 2014, 9, 2459-2467.
85. Klein S, Dell'Arciprete M L, Wegmann M, Distel L V, Neuhuber W, Gonzalez M C, et al. Oxidized silicon nanoparticles for radiosensitization of cancer and tissue cells. *BiochemBiophys Res Commun*. 2013, 434, 217-222.
86. Yadav P, Bandyopadhyay A, Chakraborty A, Islam S M, Sarkar K. Enhancing the radiotherapeutic index of gamma radiation on cervical cancer cells by gold nanoparticles. *Gold Bull*. 2019, 52(3–4), 185–196.
87. Jia T T, Yang G, Mo S J et al. Atomically precise gold-levonorgestrel nanocluster as a radiosensitizer for enhanced cancer therapy. *ACS Nano*. 2019, 13(7), 8320–8328.
88. Wu H, Lin J, Liu P D et al. Reactive oxygen species acts as executor in radiation enhancement and autophagy inducing by AgNPs. *Biomaterials*. 2016, 101, 1–9.



89. Li F, Li Z, Jin X et al. Radiosensitizing effect of gadolinium oxide nanocrystals in NSCLC cells under carbon ion irradiation. *Nanoscale Res. Lett.* 2018, 14(1), 328.
90. Jiang Y W, Gao G, Jia H R et al. Copper oxide nanoparticles induce enhanced radiosensitizing effect via destructive autophagy. *ACS Biomater. Sci. Eng.* 2019, 5(3), 1569–1579.
91. Hauser A K, Mitov M I, Daley E F, McGarry R C, Anderson K W, Hilt J Z. Targeted iron oxide nanoparticles for the enhancement of radiation therapy. *Biomaterials.* 2016, 105, 127–135.
92. Zhang H J, Patel N, Xiong J, Ding S. Targeting and noninvasive treatment of hepatocellular carcinoma in situ by ZnO nanorod-mediated concurrent chemoradiotherapy. *RSC Adv.* 2015, 5(104), 85720–85729.
93. Nakayama M, Sasaki R, Ogino C et al. Titanium peroxide nanoparticles enhanced cytotoxic effects of x-ray irradiation against pancreatic cancer model through reactive oxygen species generation in vitro and in vivo. *Radiat. Oncol.* 2016, 11(1), 91.
94. Zangeneh M, Nedaei H A, Mozdarani H, Mahmoudzadeh A, Salimi M. Enhanced cytotoxic and genotoxic effects of gadolinium-doped ZnO nanoparticles on irradiated lung cancer cells at megavoltage radiation energies. *Mater. Sci. Eng. C Mater. Biol. Appl.* 2019, 103, 109739.
95. Wang X, Zhang C Y, Du J F et al. Enhanced generation of non-oxygen dependent free radicals by Schottky-type heterostructures of Au-Bi₂S₃ nanoparticles via x-ray-induced catalytic reaction for radiosensitization. *ACS Nano.* 2019, 13(5), 5947–5958.



96. Ruan J, Wang Y, Li F et al. Graphene quantum dots for radiotherapy. *ACS Appl. Mater. Interfaces*. 2018, 10(17), 14342–14355.
97. Zare T, Fardid R, Naderi S. Synergetic effect of silver nanoparticles and UVC irradiation on H2AX gene expression in TK6 cells. *Cell J*. 2019, 21(2), 204–209.
98. Gao F, Wang D, Zhang T B et al. Facile synthesis of Bi₂S₃-MoS₂ heterogeneous nano agent as dual functional radiosensitizer for triple negative breast cancer theranostics. *Chem. Eng. J*. 2020, 395, 125032.
99. Generalov R, Kuan W B, Chen W, Kristensen S, Juzenas P. Radiosensitizing effect of zinc oxide and silica nanocomposites on cancer cells. *Colloids Surf. B Biointerfaces*. 2015, 129, 79–86
100. Zhang H J, Patel N, Ding S, Xiong J, Wu P P. Theranostics for hepatocellular carcinoma with Fe₃O₄@ZnO nanocomposites. *Biomater Sci*. 2016, 4(2), 288–298.
101. Youkhana E Q, Feltis B, Blencowe A, Geso M. Titanium dioxide nanoparticles as radiosensitisers: an in vitro and phantom-based study. *Int. J. Med. Sci*. 2017, 14(6), 602–614.
102. Wang R, Cao Z, Wei L et al. Barium tungstate nanoparticles to enhance radiation therapy against cancer. *Nanomedicine*. 2020, 28, 102230.
103. Chen Y Y, Li N, Wang J B et al. Enhancement of mitochondrial ROS accumulation and radiotherapeutic efficacy using a Gd-doped titania nano sensitizer. *Theranostics*. 2019, 9(1), 167–178.
104. Behrouzkia Z, Zohdi A R, Khalkhali H R, Mousavi F. Evaluation of gold nanoparticle size effect on dose enhancement factor in megavoltage beam



- radiotherapy using MAGICA polymer gel dosimeter. *J Biomed Phys Eng.* 2019, 9(1), 89–96.
105. Zhang X, Wang H, Coulter J A, Yang R. Octaarginine-modified gold nanoparticles enhance the radiosensitivity of human colorectal cancer cell line LS180 to megavoltage radiation. *Int J Nanomedicine.* 2018, 13, 3541–3552.
106. Jiang, Y W, Gao, G, Jia, H R, et al. Palladium nanosheets as safe radiosensitizers for radiotherapy. *Langmuir* 2020, 36, 11637–11644.
107. Kirakli E K, Takan G, Hoca S, Müftüler F Z B, Kılçar A Y, Kamer S A. Superparamagnetic iron oxide nanoparticle (SPION) mediated in vitro radiosensitization at megavoltage radiation energies. *J. Radioanal. Nucl. Chem.* 2018, 315, 595–602.
108. Huang F K, Chen W C, Lai S F, Liu C J, Wang C L, Wang C H, et al. Enhancement of irradiation effects on cancer cells by cross-linked dextran-coated iron oxide (CLIO) nanoparticles. *Phys. Med. Biol.* 2010, 55, 469–482.
109. Rezaei M, Khoshgard K, Hosseinzadeh L, Haghparast A, Eivazi MT. Application of dextran-coated iron oxide nanoparticles in enhancing the radiosensitivity of cancerous cells in radiotherapy with high-energy electron beams. *J Can Res Ther.* 2019, 15, 1352-8.
110. Habiba K, Aziz K, Sanders K, Santiago C M, Mahadevan L S K, Makarov V, Weiner B R, Morell G, Krishnan S. Enhancing colorectal cancer radiation therapy efficacy using silver nanoprisms decorated with graphene as radiosensitizers, *Sci. Rep.* 2019, 9, 1–9.
111. Saberi A, Shahbazi-Gahrouei D, Abbasian M, Fesharaki M, Baharlouei A, Arab-Bafrani Z. Gold nanoparticles in combination with megavoltage radiation



- energy increased radiosensitization and apoptosis in colon cancer HT-29 cells. *Int J Radiat Biol.* 2017, 93, 315–323.
112. Zhang X, Liu Z, Lou Z, Chen F, Chang S, Miao Y, Zhou Z, Hu X, Feng J, Ding Q et al. Radiosensitivity enhancement of Fe₃O₄@Ag nanoparticles on human glioblastoma cells. *Artif. Cells Nanomed. Biotechnol.* 2018, 46 (Suppl. S1), 975–984.
113. Tokumitsu H, Hiratsuka J, Sakurai Y, et al. Gadolinium neutron-capture therapy using novel gadopentetic acid-chitosan complex nanoparticles: in vivo growth suppression of experimental melanoma solid tumor. *Cancer Lett* 2000, 150,177-182.
114. Townley H E, Kim J, Dobson P J. In vivo demonstration of enhanced radiotherapy using rare earth doped titania nanoparticles. *Nanoscale* 2012, 4, 5043-50
115. Shao L, Gao Y, Yan F. Semiconductor quantum dots for biomedical applications. *Sensors (Basel)* 2011, 11, 11736-51.
116. Zhang Q, Yang W, Man N, et al. Autophagy-mediated chemosensitization in cancer cells by fullerene C₆₀ nanocrystal. *Autophagy* 2009, 5, 1107-1117.
117. Sayes C M, Gobin A M, Ausman K D, et al. Nano-C₆₀ cytotoxicity is due to lipid peroxidation. *Biomaterials.* 2005, 26, 7587-7595.
118. Tishler R B, Geard C R, Hall E J, et al. Taxol sensitizes human astrocytoma cells to radiation. *Cancer Res* 1992, 52, 3495-3497.
119. Anuje M, Pawaskar P N, Khot V, Sivan A, Jadhav S, Meshram J, Thombare B. Synthesis, characterization, and cytotoxicity evaluation of polyethylene glycol-



- coated iron oxide nanoparticles for radiotherapy application. *J Med Phys* 2021;46,154-161.
120. Kirakli E K, Takan G, Hoca S et al. Superparamagnetic iron oxide nanoparticle (SPION) mediated in vitro radiosensitization at megavoltage radiation energies. *J Radioanal Nucl Chem*. 2018, 315, 595–602.
121. Kehrer J P, The Haber–Weiss reaction and mechanisms of toxicity, *Toxicology*, 2000, 149 (1), 43-50
122. Subiel A, Ashmore R, Schettino G. Standards and Methodologies for Characterizing Radiobiological Impact of High-Z Nanoparticles. *Theranostics*. 2016;6(10),1651-1671.
123. Slavotinek A, McMillan T J, Steel C M. Measurement of radiation survival using the MTT assay. *Eur. J. Cancer* .1994, 30, 1376–1382.
124. Stone V, Johnston H, Schins R P F. Development of in vitro systems for nanotoxicology: Methodological considerations. *Critical Reviews in Toxicology*. 2009, 39(7), 613-626
125. Kellerer A M, Hug O. Theory of dose-effect relations. Heidelberg: Springer; 1972.
126. ICRU. Quantitative Concepts and Dosimetry in Radiobiology (Report no. 30). Measurement International Commission on Radiation Units and. Washington, DC; 1979.
127. Jain S, Coulter J A, Butterworth K T, et al. Gold nanoparticle cellular uptake, toxicity and radiosensitisation in hypoxic conditions. *Radiotherapy and Oncology*. 2014; 110: 342-7



128. Mirjolet C, Papa A L, Crehange G, et al. The radiosensitization effect of titanate nanotubes as a new tool in radiation therapy for glioblastoma: A proof-of-concept. *Radiotherapy and Oncology*. 2013; 108: 136-42.
129. Cui F B, Li R T, Liu Q, et al. Enhancement of radiotherapy efficacy by docetaxel-loaded gelatinase-stimuli PEG-Pep-PCL nanoparticles in gastric cancer. *Cancer Letters*. 2014; 346: 53-62.
130. Hainfeld J F, Dilmanian F A, Slatkin D N, et al. Radiotherapy enhancement with gold nanoparticles. *Journal of Pharmacy and Pharmacology*. 2008; 60: 977-85.
131. Robar J L, Riccio S A, Martin M A. Tumour dose enhancement using modified megavoltage photon beams and contrast media. *Physics in Medicine and Biology*. 2002; 47: 2433-49
132. Kawrakow I, Rogers D W O. The EGSnrc code system: Monte Carlo simulation of electron and photon transport. Ottawa, Canada; 2001.
133. Agostinelli S, Allison J, Amako K, et al. GEANT4-a simulation toolkit. *Nuclear Instruments and Methods in Physics Research: Section A-Accelerators, Spectrometers, Detectors and Associated Equipment*. 2003; 506: 250-303.

CHAPTER - 4

CHARACTERIZATION AND CYTOTOXICITY STUDY





4.1 Introduction

Generally, nanomaterial synthesis is classified by physical, chemical, biological or hybrid method. In the physical method, one starts with bulk matter and then goes breaking down to smaller particles till nano-scale size is achieved, a procedure called top down or destructive approach [1]. Specific examples include laser ablation, where atoms are removed from a solid through thermal or non thermal process with intense laser beam [1]. The mechanical milling is used for milling and post annealing of nanoparticles during synthesis where different elements are milled in an inert atmosphere [2]. In the chemical synthesis method, nanomaterials are synthesized by combining substances in a wet chemistry and adjusting reaction parameters. In this method, atoms, molecules or ions in solution first form nucleation and then aggregates of those species that finally end up in nano-size particles, a process called bottom-up approach [1]. Nowadays, for synthesis convenience reasons, this is the most widely used method of producing nanomaterials in industry. So, there are various methods classified under this approach including sol–gel, solvothermal, microwave irradiation, pyrolysis, chemical precipitation, micro emulsion, thermal decomposition of precursors etc [1]. In biosynthesis method, desired nanomaterials are formed using microorganisms or extracts of plants along with a precursor. Hybrid nanoparticles could be synthesized either by chemical or by physical methods. Depending on the synthesis methods, hybrid nanoparticles might provide the new chemical and physical properties and capabilities [3]. Figure 4.1 shows detail classification of nanomaterials (NM).



Figure 4.1 Classification of synthesis methods of nanomaterials

Due to their multifunctional characteristics, magnetic nanoparticles (MNPs) have interested researchers from a variety of areas, including medicine, biology and physics. There are a variety of techniques to synthesize MNPs, which have been reported as efficient synthesis approaches to produce the shape-controlled, stable, biocompatible and monodispersed MNPs in several papers [4]. MNPs have been synthesized using a variety of techniques, including co-precipitation, thermal



decomposition, solvothermal, sonochemical, microemulsion, microwave-assisted chemical vapour deposition, combustion, laser pyrolysis and carbon arc. To produce Fe_3O_4 nanomaterials of various sizes and forms, such as nanotubes, nanorods and hierarchical superstructures, several innovative and effective techniques have been established [4]. Co-precipitation is the most common and frequently used method for producing Fe_3O_4 or $\gamma\text{-Fe}_2\text{O}_3$. Co-precipitation is the most appropriate technique for the production of MNPs with regulated sizes and magnetic characteristics. Because of its simplicity of usage, it is frequently used in biological applications [5].

The distinctive characteristic determines the potential and application of a nanoparticle [4]. The use of magnetic nanoparticles in biomedical applications provides an abundance of opportunities. Nonetheless, to truly understand the interactions of these nanomaterials in biological media, detailed characterization is necessary with these complex systems [6]. Nanoparticles provide a variety of characterisation issues that impact nanoparticle characterization in a precise and suitable manner. Understanding the issues that arise during nanoparticle characterization and selecting proper characterisation approaches are therefore critical. Nanoparticle characterization is used to determine surface area and porosity, pore size, solubility, particle size distribution, aggregation, hydrated surface analysis, zeta potential, wettability, adsorption potential and shape, size of the interactive surface, crystallinity, fractal dimensions, orientation, magnetic properties and intercalation and dispersion of nanoparticles and nanotubes in nanocomposite materials [7]. UV-visible spectroscopy, atomic force microscopy (AFM), transmission electron microscopy (TEM), scanning electron microscopy (SEM), dynamic light scattering (DLS), Vibrating sample magnetometer (VSM), X-ray photoelectron spectroscopy (XPS), thermogravimetric analysis (TGA),



powder X-ray diffraction (XRD), Fourier transform infrared spectroscopy (FTIR), matrix-assisted laser desorption/ionization time-of-flight mass spectrometry (MALDI-TOF), dual polarization interferometry, nuclear magnetic resonance (NMR), nanoparticle tracking analysis (NTA) for evaluation of Brownian motion and particle size analysis; are some of the methods that can be used to determine nanoparticle parameters [7].

Because of the numerous cancer therapeutic applications of MNPs, such as drug delivery, cancer immunotherapy, magnetic hyperthermia, photodynamic therapy, and anti-cancer agents, radiosensitizer, one must investigate biocompatibility for normal tissue, tumour toxicity, pharmacokinetics, bio-distribution and others [8]. Here we will go through theoretical details about the synthesis method and characterization techniques employed for magnetic nanoparticles.

4.2 Synthesis of Magnetic Nanoparticles (MNPs) by Chemical Co-Precipitation

The methods used to produce MNPs are important to consider since their characteristics are affected not only by size and aggregation state but also by surface chemistry and synthesis process. The MNPs synthesized by physical methods such as mechanical milling are not appropriate for in vivo applications due to their broad size distribution (10–1000 nm) [9].

Therefore, the physical method is overcome by chemical wet methods, due to effectiveness in controlling nanoparticle size and high yield, which is desirable to avoid clearance by the reticuloendothelial system (RES) by opsonization [9].



Furthermore, particles of diameters of 10 to 40 nm are needed for sustained blood circulation [10].

In recent years, there has been huge interest in the study of composites such as ferrite, which can be represented by the general formula $[M^{2+}][Fe_2^{3+}]O_4$, where M^{2+} is a divalent cation of a metal (Fe, Co, Ni, Mn, Cu, Zn, and Cd). Mainly iron oxides used in the preparation of magnetic fluids are magnetite and maghemite. The chemical constitution of magnetite is $Fe^{2+}(Fe^{3+})_2(O^{2-})_4$, in which the Fe ions exist in both 2 and 3 valence states in the ratio of 1:2. This formula shows that magnetite contains both ferrous (divalent (Fe^{2+})) and ferric (trivalent (Fe^{3+})) iron cations, suggesting crystallization in an environment containing intermediate levels of oxygen [9,10]. A net spin magnetic moment exists for each Fe^{2+} and Fe^{3+} ion, which corresponds to 4 and 5 Bohr magnetons, respectively. Furthermore, the O^{2-} cations are magnetically neutral. There are antiparallel spin-coupling interactions between the Fe ions, similar in character to antiferromagnetism. It was one of the first crystal structure to be obtained using X-ray diffraction (X-RD). The structure is inverse spinel, with O^{2-} ions forming a face-centered cubic lattice and iron cations occupying interstitial sites (Fig. 4.2).

Generally, there are two types of positions that may be occupied by the iron cations, as shown in figure 4.2. For one, the coordination number is 4 (tetrahedral coordination)—that is, each Fe ion is surrounded by four oxygen nearest neighbors and the other, the coordination number is 6 (octahedral coordination). With this inverse spinel structure, half the trivalent (Fe^{3+}) ions are situated in tetrahedral sites and the other half along with Fe^{2+} cations, occupy octahedral

sites. The unit cell consists of 8 Fe^{2+} , 16 Fe^{3+} and 32 O^{2-} ions and a unit cell with a length of $a = 0.839 \text{ nm}$ [10]. Oxygen ions form a dense cubic lattice containing 32 octahedral and 64 tetrahedral sites in one unit cell.

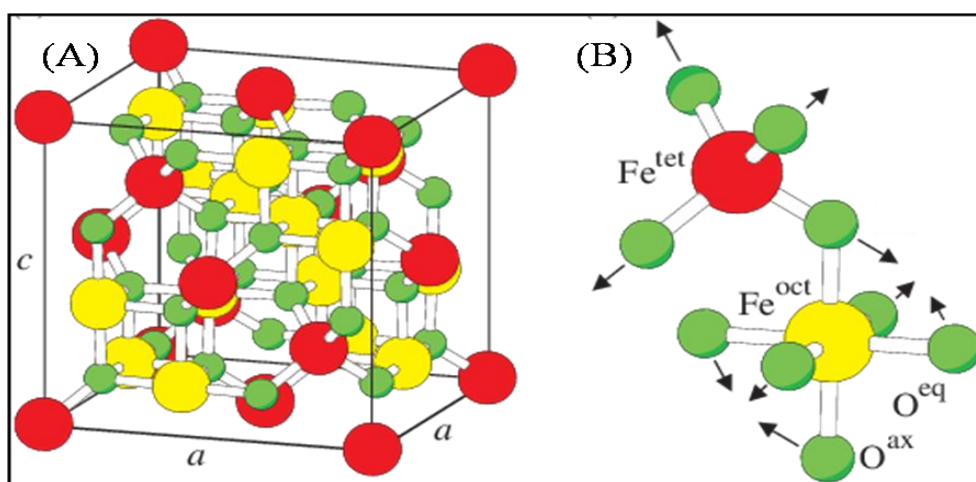
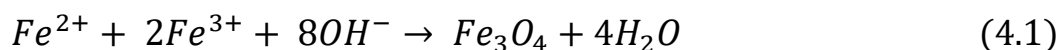


Figure 4.2 (a) Face-centred cubic inverse spinel structure of magnetite. (b) Magnification of one tetrahedron and one adjacent octahedron sharing an oxygen atom. Large spheres labelled by Fe^{tet} and Fe^{oct} represent iron atoms on tetrahedrally and octahedrally coordinated sublattices, respectively. The lower symmetry in this case also leads to the distinction between axial O^{ax} and equatorial O^{eq} atoms. Arrows indicate the shift directions of the oxygen atoms from their ideal positions. [11].

Products precipitation from solutions is one of the earliest methods for preparing NPs. Precipitation processes include dissolving metal precursors in a common solvent, such as water and then adding a precipitating agent to form an insoluble product. Precipitation processes have the benefit of producing huge amounts of particles. A homogeneous precipitating procedure, which involves the separation of the nucleation and nuclei growth is commonly used to produce uniform particles [12]. In this procedure salts (e.g., Fe^{2+} and Fe^{3+}) in 1:2 ratio were dissolved in water. A base solution [usually, KOH, NaOH, NH_3OH , or $\text{N}(\text{CH}_3)_4\text{OH}$] is added into a salt solution which is continuously stirring to

precipitate the starting material by maintaining temperature less than 100°C [13]. Magnetite NPs are protected from critical oxidation by bubbling nitrogen gases through the solution. Furthermore, as compared to techniques that do not remove oxygen, N₂ reduces particle size [12]. Resultant reaction of formation of iron oxide is shown in equation 4.1.



Precipitation of corresponding metal hydroxide is filtered followed by annealing to obtain the final mixed oxide product. The co precipitation technique also has the following advantages: high product purity, easy reproducibility, no need for organic solvents, low cost and high yield. The shape, size, content of the particles produced and morphology, on the other hand, are strongly dependent on the reaction conditions (pH, temperature, kind of basic solution, ionic strength and so on). Furthermore, iron oxide particles made this way are frequently unstable and must be stabilised by functionalizing with low molecular weight surfactants or polymers [13].

4.2.1 Steps involved during precipitation

Co-precipitation involves simultaneous occurrence of nucleation, growth, coarsening and agglomeration (shown in Fig. 4.3). Nucleation is the first step in the precipitation process when smaller size precipitates initially produce, but these precipitates tend to aggregate together into large sized particles which are thermodynamically more stable, which is known as a growth process and nuclei

of all species present must form at the same time. Procedure of precipitation discussed below in detail.

4.2.1.1 Liquid mixing/supersaturation

The initial mixing of solution components has a major impact on precipitation. More homogeneous byproducts can be obtained by good mixing, especially when co-precipitation is used. The nucleation process is primarily influenced by the stirring rate, whereas the growth rate is much less so. The rate of stirring has an effect on agglomeration as well. Changes in stirring rate and mixing method can influence aggregate size [14].

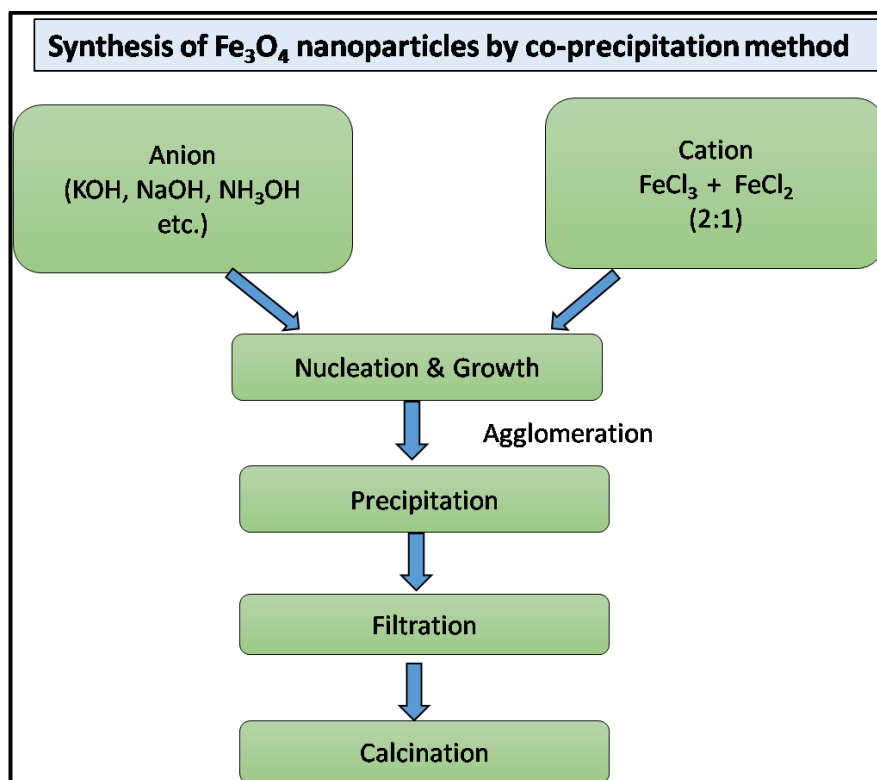


Figure 4.3 Synthesis of Fe_3O_4 nanoparticles

4.2.1.2 Nucleation and growth

The solution must be supersaturated with respect to the components to be precipitated in order for nucleation to occur. Figure 4.4 depicts the factors influencing supersaturation. The system is not stable in the supersaturated region and precipitation occurs with any minor disturbance. The supersaturation region is obtained by increasing the concentration via evaporation, increasing the pH or decreasing the temperature. A component's solubility increases with temperature. The pH affects the solubility curve as well. Solubility decreases as pH rises and the curve shifts from position 1 to position 2. Then the point A which was initially in the solution region becomes in supersaturated region (see Fig. 4.4). The point A, which was previously in the solution region, is now in the supersaturated region (See Fig. 4.4).

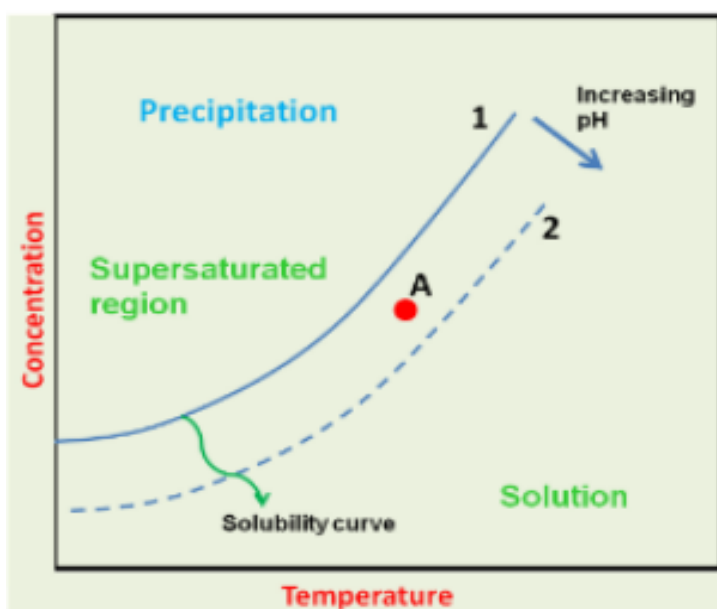


Figure 4.4 Parameters affecting supersaturation [14]

The most favourable method for precipitation is an increase in pH. The precipitation reaction is controlled by adding a basic solution to raise the pH. As



a result, the corresponding metallic hydroxide compounds can be rendered insoluble and precipitated by increasing the pH of the solution with alkaline. NaOH, KOH, NH_4OH , carbonates and bicarbonates are common reagents. Particles develop in two ways within a supersaturated region: nucleation and growth [14].

The smallest solid phase aggregate of atoms, molecules or ions is called a nucleus. A nucleus is produced during precipitation and which is capable of spontaneous growth and also a supersaturated solution is necessary for this process. Only when the concentration exceeds a critical threshold value a nucleus will produce and the precipitation will begin. As long as the concentration of the species stays above the nucleation threshold, new particles are formed. Nucleation starts with the formation of clusters which are able to grow spontaneously by the subsequent addition of monomers until a critical size is reached. Clusters smaller than this size tend to re-dissolve, while larger clusters continue to grow. As soon as the concentration falls below the critical concentration due to consumption of the precursors by nucleation or growth process, only particle growth of existing particles continues. Growth proceeds through adsorption of ions on the surface of seeded particles. This growth parameter depends on concentration, temperature and pH. Rates of nucleation and growth can be independently controlled. If nucleation is faster than growth, the system produces a narrow distribution of small particles. Fast growth results in narrow distribution of large particles [14].

4.2.1.3 Aggregation of the primary particles

Agglomeration is a critical step that results in larger and fewer but still porous particles. Aggregation is the transformation of nanometer-range primary particle clusters into micrometer-range secondary particles. These particles can be held

together by physical and chemical forces. The pores are then defined as void spaces between the primary particles and based on particle stacking their porosity is determined. Because of the extremely high supersaturation during the precipitation of most base carbonates or metal hydroxides, nucleation occurs spontaneously [14].

4.2.2 Factors influencing co-precipitation process

During the precipitation of nanoparticles, various factors such as pH, temperature, stirring velocity and so on influence purity, particle size, surface area, pore size and pore volumes, among others (shown in Fig. 4.5). These variables are discussed further below.

4.2.2.1 Effect of raw materials

During heat treatment stages, precursors are generally chosen with counter ions that break down quickly to volatile products.

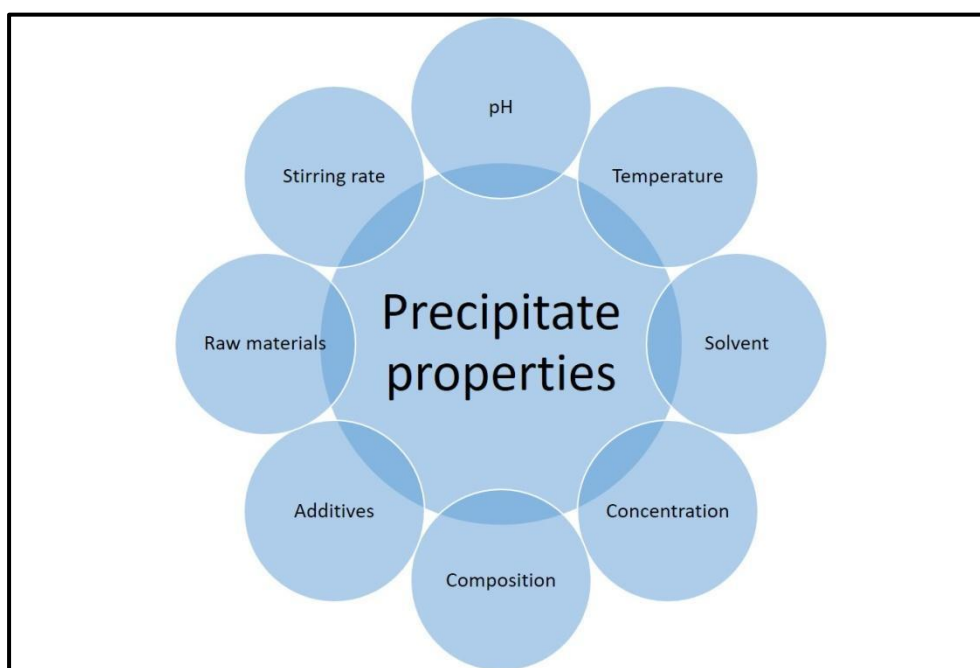


Figure 4.5 Different influencing factors affecting co -precipitation

Metal precursors such as nitrate, chlorides and sulphate salts are preferred, with ammonia, sodium carbonate and hydroxides acting as precipitating agents. In many catalytic processes, the ions chloride and sulphate act as poisons. If the precipitation must be performed in the presence of such ions, frequent washing is required to remove the ions from the precipitate [14].

4.2.2.2 Effect of pH

Degree of supersaturation i.e., the final results get affected by pH [14]. As the base amount and pH increases, the nanoparticle size decreases, albeit a small amount. At higher pH, supersaturation during co-precipitation is greater, promoting nucleation over growth, thus giving smaller particle sizes [15]. Studies have also revealed that the nanoparticle size can be altered by controlling the final pH and ionic strength of the non-complexing salt solutions. Their studies reveal that the mean particle size decreases with increasing pH and ionic strength [16]. The size reduction of magnetite nanoparticles, precipitated with a certain base, is also affected by the slow or fast addition of the basic solution to the solution of mixed Fe^{2+} and Fe^{3+} ions. The fast addition of the stoichiometric or of the more concentrated base solution to the reaction solution produces smaller size magnetite nanoparticles, in comparison to those of the corresponding magnetite obtained by slow addition of the base. The fast addition favors the continuous nucleation with respect to growth, thus enabling the formation of small size particles [15]. The nature of the precipitating base also affects the particle sizes. A reduction of magnetite size can be determined by the nature of the precipitating base in accordance with the following sequence: $(\text{C}_2\text{H}_5)_4\text{NOH} < \text{KOH} < \text{NaOH}$ [15].



4.2.2.3 Effect of temperature

The temperature of the precipitation is a key element in determining precipitate characteristics including primary size of the crystallite, surface area and phase formation. It's still impossible to anticipate the exact type and degree of the influence of precipitation temperature on characteristics, therefore it's usually chosen by trial and error. Temperature has a huge impact on nucleation rates. Most precipitation processes take place above room temperature, generally near to 373 K, for apparent reasons such as faster precipitation, for example for 9 nm size particles, the time required for complete oxidation of Fe^{2+} ions were 3 h at 80°C whereas it was about 3 months at room temperature [17]. A higher temperature may cause crystallite size to increase. This may be due to, increase in temperature increases solubility resulting in reduction of supersaturation of solvent and eventually growth rate is more producing larger size particles.

4.2.2.4 Effect of concentration

It is preferable to precipitate at high concentrations of metal ions. This increases the space time yields by reducing the vessel volume for the same mass of precipitate. Furthermore, a higher degree of supersaturation leads to faster precipitation. Because of the increased rate of nucleation, higher concentration levels result in smaller particle sizes and larger surface areas [14].

4.2.2.5 Effect of solvent

Water is almost exclusively utilised as a solvent for the production of bulk catalysts due to cost considerations. The cost of using organic solvents is significantly higher. Furthermore, the majority of metal salts employed as precursors are insoluble in organic solvents. Organic solvents are likewise

dangerous to the environment; therefore, their usage is strictly regulated. These are only utilised in a few instances where the product quality is improved by employing an organic solvent [14].

4.2.2.6 Effect of additives

Additives are materials that aren't required components of precipitation reactions. Additives can have a significant impact on the properties of precipitates. Organic molecules are the most commonly used additives, which are introduced to the precipitate to regulate the pore structure. During the calcination step, such organic molecules can be removed from the precipitate. The use of surfactants as additives in the preparation of high surface area oxides is a very promising method. Through calcinations, surfactant can be removed resulting in a well-defined pore network. Diameter of pore can be varied between 2 and 10 nm [14].

4.2.2.7 Stirring velocity

Stirring velocity affects the particle size of the magnetite nanoparticles. The dispersed phase should be largely distributed in a uniform manner over the entire liquid height for crystallization and solid catalyzed reactions, a condition that requires both higher stirring rates and power. Also, as the stirring rate increases, the reaction solution's uniformity improves and smaller particles and narrower size distributions are obtained [18].

4.3 Surface Functionalization

The physical and chemical properties of NPs may change depending upon the conditions. To prevent iron nanoparticles (NPs) from oxidation and aggregation during synthesis, Fe_3O_4 NPs are usually coated with organic or inorganic



molecules. However, it is a necessary to synthesize magnetic NPs in oxygen-free environment, most preferably in the presence of N_2 gas [19]. Furthermore, iron oxide particles produced in this manner are frequently unstable and must be stabilised by functionalizing low molecular weight surfactants or polymers [13].

On the other hand, toxicity of the NPs can be reduced by coating the surface of NPs. Surface coating, in general, can reduce the normal tissue toxicity. It also provides the stabilisation of NPs along with avoidance of toxic ion release from NPs [20]. To reach the specific site of interest NPs should have long blood circulation time. Opsonin is a serum protein, which enhances phagocytosis by adsorbing on the surface of hydrophobic NPs and decreases circulation time. Unnecessary uptake by reticuloendothelial system (RES), reduces nano-drug bioavailability as well as pose toxicity within the host. This hydrophobicity of nanoparticles is responsible for phagocytic internalization and particle clearance. As a result, coating of the hydrophobic surface of NP with a protective layer of hydrophilic substances reduces NP recognition by the immune system while increasing the likelihood of uptake by target cells. As shown in figure 4.6, this layer forms a cloud of chains on the NP surface, causing steric repulsive forces against plasma proteins and increasing the circulation time of targeted nanocarriers in the blood. Polymers such as Poly-vinyl pyrrolidone, PEG-based copolymers and PEG can be used to create hydrophilic-coated NPs [21].

PEG is a biocompatible, nonionic, flexible, hydrophilic polymer made up of repeating ethylene oxide units and acts as a surface protector. PEG coated nanoparticles have been reported to have a half-life over 7 hours while in absence of PEG it is less than a minute [23]. Also Increasing amount of PEG on nanoparticles increases blood circulation time. PEG is highly soluble in water and

not absorbed by humans, anticancer drug, organ preservation, using on tablets, they also act as lubricants and binders, nontoxic and antibacterial [24].

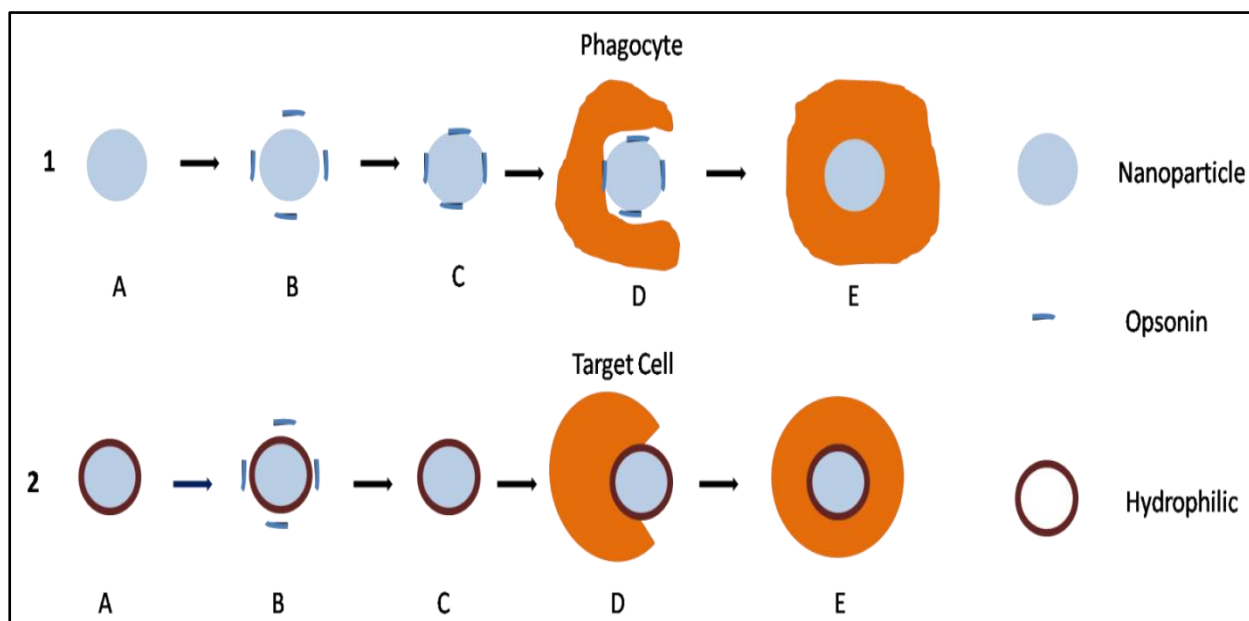


Figure 4.6 (1) uncoated hydrophobic nanoparticle pathway; (2) coated hydrophilic nanoparticle pathway

Notes: (1) (A) Nanoparticle in blood circulation; (B) opsonins recognize nanoparticle as a foreign body due to the hydrophobic surface; (C) nanoparticle opsonization; (D) and (E) phagocytosis by phagocyte and nanoparticle elimination. (2) (A) Hydrophilic polymer-coated nanoparticle in blood circulation; (B) steric hindrance maintains repulsive forces between opsonins and nanoparticle; (C) nanoparticle circulates until target site is reached; and (D) and (E) endocytosis by target cell.

4.4 Characterization of Magnetic Nanoparticles

Various characterization techniques are required to investigate the various properties of Fe_3O_4 NPs. Some methods provide different information about physical and chemical properties, while others provide information about morphology, structure and geometry. X-ray Diffraction (XRD), Fourier Transform Infrared Spectroscopy (FT-IR), Zeta measurement, Vibrating sample Magnetometer (VSM), Thermal Gravimetric Analysis (TGA), Transmission

electron microscopy (TEM) and Dynamic light scattering (DLS) techniques are used in this study.

4.4.1 Structural and phase analysis

4.4.1.1 XRD

X-ray diffraction analysis (XRD) is a methodology used in materials science to determine the crystallographic structure of a material. XRD works in which a material is irradiated with incident X-rays and then measuring the intensities and scattering angles of the X-rays that leave the material [24]. Basically, use of XRD analysis is the identification of materials based on their diffraction pattern. As well as phase identification, XRD also yields information on how the actual structure deviates from the ideal one, owing to internal stresses and defects [24]. X-rays are electromagnetic waves with a wavelength of 1 \AA . X-ray diffraction is based on constructive interference of monochromatic X-rays and a crystalline sample. These X-rays are produced by a cathode ray tube, by heating a filament to generate electrons, accelerating the electrons toward a target by applying a voltage and bombarding the target material with electrons. When electrons have sufficient energy to eject inner shell electrons of the target material, characteristic X-ray spectra are produced. These generated x-rays filtered to produce monochromatic radiation, collimated to concentrate and directed toward the sample. The interaction of the incident rays with the sample produces constructive interference (and a diffracted ray) when conditions satisfy Bragg's Law as given in equation 4.2.

$$n\lambda = 2d \cos \theta \quad (4.2)$$

Where d is the interplanar spacing, θ is the diffraction angle, λ is the X-ray wavelength and n is the order of diffraction. This law correlates the wavelength of electromagnetic radiation to the diffraction angle and the lattice spacing in a crystalline sample. These diffracted beams are then detected, processed and counted. Conversion of the diffraction peaks to d -spacings allows identification of the mineral because each mineral has a set of unique d -spacings. Generally, this is achieved by comparison of d -spacings with standard reference patterns [25].

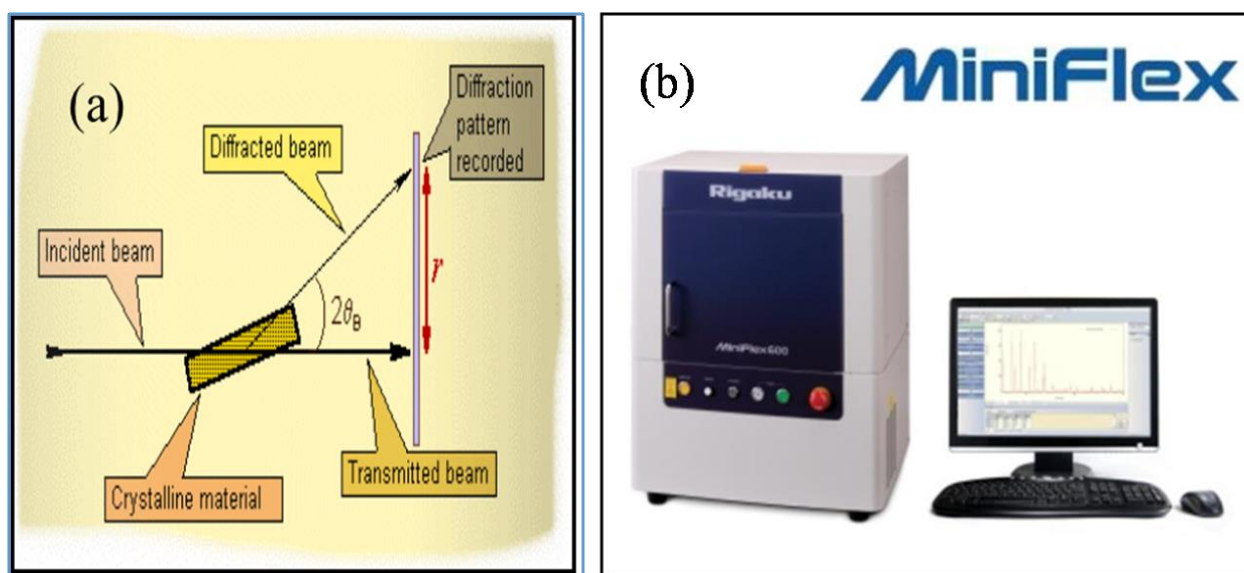


Figure 4.7 (a) Schematic diagram of X-ray Diffraction [25] and (b) XRD instrument

For X-ray diffraction, three methods are commonly used: the Laue method, the rotating-crystal method and the Powder method. The proposed work employs the Powder method, where θ is variable and λ is fixed. In particular, in the current method, the samples are finely powdered and then placed in a glass or aluminum rectangular plate. The sample is hit by a monochromatic X-ray beam. Each sample particle is a small crystal that is randomly oriented in relation to the incident X-ray beam. By detecting the directions of diffracted X-ray beams,



information about atomic arrangements can be evaluated. X-ray diffraction analysis can usually confirm the crystal and phase structure. Figure 4.7 depicts a schematic representation of the XRD system. The measured diffraction peak positions and intensities are like a fingerprint of a specific crystalline phase. The standard JCPDS powder diffraction file is used to identify crystal phases in a sample and the reflections are related to Miller indices. The Debye Scherrer formula (Equation 4.3) provides the relationship for calculating crystallite size.

$$\beta = \frac{k\lambda}{d \cos \theta} \quad (4.3)$$

Where β is full width at half maximum, K is the shape factor, λ wavelength of X-ray ($\lambda = 1.5406 \text{ \AA}$), d is the average crystallite size and θ is the Bragg angle in degree, it should be noted that the shape factor K is dimensionless and is accounting for the shape of the specimen and often has the value of 0.91 [26]

The mean size, lattice parameter and the phase composition of the crystallites of PEG coated and uncoated Fe_3O_4 NPs were calculated using XRD (RIGAKU Miniflex 600). It is equipped with a crystal monochromator employing 1.54 \AA wavelength of Cu- $K\alpha$ radiation with scanning rate of 3° min^{-1} , ranging from 20 to 80° . X'Pert High score software is used to analyze the pattern and compared with standard JCPDS Card No. 89-4319. Using the Debye Scherrer's equation the average crystallite size was calculated from the XRD peaks.



4.4.1.2 FTIR

Fourier Transform Infrared Spectroscopy (FTIR) analysis is used for the identification of organic, inorganic and polymeric materials using infrared light for scanning the samples. Variations in the characteristic pattern of absorption bands clearly indicate a change in the material composition. FTIR is useful in recognizing and characterizing unknown materials, detecting contaminants in a material, finding additives and identifying decomposition and oxidation [27]. Like a molecular "fingerprint", by measuring an infrared absorption spectrum, FTIR spectra offers information on the identification of chemical bonds in a molecule [26]. A schematic diagram of FTIR is shown in figure 4.8 (a). A typical FTIR spectrometer consists of a source, sample cell, detector, amplifier, A/D convertor and a computer. In FT-IR spectrometry, the Michelson interferometer is frequently used. The interferometer is made up of two perpendicular plane mirrors, one of which can move perpendicular to the plane. The planes of these two mirrors are divided by a semi-reflective film known as a beam splitter. The material of the beam splitter is determined by the region to be examined. Materials like germanium or iron oxide are covered onto an infrared-transparent substrate (like potassium bromide or caesium iodide) to produce beam splitters, for the mid- or near infrared regions.

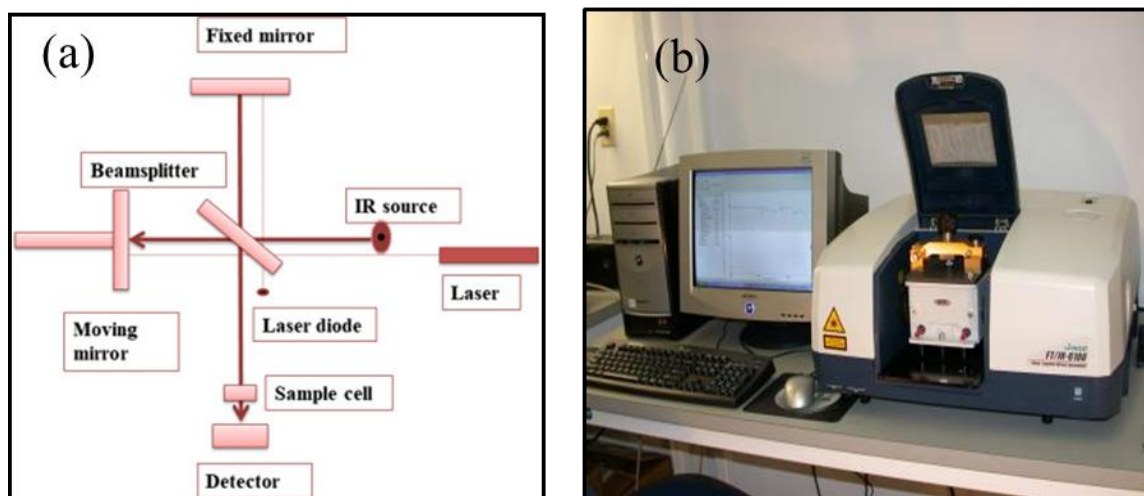


Figure 4.8 (a) A schematic diagram of FTIR (b) FTIR instrument

In this method, a chemical substance mainly exhibits selective absorption in the infrared region. The wavelength of absorption is determined by the relative masses of the atoms, bond force constants and atom geometry. Each band in a spectrum corresponds to the distinct functional groups and bonds found in a compound. Radiation generated from the source passes the sample through the interferometer and reaches the detector. The signal is amplified and converted to a digital signal by the A/D converter and amplifier, after which the signal is transferred to the computer where the Fourier transform is carried out. Infrared radiation of about $10,000\text{--}100\text{ cm}^{-1}$ is sent through the sample with some part of the radiation absorbed and some passing through. The radiation that is absorbed is converted by the sample to vibrational or rotational energy. The resultant signal obtained at the detector is a spectrum normally from $4000\text{ to }400\text{ cm}^{-1}$, which represents the sample's molecular fingerprint. Every molecule has a unique fingerprint, which makes FTIR a crucial tool for chemical identification [27].



The infrared spectra of PEG coated and uncoated Fe_3O_4 were recorded in the range of 4000 to 500 cm^{-1} on a Jasco FT/IR-6100 (Fig. 4.8(b)). The FT/IR-6100 provides a high level of functionality and high accuracy. It has highest signal-to-noise specifications (42000:1) with max resolution 0.5 cm^{-1} .

4.4.1.3 TGA

Thermogravimetric analysis (TGA) is an analytical technique used to find out a material's thermal stability and its fraction of volatile components by monitoring the weight change that occurs as a sample is heated at a constant rate. Because the sample is treated at various temperatures and with different atmospheres, the thermogravimetric method clearly belongs to the so-called thermal analysis. In a controlled dynamic environment, the method allows for simultaneous measurement of temperature, time and mass of a sample. The weight variation of the sample as a result of the thermal treatment is the basis for these types of measurements. Some mass will be lost as a result of the process in the form of volatiles or decomposition and this weight loss is typically measured with a microbalance. The sample is placed in a special "sample pan" or container designed for this type of measurement. The temperature variation is set according to a customised temperature programme that may include isothermal and ramp steps with different heating rates. The temperature is measured using thermocouples in contact with the sample container, as illustrated in figure 4.9 (a). The pan is typically placed on a sample holder, which is linked to a mass sensitive element (the microbalance) for mass measurement of the sample. The TG system (sample, sample holder, pan) is heated by an electric furnace, which in some cases can reach temperatures of up to 2000°C, depending on the materials and design of the furnace and other components.

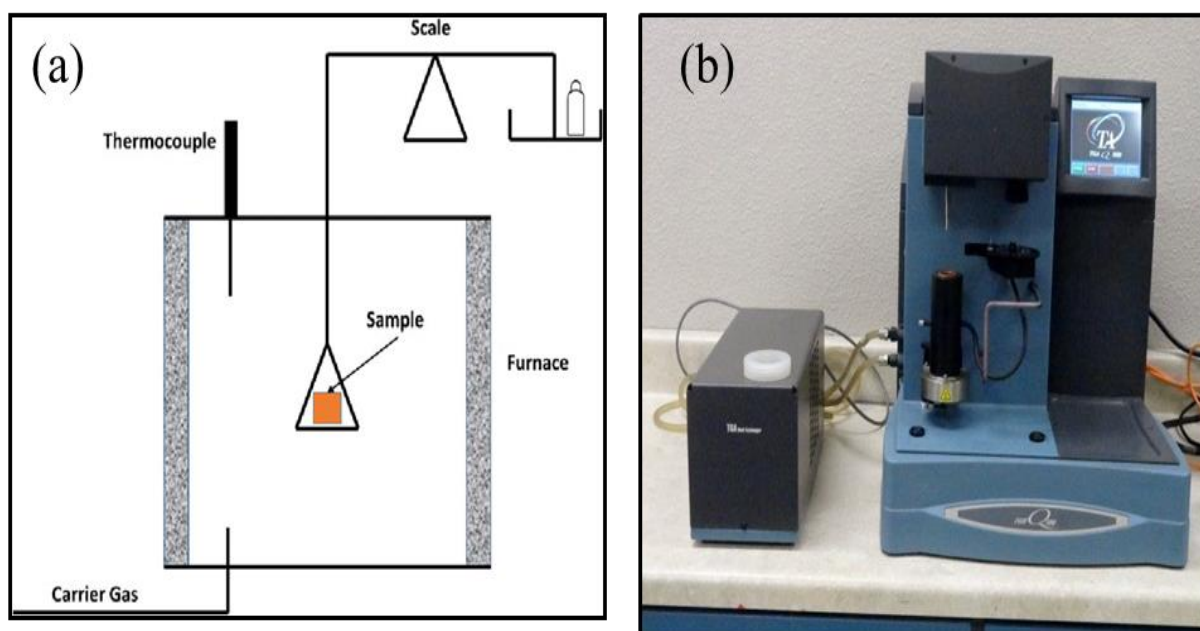


Figure 4.9 (a) Simple representation of the thermogravimetric method [33] (b) TGA instrumentation

The sample holder pans used in a TGA device can come in a variety of shapes and materials. They must be able to safely store the sample, not react with it and be appropriate for the desired temperature. Sample pans are typically made of alumina, platinum and aluminium [28]. A purge gas flowing through the balance produces an atmosphere that can be inert, such as nitrogen or argon; oxidising, such as air or oxygen; or reducing, such as forming gas (8 – 10% hydrogen in nitrogen). The purge gas's moisture content can range from dry to saturated [29].

Thermal Gravimetric Analysis was performed by TA instruments Lab Q5 (Fig. 4.9 (b)) under nitrogen gas atmosphere from 300⁰C to 600⁰C with a heating rate of 10⁰C/min. The Q50 TGA, manufactured by TA Instruments measures the change in mass of a sample with respect to temperature. It uses a sensitive micro-balance and precision temperature control. The maximum sample weight is 1 g



and resolution was 0.1 μg . Temperature range 30 -600 $^{\circ}\text{C}$ was used for the study with a heating rate of 100C/min.

4.4.2 Morphological study

4.4.2.1 TEM

Transmission electron microscopy (TEM) is a microscopy technique in which an image is created by passing an electron beam through a specimen. A suspension on a grid or an ultrathin section less than 100 nm thick are the most common specimens. The interaction of the electrons with the sample as the beam passes through the specimen creates an image. TEM is an important technique for analysing structure and behaviour that uses electrons rather than light. The TEM image provides a more detailed understanding of the morphology and a direct assessment of the nanomaterials' size distribution. This technique has been used for atomic-level chemical and structural studies as well as high-resolution imaging. The ray diagram for a transmission electron microscope is shown in schematic 4.10 (a). An electron gun at the top of the TEM produces a stream of monochromatic electrons when it is in use. The use of two coherent lenses concentrates this stream of electrons into a thin, small, coherent beam. When an electron beam is directed at a sample, a portion of it is transmitted. The objective lens focuses this transmitted portion into an image. A mandatory requirement of a sample for TEM analysis is that it be thin enough to allow electrons to pass through. For TEM, a material thickness of about 0.5 μm is recommended.

The material to be analysed is dispersed in some dispersive media (inert to powder) to generate colloidal solution, which is then dropped onto a copper or silver conducting grid (sq. size 1 m) and dried. Following that, the dried grid is employed as a specimen for TEM examination.

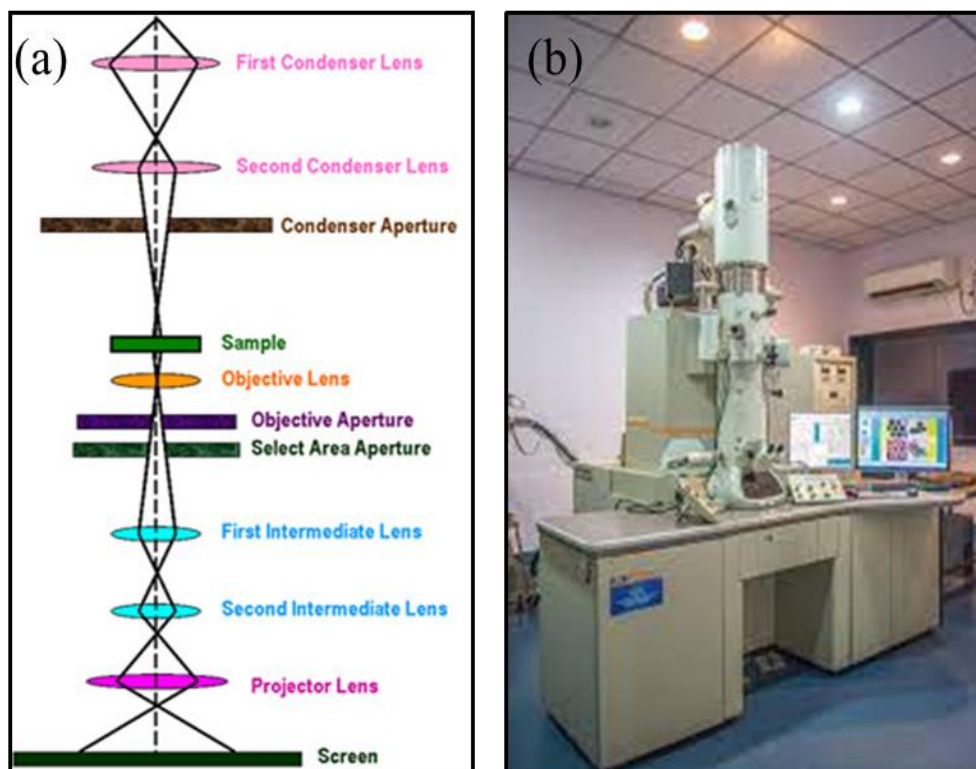


Figure 4.10 (a) Ray diagram of Transmission electron microscope [30]
(b) TEM instrumentation

The size, shape and uniformity of the NPs were analysed using a high-resolution TEM (HR-TEM) with a JEOL JEM-2100F in this study. The JEM-2100F is a multipurpose, 200 kV FE (Field Emission) analytical electron microscope. Different versions are provided to adapt to the user's purposes. The FE electron gun (FEG) produces a highly stable and bright electron probe that is never achieved with conventional thermionic electron gun. This property is essential for ultrahigh resolution in scanning transmission microscopy and in an analysis of a nano-scaled sample. It has other specifications such as spatial resolution (HRTEM): 2.3 Å (point-to-point), spatial resolution (STEM): 1.0 Å, energy resolution: 0.7 eV.



4.4.3 Colloidal stability study

4.4.3.1 Zeta potential

Magnetic nanoparticles (MNPs) should be stable in an aqueous solution for biomedical applications. As a result, MNP colloidal stability is a critical parameter that can be measured in terms of zeta potential. The electrical potential difference between the dispersion medium and the stationary layer of fluid which is attached to the dispersed particle is known as zeta potential (Fig. 4.11(a)). When all of the particles in a suspension have a large negative or positive zeta potential, they repel one another and have no tendency to group together [26].

Zeta potential is quantified of the effective electric charge on the nanoparticle's surface. When a nanoparticle has a net surface charge, the charge is “screened” by an increase in concentration of ions of opposite charge near the surface of the nanoparticle. This oppositely charged ion layer moves with the nanoparticle. The magnitude of the zeta potential gives information about particle stability. The greater the magnitude of potential exhibits increased electrostatic repulsion and therefore increased stability [31]. The line between stable and unstable suspensions is usually drawn at + 30 mV or - 30 mV. Stable particles are those with zeta potentials greater than + 30 mV or more negative than - 30 mV [26]. A small zeta potential value, on the other hand, can result in particle aggregation and flocculation due to the van der Waals attractive forces acting on them. The surface modification of NPs by nonionic polymers such as PEG aids particle stability by limiting direct interaction between cell and phagocytic systems [20].

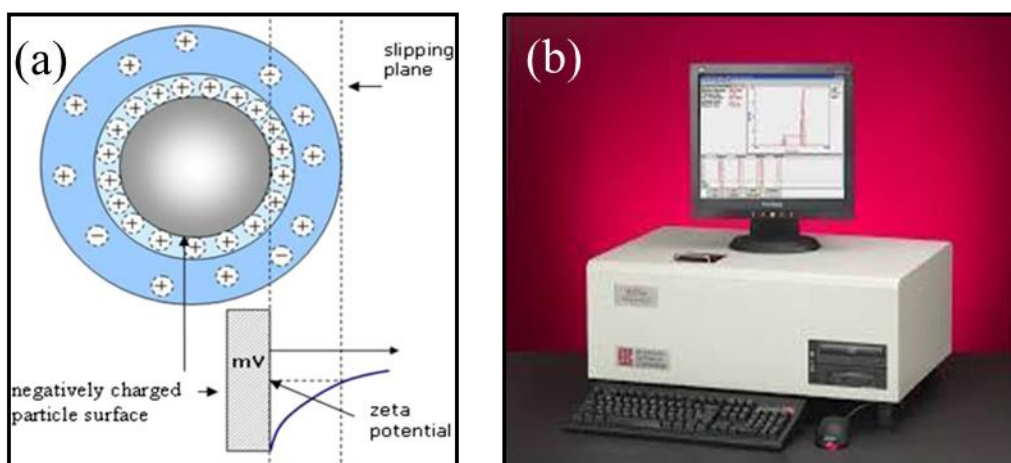


Figure 4.11 (a) Schematic diagram of electrical double layer at the surface of solution-phase nanoparticles [31]. (b) Zeta potential measurement instrumentation

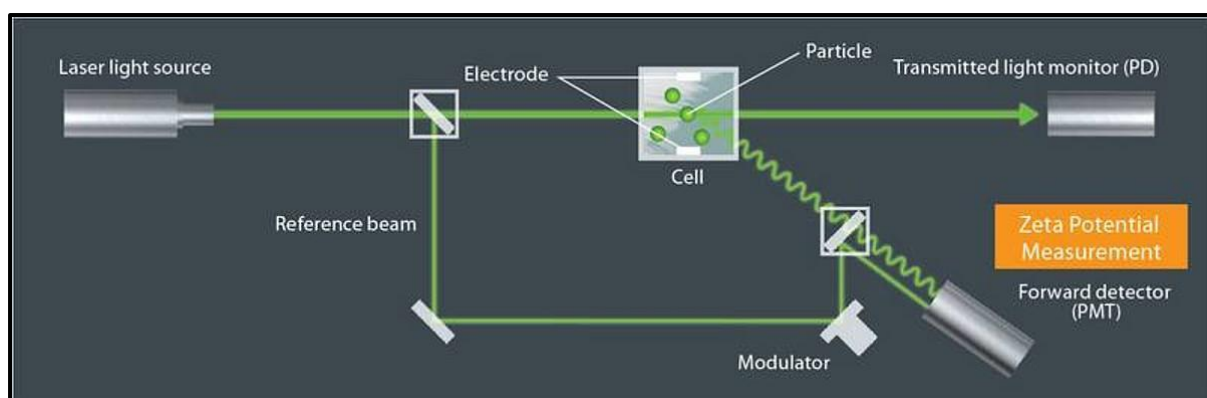


Figure 4.12 Block Diagram of Zetapotential measurements [32]

Figure 4.12 illustrates the principle of zeta potential measurement. The particle motion due to the applied electric field is measured by light scattering. Particles scatter light once illuminated with laser light. The frequency of the scattered light is a function of particle velocity due to the Doppler shift. This explicates another name for this method: laser Doppler electrophoresis. A second beam of light (the reference beam) is mixed with the scattered beam of light in order to sensitively extract the frequency shift in the scattered light. See figure 4.12 showing the scattered beam mixing with the reference beam at the zeta potential detector in



the lower right. The estimated magnitude of the frequency shift is then used to determine the particle velocity [32]. From the known applied electric field and measured particle velocity, the particle mobility is readily calculated. Zeta potential is then estimated from mobility [32].

Zeta potential of PEG coated Fe_3O_4 was carried out on 90 Plus nanoparticle size and zeta potential analyzer (Brookhaven Instruments, USA) as shown in figure 4.11(b). 90 Plus is equipped with a zeta potential analyzer which quantifies the zeta potential of the colloidal particles based on its mobility in an applied electric field. It is an absolute instrument for measuring colloids, latexes, micelles, microemulsions, proteins and other nanoparticles in the size range 1 nm - 6 microns. Based on the principles of dynamic light scattering, most measurements only take a minute or two. Measurements can be done only at two fixed angles, 15° & 90°.

4.4.3.2 DLS

The size of PEG coated Fe_3O_4 in water was studied by Dynamic Light Scattering (DLS), which is a useful parameter to decide blood half life time and biodistribution of nanoparticles. Dynamic light scattering (DLS) is based on the Brownian motion (i.e. random motion of particles in fluid results in bombardment of particles on surrounding media) of dispersed particles in liquid. When particles scatter in a liquid, they move in all directions at random. As particles collide with solvent molecules, a certain amount of energy is transferred, causing particle movement. Because the energy transfer is more or less constant, it has a significant impact on smaller particles. Smaller particles move faster than larger particles as a result of this. By measuring the speed of the particles and knowing

all other parameters that influence particle movement, one can determine the hydrodynamic diameter [33].



Figure 4.13 Zetasizer, Malvern, USA

The Stokes-Einstein equation describes the relationship between particle speed and particle size (Equation 4.4). The translational diffusion coefficient determines the particle speed (D). The equation also includes the dispersant's viscosity (η) and temperature (T) because both parameters have a direct influence on particle movement. The movement of the particles must be solely based on Brownian motion, which is a basic requirement for the Stokes-Einstein equation [33].

$$D = \frac{k_B T}{6\pi\eta a} \quad (4.4)$$

Where k_B is Boltzmann's constant, a is the radius of the spherical particle. There is no random motion if there is sedimentation, which would lead to inaccurate results. As a result, the beginning of sedimentation indicates the DLS upper size limit [33]. DLS study of PEG coated Fe_3O_4 was carried out on Zetasizer, Malvern, USA (Fig. 4.13). Instruments in the Zetasizer family are used to measure the

particle size of dispersed systems from sub-nanometer to several micrometers in diameter, using the technique called Dynamic Light Scattering (DLS).

4.4.4 Magnetic characterizations

4.4.4.1 VSM

VSM is an adaptable technique for measuring the magnetic moment of a sample when it is vibrated perpendicularly to a uniform magnetizing field. The VSM method can be used to obtain the magnetic moment information of samples based on Faraday's law of magnetic induction [34]. Law describes how an electric current produces a magnetic field and conversely, how a changing magnetic field generates an electric current in a conductor.

$$\varepsilon = -N \frac{d}{dt} (BA \cos \theta) \quad (4.5)$$

Where N is the number of wires turns in the coil, A is the coil's area and θ is the angle formed by the B field and the direction normal to the coil's surface.

VSM measures the magnetic moment of an entire sample. In this technique, a magnetic sample is mounted on the sample holder and placed between the electromagnet poles, typically oriented horizontally (see Fig. 4.14 (a)). There are a few types of sample holders, as shown in figure 4.14 (b); depending on the types of measurement to be performed, there are both in-plane and/or out-of-plane sample holders [34]. The sample to be studied is put in a continuous magnetic field during VSM experiments. If the sample is magnetic, the magnetic domains or individual magnetic spins will align with the applied magnetic field, magnetising the sample.

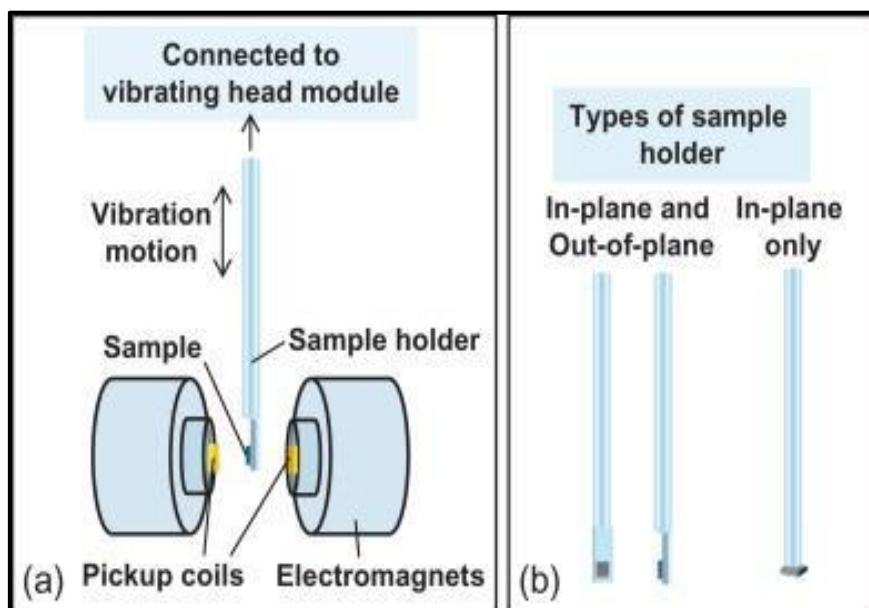


Figure 4.14 Schematic diagram of (a) part of the VSM setup and (b) types of sample holder used in VSM [34].

The magnetic dipole moment of the sample produces a magnetic field around it as a result of the applied magnetic field. The detecting coils will be induced by the oscillatory movement of the magnetised sample. The induced voltage is proportional to the sample's magnetization, which may be changed by changing the electromagnet's dc magnetic field. The superparamagnetic property of MNPs at ambient temperature is an important phenomenon for biomedical applications [26].

The magnetic properties of PEG coated Fe_3O_4 nanoparticles were measured using EG&G PAR 4500 Vibrating Sample Magnetometer (VSM) at 300K.

4.5 Biocompatibility Study: Cytotoxicity Assays

Nanomaterial (NM) research has in part been focused on their use in biomedical applications for more than several decades. However, in recent years this field



has been growing to a much more advanced stage by carefully controlling the size, shape and surface-modification of nanoparticles [35]. According to a consensus conference of the European Society for biomaterials in 1986, the biocompatibility is defined as the ability of a material to present appropriate host response in a particular application. The obscurity of the term reflects the ongoing development of insights into how biomaterials interact with the human body and eventually how those interactions decide clinical success. It is worth noting that the interactions between a material and a host are affected by several parameters including the host factors, the properties of the material, the site and duration of the exposure. To understand the type and scale of these interactions, nanomaterials should be tested for potential toxicity in a variety of in vitro and in vivo studies. However, there are no harmonized standards for assessing toxicity and biocompatibility of nanomaterials in biological systems and the rules are still being investigated [36].

Magnetic nanoparticles (MNP) have a particle size within the nanoscale with magnetic properties. Variety of metals can be used to convey the magnetic properties of MNPs; nickel, cobalt and iron have been demonstrated to be such examples. Organic and inorganic polymers including RGD peptides, fibronectin, dextran and PEG can be used to surface functionalize the magnetic core resulting in improved biocompatibility by protecting biological entities from adverse toxic reactions [37].

In in vitro research, cytotoxicity is one of the most significant parameters for biological evaluation. There is a need for affordable, accurate, and repeatable short-term cytotoxicity and cell viability assays in order to determine cell death



for cancer and biocompatibility for normal cells. These tests can be divided into four categories: dye exclusion assays, colorimetric assays, fluorometric assays and Luminometric assays. It is critical to select the most appropriate method from among these assays in order to acquire precise and trustworthy findings. Different aspects must be considered when choosing the cytotoxicity and cell viability assays to be utilised in the study, such as availability at the laboratory where the study will be conducted, test chemicals, detection mechanism, specificity and sensitivity.

For cytotoxicity studies of chemicals and drug screening, in-vitro cell viability and cytotoxicity assays with grown cells are routinely utilised. In recent years, there has been a growing interest in the use of these tests. These tests are currently being utilised in oncological studies to measure both chemical toxicity and tumour cell growth inhibition during medication development. They are quick and do not necessitate the use of animals. They can also be used to test a large number of sample materials. Various cell activities such as cell membrane permeability, enzyme activity, cell adherence, ATP synthesis, co-enzyme formation and nucleotide absorption activity are used in cell viability and cytotoxicity experiments [38]. In vitro cytotoxicity or cell viability assays provide a number of advantages including speed, cost saving, the ability to automate and studies utilising human cells may be more relevant than some in vivo animal experiments. They do, however, have significant drawbacks because they are not yet technologically proficient enough to completely replace animal tests [39]. Although cytotoxicity and cell viability assays are classified in a variety of ways, as shown in figure 4.15, these assays are classified based on the measurement kinds of end points (colour changes, fluorescence, luminescence and so on).

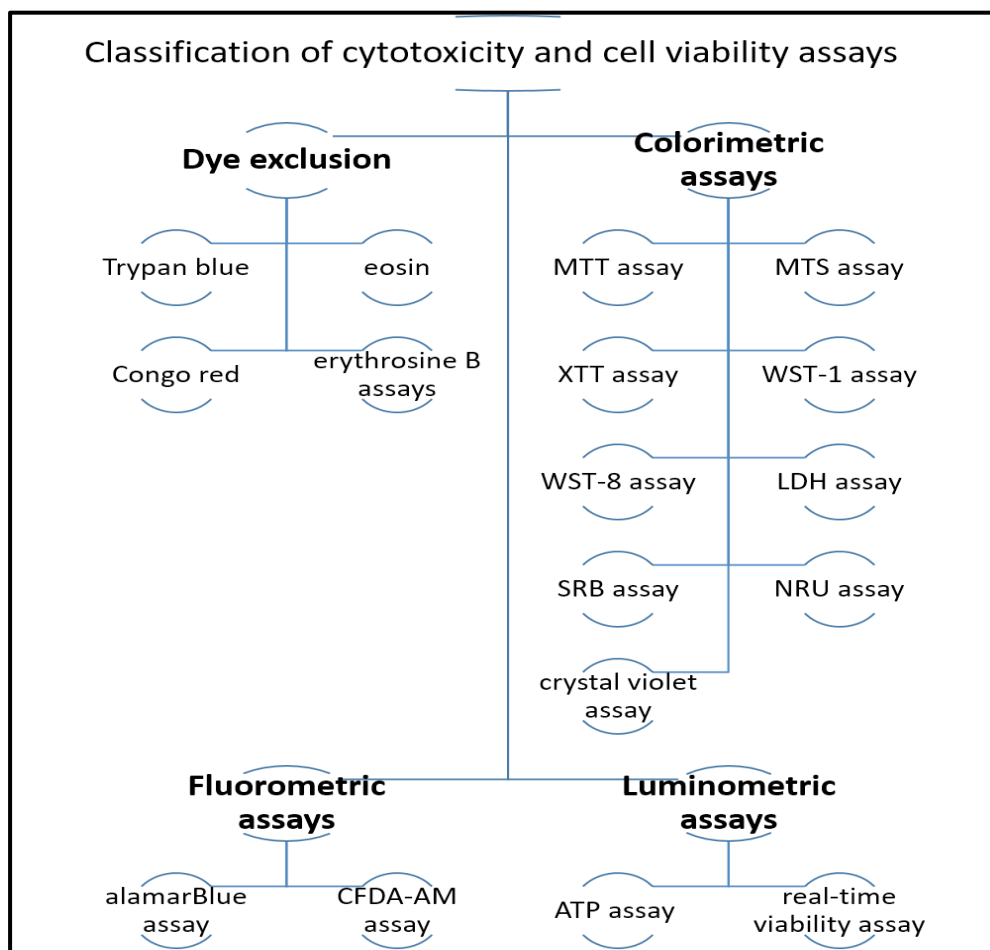


Figure 4.15 Different types of cell viability assay

Compared to other types, MTT assay is far superior because it is easy to use, safe, has a high reproducibility and is commonly used to determine both cell viability and cytotoxicity tests [40]. The MTT assay is used to assess cellular metabolic activity as an indicator of cell viability, proliferation and cytotoxicity. This colorimetric assay is based on the reduction of a yellow tetrazolium salt (3-(4,5-dimethylthiazol-2-yl)-2,5-diphenyltetrazolium bromide or MTT) to purple formazan crystals by metabolically active cells (Fig. 4.15). The viable cells contain NAD(P)H-dependent oxidoreductase enzymes which reduce the MTT to formazan. The insoluble formazan crystals are dissolved using a solubilization solution like Dimethyl sulfoxide (DMSO) and the resulting-colored solution is

quantified by measuring absorbance at 400-600 nanometers using a multiwell spectrophotometer. The darker the solution, the greater number of viable, metabolically active cells is present [41].

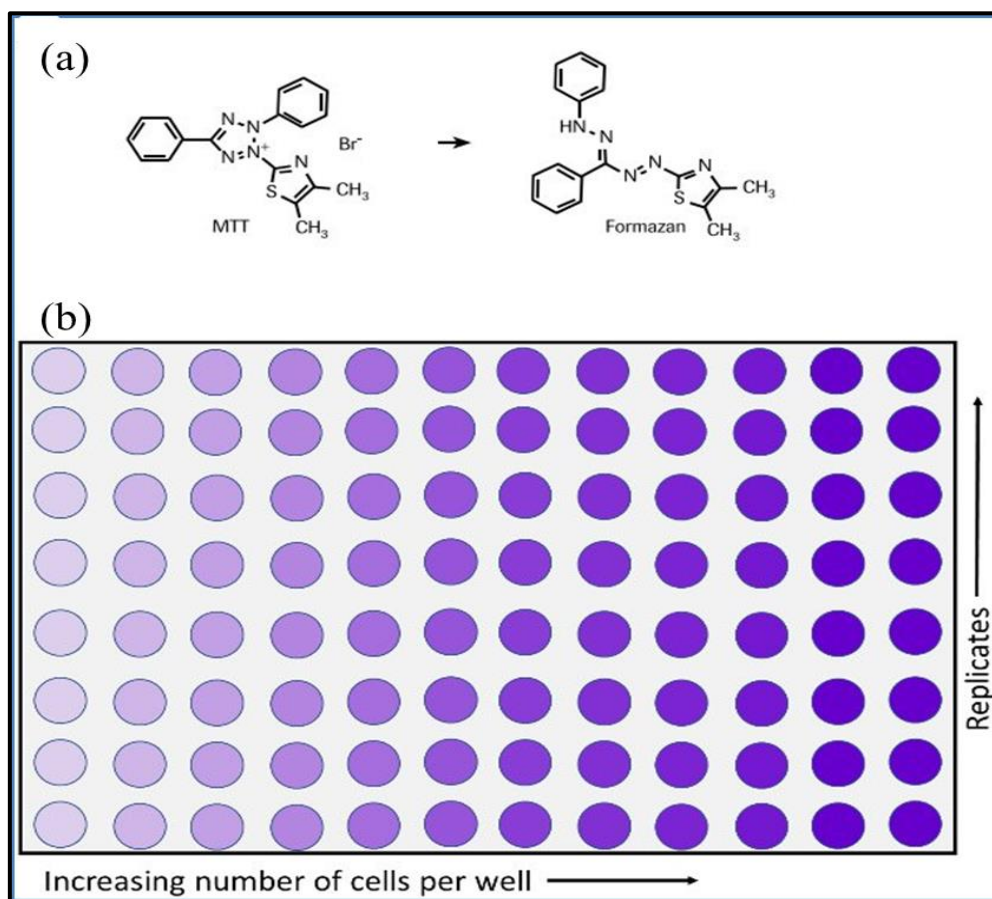


Figure 4.16 (a) Metabolism of MTT to a formazan salt by viable cells as shown in a chemical reaction and (b) in a 96-well plate [41].



References

1. Weldegebrieal G K. Synthesis method, antibacterial and photocatalytic activity of ZnO nanoparticles for azo dyes in wastewater treatment: A review. *Inorganic Chemistry Communications*. 2020, 120, 108140.
2. Ealias A M, Saravana kumar M P. A review on the classification, characterisation, synthesis of nanoparticles and their application, 2017 IOP Conf. Ser.: Mater. Sci. Eng. 2017, 263,032019.
3. Tri P N, Ouellet-Plamondon C , Rtimi S, Assadi A A, Nguyen T A. Methods for synthesis of hybrid nanoparticles. In *Noble Metal-Metal Oxide Hybrid Nanoparticles*. Woodhead Publishing. 2019, 51–63.
4. Ajay V R, Krishnan K, Abitha V K, Thomas S. Chapter 5 - Methods for Synthesis of Nanoparticles and Fabrication of Nanocomposites, Editor(s): Bhagyaraj S M, Oluwafemi O S, Kalarikkal N, Thomas S. In *Micro and Nano Technologies, Synthesis of Inorganic Nanomaterials*, Woodhead Publishing, 2018, 121-139.
5. Majidi S, Sehrig F Z, Farkhani S M, Goloujeh M S, Akbarzadeh A. Current methods for synthesis of magnetic nanoparticles, *Artificial Cells, Nanomedicine, and Biotechnology*. 2016, 44(2), 722-734.
6. Sandler S E, Fellows B, Mefford O T. Best Practices for Characterization of Magnetic Nanoparticles for Biomedical Applications. *Anal. Chem*. 2019, 91 (22), 14159–14169.
7. Patra J K, Baek K H. Green nanobiotechnology: factors affecting synthesis and characterization techniques. *J Nanomater*. 2014, 219.
8. Mukherjee S, Liang L, Veiseh O. Recent Advancements of Magnetic Nanomaterials in Cancer Therapy. *Pharmaceutics*. 2020, 12(2), 147.



9. Kesler S E, Simon A F. Mineral resources, economics and the environment (2nd Ed.). Cambridge, United Kingdom: Cambridge University Press. 2015.
10. Cornell R M, Schwertmann U. The Iron Oxides. VCH, New York, 1996.
11. Friák M, Schindlmayr A, Scheffler M. Ab initio study of the half-metal to metal transition in strained magnetite. New J. Phys. 2007, 9, 5.
12. Majidi S, Sehrig F Z, Farkhani S M, Goloujeh M S, Akbarzadeh A. Current methods for synthesis of magnetic nanoparticles, Artificial Cells, Nanomedicine and Biotechnology. 2016, 44(2), 722-734.
13. Nawaz M, Sliman Y, Ercan I, Lima-Tenório M K, Tenório-Neto E T, Kaewsaneha C, Elaissari A. Magnetic and pH-responsive magnetic nanocarriers. Stimuli Responsive Polymeric Nanocarriers for Drug Delivery Applications. 2019, 37–85.
14. https://edurev.in/studytube/Precipitation-and-co-precipitation--Catalyst-Scien/2e9cc4ef-2608-483b-bd88-ae4dbeb08b00_t
15. Mascolo M C, Pei Y, Ring T A. Room Temperature Co-Precipitation Synthesis of Magnetite Nanoparticles in a large pH Window with Different Bases. Materials (Basel). 2013, 6(12), 5549-5567.
16. Vayssieres L, Chanaec C, Tronc E, Jolivet J P. Size Tailoring of Magnetite Particles Formed by Aqueous Precipitation: An Example of Thermodynamic Stability of Nanometric Oxide Particles. J. Colloid Interf. Sci. 1998, 205 (2) 205-212.
17. Tang J, Myers M, Bosnick K A, Brus L E. Magnetite Fe₃O₄ Nanocrystals: Spectroscopic Observation of Aqueous Oxidation Kinetics. J. Phys. Chem. B. 2003, 107(30), 7501–7506.



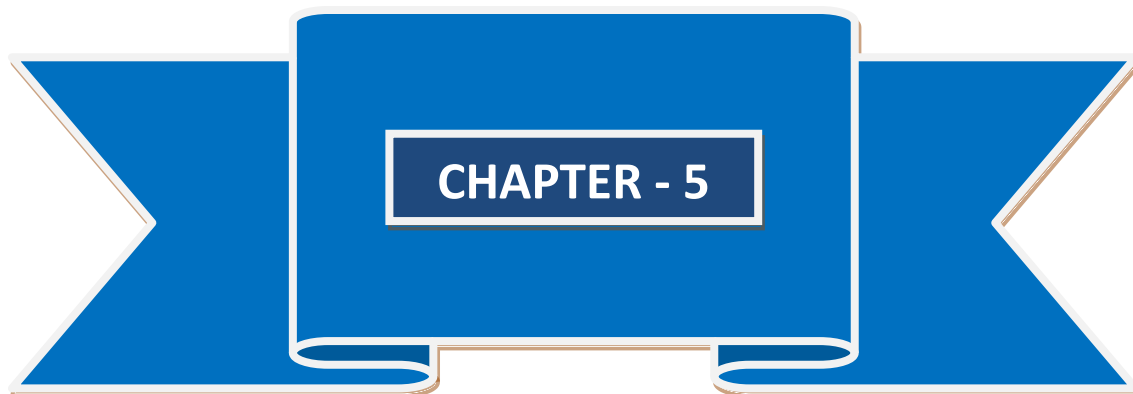
18. Valenzuela R, Fuentes M C, Parra C, Baeza J, Duran N, Sharma S, Knobel M, Freer J. Influence of stirring velocity on the synthesis of magnetite nanoparticles (Fe_3O_4) by the co-precipitation method. *J. Alloys Compd.* 2009, 488, 227–231.
19. Ali A, Zafar H, Zia M, et al. Synthesis, characterization, applications, and challenges of iron oxide nanoparticles. *NanotechnolSciAppl.* 2016 9, 49-67.
20. Anuje M, Sivan A, Khot V and Pawaskar P. Chapter 10 Cellular interaction and toxicity of nanostructures. In Thorat N, Bauer J (eds). *Nanomedicines for Breast Cancer Theranostics.* 2020, 203.
21. Murugan K, Choonara Y E, Kumar P, Bijukumar D, du Toit L C, Pillay V. Parameters and characteristics governing cellular internalization and trans-barrier trafficking of nanostructures. *Int J Nanomedicine.* 2015, 10, 2191–2206.
22. Yoo J, Chambers E, Mitragotri S. Factors that control the circulation time of nanoparticles in blood: challenges, solutions and future prospects. *Curr. Pharm. Des.* 2010, 16, 2298–2307.
23. Anbarasu M, Anandan M, Chinnasamy E, Gopinath V, Balamurugan K. Synthesis and Characterization of Polyethylene Glycol (PEG) Coated Fe_3O_4 Nanoparticles by Chemical Co-Precipitation Method for Biomedical Applications. *SpectrochimActa A Mol. Biomol. Spectrosc.* 2015, 135, 536-539.
24. <https://www.jove.com/science-education/10446/x-ray-diffraction>
25. www.micro.magnet.fsu.edu/primer/java/interference/index.html



26. Studies on surface functionalization of superparamagnetic $\text{La}_{0.7}\text{Sr}_{0.3}\text{MnO}_3$ nanoparticles for cancer hyperthermia therapy. Ph.D. thesis submitted to D.Y. Patil University by Swati Jadav.
27. Deena T, Samuel E J J, Roopan S M. Chapter 12 - Nanoparticle characterization techniques, Editor(s): Ashutosh Kumar Shukla, Siavash Irvani, In Micro and Nano Technologies, Green Synthesis, Characterization and Applications of Nanoparticles, Elsevier, 2019, 303-319.
28. De Blasio C. Thermogravimetric Analysis (TGA). In: Fundamentals of Biofuels Engineering and Technology. Green Energy and Technology. Springer, Cham. 2019.
29. Prime B R, Bair H E, Vyazovkin S, Gallagher P K, Riga A. Thermogravimetric analysis (TGA). In: Menczel J D, Prime B R. (Eds.), Thermal Analysis of Polymers, Fundamentals and Applications. John Wiley, New Jersey. 2009, 241–317.
30. <http://www.nanoscience.gatech.edu/zlwang/image/research/tem/fig1.jpg>
31. Vijayakumar S. Chapter 15 - Stability Studies on Nanomaterials Used in Drugs, Editor(s): Shyam S. Mohapatra, Shivendu R, Nandita D, Raghvendra K M, Thomas S. In Micro and Nano Technologies, Characterization and Biology of Nanomaterials for Drug Delivery, Elsevier, 2019, 425-444.
32. https://www.horiba.com/en_en/zeta-potential/
33. <https://wiki.anton-paar.com/us-en/the-principles-of-dynamic-light-scattering/>
34. Adeyeye A O, Shimon G. Chapter 1 - Growth and Characterization of Magnetic Thin Film and Nanostructures, Editor(s): Robert C, Zbigniew C, Robert L S. Handbook of Surface Science, North-Holland. 2015, 5, 1-41.



35. Gurunathan S, Kim J H. Synthesis, toxicity, biocompatibility, and biomedical applications of graphene and graphene-related materials. *Int J Nanomedicine*. 2016, 11, 1927-1945.
36. Adabi M, Naghibzadeh M, Adabi M, Zarrinfard M A, Esnaashari S S, Seifalian A M, Faridi-Majidi R, Tanimowo Aiyelabegan H, Ghanbari H. Biocompatibility and nanostructured materials: applications in nanomedicine. *Artif Cells Nanomed Biotechnol*. 2017, 45(4), 833-842.
37. Markides H, Rotherham M, El Haj A J. Biocompatibility and Toxicity of Magnetic Nanoparticles in Regenerative Medicine. *Journal of Nanomaterials*. 2012, 1–11.
38. Ishiyama M, Tominaga H, Shiga M, Sasamoto K, Okhura Y, Ueno K A. Combined assay of cell viability and in vitro cytotoxicity with a highly water-soluble tetrazolium salt, neutral red and crystal violet. *Biological & Pharmaceutical Bulletin*. 1996, 19(11), 1518-1520.
39. Chrzanowska C, Hunt S M, Mohammed R, Tilling P J. The use of cytotoxicity assays for the assessment of toxicity. In: EHT 9329, Final Report to the Department of the Environment. 1990
40. Stone V, Johnston H, Schins R P F. Development of in vitro systems for nanotoxicology: Methodological considerations. *Critical Reviews in Toxicology*. 2009, 39(7), 613-626.
41. <https://www.sigmaaldrich.com/IN/en/technical-documents/protocol/cell-culture-and-cell-culture-analysis/cell-counting-and-health-analysis/cell-proliferation-kit-i-mtt>



PEG COATED SPION'S RADIOSENSITIZER EVALUATION

**Part of this chapter included in research paper published in
Journal of Medical Physics**

Original Article

Synthesis, Characterization, and Cytotoxicity Evaluation of Polyethylene Glycol-Coated Iron Oxide Nanoparticles for Radiotherapy Application

Madhuri Anuje, Padmaja N. Pawaskar, Vishwajeet Khot, Ajay Sivan¹, Satish Jadhav, Jagruti Meshram, Balu Thombare²

Department of Medical Physics, Center for Interdisciplinary Research, D.Y. Patil Education Society (Deemed to be University), Kolhapur, ¹Department of Radiotherapy, Integrated Cancer Treatment and Research Centre, ²Department of Physics, Savitri Bai Phule Pune University, Pune, Maharashtra, India



PEG



FeCl_2



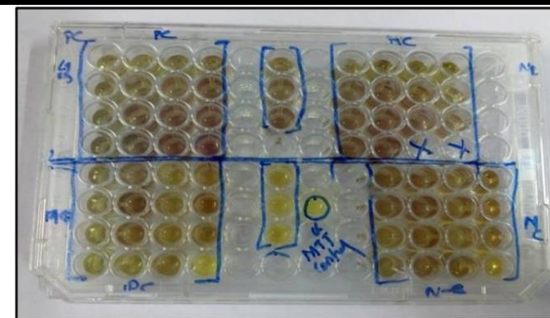
FeCl_3



KOH



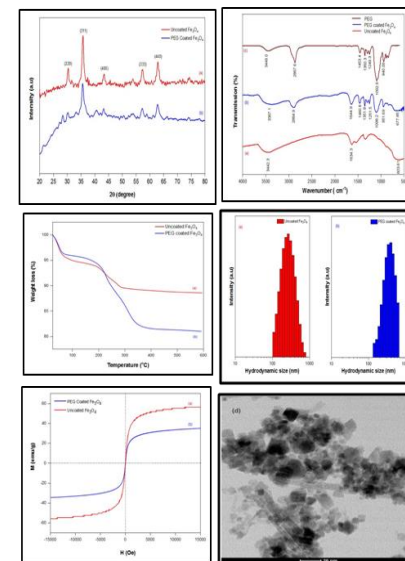
Synthesis by Co-precipitation



MTT Assay



PEG coated Fe_3O_4



Characterizations

5.1 Introduction

Nowadays, cancer is one of the prime causes of morbidity and mortality in the world. The ideal aim of radiotherapy is delivering a lethal radiation dose to tumor cells while reducing radiation exposure to healthy tissues around the tumor. One way to increase the dose in the tumor cells is the use of nanoparticles (NPs) as radiosensitizer substances in these cells [1]. Superparamagnetic iron oxide nanoparticles are mainly made up of either magnetite (Fe_3O_4) or maghemite ($\gamma \text{Fe}_2\text{O}_3$). These are particularly valuable because of their superparamagnetic properties, which enable them to be guided and confined to a specific organ using external magnetic force [2]. Before its application as a radiotherapy sensitizer one needs to study its properties such as size, structure, functional group, shape, colloidal stability, surface functionalizations, magnetic properties, biocompatibility and cytotoxicity. These properties exhibit nanoparticle behavior in in-vivo and in -vitro studies.

In order to increase blood circulation time and stability and for prevention from opsonization, Fe_3O_4 nanoparticles must be coated with polymers such as Poly (ethylene) Glycol (PEG). Surface functionalization of NPs confirmed with different characterizations. In this study PEG coated Fe_3O_4 nanoparticles synthesized by chemical co-precipitation method and X-ray powder diffraction (X-RD), Fourier transform infrared spectroscopy (FTIR), Thermogravimetric analysis (TGA), Zeta-Potential Measurements, Dynamic Light Scattering (DLS), Transmission electron microscopy (TEM), Vibrating-sample magnetometer (VSM) and cytotoxicity study has been carried out. X-RD, FTIR and TGA results show that Fe_3O_4 nanoparticles have been functionalized with PEG molecules during the course of synthesis. Synthesized nanoparticles should have good stability which has been confirmed from zeta potential. DLS results



reveal that PEG coated Fe_3O_4 has greater hydrodynamic size than bare. TEM micrograph demonstrated that nanoparticles are roughly spherical and size is in the 10 – 20 nm range. Saturation Magnetization value of PEG coated and bare Fe_3O_4 also confirms coating and shows superparamagnetic behavior. Cytotoxicity study indicated that PEG coated Fe_3O_4 is biocompatible on L929 and toxic on MCF-7. These characterized properties of nanoparticles of PEG coated Fe_3O_4 shows that it may be capable to work as a radiosensitizer in radiotherapy, in order to increase therapeutic efficacy so that it minimizes painful side effects of radiation.

5.2 Experimental

5.2.1 Synthesis and characterization of PEG coated and uncoated Fe_3O_4 Nanoparticles

Iron (III) chloride anhydrous (FeCl_3 , 96%), Ferrous chloride hydrated (FeCl_2 , 98%), Potassium hydroxide pellets (KOH), polyethylene glycol (PEG 400) were purchased from Sigma-Aldrich. All these chemicals were used directly without further purification.

Synthesis of PEG coated and uncoated Fe_3O_4 nanoparticles

PEG coated Fe_3O_4 were synthesized by chemical co-precipitation method [15]. Experimental setup is as shown in figure 5.1. In a beaker containing 100 ml of distilled water, 2 M of ferric chloride, 1 M of ferrous chloride and 10 ml of PEG 400 were added and stirred for 30 min. 1 M of KOH pellets dissolved in 100 ml distilled water was taken in a burette and added drop wise to the beaker containing aqueous solution of FeCl_3 , FeCl_2 and PEG for 45 minutes to obtain homogenous solution.



Figure 5.1 Experimental setup of synthesis of PEG coated Fe_3O_4

Temperature was maintained at 90°C with a stirring rate of 1100 rpm. The solution appears black in colour. When the required condition for precipitation was achieved, the solution allowed settling down as shown in figure 5.2 (a). Precipitate was magnetically separated using a permanent magnet and washed 3-4 times and kept in the oven at 90°C for 12 hours. Figure 5.2 (b) shows behavior of nanoparticles in presence of magnetic field i.e., nanoparticles align in the direction of applied magnetic field. For synthesis of bare Fe_3O_4 ; 2 M of ferric chloride and 1 M of ferrous chloride were taken in a beaker containing 100 ml of distilled water. 1 M of KOH pellets dissolved in 100 ml distilled water and added drop wise to the beaker containing aqueous solution of FeCl_3 , FeCl_2 under nitrogen atmosphere with stirring rate 1100-1200 rpm and temperature maintained the same as above.

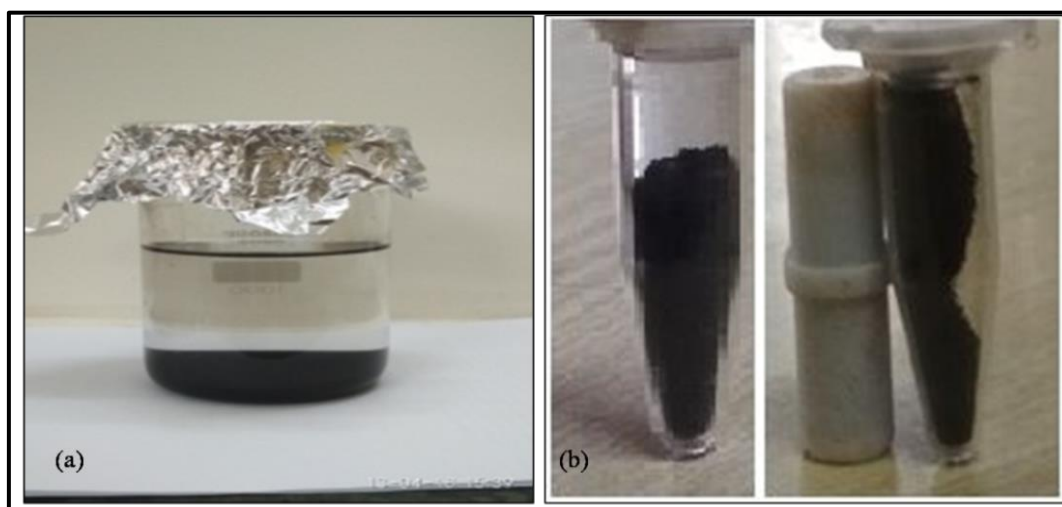


Figure 5.2 (a) Precipitation of iron oxide nanoparticles, (b) Nanoparticles in absence and presence of magnet

Characterization

The X-ray diffraction patterns of PEG coated Fe_3O_4 nanoparticles were performed on an X-ray diffractometer (Bruker AXS D8 advance). The infrared spectra were recorded in the range of 4000 to 500 cm^{-1} on a Fourier Transform Infrared Spectrometer (Jasco FT/IR-6100). Thermal Gravimetric Analysis was performed by TA instruments Lab Q50 under nitrogen gas atmosphere from 300°C to 600°C with a heating rate of $10^\circ\text{C}/\text{min}$. Zeta potential was carried out on a 90 plus particle size analyzer, Brookhaven, USA. Dynamic light scattering for hydrodynamic size determination was performed on Zetasizer, Malvern Instruments Ltd. 2 mg of PEG coated nanoparticles was dissolved in 2 ml of distilled water and Sonicated for 2 to 3 minutes. Supernatant of the solution is taken to study hydrodynamic size. Nanoparticle size was determined by transmission electron micrograph taken on JEOL JEM-2100F Field Emission Gun Transmission Electron Microscope (HR-TEM). The magnetic properties of PEG coated Fe_3O_4 nanoparticles were measured using EG & G PAR 4500 Vibrating Sample Magnetometer (VSM) at 300K .

5.2.2 In vitro cytotoxicity study of PEG coated and uncoated Fe₃O₄ nanoparticles

Materials

L-929 Mouse Fibroblast & MCF-7 breast cancer cell, Dulbecco's Modified Eagle Medium (DMEM) containing 10% FBS, Neubauer's Chamber, 96 well Tissue culture treated plate, EZ count MTT Cell Assay Kit (HiMedia), Phosphate buffered saline, T25 flasks (Thermo), Thermo scientific Nalgene syringe filter (0.2 μ m PES). Culture flasks incubated in the CO₂ Incubator at 37°C with 5.0 % CO₂. MTT Assay done at APT Research Foundation, Pune, Maharashtra, India. All experiments were carried out in triplicate. The cell survival values presented in the figures show the mean \pm standard. The cell survival value among the different groups was compared using Two tailed unpaired t-Test with $p \leq 0.05$ considered significant.

Cell culture

In the 96 well tissue culture treatment plate, 10⁴ cells/well were added (cell count was taken using a Neubauer's chamber) (as shown in Fig. 5.3). For 24 hours, the plate was incubated at 37°C in a 5% CO₂ incubator. The plate was examined under an inverted microscope after 24 hours of incubation to verify the morphology of the cells and the confluency of the wells in the 96 well plates. The sterile test sample was suspended at a predetermined concentration in DMEM containing 10% FBS and dilutions were made appropriately. 100 μ l of each of the test samples at various concentrations, as well as the positive control (doxorubicin) and normal control (cells with medium and no test sample), were added. After adding the sample, the plate was incubated for 24 hours at 37°C in a 5% CO₂ incubator.

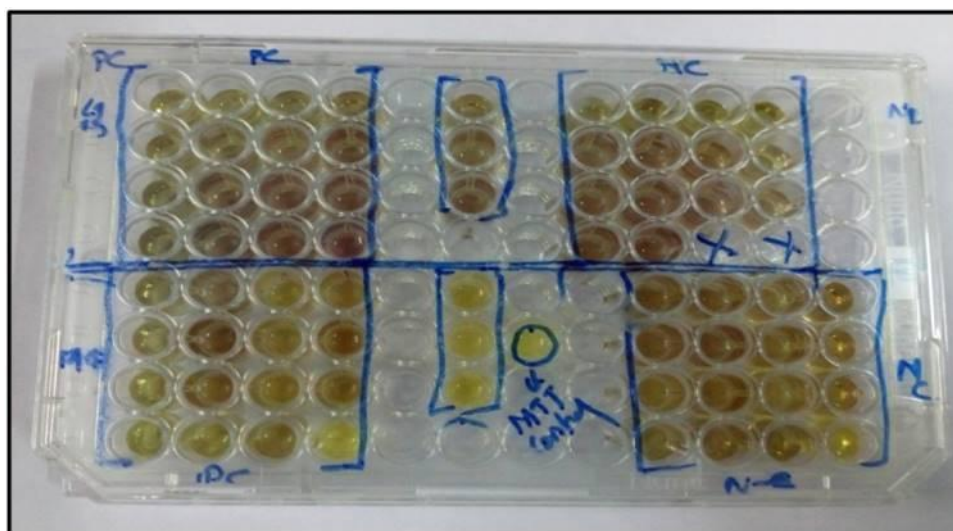


Figure 5.3 Tissue culture well plate

The plate was examined under an inverted microscope after 24 hours of incubation and images of the recorded observations were made. The test sample was withdrawn and 90 μ l of fresh DMEM with 10% FBS was added. Then, in each well, 10 μ l of MTT reagent was applied. The plate was wrapped in aluminium foil and incubated for 4 hours at 37°C in a 5% CO₂ incubator. After 4 hours of incubation, the entire medium was removed by flicking the plate and 100 μ l of solubilisation buffer was added to each well, which was then incubated for 20 minutes at 37°C in a 5% CO₂ incubator. On a 96 well Plate reader, absorbance was measured at 570 nm and 630 nm after incubation.

5.3 Results and Discussion

5.3.1 Structural analysis

5.3.1.1 X-ray diffraction (X-RD)

The X-ray diffraction pattern was obtained of synthesized bare Fe₃O₄ and PEG coated Fe₃O₄ nanoparticles were characterized by X-ray diffraction technique using Bruker AXS D8 advance (Cu K α , λ =1.5406 Å radiation) and XRD was



taken every time to confirm its structure. Size of nanoparticles was calculated for high intense peak of (311) using Scherrer's relation (5.1) as

$$D = \frac{K\lambda}{\beta \cos \theta} \quad (5.1)$$

Where, β is the full width at half maxima, K is a shape factor constant (0.91) and λ is the wavelength of Cu-K α X-ray source (1.5406 Å)

We have synthesized PEG coated and bare Fe₃O₄ and XRD was taken every time to confirm its structure. Size of nanoparticles calculated using Scherrer formula, which is in the range of 8 – 12 nm. The X-RD pattern reveals the formation of single-phase PEG coated Fe₃O₄ and uncoated Fe₃O₄, with lattice constants, a , 8.3578 Å and 8.331 Å respectively, which is very close to reported value of magnetite (JCPDS Card No. 89-4319, a =8.3952 Å). The crystalline size of PEG coated Fe₃O₄ and bare Fe₃O₄ are estimated to be about 9.86 nm and 10.94 nm from X-ray line broadening as shown in figure 5.4 (b) and (a). The crystalline size with repeated synthesis found to be 9.85 nm and 10.00 nm for PEG coated Fe₃O₄ (Fig. 5.5 (b)) and without (Fig. 5.5 (a)) PEG coated Fe₃O₄ respectively.

The diffraction peaks at $2\theta = 30.36^\circ$, 35.72° , 43.44° , 57.26° and 62.92° can be assigned to the (220), (311), (400), (333) and (440) planes respectively, which indicates cubic crystal structure of pure Fe₃O₄. Figure clearly shows that diffraction peaks for uncoated Fe₃O₄ (Fig. 5.4 (a)) are stronger in intensity and narrower as compared to PEG coated Fe₃O₄ (Fig. 5.4 (b)).

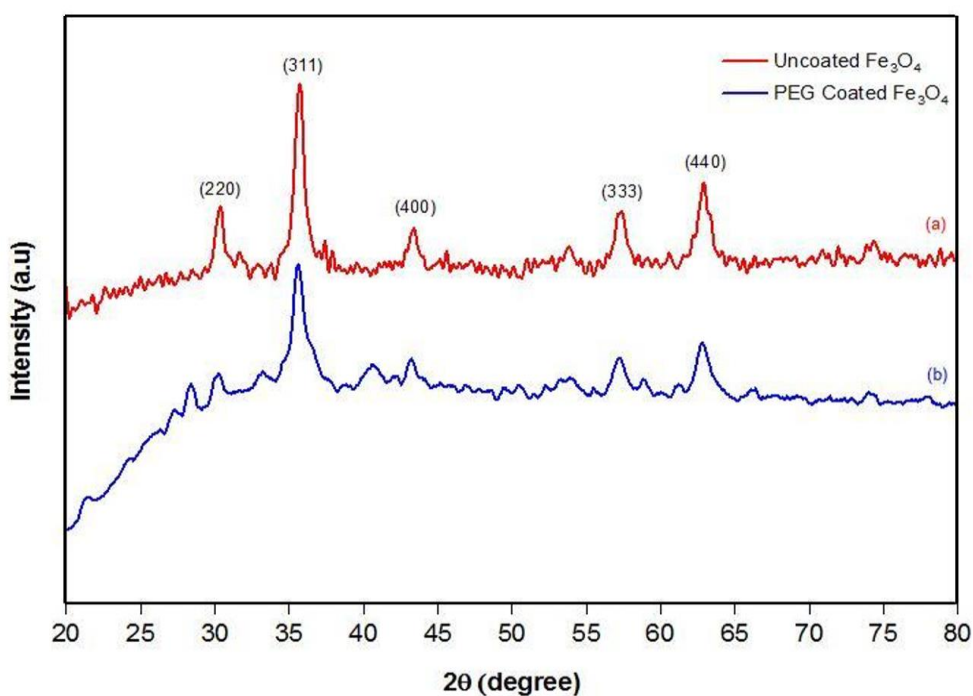


Figure 5.4 (a) X-RD spectra of uncoated Fe_3O_4 and (b) PEG coated Fe_3O_4 .

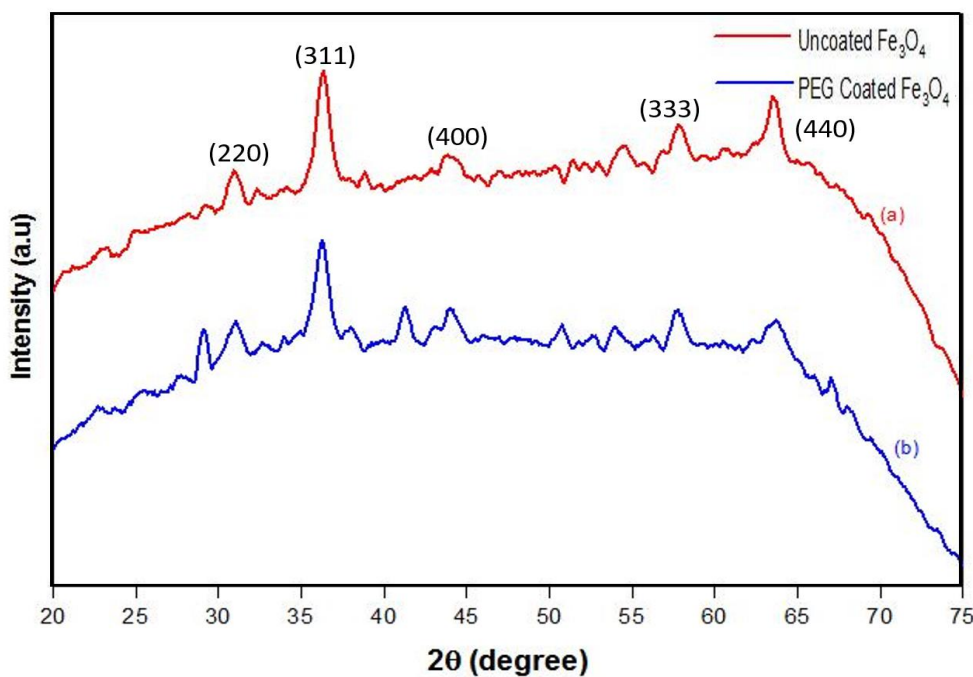


Figure 5.5 (a) X-RD spectra of uncoated Fe_3O_4 and (b) PEG coated Fe_3O_4 .



It has been observed that coating reduces crystalline size of nanoparticles [3]. It may be due to the coating preventing agglomeration of particles. During the synthesis most nano-objects are used in the form of a suspension having been dispersed in an aqueous medium. To stabilize such suspensions and to prevent sedimentation or agglomeration, molecules or polymers are coated to the particle surface [4]. Also, we can assume that due to surface coating, nucleation rate is higher compared to growth which results in formation of large numbers of smaller particles (as discussed in chapter 4, section 4.2.1).

5.3.1.2 Fourier transform infrared spectrometry (FTIR)

The presence of PEG molecules confirmed by FTIR studies as shown in figure 5.6, FTIR was carried out for the 500 cm^{-1} - 4000 cm^{-1} wavenumber interval. The data plot transmits the wave number of infrared lights in the form of sharp absorption peaks in certain wavenumbers resulting from the vibration of certain functional groups. In PEG spectra (Fig. 5.6 (c)) absorption peak seen at 1092.6 cm^{-1} is due to C-O-C ether stretch band [5]. $-\text{CH}_2$ bending bands appear at 1453.40 cm^{-1} and 1249.3 cm^{-1} . The peak at 940.09 cm^{-1} corresponds to the out of plane bending vibration of $-\text{CH}$ band [5]. Infra- red wavenumber absorption occurred at 2867.6 cm^{-1} is due to $-\text{CH}$ stretching vibration band [6]. In the pure Fe_3O_4 spectrum (Fig. 5.6 (a)), it is identified that the occurrence of bending vibration of H-O-H at 1634.3 cm^{-1} is due to adsorbed water [7]. Stretching vibration of Fe-O functional group occurs for absorption of infrared wavenumber at 603.61 cm^{-1} . In PEG coated Fe_3O_4 FTIR spectra (Fig. 5.6 (b)) main absorbance of ether stretch band seen at the 1098.2 cm^{-1} . Bending vibrations of $-\text{CH}_2$ and $-\text{CH}$ bands are seen at 1460.08 cm^{-1} , 1251.5 cm^{-1} and 951.69 cm^{-1} respectively. Also, H-O-H bending is seen around 1644.9 cm^{-1} . Fe-O vibration in PEG coated appeared around 677.85 cm^{-1} . The broad peak in between $3400 - 3028\text{ cm}^{-1}$ in all of these spectra

of PEG, PEG coated and Iron oxide belongs to the attached hydroxyl group (Table 5.1) [7]. The presence of C-O-C ether stretch, -CH₂ bending, -CH bending, -CH stretching and Fe-O stretching vibration in PEG coated Fe₃O₄ confirms Fe₃O₄ is coated with PEG on its surface.

Table 5.1 Functional group bonds of Fe₃O₄nanoparticles [7].

Sr. No	Wavenumber (cm ⁻¹)	Functional Group
1	658-506	Fe-O Stretching
2	1672-1367	H-O-H Bending
3	3400-3028	O-H Stretching
4	2920-2855	C-H Stretching

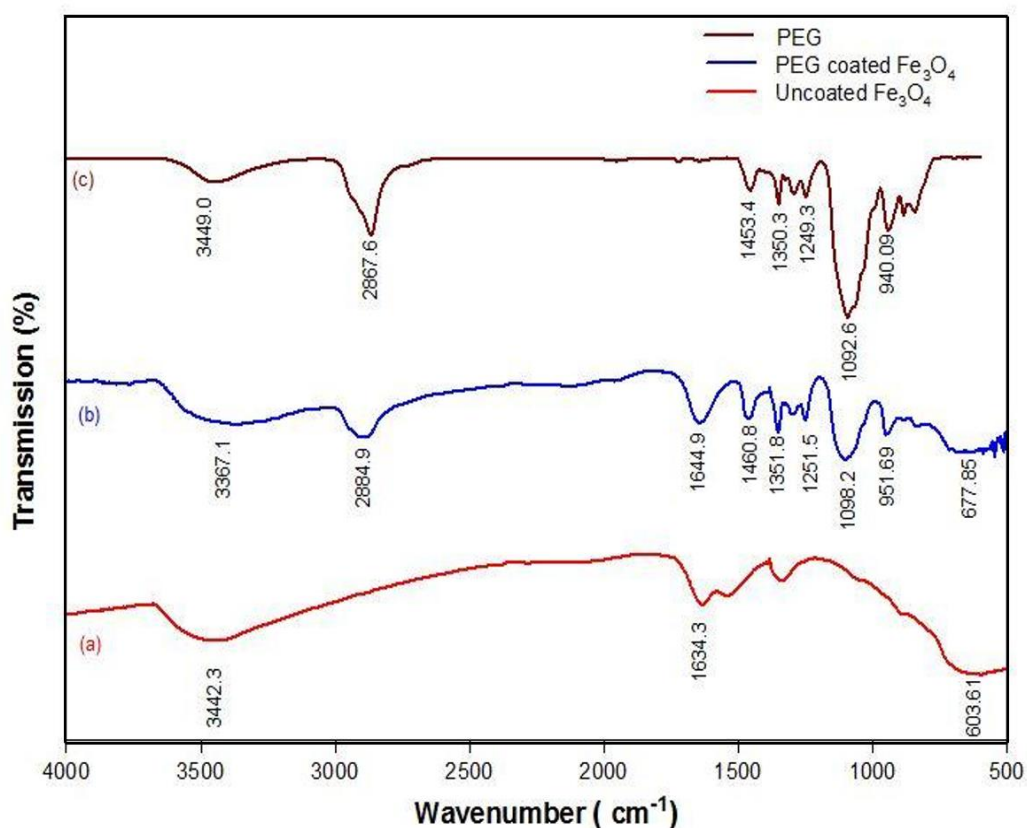


Figure 5.6 FTIR spectra of (a) uncoated Fe₃O₄, (b) PEG coated Fe₃O₄ and (c) PEG

5.3.1.3 Thermal gravimetric analysis (TGA)

Figure 5.7 shows thermo-gravimetric analysis of bare Fe_3O_4 and PEG coated Fe_3O_4 nanoparticles. The TGA curve shows that decomposition of PEG coat (curve 5.7 (b)) of nanoparticles started around 194°C and ended around 375°C . Indicating the total weight loss of 18.13% results from decomposition of PEG polymers from the surface of PEG coated Fe_3O_4 nanoparticles. From uncoated Fe_3O_4 (curve 5.7 (a)) it is seen that decomposition started around 179°C and percentage weight loss is about 10.4%. The increment in onset decomposition temperature about 15°C of PEG coated nanoparticles and difference in percentage weight loss confirms strong attachment of PEG molecules on surfaces of Fe_3O_4 nanoparticles.

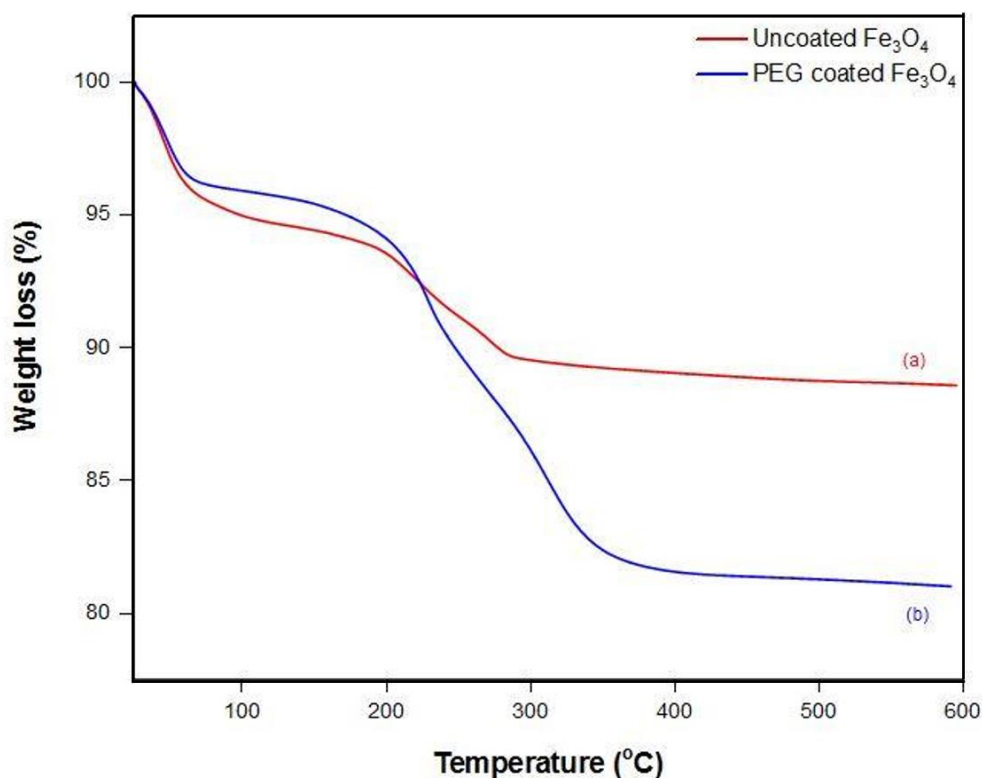


Figure 5.7 (a) TGA curves of uncoated Fe_3O_4 and (b) PEG coated Fe_3O_4



5.3.2 Colloidal stability study

5.3.2.1 Zeta potential measurements

Higher colloidal stability of the nanoparticles is due to stronger charge on the surface and hence will lead to longer shelf life [8]. Colloidal stability of PEG coated Fe_3O_4 was studied by Zeta Potential Measurements. Average Zeta Potential value for PEG coated Fe_3O_4 found to be 32.65 mV [9]. Under the applied electric field, the specimen particles dissolved move toward the electrode of opposite charge. The intensity fluctuations of the laser light scattered by the sample particles proportional to their electrophoresis mobility (velocity) are transformed into the zeta potential values. Zeta potential value determines stability of colloidal systems. Colloidal systems with zeta-potential higher than 30 mV are strongly charged and become stable due to particle–particle repulsion, thus avoiding agglomeration of particles and provides control over the size of NPs.

5.3.2.2 Dynamic light scattering (DLS)

The size of PEG coated Fe_3O_4 in water was studied by Dynamic Light Scattering (DLS), which is a useful parameter to decide blood half lifetime and bio distribution of nanoparticles. Greater amount of PEG coverage increases the blood circulation time [10]. Here 10 ml of PEG 400 concentration used during synthesis, showed hydrodynamic size around 342 - 396 nm as shown in figure 5.8 (b). This may be due to formation of extended hydrogen bond networks between ethylene groups present on the surface of nanoparticles and water molecules in the neighborhood. In all the cases the hydrodynamic sizes are higher as compared to particle size obtained from XRD and TEM. The higher diameter value obtained in DLS measurement may also be due to aggregation of nanoparticles and the contributions from solvent molecules being adsorbed on the

particle surface, canted surface [11]. Hydrodynamic size for uncoated Fe_3O_4 is about 229 - 265 nm (Fig. 5.8 (a)). For coated nanoparticles hydrodynamic size is greater due to presence of PEG on Fe_3O_4 .

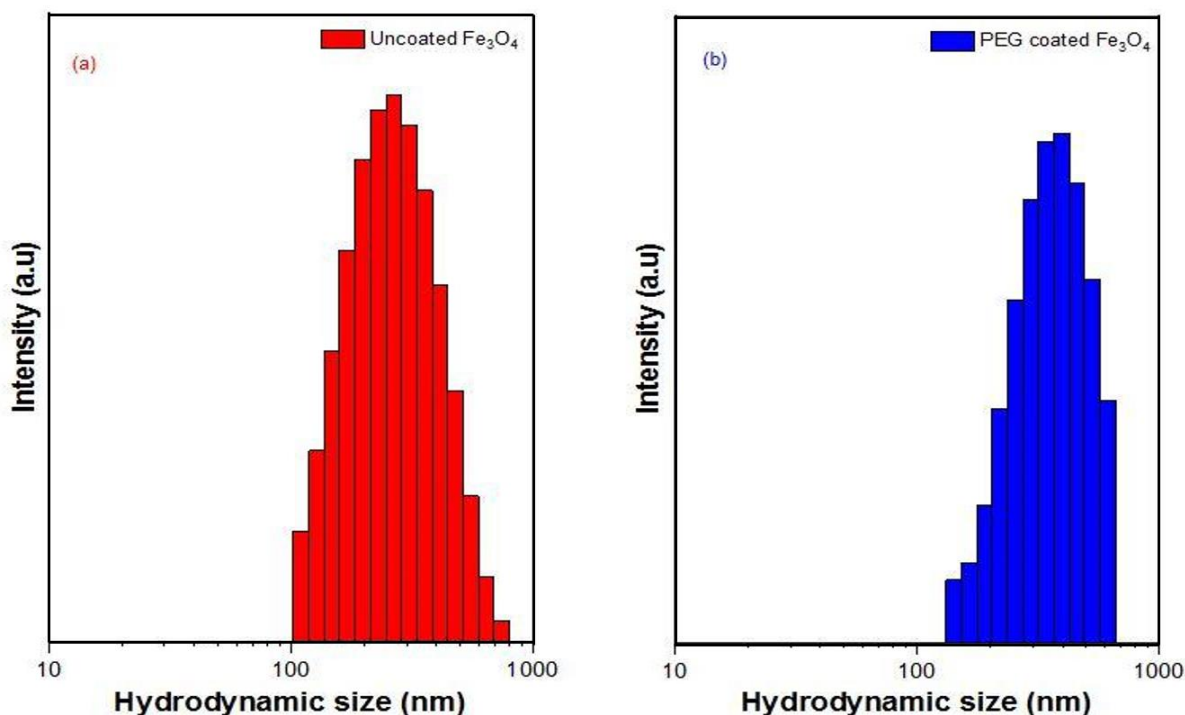


Figure 5.8 Hydrodynamic size of (a) uncoated Fe_3O_4 and (b) PEG coated Fe_3O_4

5.3.3 Morphological study

5.3.3.1 High resolution- transmission electron microscopy (HR-TEM)

High resolution transmission electron microscopy (HR-TEM) study was carried out for PEG coated Fe_3O_4 nanoparticles to have the detailed information about size, shape, structure and morphology of the nanoparticles.

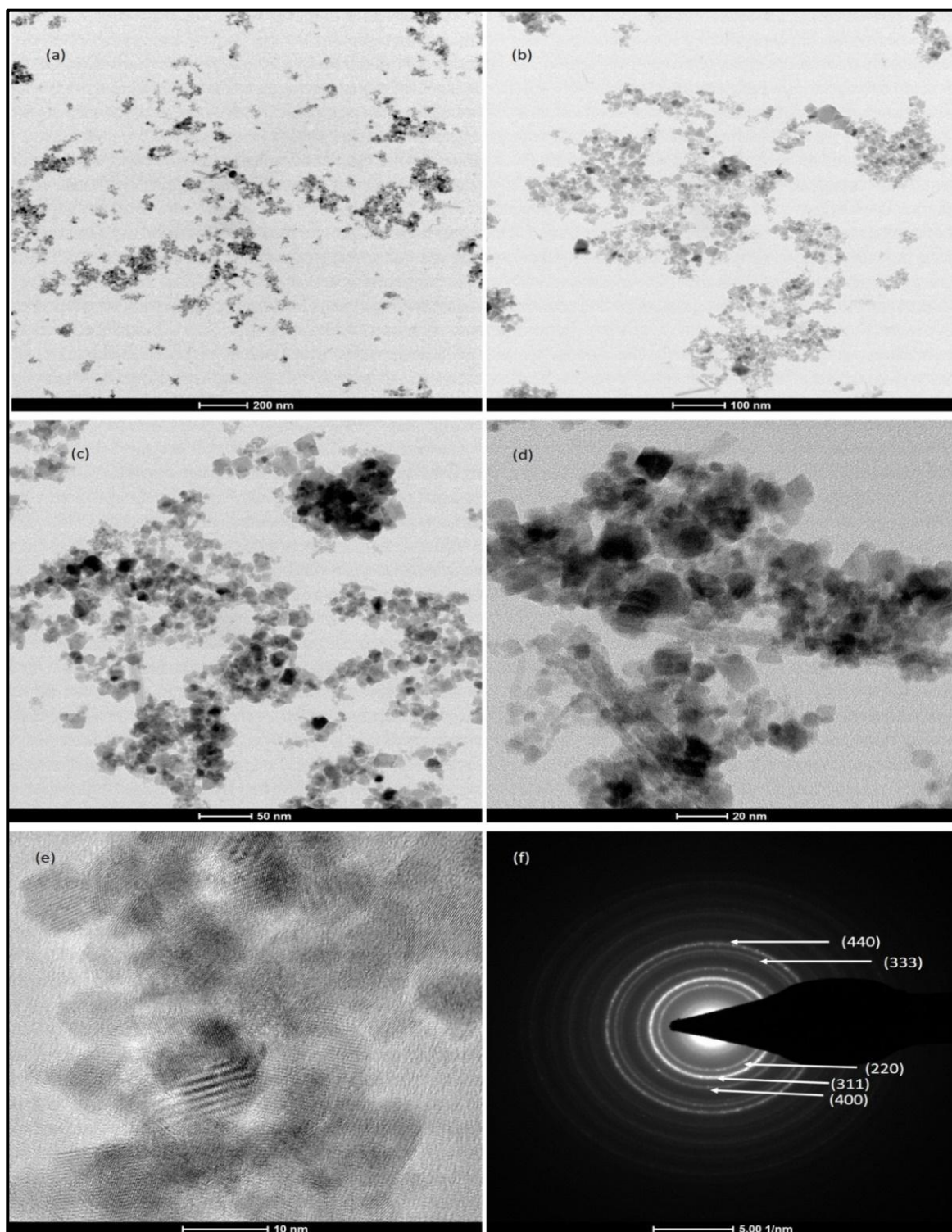


Figure 5.9 HR transmission electron microscope micrographs of polyethylene glycol coated Fe_3O_4 nanoparticles of resolution 200 nm (a), 100 nm (b), 50 nm (c), 20 nm (d), 10 nm (e), and SAED pattern (f) of polyethylene glycol coated Fe_3O_4

HR-TEM images, figure 5.9 (a), (b), (c), (d) and (e) of PEG coated Fe_3O_4 nanoparticles exhibit polygonal structure with the size distribution between 10 and 20 nm. TEM micrographs of Fe_3O_4 nanoparticles exhibit a well-defined, homogeneous and roughly spherical shape. This may be due to the PEG coating acting as stabilizer and dispersing agent. Particle diameter was calculated by image J software, which is in consistency with particle size calculated by XRD results ($d_{\text{X-RD}} = 9.86\text{nm}$). The Selected Area Electron Diffraction (SAED) pattern (Fig. 5.9 (f)) shows only diffraction intensity associated with crystalline Fe_3O_4 which is similar to XRD result.

5.3.4 Magnetization study (VSM)

Figure 5.10 shows magnetic field vs. magnetic moment (M–H) curve for bare Fe_3O_4 and PEG coated Fe_3O_4 nanoparticles exhibiting superparamagnetic behavior with zero coercivity (C_e) and zero remanence (M_r). The magnetic nanoparticles in magnetic fields get agglomerate due to magnetic dipole attraction and will be reduced after removal of magnetic field resulting in no residual magnetization before and after removal of magnetic field [12]. This superparamagnetic behavior of magnetic nanoparticles is preferred for biomedical applications. This fact of nonexistence of coercive forces and remanence prevents magnetic dipolar interactions between nanoparticles and their aggregation, which could lead to serious adverse problems such as the formation of clots in the blood circulation system [13]. Saturation Magnetization values from graph for PEG coated (Fig. 5.10 (b)) and bare Fe_3O_4 (Fig. 5.10 (a)) are about 34 emu/g and 56 emu/g respectively, which are smaller than theoretical value of bulk Fe_3O_4 ($M_s = 92 \text{ emu/g}$) since M_s decreases with decreasing particle size [12] ($d_{\text{X-RD}}$ values for PEG coated $\text{Fe}_3\text{O}_4 = 9.86 \text{ nm}$ and $\text{Fe}_3\text{O}_4 = 10.94 \text{ nm}$). This may be due to Fe_3O_4 nanoparticles with a bare surface tend to agglomerate

because of strong magnetic attractions between the particles. It has been reported that for biomedical application M_s of 7 - 22 emu/g is adoptable [14, 15]. The achieved M_s value of 34 emu/g for PEG coated Fe_3O_4 nanoparticles can be acceptable for biomedical applications.

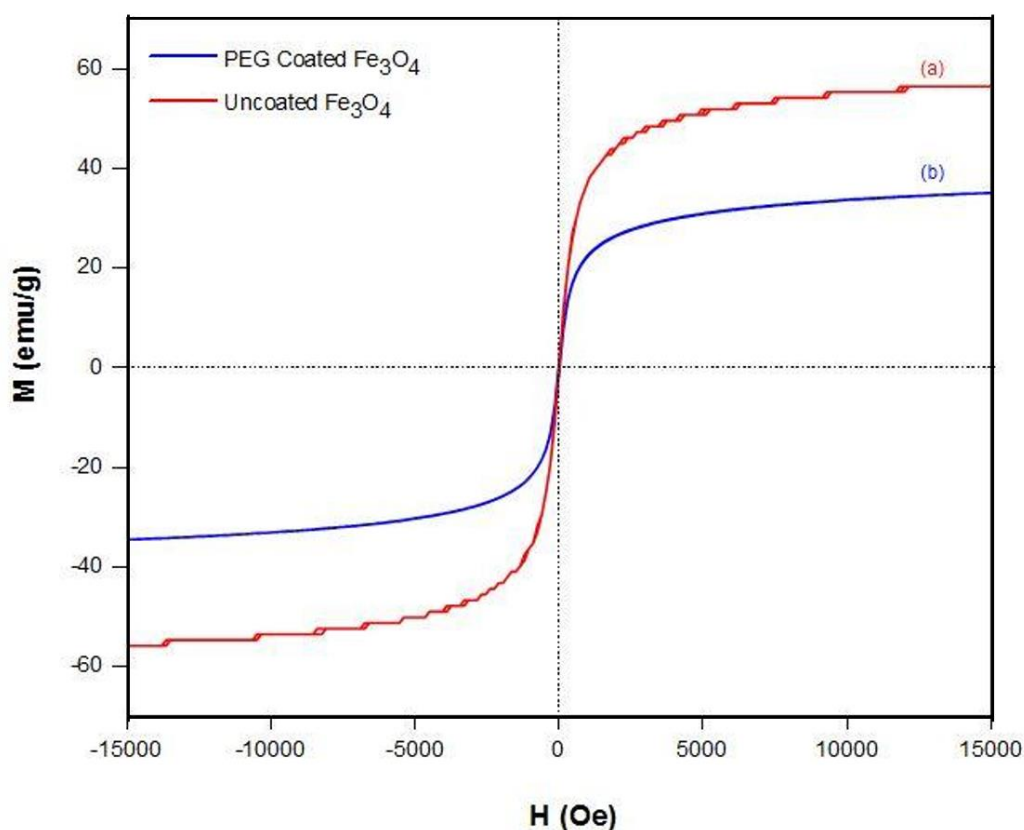


Figure 5.10 Magnetization curve for (a) Uncoated Fe_3O_4 , (b) PEG coated Fe_3O_4

5.4 Cytotoxicity Study (MTT assay)

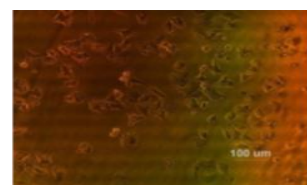
Cell viability study has been carried out of PEG 400 coated and uncoated Fe_3O_4 for four different concentrations 0.1 mg/ml, 0.15 mg/ml, 0.2 mg/ml and 0.25 mg/ml for both L929 normal and MCF-7 cancer cell lines. Micrographs were taken during the experiment as shown in figure 5.11. Liu et.al studied

biocompatibility of polyethylene glycol derivatives on L929 cell lines and found that PEG-1000 and PEG-4000 are moderate cytotoxic to L929 while PEG-400 and PEG-2000 are non-cytotoxic. So, PEG-400 might be a suitable coating for the cytotoxicity study [16]. In this study, as concentration increases cell viability decreases as shown in figure 5.12, while 0.25 mg/ml concentrations of both the nanoparticles show greater toxicity in both the cell lines. 78% killing is observed on the MCF-7 cell line, for 0.25 mg/ml PEG-coated Fe_3O_4 NPs whereas 0.01 mg/ml doxorubicin shows 86% cell death. Doxorubicin shows cytotoxic effect on cancer cell line as well as normal cell line (Fig. 5.12 (c) and (d), check bar diagram of positive control (PC) showing L929 cell killing) which confirms the drug has side effects on normal tissue along with better tumor control.

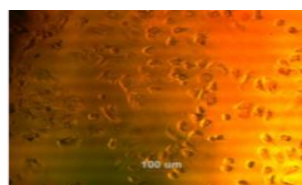
It has been observed that PEG coated Fe_3O_4 showing greater cell viability compared to bare in both cell lines ($p < 0.05$) but L929 cell line has a greater percentage of viability compared to MCF-7 which shows PEG coated Fe_3O_4 are biocompatible [Fig. 5.12 (e) and (f)]. According to our study percentage of MCF-7 cell killing observed for PEG-coated Fe_3O_4 for 0.1 mg/ml, 0.15 mg/ml, 0.2 mg/ml and 0.25 mg/ml were about 45.67%, 51.3%, 65.23% and 78.56%, respectively, while for L929 cell line it was 44.33%, 46.44%, 49.49% and 55.67%. It shows that there is higher cell killing observed for MCF-7 compared to L929 cell lines, especially for 0.2 and 0.25 mg/ml. For MCF-7 cancer cell lines, percentage of killing observed for uncoated Fe_3O_4 , for 0.1 mg/ml, 0.15 mg/ml, 0.2 mg/ml, 0.25 mg/ml were about 55.67%, 61.34%, 66.67% and 85% respectively while for L929 cell lines it was 55.67%, 59.8%, 68.04% and 75.26% respectively. It shows that there is not much difference in cell killing for uncoated Fe_3O_4 for MCF-7 and L929 cell lines except 0.25 mg/ml.



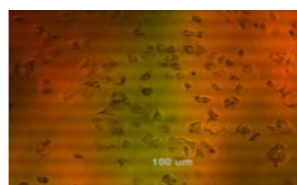
From these studies, it has been observed that PEG coated Fe_3O_4 nanoparticle (0.25 mg/ml) has nearly equivalent cytotoxic effect on MCF-7 cancer cell lines and is biocompatible on L929 cell lines as compared to standard drug (0.001 mg/ml). ROS production for cancer cell killing further may be enhanced while it used as radiosensitizer.



MCF-7 coated 0.1 mg/ml



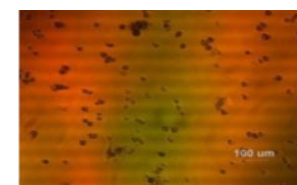
MCF-7 coated 0.15 mg/ml



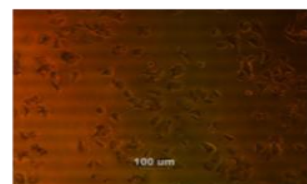
MCF-7 coated 0.2 mg/ml



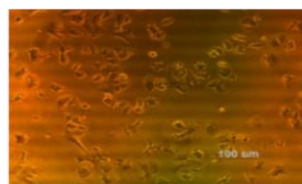
MCF-7 coated 0.25 mg/ml



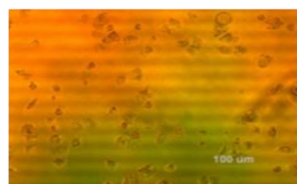
MCF-7 Positive Control



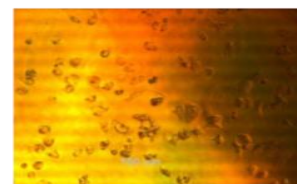
MCF-7 uncoated 0.1 mg/ml



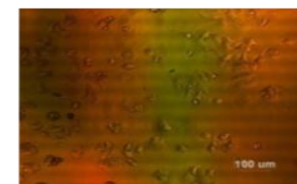
MCF-7 uncoated 0.15 mg/ml



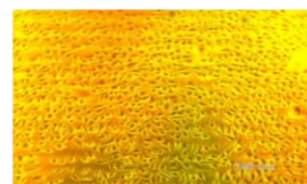
MCF-7 uncoated 0.2 mg/ml



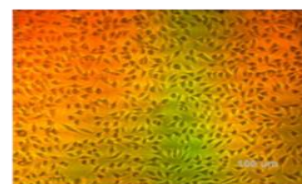
MCF-7 uncoated 0.25 mg/ml



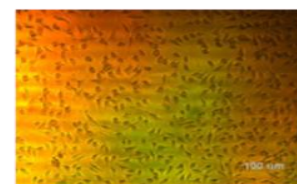
MCF-7 Negative Control



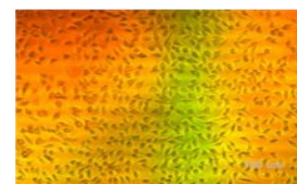
L929 coated 0.1 mg/ml



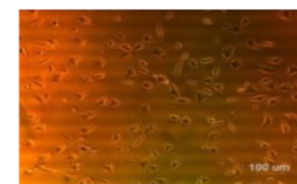
L929 coated 0.15 mg/ml



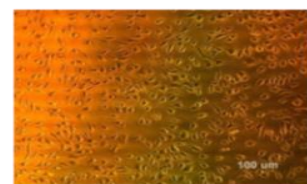
L929 coated 0.2 mg/ml



L929 coated 0.25 mg/ml



L929 Positive Control



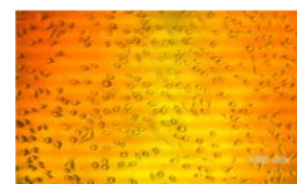
L929 uncoated 0.1 mg/ml



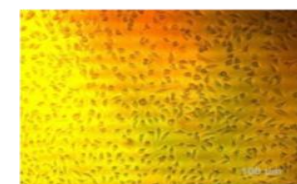
L929 uncoated 0.15 mg/ml



L929 uncoated 0.2 mg/ml



L929 uncoated 0.25 mg/ml



L929 Negative Control

Figure 5.11 Micrographs taken during the experiment

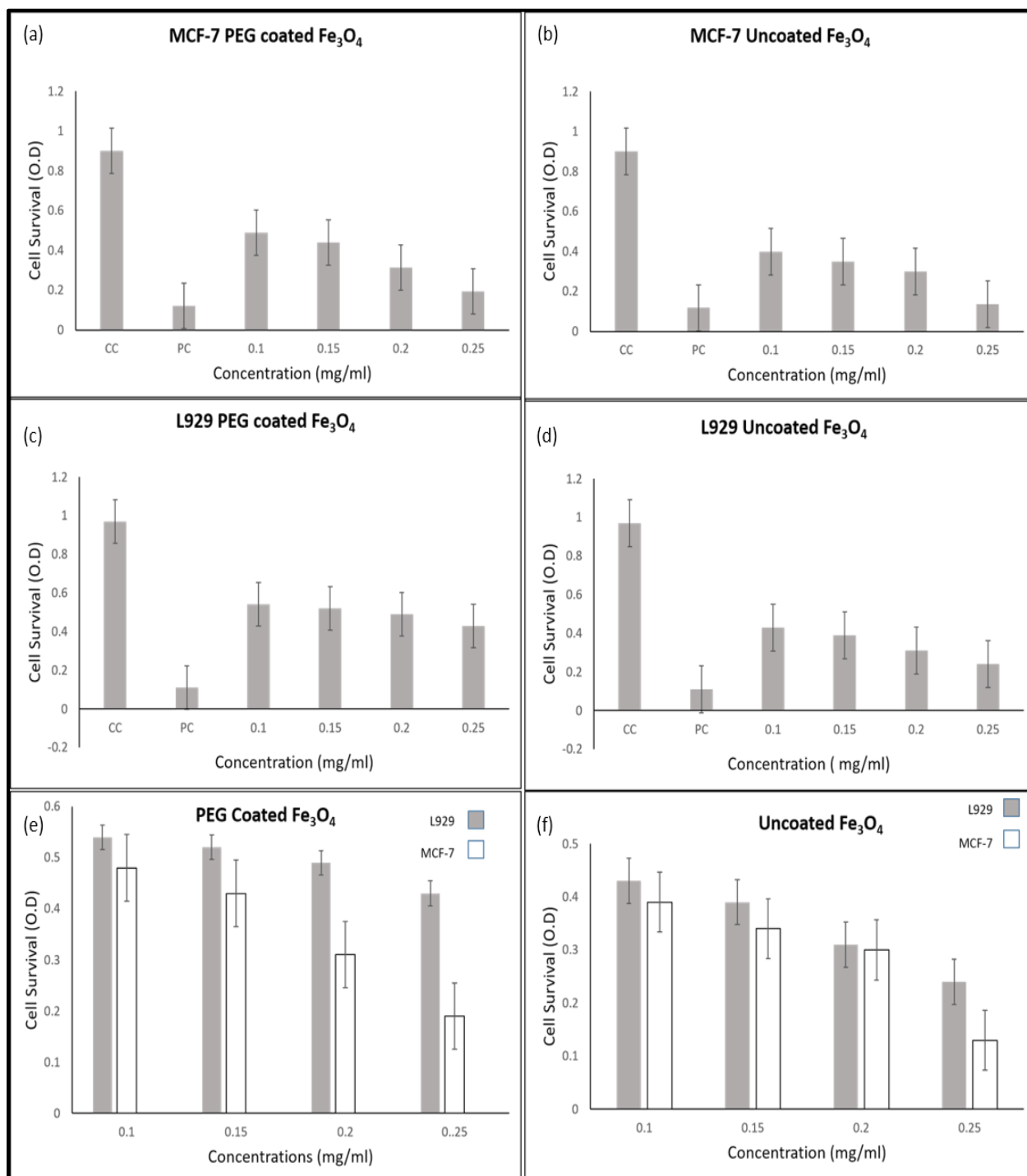


Figure 5.12 Concentration dependent cytotoxicity of (a) PEG coated Fe_3O_4 on MCF-7, (b) uncoated Fe_3O_4 on MCF-7, (c) PEG coated Fe_3O_4 on L929 and (d) uncoated Fe_3O_4 on L929 cell lines. (e) Comparison study of effect of PEG coated Fe_3O_4 on L929 and MCF-7 cell line. It's observed that reduction in percentage of cell survival for MCF-7 compared to L929 were 5.1%, 8.1%, 17.7% and 23.7% for concentrations 0.1, 0.15, 0.2 and 0.25 mg/ml respectively and (f) Comparison study of effect of uncoated Fe_3O_4 on L929 and MCF-7 cell lines. It's observed that reduction in percentage of cell survival for MCF-7 were 3.1%, 4.2%, 1% and 10.5%

5.5 Conclusion

The main goal of radiotherapy is to increase sensitivity of tumors in order to kill effectively while minimizing normal tissue dose. This can be achieved by using PEG coated Fe_3O_4 nanoparticles. Due to radiation exposure, surface coverage containing PEG may be partially or fully destroyed. So Fe^{2+} ions are easily accessible and act as a more efficient catalyst by taking part in the Haber- Weiss reaction for production of ROS species to enhance radiation treatment of cancer therapy. In this review we briefly summarize synthesis, characterization and cytotoxicity study in order to assess whether a PEG coated Fe_3O_4 nanoparticle is a suitable candidate for radiotherapy sensitizer. Findings of size, shape, stability and superparamagnetic behavior are observed to be much suitable for biomedical applications. XRD and TEM study reveals the size of the nanoparticle is in between 8 to 20 nm. PEG coating is confirmed using FTIR, TGA and DLS studies while zeta-potential and VSM study corroborate its stability and superparamagnetic behaviors.

In cytotoxicity study, the percentage of cell killing observed for PEG coated Fe_3O_4 is higher for MCF-7 compared to L929, this shows it is biocompatible. Percentage of cell killing observed for both MCF-7 and L929 is greater for bare Fe_3O_4 compared to PEG coated Fe_3O_4 . In all cases 0.25 mg/ml showed higher cell killing. Here, coating improves the biocompatibility nature of nanoparticles which makes it an appropriate contender. Overall, PEG coated Fe_3O_4 can act as a radiosensitizer in radiotherapy which may promote new opportunities for progress in cancer radiotherapy to improve clinical efficacy in different cancers.

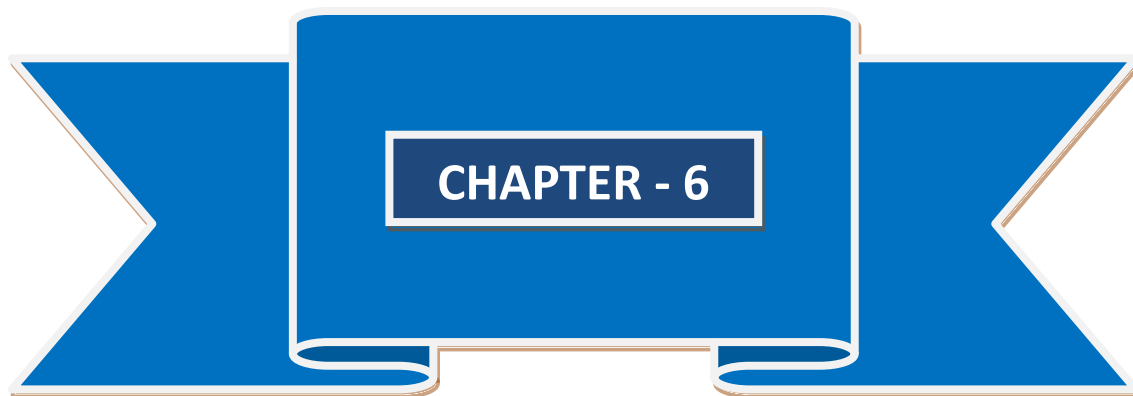


References

1. M. Rezaei, K. Khoshgard, L. Hosseinzadeh, A. Haghparast, M.T. Eivazi, Application of Dextran-coated Iron Oxide Nanoparticles in Enhancing the Radiosensitivity of Cancerous Cells in Radiotherapy With High-energy Electron Beams, 2019, [https:// doi.org/10.4103/jcrt.JCRT_19_17](https://doi.org/10.4103/jcrt.JCRT_19_17)
2. Wadajkar A S, Menon J U, Kadapure T, et al. Design and Application of Magnetic-based Theranostic Nanoparticle Systems. Recent Pat Biomed Eng 2013,6,47-57
3. Anbarasu M, Anandan M, Chinnasamy E. Gopinath V, Balamurugan K. Synthesis and Characterization of Polyethylene Glycol (PEG) Coated Fe₃O₄ Nanoparticles by Chemical Co-Precipitation Method for Biomedical Applications. SpectrochimActa A Mol. Biomol. Spectrosc 2015,135,536-539.
4. <https://nanopartikel.info/en/basics/cross-cutting/coatings-for-nanomaterials/>
5. Masoudi A, Hosseini H R M, Shokrgozar M A, Ahmadi R, Oghabian M A. The effect of poly (ethylene glycol) coating on colloidal stability of superparamagnetic iron oxide nanoparticles as potential MRI contrast agent. Int. J. Pharm 2012, 433,129–141.
6. Shameli K, Ahmad M B, Jazayeri S D et al. Synthesis and characterization of polyethylene glycol mediated silver nanoparticles by the green method. International Journal of Molecular Sciences 2012,13,6639–6650.
7. Malega F, Indrayana I, Suharyadi E. Synthesis and characterization of the microstructure and functional group bond of Fe₃O₄ nanoparticles from natural iron sand in Tobelo North Halmahera. JurnalIlmiahPendidikanFisikaAl-Biruni 2018, 7, 13-22
8. Chapter 5: Gumustas M, SengelTurk C T, Gumustas A, Ozkan S A, Uslu B. Effect of polymer-based nanoparticles on the assay of antimicrobial drug



- delivery systems. In: Grumezescu, A M Editor. Multifunctional Systems for Combined Delivery, Biosensing and Diagnostics. Elsevier: Amsterdam, the Netherlands; 2017, 67–108.
9. Fonte P, Andrade F, Araujo F, Andrade C, Neves J, Sarmento B. Chitosan-coated solid lipid nanoparticles for insulin delivery. *Methods Enzymol* 2012, 508, 295–314.
 10. Yoo J, Chambers E & Mitragotri S. Factors that control the circulation time of nanoparticles in blood: challenges, solutions and future prospects. *Curr. Pharm. Des* 2010, 16, 2298–2307
 11. Abhiram A. et al. Synthesis of poly (ethylene glycol) (PEG)-capped Fe_3O_4 nanoclusters by hydrothermal method. *IOP Conf. Ser.: Mater. Sci. Eng.* 2019, 577, 012153
 12. Shete P B, Patil R M., Ningthoujam RS, Ghosh SJ, Pawar SH. Magnetic core shell structures for magnetic fluid hyperthermia therapy application. *New J. Chem* 2013, 37, 3784–3792.
 13. Bañobre-López M, Teijeiro A, Rivas J. Magnetic nanoparticle-based hyperthermia for cancer treatment. *Rep. Pract. Oncol. Radiother* 2013, 18, 397–400.
 14. N.A. Brusentov, V V. Gogosov, T.N. Brusentov, A V. Sergeev, N Y. Jurchenko, A.A. Kuznetsov, O.A. Kuznetsov, L.I. Shumakov, J. Magn. Mater. 2001, 225, 113–117.
 15. C.J. Xu, K M. Xu, H W. Gu, X F. Zhong, Z H. Guo, R. Zheng, X. Zhang, B. Xu., Dopamine as A Robust Anchor to Immobilize Functional Molecules on the Iron Oxide Shell of Magnetic Nanoparticles. *J. Am. Chem. Soc.* 2004, 126, 3392–3401
 16. Liu G, Li Y, Yang L, Wei Y, Wang X, Wang Z et al. Cytotoxicity study of polyethylene glycol derivatives *RSC Adv* 2017, 7, 18252–18259



PEG COATED SPION AS A RADIOSENSITIZER

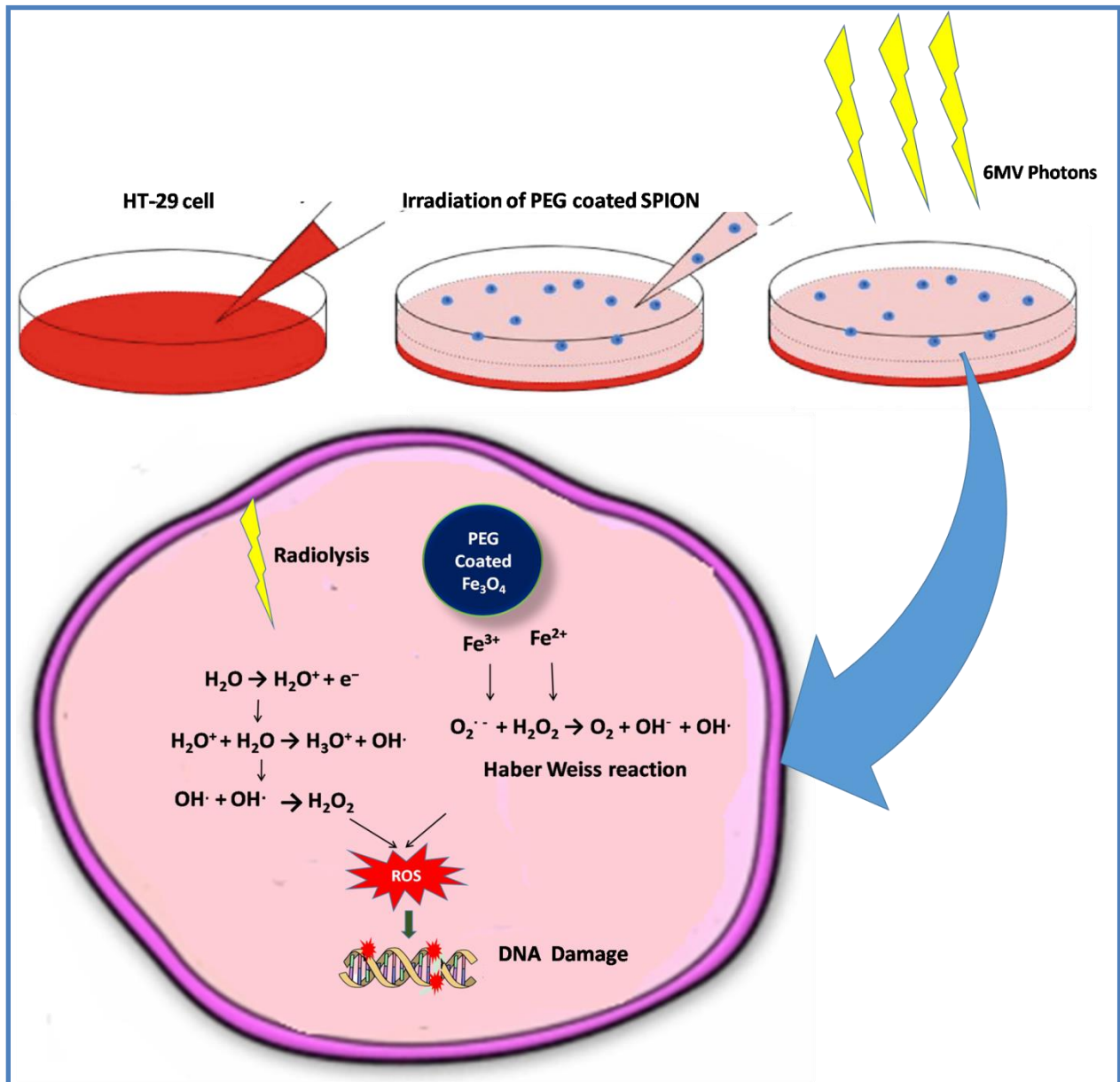
**Part of this chapter included in research paper accepted in
Journal of Medical Physics**

Original Article

Use of Poly (Ethylene Glycol) Coated Superparamagnetic Iron Oxide Nanoparticles as Radio Sensitizer in Enhancing Colorectal Cancer Radiation Efficacy

Madhuri Anuje^{1,2}, Padamaja Pawaskar¹, Ajay Sivan², Chandrakant Lokhande¹, Imtiaz Ahmed³, Dhanashree Patil⁴

¹Department of Medical Physics, Center for Interdisciplinary Research, DY Patil Education Society (Deemed to be) University, Kolhapur, ²Integrated Cancer Treatment and Research Centre, Pune, Maharashtra, ³Department of Radiation Oncology, KLES Belgaum Cancer Hospital, ⁴Dr. Prabhakar Kore Basic Science Research Centre, KLE Academy of Higher Education and Research (KLE University), Belgaum, Karnataka, India





6.1 Introduction

Radiotherapy plays a crucial role in treatment of cancer in about 50% cases [1]. Most important concern in and disadvantage of radiotherapy is that ionizing radiation affects both healthy tissue and solid tumors. With increasing radiation doses to achieve tumor control, tissue surrounding the target tumor gets damaged which is a limitation in escalation of dose beyond which radiotherapy cannot be sustainably employed to treat cancers. The use of nanoparticles (NPs) as radiosensitizer agents in tumour cells is one of the methods of increasing the dose in these cells. As discussed in Chapter 3 Section 3.2, several different nanoparticles have been reported for enhancing the effect of radiation on various cancer cells. We reviewed 68 radiosensitization research papers from 2008 to 2020 and tabulated on the basis of the nanoparticle size, concentrations, cell lines, energy used, amount of dose delivered and final SER/DMF/DEF values. We observed that the most commonly used nanoparticle is gold (Au) and the most commonly used cell line is breast cancer cell line (MCF-7). In our study, we decided to use the radioresistant colorectal cancer cell line HT-29.

We started with the MCF-7 breast cancer cell line, which we used to carry out a cytotoxicity study on. In our study, the MCF-7 cell line showed 80.7 % cell killing at 0.25 mg/ml concentration, while the normal (L929) and HT-29 cell lines showed 57 % and 38.7 % cell killing, respectively (as shown in Fig. 6.1) [17]. In comparison to normal L929 and HT-29 cell lines, MCF-7 exhibits excessive sensitivity to SPIONs. As a result, according to our findings, there may be no need to investigate radiosensitization in MCF-7. HT-29 cells, on the other hand, are radioresistant and their cytotoxicity when exposed to only radiation or nanoparticles is very low. In order to achieve better tumour control, we

investigated the cytotoxicity of HT-29 by combining different concentrations of SPIONs and radiation.

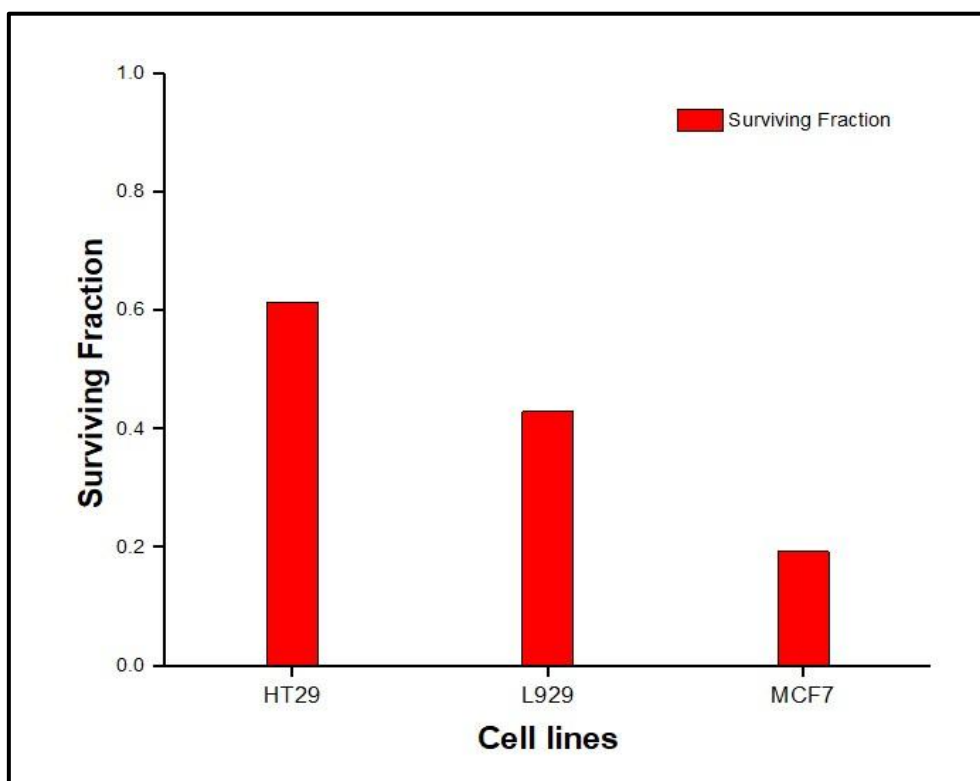


Figure 6.1 Comparison of cytotoxicity for different cell lines

Globally, colorectal cancer (CRC) is the third most common type of cancer, making up about 10.2% of all cases [2]. In 2018, there were 1.84 million new cases and 880,792 deaths from the disease [2]. CRC is more common in developed countries, where more than 65% of cases are found [3]. The role of radiotherapy in rectal cancer has more meaningful application from anatomical perspective as rectum is a relatively fixed structure in the pelvis and it is situated below the organs that have limited tolerance to radiotherapy [4]. Traditionally, CRC is treated with surgery in the early stages, while a combination of preoperative chemo-radiation therapy (CRT) and surgery is used in the more



common locally advanced stages [5]. Preoperative CRT results in only about 15% of patients achieving a complete pathological response, i.e., no viable tumor remains within the surgical specimen at the time of surgery [6, 7]. Also, in lower third rectal cancers with wait and watch policy post radio-chemotherapy for organ preservation has shown encouraging results [8]. In order to achieve greater therapeutic ratio, greater radiation doses can be used to improve tumor downstaging and local control of tumors [7]. However, the dose escalation also increases the risk of toxicity and exceeds the tolerance of adjacent healthy tissue [7]. A better alternative way is to combine standard-dose radiotherapy with radiosensitizers to enhance the radiation therapy efficacy locally within tumors while saving adjacent healthy tissues [5,9].

6.2 Methods and Materials

Aim of the radiotherapy is to deliver a lethal dose to the tumor while reducing impact to the normal tissue. This reduction in impact can be achieved by having a greater therapeutic ratio while using radiosensitizer such as nanoparticles. This study investigates the potential of radio sensitization enhancement of superparamagnetic iron oxide nanoparticles (SPIONs) on HT-29 cell lines with different concentrations (0.007 to 0.25 mg/ml) and different radiation doses (0.5 to 2 Gy) of 6MV photon beam. This research was conducted at KLE's Belgaum Cancer Hospital, Belgaum. Figure 6.2 depicts the steps involved in the radio sensitization enhancement of SPIONs on HT-29 cell lines.

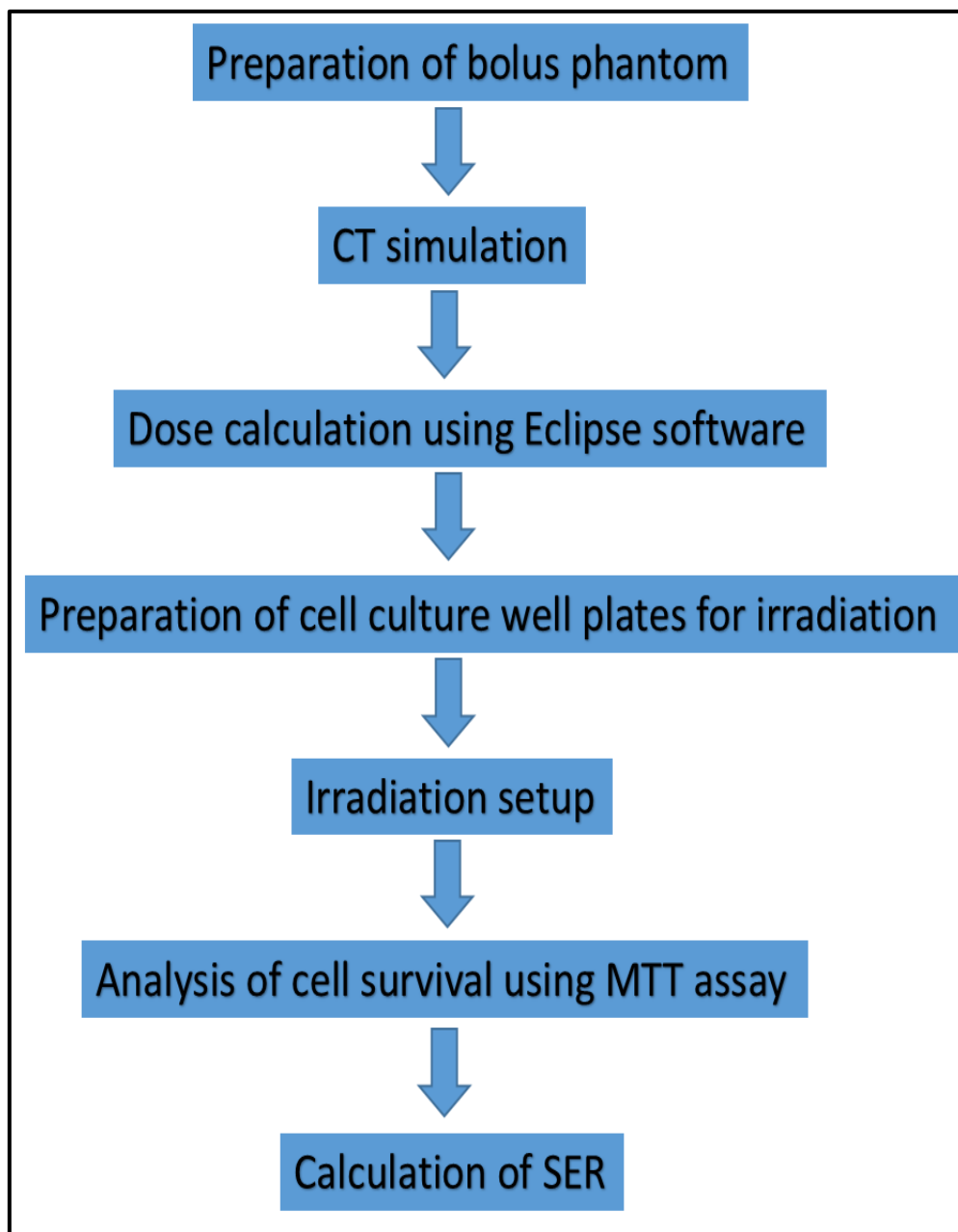


Figure 6.2 Steps involved in experiment of radio sensitization enhancement of SPIONs on HT-29 cell lines.

6.2.1 Preparation of bolus phantom

Radiation cannot be directly exposed to 96-well culture plates. We need to ensure whether the prescribed dose and the actual dose delivered are the same. We must also make proper arrangements for exposure to the well plate in order to deliver the prescribed dose to the culture. All other parameters, such as field size, distance from source to axis and energy must be considered.

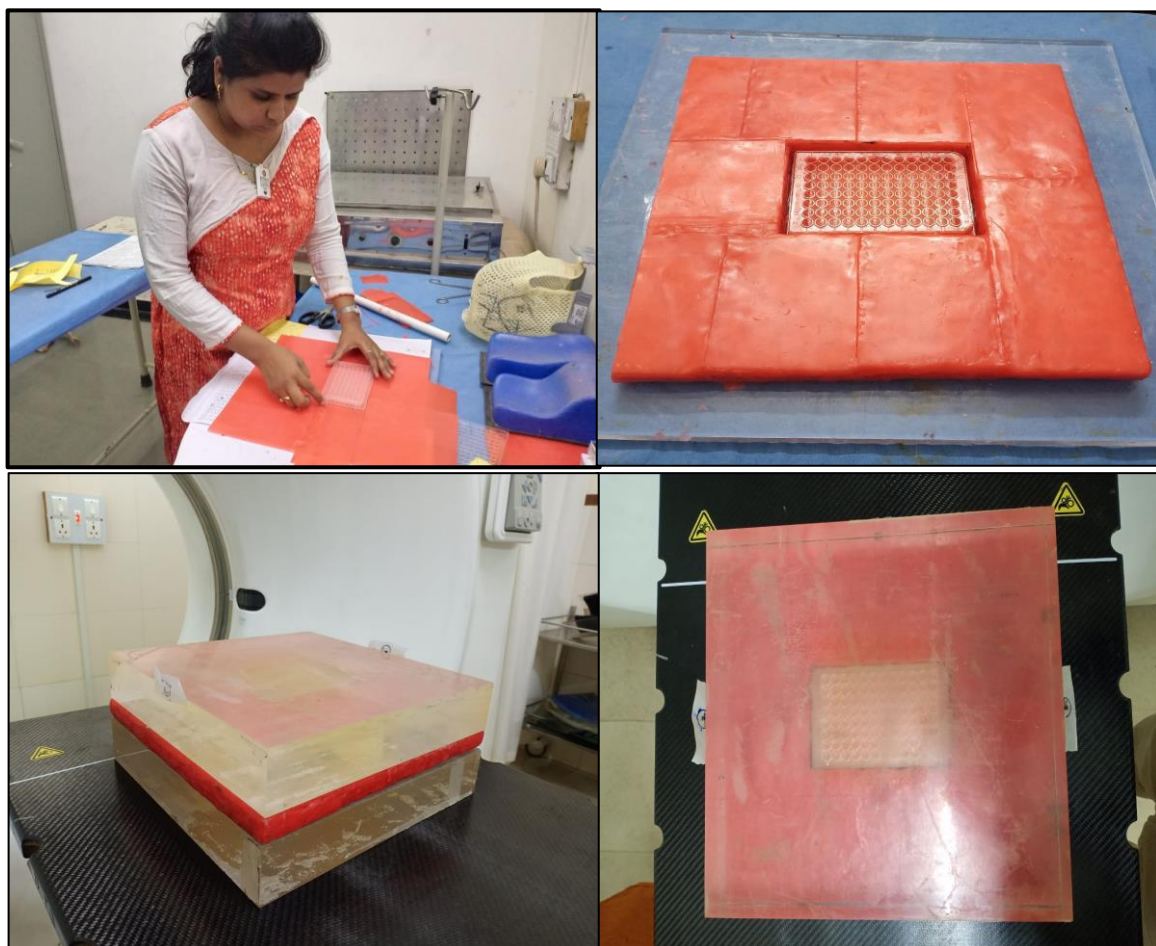


Figure 6.3 Preparation of wax bolus phantom (a) and (b), 96 well Cell culture plate sandwiched in between two solid water phantom (c) and (d)

The cell culture plate sandwiched between two solid water phantoms (thickness 5 cm of each and 40 cm x 40 cm size) in order to attain electronic equilibrium



and cell culture plate kept at centre while the remaining space filled with tissue equivalent wax bolus. Preparation of wax bolus is as shown in figure 6.3 (a) and (b). In radiation therapy, bolus is a material which has properties equivalent to tissue when irradiated. Tissue equivalent material could bring scattered photons of lower energy which interact by photoelectric effect. Solid phantoms made up of Polymethyl methacrylate (PMMA), are widely used in radiotherapy for routine dosimetric quality assurance tests, primarily due to their ease of use compared to scanning water tanks [10].

6.2.2 CT simulation

Figure 6.4 shows the phantom positioned on the CT couch with 96 well tissue culture plates filled with water. The lasers are activated and positioned at the midline in accordance with the region of interest. GE Lightspeed Plus 4 Slice CT Scan Machine used for CT simulation.

6.2.3 Irradiation planning

Images of 2.5 mm thickness acquired using CT scanner were sent to treatment planning software in the TPS room through Digital Image Communication in Medicine (DICOM). Eclipse version 11.0.31 software used for planning purposes. Dose calculated using Analytical Anisotropic Algorithm (AAA). Figure 6.5 shows dose distribution.

It was planned in order to get maximum dose at tissue culture. Clinical factors like gantry angle, source axis distance and field size were determined by the dose distribution at that depth. MUs calculated according to different doses i.e., 0.5 to 2 Gy.



Figure 6.4 Setup for CT Simulation

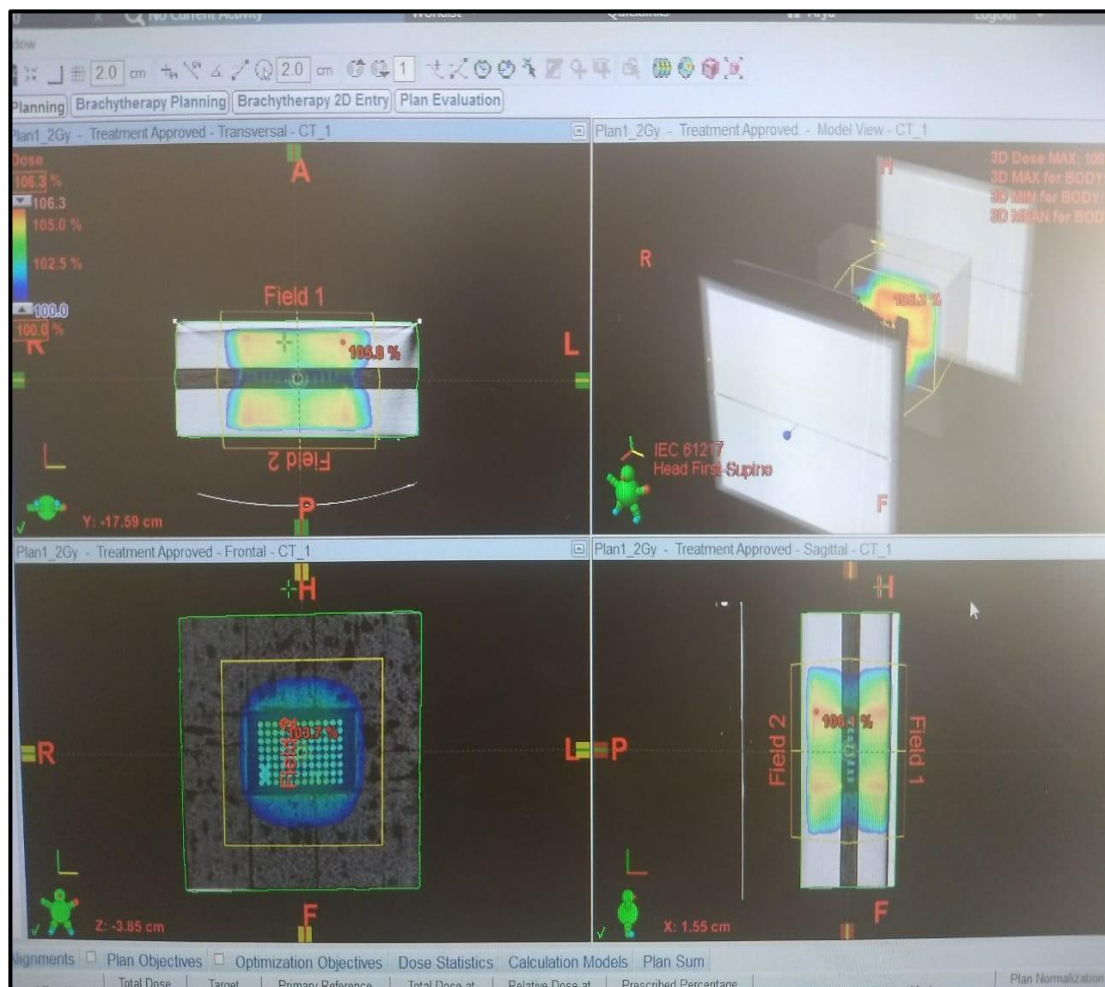


Figure 6.5 Dose calculation using treatment planning software

6.2.4 Cell culture well plates for radiation exposure

In vitro growth inhibition effect of the test compound was assessed by colorimetric or spectrophotometric determination by conversion of MTT to “Formazan blue” by living cells. 1×10^5 cells/ml HT-29 cell suspension was seeded into each well in a 96 well microtiter plate and the final volume was made up to 150 μ l by adding DMEM media and incubated overnight. Dilutions of the test compounds i.e., PEG coated SPIONs were prepared in DMEM media.



Figure 6.6 Tissue culture well plates ready for irradiation

100 μ l of the test compounds with different concentrations of 0.007, 0.015, 0.031, 0.062, 0.125 and 0.25 mg/ml were added to the wells and normal control (cells with medium and no test sample), incubated for 24 h, in presence of 5 % CO₂, at 37°C into CO₂ incubator. Figure 6.6 shows four different well plates ready for irradiation for different doses 0.5, 1, 1.5 and 2 Gy.

6.2.5 Irradiation setup

Irradiation of HT 29 cell lines was done using Megavoltage X-ray beam (6 MV) produced by Varian Clinac-iX in the Radiation Oncology Department of KLE's Belgaum Cancer Hospital, Belgaum (Karnataka, India). Cells were cultured in 96 well plates and incubated for 24 h with PEG coated Fe₃O₄ nanoparticles at different concentrations of 0.007 to 0.25mg/ml and normal control as mentioned above. Figure 6.7 shows the schematic of the radiation experiment. The cell

culture plate is sandwiched between two solid water phantoms (thickness 5 cm of each) in order to attain electronic equilibrium and the remaining space filled with tissue equivalent wax bolus as shown in figure 6.7 (a). Water equivalent material could bring scattered photons of lower energy which interact by photoelectric effect. In this study we kept 96 well plates at 5 cm depth instead of d_{max} because the energy held by the scattered photon is related to the energy of the incident photon. Therefore, backscattered photons which carry less energy are interesting for X-rays-nanoparticles interactions purposes, thus the cells should be located in a low dose gradient: after the depth of the maximum dose and inside the beam, off the penumbra region [11].

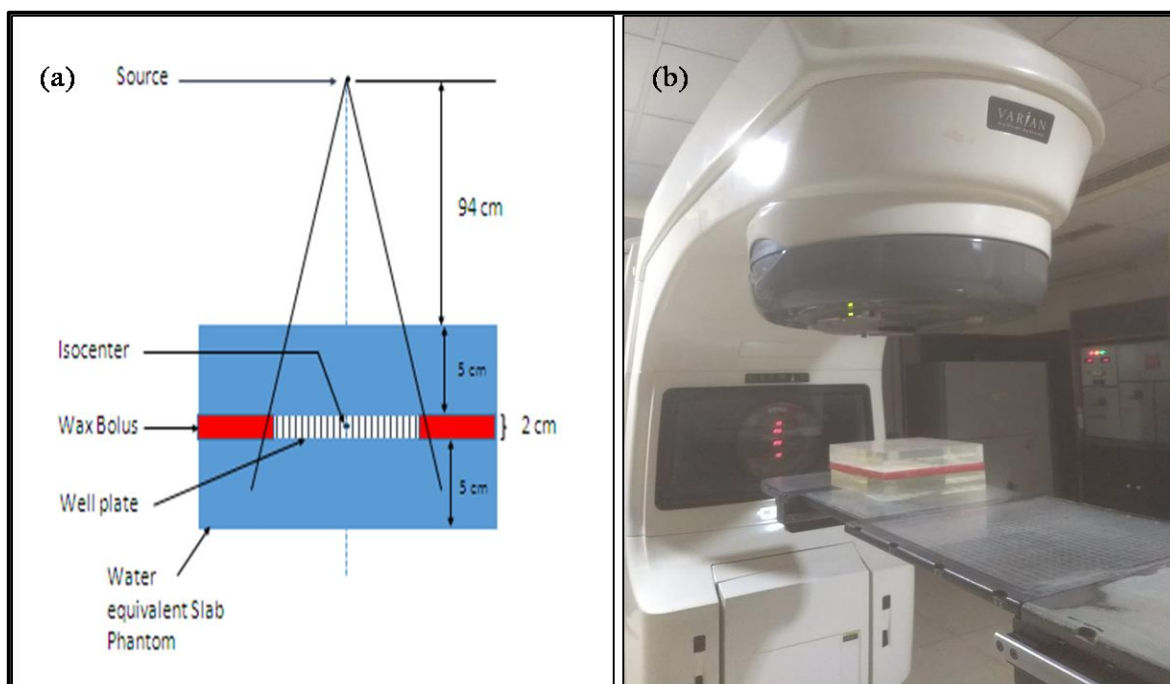


Figure 6.7 Schematic of standard irradiation setup (a), Irradiation of HT-29 cells under linear accelerator

The cell plates were kept at clinical distance from source i.e., at 100 cm and 20 cm x 20 cm field size kept open as shown in figure 6.7 (b). Irradiation was done



for different doses such as 0.5, 1, 1.5 and 2 Gy using Anterior-Posterior (AP) and Posterior-Anterior parallel opposed technique.

6.2.6 Analysis of cell survival using MTT assay

After exposure to 6 MV X-ray beams under linear accelerator machine and cell culture kept for 72 h incubation. After 3 days, 20 μ l of 5 mg/ml MTT reagent was added to the wells. The plate was kept for 4 h. incubation in a dark place at room temperature. (The plate was covered with aluminum foil, since the MTT reagent is photosensitive). The supernatant was carefully removed without disturbing the precipitated Formazan crystals and 100 μ l of DMSO was added to dissolve the crystals formed. The optical density (OD) was measured at a wavelength of 492 nm. The study was performed in triplicates and the result represents the mean of three readings. Surviving fraction of cells calculated using the formula, $S.F = \text{Mean OD}_{NP} / \text{Mean OD}_{CONT}$.

Same experiment has been performed on HT-29 cell lines with 0.007, 0.015, 0.031, 0.062, 0.125 and 0.25 mg/ml concentrations of SPIONs nanoparticles and control cells (cells with medium and no test sample), incubated for 96 h, in presence of 5 % CO₂, at 37°C into CO₂ incubator. Optical density was measured without any radiation exposure. Incubation period was kept the same as above.

6.2.7 Sensitization enhancement ratio (SER)

The SER is the ratio of cell survivals of radiation alone versus radiation along with cell sensitizer. If value is greater than one, then the addition of the agents is functioning as a radiosensitizer. If it is less than one, then the drug is a radioprotector [12]. Sensitizer enhancement ratio (SER) values for 0.5, 1, 1.5 and 2 Gy calculated by using formula given in equation 6.1 [13].



$$SER_{xGy} = \frac{SF_{xGy,Cont}}{SF_{xGy,NP}} \quad (6.1)$$

SER values calculated for different doses and different concentration are tabulated in table 6.1.

Table 6.1 SER values for different concentration SPIONs for various doses of radiations

Dose (Gy)	SER _{0.007}	SER _{0.015}	SER _{0.031}	SER _{0.062}	SER _{0.125}	SER _{0.25}
0.5	0.94	1.00	1.09	1.14	1.19	1.50
1	0.93	1.02	1.11	1.14	1.17	1.61
1.5	0.98	1.06	1.12	1.14	1.19	1.67
2	1.05	1.11	1.12	1.14	1.21	1.74

6.3 Results

6.3.1 Cytotoxicity evaluation of PEG coated SPIONs

Figure 6.8 shows cytotoxicity of PEG coated Fe₃O₄ nanoparticles for different concentrations such as 0.007, 0.015, 0.031, 0.062, 0.125 and 0.25 mg/ml without radiation exposure. Percentage cell viability of HT 29 cancer cells incubated for 96 hours with Fe₃O₄ nanoparticles are 91.4%, 88.2%, 81.6%, 76.5%, 72.3% and 61.3% respectively. Result shows that as concentration increases cell killing increases. In this study all the tested concentrations did not have considerable cytotoxicity.

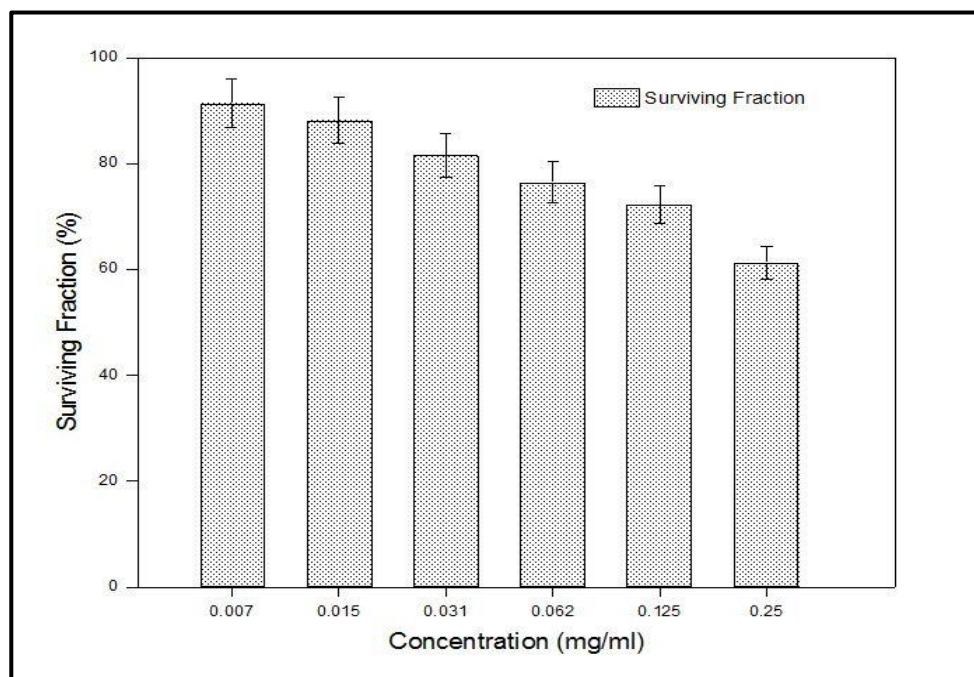


Figure 6.8 Percentage of HT-29 cell survival for different nanoparticle concentrations

6.3.2 Radiosensitization enhancement by PEG coated SPIONs

HT-29 colorectal cancer cell lines were exposed with only radiation and radiation along with nanoparticles. Percentage cell viability observed for only radiation doses of 0.5, 1, 1.5 and 2 Gy are 83.4%, 79.6%, 79.0% and 78.5%. Cell killing for only radiation observed is not significant ($p > 0.05$). When radiation combined with higher nanoparticle concentration i.e 0.25 mg/ml for doses 0.5, 1, 1.5 and 2 Gy, percentage cell viability observed to be 55.3%, 49.3%, 47.1% and 44.9% respectively showing that when radiation combined with different nanoparticle concentration for doses 0.5, 1, 1.5 and 2 Gy, cell killing increased by 28.1%, 30.3%, 31.9% and 33.6% respectively.

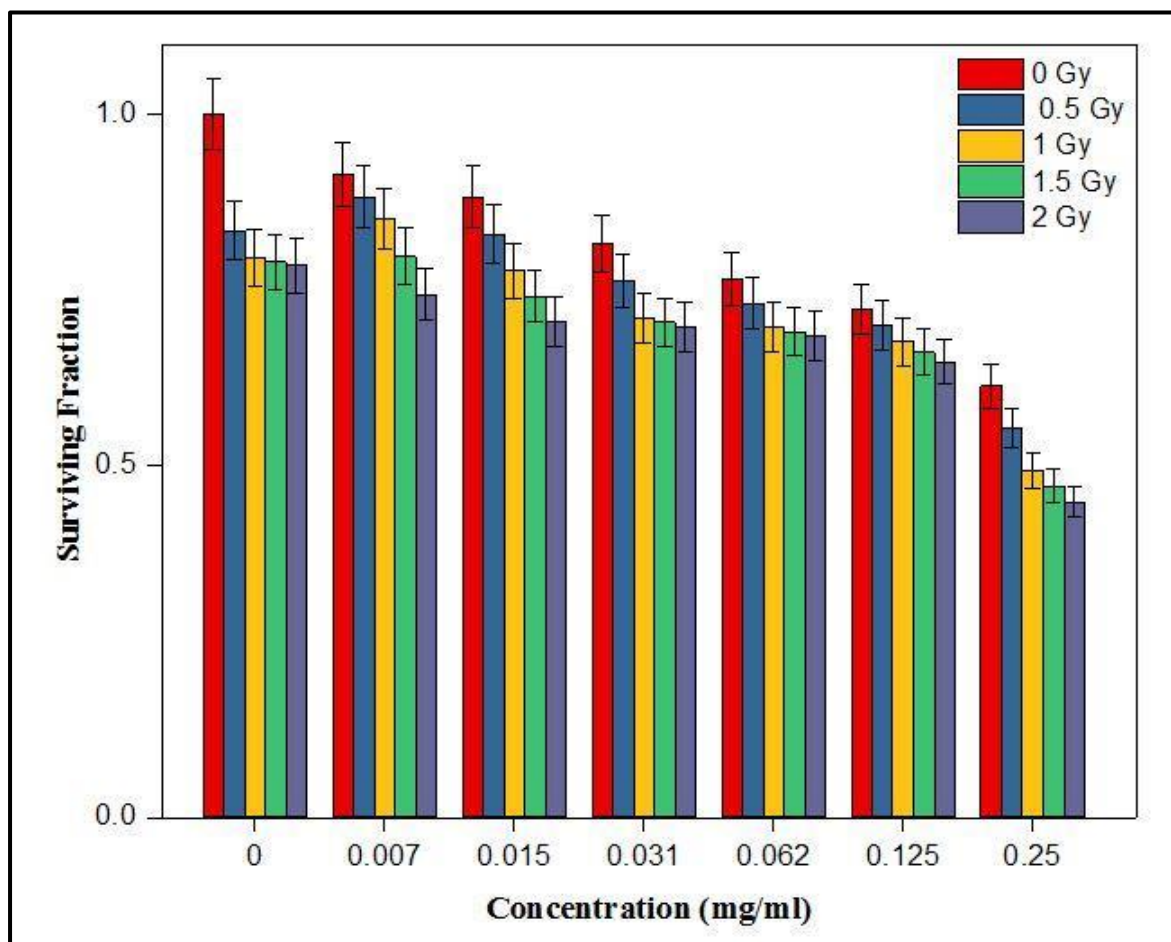


Figure 6.9 Percentage of HT-29 cells survival for different concentration and at various doses of photon beam

Dose response curves for different concentrations are as shown in figure 6.9. Percentage cell viability of HT-29 cells decreases with increasing concentrations of SPIONS as well as radiation doses. SER values for each dose for different concentrations are as shown in figure 6.10. Greater the SER value, radiosensitization by nanoparticles will be higher. In, SER values increase from 0.94 to 1.74 for concentration from 0.007 to 0.25 mg/ml considering all the doses. Higher sensitization observed for 0.25 mg/ml concentrations than others. SER values are observed to be less than one for doses 0.5, 1 and 1.5 Gy of the concentration 0.007 mg/ml (as shown in table 6.1).

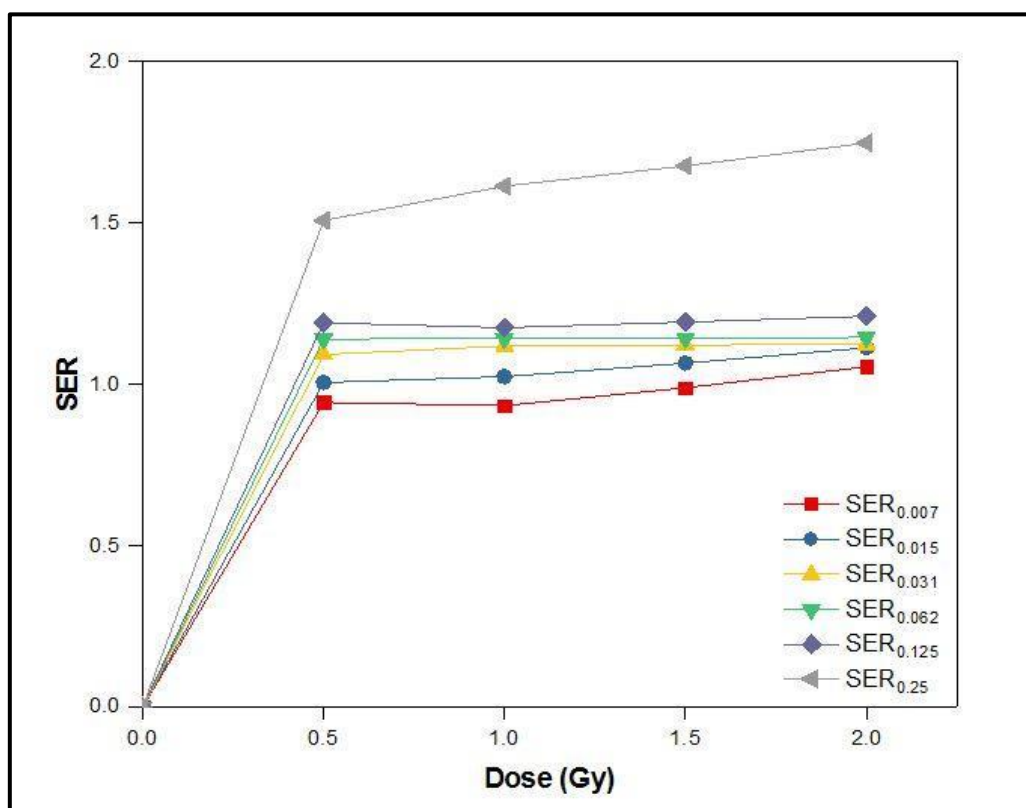


Figure 6.10 Sensitization enhancement factor values of photon beam irradiations for different concentration and various doses.

In summary, there is significant correlation in the percentage cell viability observed for HT-29 cells incubated with different concentrations of SPIONs and SPIONs along with different radiation doses of 6 MeV photon beam with r^2 value of 0.91 ($p=0.003$). Also, statistically significant difference in percentage of cell survival was observed between groups in which cells were exposed with only radiation doses and groups receiving radiation doses along with different SPIONs concentration with r^2 value of 0.97 ($p = 0.02$).



6.4 Discussion

Each substance used for cancer diagnosis or therapy is affected by biocompatibility and complicated metabolism. Therefore, the possibility of using one substance for different tasks (multifunctionality) is particularly attractive [14]. Especially SPIONs have essential properties such as excellent biocompatibility, superparamagnetism [15], physically and chemically stable, environmentally safe, ease of synthesis process and surface treatment [16]. Our present results show SPIONs can be used as radiotherapy sensitizers. One of the important steps toward the widespread usage of such nanoparticles is an assessment of the toxicity effect of these nanoparticles due to ROS production. Cytotoxicity has been assessed on different biological models using in vitro as well as in vivo studies. The in vitro studies are of more interest due to its simplicity, lower cost and better control [17]. SPIONs have lower Z (26 vs. 79) and lower X-ray absorption enhancement factor (1.2 vs. 1.6 respectively) compared to gold nanoparticles (GNPs) at keV energy level according to Roeske's theoretical calculation [18]. SPIONs might still act as effective radiosensitizers at MV energies according to our and others results.

Huang et. al estimated dose enhancement factors (DEF) in the case of cervical cancer cells (HeLa cell), are 1.6, 1.4 & 1.33 for while in the case of EMT cell, 1.6, 1.33 & 1.44 for doses 1, 2 & 4 Gy respectively. Here DEF values found to be decreasing with increasing doses for same concentration [14]. Kirakli et. al carried out in vitro study of SPIONs on human breast adenocarcinoma cell line (MCF-7), human mammary gland carcinoma cell line (MDAMB-231) and human ovarian carcinoma cell line (MDAH-2774) with radiation exposure of doses 0,2,4,6, and 8 Gy at 6 MV energy for different concentrations such as 0.0125, 0.025, 0.05, 0.1 and 0.125 mg/ml. This study demonstrates that the highest



radiosensitization was seen in MCF-7 and MDAH-2447 cells at 2 Gy (NER: 1.49 and 1.39 respectively). Nanoparticle enhancement ratio (NER) values decrease with increasing doses [19]. Khoei et. al. studied the sensitization effect of NH₂-NanoMag on human prostate cancer DU145 cells. Dose enhancement factor (DEF) is approximately 1.2 at different doses in the range of 2–8 Gy of 6 MV X-ray radiation. In this study 1, 2 and 3 mg/ml concentrations were used and percentage cell viability found to be decreasing with concentrations [20]. Razaei et.al carried out the cytotoxicity evaluation of dextran-coated iron oxide nanoparticles (IONPs) at different concentrations (0.010, 0.040, and 0.080 mg/ml) with different doses (0, 2, 4, 6, and 8 Gy) of 6 and 12 MeV electron beams on HeLa and MCF-7 cell lines. Toxicity results of the nanoparticles at 0.010 and 0.040 mg/ml concentrations showed no significant cytotoxicity effect. The radiosensitivity enhancement induced by the nanoparticles in MCF-7 cell line was more than it in HeLa cell line. Greater radiosensitization observed for 12 MeV (1.17-1.32 for HeLa, and 1.29-1.35 for MCF-7) compared to 6 MeV (1.13-1.25 for HeLa, and 1.26-1.29 for MCF-7) at 0.01, 0.04 and 0.08 mg/ml concentrations [17].

Compared to these studies we found greater radiosensitization by PEG coated SPIONs for concentration 0.25 mg/ml at 2 Gy dose of 6 MV photon beam (SER: 1.74). We have studied biocompatibility of PEG coated SPIONs on normal cell lines i.e L929, results show about 57% cell killing for 0.25 mg/ml concentration [21]. As we increase concentration above 0.25 mg/ml, normal cell killing also increases which will not be useful. Also there has been no study found that SPIONs are treated on colorectal cancer cell lines (HT-29). In our study we found that radiosensitization increases with concentration of nanoparticles which is consistent with other studies. We compared the percentage cell viability of cell

lines exposed to only radiation (i.e., control) with radiation and nanoparticles combination, for all concentrations as shown in figure 6.9.

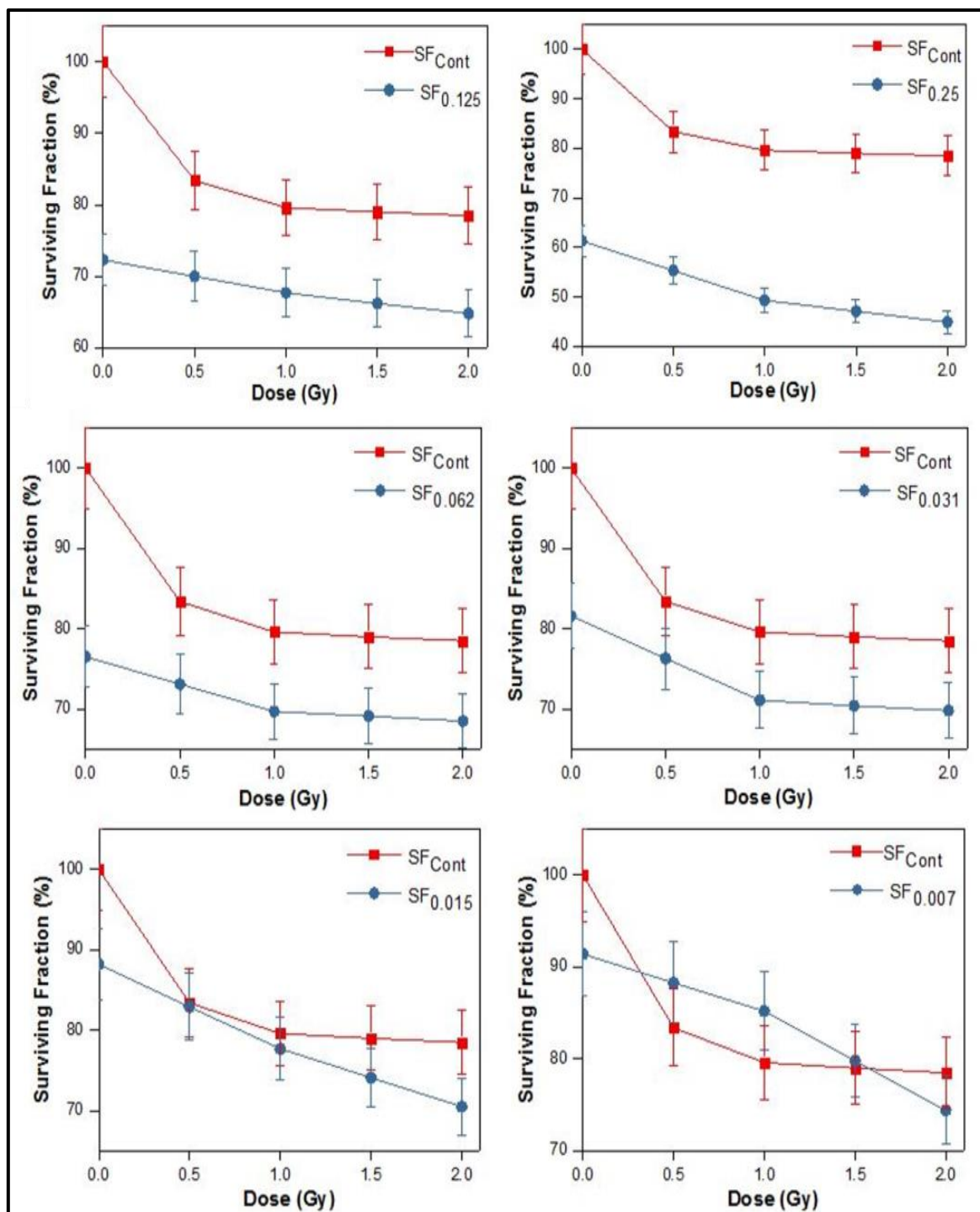


Figure 6.11 Comparison of surviving fraction of cells exposed to radiation dose alone (Control) with radiation dose exposed with SPIONs concentrations.



It has been seen that percentage cell viability of HT-29 cells is reduced by minimum 20 % when it is exposed with a combination of radiation doses & concentrations (0.031, 0.062, 0.125 and 0.25 mg/ml) compared to radiation doses alone. Figure 6.11 explains how percentage cell viability is effectively reduced but for lower two concentrations, percentage cell viability is observed to be nearly the same for radiation alone and radiation along with SPIONs. So, concentrations 0.031, 0.062, 0.125 and 0.25 mg/ml might be applicable to work as radiotherapy sensitizer in colorectal cancer.

SER values calculated for each dose and concentration is tabulated as shown in table 1. As doses increase there is a slight increment observed in SER values for concentrations 0.007, 0.015, 0.031, 0.062 and 0.125 mg/ml but for 0.25 mg/ml concentration of nanoparticles, SER values increase effectively with doses (see Table 6.1).

Fe_3O_4 was found to be cytotoxic as it contains Fe^{2+} ions and helps in the formation of reactive oxygen species (ROS) which leads to cell death through damage of mitochondria [15]. The pathway of production of ROS is the Haber-Weiss reaction which results in the generation of the highly reactive hydroxyl radical from the reaction between superoxide and hydrogen peroxide [15]. Radiation therapy promotes production of superoxide anion through leakage of electrons from the electron transport chain. The reaction can then be catalysed by iron oxide nanoparticles, resulting in highly reactive oxygen species [22]. This is an important parameter in use of SPIONs as a radiotherapy sensitizer. Cytotoxicity of nanoparticles is the combined effect of ROS production by radiation and SPIONs. It depends on several factors such as size, concentration, incubation time of nanoparticles, cell line, amount of radiation doses, energy and type of



radiation [17]. In above cases as concentration of nanoparticles, amount of radiation doses delivered and energy of radiation varies, the sensitization effect on cell lines also changes [14,17,20,22]. On the other hand, iron is an essential factor for cell growth and its multiplication in view of its role in the activity of DNA synthesis and for the reduction of ribonucleotides to deoxyribonucleotides. It needs a continuous supply of iron to maintain activity. Thus, the essentiality of this metal together with its potential toxicity, suggests that cellular iron metabolism needs to be highly regulated [23]. In our study we found that cells exposed to SPIONs of concentrations 0.007 and 0.014 mg/ml for 0.5, 1, 1.5 and 2 Gy have shown slightly greater percentage cell viability compared to only radiation doses as shown in figure 6.8 (see bar diagram for 0 concentration i.e., only radiation doses and 0.007 - 0.014 mg/ml concentration of SPION), which is controversial. This suggests that these two concentrations promote cell growth and effective cell killing is observed for concentration onwards 0.031 mg/ml up to 0.25 mg/ml suggesting that these concentrations may be applicable for radiotherapy to work as sensitizer.

Various studies revealed that within a 1-100 nm range, 50 nm NPs show maximum cellular uptake, with 14-20 nm NPs having a higher endocytotic rate than the 100 nm NPs [24]. Additionally, coated NPs (surface charged) display internalization more readily than their plain counterparts because of increased surface potential resulting in higher affinity for cells. Synthesized PEG coated Fe_3O_4 nanoparticles are biocompatible, stable, super paramagnetic and of size in the range of 10-20 nm [21]. In summary, PEG coated Fe_3O_4 nanoparticles are well suited to work as radiotherapy sensitizers in colorectal cancer. Side effects on normal tissue due to incremental doses to achieve better tumor control probability (TCP) can be reduced using the sensitization effect of nanoparticles.



6.5 Conclusion

These results reveal that PEG coated super paramagnetic iron oxide nanoparticles have synergistic effect on HT-29 cell lines while it is used along with radiation doses of MV energy x-rays. Greater SER values obtained while using SPIONs as a radiosensitizer. In case of colorectal cancer, local tumor control (tumor control probability, TCP) can be achieved at a minimum risk of normal tissue complications (normal tissue complication probability, NTCP) by using SPIONs.



References

1. Jafari S, Cheki M, Tavakoli M, Zarrabi A, Sani K G and Afzalipour R. Investigation of Combination Effect Between 6 MV X Ray Radiation and Polyglycerol Coated Superparamagnetic Iron Oxide Nanoparticles on U87-MG Cancer Cells. J. Biomed. Phys. Eng. 2018
2. Forman D, Ferlay J. "Chapter 1.1: The global and regional burden of cancer". In Stewart B W, Wild CP (eds.). World Cancer Report.the International Agency for Research on Cancer, World Health Organization. 2014,16–53. ISBN 978-92-832-0443-5.
3. Bosman, Frank T. "Chapter 5.5: Colorectal Cancer". In Stewart, Bernard W.; Wild, Christopher P (eds.). World Cancer Report.the International Agency for Research on Cancer, World Health Organization. 2014, 392–402. ISBN 978-92-832-0443-5.
4. Agranovich A, Berthelet E. Radiotherapy for Colorectal cancer. BC Medical Journal. 2000;42(3):139-141.
5. Habiba K, Aziz K, Sanders K. et al. Enhancing Colorectal Cancer Radiation Therapy Efficacy using Silver Nanoprisms Decorated with Graphene as Radiosensitizers. Sci Rep. 2019,9,17120.
6. Agarwal A. et al. Quantified pathologic response assessed as residual tumor burden is a predictor of recurrence-free survival in patients with rectal cancer who undergo resection after neoadjuvant chemoradiotherapy. Cancer, 2013,119,4231–4241.
7. Gunther J R. et al. Preoperative radiation dose escalation for rectal cancer using a concomitant boost strategy improves tumor downstaging without increasing toxicity: A matched-pair analysis. Adv. Radiat. Oncol. 2017,2, 455–464.



8. Habr-Gama A, Perez R. O, Nadalin W et al. Operative versus nonoperative treatment for stage 0 distal rectal cancer following chemoradiation therapy: long-term results. *Ann Surg.* 2004,240,711-717.
9. Wardman, P. Chemical radiosensitizers for use in radiotherapy. *Clin. Oncol.* 2007, 19,397–417.
- 10 Maegan A. Gargett, Adam R. Briggs, Jeremy T. Booth, Water equivalence of a solid phantom material for radiation dosimetry applications, *Physics and Imaging in Radiation Oncology*, Volume 14, 2020, 43-47, ISSN 2405-6316
- 11 Retif P, Pinel S, Toussaint M, Frochot C, Chouikrat R, Bastogne T, Barberi-Heyob M, Nanoparticles for Radiation Therapy Enhancement: the Key Parameters. *Theranostics.* 2015,5(9),1030-44
- 12 Young SW, Qing F, Harriman A, et al. Gadolinium (III) texaphyrin: a tumor selective radiation sensitizer that is detectable by MRI. *ProcNatlAcadSci U S A* 1996, 93, 6610-6615
- 13 Subiel A, Ashmore R, Schettino G. Standards and methodologies for characterizing radiobiological impact of high-Z nanoparticles. *Theranostics.* 2016, 6, 1651–71.
- 14 Huang F K, Chen W C, Lai S F, Liu C J, Wang C L, Wang C H, Chen H H, Hua T E, Cheng Y Y, Wu M K, Hwu Y, Yang C S, Margaritondo G, Enhancement of irradiation effects on cancer cells by cross-linked dextran-coated iron oxide (CLIO) nanoparticles. *Phys Med Biol.* 2010,55(2),469–482.
- 15 Klein S, Sommer A, Distel L V, Neuhuber W, Kryschi C. Superparamagnetic iron oxide nanoparticles as radiosensitizers via enhanced reactive oxygen species formation. *Bio. Chem.Biophys. Res. Commun.* 2012, 425,393–397.
- 16 Ghazanfari M R, Kashefi M, Shams SF, Jaafari M R, Perspective of Fe₃O₄ nanoparticles role in biomedical applications, *Biochem. Res. Int.* 2016, 7840161(32 pages).



- 17 Rezaei M, Khoshgard K, Hosseinzadeh L, Haghparast A, Eivazi M T, Application of dextran-coated iron oxide nanoparticles in enhancing the radiosensitivity of cancerous cells in radiotherapy with high-energy electron beams. *J. Cancer Res. therapeutics* 2019,15(6), 1352-1358.
- 18 Roeske J C, Nunez L, Hoggarth M, Labay E, Weichselbaum R R. Characterization of the theoretical radiation dose enhancement from nanoparticles. *Technol Cancer Res Treat.* 2007, 6(5),395–401
- 19 Kirakli E K, Takan G, Hoca S, Müftüler F Z B, Kılçar A Y, Kamer S A. Superparamagnetic iron oxide nanoparticle (SPION) mediated in vitro radiosensitization at megavoltage radiation energies. *J. Radioanal. Nucl. Chem.* 2018, 315, 595–602
- 20 Khoei S, Mahdavi S R, Fakhimikabir H, Shakeri-Zadeh A, Hashemian A. The role of iron oxide nanoparticles in the radiosensitization of human prostate carcinoma cell line DU145 at megavoltage radiation energies. *Int J Radiat Biol.* 2014,90(5),351–356.
- 21 Anuje M, Pawaskar P N, Khot V, Sivan A, Meshram J, Thombare B. Synthesis and cytotoxicity evaluation of poly (ethylene) glycol coated iron oxide nanoparticles for radiotherapy application. *J Med Phy*, 2021, 46(3), 154-161.
- 22 Hauser A K, Mitov M I, Daley E F, McGarry R C, Anderson K W, Hilt J Z. Targeted iron oxide nanoparticles for the enhancement of radiation therapy. *Biomaterials.* 2016,105,127–35.
- 23 Mario Cazzola, Gaetano Bergamaschi, Laura Dezza, and Paolo Arosio Manipulations of Cellular Iron Metabolism for Modulating Normal and Malignant Cell Proliferation: Achievements and Prospects *Blood* 1990,75(10),1903-19.



- 24 Anuje M, Sivan A, Khot V and Pawaskar P N. "Chapter 10 Cellular interaction and toxicity of nanostructures". In Thorat N, Bauer J (eds). Nanomedicines for Breast Cancer Theranostics. 2020,203. ISBN: 9780128200179

CHAPTER - 7

SUMMARY AND CONCLUSION





7.1 Introduction

In this section we have summarized all previous six chapters. First chapter introduces principle of radiotherapy, steps involved in radiotherapy procedure and advancement in radiotherapy techniques. Properties and applications of magnetic nanoparticles has been portrayed in chapter 2. Different kinds of nanoparticle mediated radiosensitizers and classification of assessment of radiosensitization by nanoparticles based on cell survival data included in chapter 3. Chapter 4 sum up theory behind synthesis, characterizations and cytotoxicity study of nanoparticles. In detail, it explains about steps involved during precipitation, factors affecting co-precipitation method, principles of instruments used for characterization and different in vitro techniques used for cytotoxicity evaluation. In order to evaluate suitability of PEG coated SPIONs for radiosensitization, different characterization techniques have been carried out such as XRD, FTIR, Zeta-Potential, DLS, TGA, TEM, VSM and MTT assay. Results of these experiments have been discussed in chapter 5. After assessment of suitability of PEG coated SPIONs we found it can be applicable for biomedical applications. In chapter 6, we carried out radiotherapy experiments. HT-29 cell line exposed with PEG coated SPIONs along with radiation and then MTT assay has been carried out. Cell survival of HT-29 cells has been observed and calculated in the form of SER. During exposure of well plate, all the parameters such as preparation of bolus phantom, CT simulation, dose calculation, cell culture preparation, irradiation setup, analysis of cell survival using MTT assay and SER calculation have been described in detail.

In our research we have chosen SPION for radiosensitization due to their advantages over another nanoparticle sensitizer as mentioned previously. When HT-29 cells

were treated with different concentrations of PEG coated SPIONs and various doses, we observed cell killing as given in Table 7.1. When HT-29 cells were exposed to 2 Gy (only radiation) we found 21.5 % of cell killing. As this radiation dose combined with different nanoparticle concentrations, percentage of cell killing increases up to 55.1 %. We can achieve higher therapeutic efficiency using SPIONs while it is used along with standard dose fraction i.e., 2 Gy compared to single radiation dose alone. Also, in order to minimize normal tissue complication probability (NTCP) while achieving tumor control probability (TCP), use of SPION might be a good option.

Table 7.1 Cell killing observed for HT-29 cell line while treated with different doses and concentration of SPIONs

Concentration (mg/ml)	Percentage of Cell Killing (Avg. reading)				
	0 Gy	0.5 Gy	1 Gy	1.5 Gy	2 Gy
0	0	16.6	20.4	21	21.5
0.007	8.6	11.7	14.8	20.2	25.6
0.015	11.8	17.1	22.3	25.9	29.5
0.031	18.4	23.7	28.9	29.6	30.2
0.062	23.5	26.9	30.3	30.9	31.1
0.125	27.7	30	32.3	33.8	35.2
0.25	38.7	44.7	50.7	52.9	55.1



For example, 21.5 % cell killing observed for 2 Gy radiation dose alone, same or greater percentage cell killing observed while using dose less than standard dose (2 Gy) with nanoparticles. i.e., percentage cell killing observed when 0.5 Gy combined with 0.031 concentration, 1 Gy combined with 0.015 and 1.5 Gy combined with 0.015 concentrations (See table 7.1). In summary, limitation of radiotherapy (i.e. escalation of dose beyond which radiotherapy cannot be sustainably employed to treat cancers) may be overcome by using radiosensitizer.

7.2 Major Conclusions

- PEG coated SPIONs successfully synthesized using Chemical co-precipitation method.
- Synthesized NPs accomplish all those requirements to be used for cancer radiotherapy application which involves particle size, superparamagnetism, colloidal stability, biocompatibility for normal cell and cytotoxicity for tumor.
- Iron oxide nanoparticles successfully functionalized with Poly (ethylene) Glycol (PEG) and coating also confirmed using XRD, FTIR, TGA, DLS and VSM.
- Cytotoxicity study of PEG coated SPIONs using MTT assay shows PEG coated SPIONs are biocompatible on L929 cell lines (Normal cell) and cytotoxic effect on MCF-7 (Breast cancer cell line). It shows greater cytotoxicity for MCF-7, which reveals that it can also be used alone for breast cancer treatment.
- From our study, we found that four concentrations of PEG coated SPIONs such as 0.031, 0.062, 0.125 and 0.25 mg/ml might be suitable for radiotherapy enhancement in the HT-29 cell line.



- Role of PEG coated SPIONs studied to work as an effective radiosensitizer for HT-29 for the first time in the literature.
- The goal of radiotherapy i.e. achieving better tumor control while minimizing damage to healthy tissue can be fruitfully achieved using PEG coated SPIONs.

7.3 Future Scopes

- In-vitro study of PEG coated SPION to work as a radiosensitizer was carried out but there is need to assess biological effectiveness of this drug as a radiosensitizer in animal models (In vivo).
- Mostly colorectal cancer is treated with preoperative chemoradiotherapy. In future study, there will be good option to combine radiotherapy along with sensitizer and chemotherapy which may increase fruitfulness of PEG coated SPIONs
- Combining hyperthermia with radiotherapy along with SPIONs on HT-29 might be efficacious for future research.
- Other than HT-29, other radioresistant cell lines also can be investigated for radiosensitization along with SPIONs.

ABBREVIATIONS

3D CRT	Three-Dimensional Conformal Radiation Therapy
AAA	Analytical Anisotropic Algorithm
AFM	Atomic Force Microscopy
AMF	Alternating Magnetic Field
BEV	Beam's Eye View
CNTs	Carbon Nanotubes
CRT	Chemo-Radiation Therapy
CT	Computed Tomography
CTV	Clinical Target Volume
DEF	Dose Enhancement Factor
DICOM	Digital Imaging and Communications in Medicine
DMEM	Dulbecco's Modified Eagle Medium
DMF	Dose Modification Factor
DMR	Dose Modifying Ratio
DNA	Deoxyribonucleic Acid
DRR	Digitally Reconstructed Radiographs
DSB	Double Strand Breaks
DVH	Dose Volume Histograms
EBRT	External Beam Radiation Therapy
EPID	Electronic Portal Imaging Device
EPR	Enhanced Permeability and Retention
FBS	Fetal Bovine Serum
FTIR	Fourier Transform Infrared Spectroscopy
GNP	Gold Nanoparticles
GTV	Gross Target Volume
HDR	High Dose Rate

HR-TEM	High Resolution - Transmission Electron Microscope
IARC	International Agency for Research on Cancer
ICRP	International Commission on Radiological Protection
ICRU	International Commission on Radiation Units and Measurement
IGRT	Image Guided Radiation Therapy
IM	Internal Margin
IMRT	Intensity-Modulated Radiation Therapy
ISO	International Organization for Standardization
keV	Kilo Electronvolt
KV	Kilo Voltage
LDR	Low Dose Rate
LET	Linear Energy Transfer
LINACS	Linear Accelerators
LQ	Linear Quadratic
MALDI-TOF	Matrix-Assisted Laser Desorption/Ionization Time-Of-Flight Mass Spectrometry
MC	Monte Carlo
MDR	Medium Dose Rate
MeV	Mega Electronvolt
MID	Mean Inactivation Dose
MLC	Multi Leaf Collimator
MNPs	Magnetic Nanoparticles
MRI	Magnetic Resonance Imaging
MTT	Methylthiazol-Tetrazolium
MV	Mega Voltage
NCT	Neutron Capture Treatment
NIH	National Institutes of Health
nm	Nanometer

NMR	Nuclear Magnetic Resonance
NMs	Nanomaterials
NPs	Nanoparticles
NRC	National Research Council
NTA	Nanoparticle Tracking Analysis
NTCP	Normal Tissue Complication Probability
OAR	Organ at Risk
OBI	On Board Imagers
PACS	Picture Archive and Communication System
PDR	Pulsed Dose Rate
PEG	Polyethylene Glycol
PET	Positron Emission Tomography
PRV	Planning Organs at Risk Volume
PTV	Planning Target Volume
REF	Radiation Enhancement Factor
RER	Radiation Enhancement Ratio
RES	Reticuloendothelial System
ROI	Region of Interest
ROS	Reactive Oxygen Species
RT	Radiation Therapy
SAD	Source to Axis Distance
SAR	Specific Absorption Rate
SBRT	Stereotactic Body Radiation Therapy
SEM	Scanning Electron Microscopy
SER	Sensitizer Enhancement Ratio
SF	Surviving Fraction
SM	Setup Margin
SPECT	Single Positron Emission Computed Tomography

SPIONs	Super Paramagnetic Iron Oxide Nanoparticles
SPNs	Superparamagnetic Nanoparticles
SRS	Stereotactic Radiation Surgery
SSB	Single Strand Breaks
SSD	Source to Surface Distance
TBI	Total Body Irradiation
TCP	Tumor Control Probability
TLD	Thermoluminescent Dosimeter
TPS	Treatment Planning Systems
TV	Treatment Volume
VSM	Vibrating Sample Magnetometer
WHO	World Health Organization
XPS	X-Ray Photoelectron Spectroscopy
XRD	X-Ray Diffraction

Curriculum vitae



Madhuri Anuje Kawade



Personal Information

Name	Madhuri Anuje Kawade
Date of Birth	02/08/1990
Place of Birth	Sangli
Marital Status	Married

Contact Information

Address	A1201, Citron Society, Kesnand road, Wagholi, Tal - Haveli, Dist-Pune
Mobile	7038597707, 9890041633
E-Mail	anuje.madhuri@gmail.com
e-Lora ID	16-35288

Objective

Medical Physicst cum RSO, Research Scholar

To reach the position of an excellent Medical Physicist / RSO through hard work and dedication towards the job, assigned to me, as well as for the organization. Also confident Research Scholar with a commitment to excellence and a background in Medical Physics.

Accreditation

Jan 2017	Radiological Safety Officer level III (RSO-III) Bhabha Atomic Research Centre (BARC), Mumbai
May 2015	Medical Physics Competency Test (MPCT) Bhabha Atomic Research Centre (BARC), Mumbai

Education

2014 - till today	Ph.D. Scholar in Medical Physics D.Y Patil University Kolhapur
2011-2013	M.Sc. Medical Physics D.Y Patil University Kolhapur
2008-2011	B.Sc. Physics Jaysingpur College, Jaysingpur
2006-2008	Higher Secondary Shri Datta Kanistha Mahavidyalay, Kurundwad
2006	Secondary Shri Datta Vidya Mandir, Narasobawadi

Work Experience

August 2017 till Today	Medical Physicist Cum Radiological Safety Officer BSDTs Integrated Cancer Treatment & Research Centre, Wagholi, Pune
-------------------------------	--

Role & Responsibility

The Radiological Safety Officer shall:-

- (a) carry out routine measurements and analysis on radiation and radioactivity levels in the controlled area, supervised area of the radiation installation and maintain records of the results thereof;
- (b) the safe storage and movement of radioactive material within the radiation installation;
- (c) ensure that -
 - i. reports on all hazardous situations along with details of any immediate remedial actions taken are made available to the employer and licensee for reporting to the competent authority and a copy endorsed to the competent authority(AERB);

- ii. quality assurance tests of structures, systems, components and sources, as applicable are conducted; and
 - iii. monitoring instruments are calibrated periodically.
- (d) Treatment Planing and Manual Time Calculation for Bhabhatron II Telecobalt Machine

Nov 2016 - Aug 2017
Jan 2014- Sept 2015

Assistant Professor (Medical Physics)
 D. Y. Patil University, Kolhapur

Conferences

2019

1) Participated in oral presentation on topic titled “Role of Superparamagnetic Nanoparticles as a Radiation Therapy Sensitizer in colorectal cancer” in international conference on ‘cancer Biology: Basic science to Translational Research’ (CBTR-2020) held on 17Th -18th January 2020. Organized by department of stem cell and regenerative medicine and D.Y. Patil medical college.

2018

2) Presented paper Poster titled “Role of Superparamagnetic Nanoparticles as a Radiation Therapy Sensitizer” in ‘39th Annual National conference of Association of Medical Physicists of India (AMPICON-2018)’ Nov 2-4,2018, Chennai Trade Centre, Chennai, Organized by the TN & PY chapter of AMPI

3) Participated Workshop on “ Quality Assurance of Advanced Imaging Systems used in Radiodiagnosis and Radiotherapy” Feb 23-24, 2018, Jointly Organized by Radiological Physics and Advisory Division, P.D.Hinduja National Hospital and Western Chapter of AMPI at CT &

CRS, RP & AD, BARC, Anushaktinagar, Mumbai - 400094.

4) Participated “Annual conference of Association of Medical Physicist of India (NC)” Feb 17-18,2018
Organized by Swami Rama Himalayan University, Jolly Grant, Dehradun, Uttarakhand, India.

2017

5) Attended National Symposium on Medical Physics of AMPICON_WC- 2017, ‘The Present Challenges and Future Expectations of Physics in Oncology’ held on 6th -7th May-2017 Organized by Aditya Birla Memorial Hospital, Pune.

6) Certified for delivering guest lecture on “Medical Instrumentation Techniques- I ” 24th- 29th Apr 2017, organized by Institutional Research Committee(IRC), D.Y.Patil University,Kolhapur.

7) Participated Workshop on “Nuclear Energy and Health Care (NEHCA- 2017)”, held on 19th Feb 2017 under ‘Innovative Technologies for Rural Development and Their Commercialization (ITRDC- 2017) Organized by Centre for Research and Technology Developments, Sinhagad Institute Solapur in collaboration with Indian Medical Association, Solapur and BHABHA ATOMIC RESEARCH CENTRE, MUMBAI.

2015

8) Participated & Presented Poster in “Annual Meet on Advanced Research” 17th March, 2015, Organized by D.Y.Patil Univeristy, kolhapur.

9) Participated “Workshop on Applications of Statistics In Medical Research” 19th and 20th Jan 2015, Conducted by Univeristy Research cell of D.Y.Patil Univeristy, kolhapur.

2014

10) Attended “35th Annual conference of Association of Medical Physicist in India” AMPICON 2014, 20th to 22nd

November 2014, organized by the Department of Radiotherapy & Oncology Rural Medical College Hospital, Pravara Institute of Medical Science-Deemed University (PIMS-DU), Loni, Maharashtra.

11) Attended International Workshop on "Ph.D. program for medical innovations", (IWPPMI-2014), Feb 16th and 17th, 2014 organized by Centre for Interdisciplinary Research, D.Y. Patil University, Kolhapur.

2012

12) Attended "Radiological Imaging and advances", IRIA CME, Kolhapur 2012, 25th & 26th AUGUST 2012 organized jointly by Indian Radiological & Imaging association, Indian college of Radiology and Imaging and D.Y. Patil University, Kolhapur

2011

13) Attended Symposium on, "Nuclear Energy and Health Care", A multimedia Event, October 22nd - 24th 2011, organized by Centre for Interdisciplinary Research, D.Y. Patil University, Kolhapur in collaboration with Indian nuclear Society, Mumbai.

Publications

2021

1) Anuje M, Pawaskar P.N., Khot, Sivan A, Meshram J, Thombare. **Synthesis and cytotoxicity evaluation of poly (ethylene) glycol coated iron oxide nanoparticles for radiotherapy application.** Journal of Medical Physics. volume 46, 2021, Page No 154-161.

2) Anuje M, Pawaskar P.N., Sivan A, Lokhande C.D. and Patil Dhanashree. **Use of Poly (Ethylene Glycol) coated Superparamagnetic Iron Oxide Nanoparticles as a radiosensitizer in enhancing colorectal cancer radiation efficacy.** Journal of Medical Physics (Accepted)

2020 3) Anuje M, Sivan A, Khot V and Pawaskar P. “**Chapter 10 Cellular interaction and toxicity of nanostructures**”. In Thorat N, Bauer J (eds). Nanomedicines for Breast Cancer Theranostics. 2020:203. ISBN: 9780128200179

2019 4) Anuje M, Bauer J and Thorat N. “**Chapter 7 Radiotherapy and breast cancer nanomedicine**”. In Thorat N, Bauer J (eds). External Field and Radiation Stimulated Breast Cancer Nanotheranostics. 2019:7-9. ISBN: 978-0-7503-2416-8.

2018 5) Anuje M, Pawaskar P.N., **Role of superparamagnetic nanoparticle as radiation therapy sensitizer**. Journal of Medical Physics, 2018: 43(1): 48-49 (Abstract)

2017 6) Anuje M, Phadatare M, Ahmed I, Sougoumarane D. **Protocol to calculate margin from Clinical Target Volume (CTV) to Planning Target Volume (PTV)**. Annual journal of university Research, Volume 7, 2017, page No.374

Skills

Professional

- (a) Radiation Safety & Survey
- (b) Radiation Therapy Treatment Planning
- (c) Quality Assurance
- (d) Medical Imaging
- (e) Dosimetry

Computer

Microsoft Office (MS Word, MS Excel, MS

Languages

Marathi	Mother tounge
----------------	---------------

English, Hindi, Kannada	Expert
--------------------------------	--------

Other	
-------	--

Hobbies	Watching TV, Cooking, Listening Music
----------------	---------------------------------------

References

Prof. (Dr.) S.H. Pawar	Former Vice chancellor, D. Y. Patil University, Kolhapur-416006, Maharashtra, India. Cell No. 09822878226 E-mail: shpawar1946@gmail.com
-------------------------------	---

Dr. P.N. Pawaskar (Ph.D Guide)	Assistant Professor, Department of Medical Physics, D. Y. Patil University, Kolhapur-416006, Maharashtra, India. Cell No. 09028074295 Email : samgrish@gmail.com
---------------------------------------	--

Dr. Jagdish Shinde	Radiation Oncologist, Aditya Birla Memorial, Pune, Maharasthtra, India Cell no.09890233887
---------------------------	--

D. Sougoumarane	Chief Medical Physicist & RSO, Dept. of Radiotherapy, Belgaum Cancer Hospital, Belgaum Mobile No: +91-8951768508 Email : dsougoumarane1969@gmail.com
------------------------	--

Declaration

I hereby declare that the above mentioned
information is correct to best of my Knowledge.

Place-Pune

Date- 23/10/2021

Madhuri Anuje Kawade
